INVESTIGATION OF THE JET NOISE PREDICTION THEORY AND APPLICATION UTILIZING THE PAO FORMULATION

Final Technical Report

This research work was supported by
the National Aeronautics and Space Administration
George C. Marshall Space Flight Center
Contract NAS8-28588

The University of Alabama in Huntsville
Division of Graduate Programs and Research

P. O. Box 1247
Huntsville, Alabama 35807

November 1973

INVESTIGATION OF THE JET NOISE PREDICTION THEORY AND APPLICATION UTILIZING THE PAO FORMULATION

Final Technical Report

This research work was supported by
the National Aeronautics and Space Administration
George C. Marshall Space Flight Center
Contract NAS8-28588

The University of Alabama in Huntsville
Division of Graduate Programs and Research

P. O. Box 1247
Huntsville, Alabama 35807

November 1973

ACKNOWLEDGEMENT

The author wishes to express his appreciation to Mr. Gilbert A. Wilhold and Mr. Jess H. Jones of the Unsteady Gasdynamics Branch, NASA-MSFC, for their continuous support on this rocket noise research project, which leads to the completion of an advanced theory on rocket noise, and the development of the theoretical results for direct engineering applications. The author wishes also to thank Mrs. Marion S. Bishop of the Computer Services Center at The University of Alabama in Huntsville for her excellent work in computer programming, whereby the numerical results are rendered in an elegant form as suitable for engineering applications.

PREFACE

The complete development of this advanced rocket noise theory and application is performed under the sponsorship of three NASA-MSFC contracts: NAS8-25893 and NAS8-26915 to Wyle Laboratories Eastern Operations, and NAS8-28588 to the University of Alabama in Huntsville. The first contract was awarded to Wyle Laboratories in February 1970. In the course of this study, numerous reports and technical papers have been published to mark various phases of progress:

1. "Analytical properties of noise generating mechanisms in a supersonic shear layer," NASA CR-1848, Wyle Laboratories, May 1971.
2. "A generalized theory on the noise generation from supersonic shear layers," Journal of Sound and Vibration, V. 19, pp. 401-410, April 1971.
3. "Applications of the generalized aerodynamic noise theory," AIAA paper 71-584, presented at the AIAA 4th Fluid and Plasma Dynamics Conference, Palo Alto, Calif., June 1971.
4. "Applications of the generalized jet noise theory," Wyle Laboratories Research Staff Report WR-72-5, March 1972.
5. "Developments of a generalized theory of jet noise," AIAA Journal v. 10, pp. 596-602, May 1972.
6. "An analysis of jet noise directivity," AIAA paper 73-185, presented at the AIAA 11th Aerospace Sciences Meeting, Washington, D. C., January 1973.
7. "Aerodynamic noise emission from turbulent shear layers," J. Fluid Mechanics, V. 59, pp. 451-479, July 1973.

At the conclusion of the present contract, the studies have come to a major milestone. Namely, the application of the theory to practical engineering problem has been realized. It is therefore hopeful that from this point on, the application will aid the development of accurate methods of noise prediction which would rely less on empirical approach, and place the engineering prediction of rocket and other types of jet propulsion noise on a solid analytical basis.

In the course of this study, the superb technical coordination of the NASA-MSFC Unsteady Gasdynamics Branch, the technical resources of Wyle Laboratories and the Fluid and Thermal Engineering Department (presently the Mechanical Engineering Department) of The University of Alabama in Huntsville, have been most valuable for enhancing the progress of this work, for which the author wishes sincerely to acknowledge.

ABSTRACT

The present report describes the application of the Phillips theory to engineering calculations of rocket and high speed jet noise radiation. It contains the detailed derivation of the theory, the composition of the numerical scheme, and discussions of the practical problems arising in the application of the present noise prediction method. Although the present method still contains some empirical elements, yet it provides a unified approach in the prediction of sound power, spectrum, and directivity. It is expected that the present method would permit great improvement in the accuracy of jet and rocket noise prediction.

TABLE OF CONTENTS

1.0 INTRODUCTION

For the past decade, rocket noise prediction for engineering application has relied on empirical methods. Although the predictions have been accurate in general, there is a need to understand the basic mechanism of rocket noise. The accuracy of the empirical methods rests heavily upon the large amount of experimental data as accumulated through various measurements of engine test firing and actual vehicle launch. As for the noise of recently developed rocket engines, the data base will not be sufficient for practical applications if empirical techniques are used. Furthermore, the existing empirical approach is limited in scope. Reliable directivity patterns and sound source location can not be established by using experimental data alone. Therefore, an advanced rocket noise theoretical model is clearly in demand.

The present report describes the result of a jet noise theory based on the Phillips convected wave equation. Effects of high speed convection, refraction, and other aero-acoustic interactions in the flow regime are included in the theory. After preliminary calculation has indicated that the theory is capable of providing accurate description of jet and rocket noise, the numerical model for direct engineering application was constructed.

The main advantage of the present numerical model is the simplicity of input parameters. A typical set of input includes four key parameters: the maximum convection Mach number, the maximum speed of sound ratio, the spatial scale and the scale ratio for the local turbulence. The typical output is nondimensional. In case dimensional quantity or change of reference scale is desired, two scale factors may be added to the list of input quantities. These factors will place the predicted frequency and intensity of sound at their proper values. The most important aspects of this method are perhaps the items as given below:

(a) Accurate determination of the directivity pattern, especially in the upstream directions. Since the launch vehicle structure is exposed to the upstream sound field of the rocket exhaust flow, accurate prediction of the upstream directivity can effectively reduce the load uncertainty for the vehicle structure.

(b) The correct trends of sound power level and spectrum. In the low supersonic and transonic velocity range, the sound power as a function of convection Mach number has been a source of disagreement between experiments and previous theories. The present calculation provides the correct observed characteristic frequency of jet noise throughout this range, and the U^8-law is reproduced without any irregularity for transonic convection velocities.

(c) The allocation of sound source at different frequencies as a function of direction. Since the Doppler effect causes the frequency to be different in different directions for sound emitted from the same source, the sound source location is expected to be different for sound emission in different directions at a given frequency. There has been some efforts to infer the apparent source location from experimental data. However, a systematic approach is not available among the empirical noise prediction methods. In most cases, fixed source locations are assigned for a given class of launch configurations.

It should be noted that the present numerical model does carry a small number of empirical parameters such as the structural constants of the turbulence. These constants will be determined by numerical iteration such that the prediction and the experimental data are brought into agreement. The advantages of the present method over the conventional empirical technique are its power of extrapolation and its unification of spectral and directional calculations under one theory.

The present theory does not completely explain all the important trends of rocket noise emission. One of the most important discrepancy is the sound source strength per unit length in the mixing region of the flow. The theory indicates that the source strength is constant in this zone, while experimental data indicates that the source strength is a linear function of x/D. Further analytical study is clearly required to determine the correct dynamical process. In the present model, an empirical correction is applied. Another obvious omission in the present theory is the effect of scattering. In high velocity jets, the turbulent intensity is a significant fraction of the local speed of sound. Such local velocity fluctuations can produce

significant refraction of sound and possibly some additional aerodynamic attenuation. Its effect on directivity and sound power should be evaluated. In the present calculations, the predicted intensity near the peak angles is sometimes higher than the observed values. The omission of scattering effect may account for such a difference.

In the remainder of this report, the theory, the numerical model, and discussion of results are given in separate sections. The numerical results of an example are given in Appendix A; the listing of the computer program is given in Appendix B; and the details of the Phillips theory are given in Appendix C. Appendix C is in fact a reprint of a paper as published in the Journal of Fluid Mechanics.

2.0 A NUMERICAL MODEL FOR JET NOISE EMISSION

2.1 Solutions to the Phillips convected equation.

The Phillips theory deals with noise emission from turbulence in a parallel shear layer, in which refraction, convection, and other first order aero-acoustic interactions are taken into account. As the general Phillips convected wave equation is restricted to a plane parallel shear layer, it can be reduced to an ordinary differential equation by means of Fourier transformation over the homogeneous coordinates. The ordinary differential equation can then be solved by means of the WKBJ method. For a small volume of turbulence, its far-field noise radiation can be obtained in closed form, as described in Appendix C. Noise radiation in different directions is governed by three different solutions:

$$\overline{\Phi_o \Phi_o^*}(\underset{\sim}{y}) = \frac{3\sqrt{2}\,\gamma^2 \pi^{3/2} v_o^4 M^4 M_c^4 \alpha^4 q_\infty}{r^2 A^2 L_1 q_o} \frac{A}{(1 - M_c \cos\theta)} \left\{A^2 + \alpha^2 M_c^2\right\}^{-5/2} \tag{1}$$

$$\overline{\Phi_1 \Phi_1^*}(\underset{\sim}{y}) = \frac{160 \times 2^{2/3} \gamma^2 \pi^2 v_o^4 M^8 A_i^2(0) \alpha^{13/3} \tan\theta}{r^2 A^2 L_1^{4/3} \Omega^{1/3}} \Gamma\left(\frac{2}{3}\right) \{\cos\theta\}^{13/3}$$

$$\times \left(\frac{M_c}{M}\right)^{13/3} \{(1 - M_c \cos\theta)^2 + \alpha^2 M_c^2 \cos^2\theta\}^{-8/3} \tag{2}$$

$$\overline{\Phi_1 \Phi_1^*}(\underset{\sim}{y}) = \frac{3\sqrt{2}\,\gamma^2 \pi^{3/2} v_o^4 M^4 M_c^4 \alpha^4 q_\infty}{r^2 A^2 L_1 q_o} \frac{F(b)}{F(0)} \cos^4\theta$$

$$\times \{(1 - M_c \cos\theta)^2 + \alpha^2 M_c^2 \cos^2\theta\}^{-5/2} \tag{3}$$

The above equations are identical to Equations (C82), (C84), and (C85)*, respectively in Appendix C. Equation (1) is the so called accoustical solution. It governs mainly

* The prefix C is a designation of equation numbers in Appendix C.

the upstream noise radiation. The source function is the acoustic components of the turbulence, and the emitted sound reaches the far field without passing through any transition point.

Equations (2) and (3) have hydrodynamical components of the turbulence as the source function for noise emission. In both of these latter cases, one transition point occurs between the sound source and the far field. For equation (2), the source volume is located in the neighborhood of a transition point. For Equation (3), the source volume is far behind the transition point. Equation (3) demonstrates very well the mechanisms of sound emission from a shear layer as described by the Phillips convected wave equation. The refraction in the flow regime is described by

$$\frac{q_\infty}{q_o} = A \sin\theta \left\{ \left| (1 - M_c \cos\theta)^2 - A^2 \cos^2\theta \right| \right\}^{-1/2} \qquad (4)$$

The degenerated form of the refraction factor is represented by $\tan\theta$ in Equation (2). The refraction effects in the shear flow changes the direction of a ray tube, in the sense of geometrical acoustics, as well as its cross sectional area. For a given amount of energy flux in the tube, the intensity changes as the area of the tube changes. The factor $F(b)/F(0)$ in Equation (3) is the aerodynamic attenuation factor. As the pressure fluctuations from the source finds its way through the hydrodynamic zone of wave propagation, the amplitude of the signal is attenuated. The attenuation is a function of frequency and the location of the transition point relative to the source location (see Eq. (C78)). The function $F(b)$ represents the integrated attenuation over the entire spectrum. In the remaining terms of Equation (3), the coupled effect of refraction and convection are represented. The numerical value of the coupled convection factor may have significantly different value as compared to the Lighthill convection factor of

$$C^5 = \left[(1 - M_c \cos\theta)^2 + \alpha^2 M_c^2 \right]^{-5/2}$$

In Equation (1), the coupling of refraction and convection is so strong such that the convection factor is reduced to a constant for all upstream directions. The directivity for upstream radiation is purely the result of refraction and the Doppler

effect. Since in Equations (1) and (2) the sound source is either near or above the transition point, the pressure wave does not pass through a hydrodynamical zone. There is no aerodynamic attenuation for these two solutions. For equation (3), the definition of F(b) and its argument can be given as:

$$F(b) = \int_b^\infty e^{b^2-u^2} (u-b)^4 \, du \tag{5}$$

$$b = \frac{2\sqrt{2}\ M\ W(y,\theta)\cos\theta}{\sqrt{\mu}\ L_t \left\{(1-M_c\cos\theta)^2 + \alpha^2 M_c^2 \cos^2\theta\right\}^{1/2}} \tag{6}$$

$$\mu \begin{cases} 1 & \text{for self noise} \\ 2 & \text{for shear noise} \end{cases}$$

where $W(y, \theta)$ is a function related to the WKBJ transformation:

$$W(y,\theta) = \int_{y_o}^{y} \left\{\frac{(1-M_c\cos\theta)^2}{A^2} - \cos^2\theta\right\}^{1/2} dy \tag{7}$$

In the above equation, y_o denotes the location of the transition point for a given direction θ. It can be noted from Eq. (5) that the value of F(b) is purely numerical. All the aero-acoustic parameters are related to this function through the definition of b. The integral in Eq. (5) can be evaluated easily by numerical means. The graphical representation of F(b) is given in Figure 1. Equation (7) indicates that the value of $W(y, \theta)$ depends only on the mean flow properties of the shear layer. In the present numerical model, the velocity profile of the shear flow is assumed to be a Gaussian function:

$$U(y) = U_{max}\, e^{-2y^2} \tag{8}$$

The temperature and density variation in the shear layer is represented via the local speed of sound ratio: $A = c/c_o$. The profile of A is assumed to be a straight line:

$$A(y) = 1 + y(A_{max} - 1) \quad \text{for } y \leq 1;$$
$$A(y) = 1 \quad \text{for } y > 1. \tag{9}$$

Hence, the input parameters for the mean flow of a given turbulent shear layer will be A_{max} and $M_{max} = U_{max}/c_o$.

The sound field as produced by a small volume of turbulence may be divided into a maximum of four zones. The dividing angles are:

$$\cos \theta_1 = 1/(M_c - A), \quad \theta_1 = 0 \text{ if } (M_c - A) \leq 1, \tag{10}$$

$$\cos \theta_2 = 1/(M_c + A), \tag{11}$$

$$\cos \theta_3 = 1/(M_c - A), \quad \theta_3 = \pi \text{ if } (M_c - A) \geq -1. \tag{12}$$

In each zone, the solution to the convected wave equation is different. The proper solution in each zone is given in the following table:

TABLE 1. ZONES AND SOLUTIONS

Zone	Angular Limits	Type of Solution	Equation
1	$0 - \theta_1$	S2	1 (C82)
2	$\theta_1 - \theta_2$	S1b	3 (C85)
3	$\theta_2 - \theta_3$	S0	1 (C82)
4	$\theta_3 - 180^\circ$	S1b	3 (C85)

Zone 1 exists only if the convection Mach number is very large such that $M_c - A > 1.0$, while zone 4 exists only for low convection velocities where $A - M_c > 1.0$. In the neighborhood of the dividing angles, the solution is governed by either Equation (C83) or (C84). Analytically, these solutions are brought into effect because the source is located in the neighborhood of a transition point.

Equation (C83) is applicable under two conditions: either the radiation frequency is very low, or the velocity gradient vanishes at the transition point. The first condition is academic because the WKBJ transformation is not applicable at low frequencies. For a Gaussian velocity profile, the second condition is met only at the centerline of the profile. In this case, Equations (C83) and (C84) are quite similar. The velocity gradient Ω in Eq. (C84) is substituted by the curvature of the velocity profile Ω' in Eq. (C83). It should be noted that the sound intensity depends only on fractional powers of these quantities. In addition, Eq. (C83) takes over only if the velocity gradient goes to zero. For a Gaussian velocity profile, the magnitude of Ω and Ω' is approximately the same. Over a large portion of the profile, the non-dimensional value of Ω is approximately 1.0. The exponential indices of the convection factor in these equations are different by only a very small fraction. Hence, the sound radiation near a dividing angle and at the center of the profile is represented by using only Eq. (C84). As a further simplification, the value of Ω is set identically to 1.0 throughout the thickness of the shear layer. The error introduced by these approximations should be very small. The solution in Zone 1 is classified under S2 because the radiated sound wave passes through two transition points in the shear layer before it reaches the far field. Locally, the sound source is the acoustic component of the turbulence, the asymptotic formula for S2 emission under such conditions is identical to (C82) except for an attenuation factor. This is because the pressure wave will be attenuated heavily in the elliptic zone between the two transition points. In the numerical calculation, the factor $F(b)/F(0)$ will be taken into account for Zone 1.

The small volume assumption stipulates that the change of wavenumber and convection velocity through the turbulent volume is small. Such conditions are not met in mean flows with convection Mach numbers greater than 3.0. Equation (2) can be taken as an example. In this solution, the source function is assumed to be in the neighborhood of a transition point. At the transition point, the wavenumber vector is actually parallel to the shear layer, which is described mathematically in Equation (2). However, before the pressure wave left the turbulence volume, the effect of local convection would have changed the wavenumber vector

to a direction of more than 60 degrees away from the plane of the shear layer. As a result, the sound intensity is over-estimated. As a simple approximation, the mean value of the wavenumber vector should be used in Equation (2). Adequate numerical modification in the computer program has been made to correct for this discrepancy. Similar adjustments are also necessary for Equations (1) and (3). In the neighborhood of the dividing angles, Equations (1) and (3) become singular because q_o approaches zero. The governing solution in such regions is Equation (2). In the present program, the domain of application of Equation (2) is defined as within 2.45 degrees on either side of the dividing angles. Numerical calculations have shown that the three solutions join smoothly with this definition of domain if the convection Mach number is between 0.8 and 10. For convection Mach numbers smaller than 0.8, the domain of Equation (2) spans over a wider angle. An empirical domain greater than $\pm$ 2.45 degree should be defined.

2.2 The turbulence structure.

The solutions (C82) to (C85) are obtained from the general solutions of the Phillips equation by assuming a Gaussian turbulence structure. The Gaussian structure is defined by two constants: the spatial scale and the time scale. In most cases, the time scale is defined indirectly through a nondimensional scale ratio α. In the present work, the turbulence is defined as follows:

$$\overline{v_i v_j}\,(\underset{\sim}{k}, \omega) = \frac{v_o^2 L_1^3 L_t}{32\pi^2} \left[(kL_1)^2 \delta_{ij} - L_1^2 k_i k_j \right] \times \exp -\frac{1}{4}\left[(kL_1)^2 + (\omega L_t)^2 \right] \quad . \tag{13}$$

This is indeed one of the simplest form of an incompressible, isotropic turbulence which satisfies only the kinematical compatibility condition. The analytical form of Equations (C82) to (C85) is common to all the turbulence source functions in the form as given below:

$$\overline{v_i v_j}\,(\underset{\sim}{k}, \omega) = v_o^2 \left\{ (kL_1)^2 \delta_{ij} - L_1^2 k_i k_j \right\} F\left\{ (kL_1)^2 + (\omega L_t)^2 \right\} \qquad (14)$$

This is a broad class of function which includes most of the empirical formulae as used for describing turbulence structure of isotropic turbulence as well as wall turbulence. If any function in the form of Equation (14), other than the Gaussian function, is chosen as the source function, the only changes in Equations (C82) to (C85) will be the numerical constants and the definition of F(b). It should be noted that the Gaussian spectrum drops off very rapidly beyond the peak of the spectrum. Therefore, it is difficult to use the Gaussian model for narrow band noise prediction. Equation (14) would allow much greater freedom in the choice of the spectral distribution of the source function.

Calculations have shown that the structure of turbulence has great influence on the quality and quantity of sound radiation, if the turbulence intensity remains fixed. Sound power, directivity, and frequency characteristics of jet noise radiation can be related to L_1, L_t, and α through formulae as given previously in this chapter.

In the range of $M_j < 2.0$, the sound power production is strongly influenced by the factor α. From equations (1) to (3), it can be seen clearly that the farfield noise intensity is proportional to α^4. For greater convection Mach numbers, the convection factor in these formulae provides an α^{-5} factor in the same formulae. Hence, the dependence of sound power on α diminishes rapidly in the very high convection Mach numbers range. The self noise intensity is inversely proportional to the spatial scale length. However, this is not an important factor for overall sound power because the shear noise would increase in direct proportion to L_1.

The directivity of sound emission in the downstream direction is heavily influenced by refraction and aero-acoustic attenuation. While the refraction effect is fixed for given mean flow conditions, the aero-acoustic attenuation is determined by both the mean flow and the characteristic frequency of the turbulence. According to Figure 1 , the logarithmic value of F(b) is almost a linear function of its argument b. According to Equation (6), the value of b is inversely proportional

to the temporal scale of the turbulence L_t. The aerodynamic attenuation is the largest near the axis of the jet. A small change of L_t may change the sound intensity by several decibel.

The dependence of far field sound frequency on the turbulence structure is rather interesting. In the lower convection Mach number range of $M_j \leq 0.6$, the sound frequency is determined by L_t and the Doppler effect. However, the radiated sound frequency is determined entirely by the spatial scale L_1 for supersonic convection Mach numbers. This phenomenon can be described physically in the contest of the Phillips theory. In the low convection Mach number range, the limiting case of a turbulent sound source is one that remains almost stationary in space. It is then obvious that the sound source must oscillate in time in order to radiate sound. Therefore, the sound frequency will be governed by the temporal scale of the turbulence. The Doppler shift will further modify the radiated sound frequency. In the supersonic convection regime, the picture is quite different. The principal source of sound is the nearly frozen components of the turbulence. In the Phillips description of sound propagation, the far field sound is related to the turbulence such that the wavenumber in the turbulence should be the same as the projection of the sound wavenumber vector on the plane of the shear layer. Therefore, it is the spatial distribution of the source function that dictates the frequency of sound emission. In the next section, the analytical derivation of the above results will be discussed.

It is difficult to determine the turbulence intensity in a rocket exhaust flow. For low speed jets, it was found (Reference 1) that the turbulent intensity is in the order of 0.16. For the present study, however, a systematic method is needed for defining the turbulence intensity at all stations of the rocket exhaust flow. In the absence of available experimental data, the turbulence intensity for the rocket exhaust flow will be inferred indirectly.

A method for calculating the free mixing of two dissimilar gases is given by Donaldson and Gray in Reference 2 . The key parameter which governs the mixing process is a mixing parameter as defined after the Prandtl mixing length hypothesis:

$$K = \frac{\rho \overline{u'v'}}{\frac{1}{2} \rho U_b (\partial U/\partial y)} \tag{15}$$

As a result of extensive numerical experiment by Donaldson and Gray using their theory, it was found that the mixing parameter is a universal function of the true Mach number at the half velocity point of the velocity profile. This Mach number is designated in Reference 2 as M_5. The dependence of K on M_5 is given in Figure 2 . From this figure, one can observe that the value of K varies from 0.0475 in the low M_5 range, to approximately 0.01 for M_5 in the neighborhood of 2.0. According to the definition of K as given in Equation (15), the value of the mixing parameter is proportional to the mean square value of the turbulence intensity of 0.160 in low speed jets.

In the computer program, the value of turbulence intensity is fixed at 0.16 for the calculation of sound emission from an individual slice of jet. Since the Donaldson and Gray results of jet mixing for rocket exhaust flows are available, (Reference 2), the adjustment to the turbulence intensity will be given to the numerical model via an input parameter. Details of this input parameter will be discussed in Section 2.4.

2.3 The peak frequency and the band number.

The narrow band solutions for a Gaussian source function is given by Equations (C70), (C73), (C75), and (C78). In these equations, the frequency is non-dimensional, and it is related to the Strouhal number via:

$$St^* = \omega/2\pi \tag{16}$$

The asterisk signifies that this Strouhal number is defined in reference to the local convection velocity and length scale. In a rocket noise calculation which includes many slices of the exhaust flow, it is necessary to refer all calculated values of frequency to the standard Strouhal number in which the exit diameter and velocity are the references. Therefore,

$$St = St^* \frac{U_x D}{U_j L} = s_f St^* \tag{17}$$

where s_f is called the frequency scale factor. This is given as an input parameter to the computer program for each slice of the jet.

Each volume of turbulence produces a broad band radiation of noise in the far field. The shape of the spectrum is dependent upon the assumed function of the turbulence structure. For the Gaussian structure, the peak frequency for radiated noise in a given direction can be obtained from the narrow band solutions. General formulae have been obtained for both the shear noise and the self noise:

$$\text{(Shear noise)} \qquad St^* = \frac{1}{4\pi a^2} \left\{ -d + \sqrt{d^2 + 4a^2} \right\} \tag{18}$$

$$\text{(Self noise)} \qquad St^* = \frac{1}{4\pi a^2} \left\{ -d + \sqrt{d^2 + 8a^2} \right\} \tag{19}$$

where

$$\text{(S1)} \qquad a^2 = \frac{1}{8} \left\{ (1 - M_c \cos\theta)^2 + \alpha^2 M_c^2 \cos^2\theta \right\} L_t^2$$

$$\text{(S0)} \qquad a^2 = \frac{1}{8} (1 - M_c \cos\theta)^2 (\alpha^2 M_c^2 + A^2) L_t^2 \tag{20}$$

$$d = M W (y, \theta) \cos\theta \tag{21}$$

It can be seen from the above formulae that the attenuation factor plays an important role in the determination of peak frequency along directions close to the jet axis. In some experimental studies, it has been observed that the

characteristic frequency for noise radiation near the jet axis is significantly lower than predictions according to the convective effect. In Reference 5, this is called the reversed Doppler shift. Two mechanisms in the Phillips theory may be taken to explain this effect. The aero-acoustic attenuation for shear noise is much smaller than for self noise at small values of θ. As a result, the spectrum is dominated by the shear noise. Since the shear noise has a lower peak frequency, the observed spectrum has a trend which runs against the Doppler shift effect. The second reason is perhaps the more important one. The aero-dynamic attenuation coefficient in directions close to the jet axis is very large. Since the attenuation, in decibels, is directly proportional to frequency, the higher frequency part of the radiated noise spectrum will be heavily attenuated. As a consequence, the peak frequency of the radiated noise spectrum will be shifted to a much lower frequency.

It is also evident from the above formulae that the ratio of the peak frequencies of self noise and shear noise is not a constant. According to calculations obtained so far, the ratio is generally within one or two one-third-octaves. The above formulae are also sufficient to prove that L_t dominates the radiated sound frequency in the low Mach number range, and the L_1 dominates the frequency characteristics in the high Mach number range. For all practical purposes of the present discussion, the peak Strouhal number as given by Equations (18) and (19) can be taken as μ/a, where μ is different from self noise and shear noise. For small Mach numbers, the value of a is proportional to L_t. For downstream radiations at large convection Mach numbers, however, the value of a is proportional to $\alpha M_c L_t$. According to the definition of α, the latter quantity is identical to ML_1. Since M is a constant, the peak frequency is determined by L_1. It is interesting to note that this phenomenon is not unique for the Phillips theory. Identical conclusions can be derived from the Lighthill theory.

In the output of the computation, the frequency is represented in terms of band numbers. It is defined as:

$$N = \text{Integer} \left\{ 3 \log \left(\omega / 0.002\pi \right) \; / \log 2 + 0.5 \right\} \qquad (22)$$

Table 2: Band Number N, and the Corresponding Center Strouhal Number.

N	Center St.	N	Center St.
0	0.00100	30	1.02400
1	0.00126	31	1.29016
2	0.00159	32	1.62550
3	0.00200	33	2.04800
4	0.00252	34	2.58032
5	0.00317	35	3.25100
6	0.00400	36	4.09600
7	0.00504		
8	0.00635		
9	0.00800		
10	0.01008		
11	0.01270		
12	0.01600		
13	0.02016		
14	0.02540		
15	0.03200		
16	0.04032		
17	0.05080	-1	0.0007937
18	0.06400	-2	0.0006300
19	0.08063	-3	0.0005000
		-4	0.0003969
		-5	0.0003150
20	0.10159	-6	0.0002500
21	0.12800	-7	0.0001984
22	0.16127	-8	0.0001575
23	0.20319	-9	0.0001250
24	0.25600		
25	0.32254		
26	0.40637		
27	0.51200		
28	0.64508		
29	0.81275		

Each number represents a one-third-octave band. The center frequency for band 0, 10, and 20 are St = 0.001, 0.01, and 0.1, respectively. A complete list of center frequencies are given in Table 2 . There are some advantages of using this system. First, the output is compact and easy to comprehend. Second, the band number is an integer, and it can be used as an index for the construction of an overall noise spectrum. Noise radiation of the same frequency from different slices and segments of the jet can be easily located via the band number, and summed. Third, the calculated peak frequency cannot be considered as accurate because the definition of the turbulence structure is empirical. It is perhaps more realistic to represent the peak frequencies in terms of one-third octave bands rather than their calculated numerical values.

2.4 The calculation of sound intensity and sound power.

Equations (1) through (3) give the mean square sound pressure in nondimensional form. For practical applications, it is more convenient to compute sound intensity in common engineering terms. In metric system, the sound pressure is commonly given in decibel levels with a reference root mean square pressure of $2 \times 10^{-5}\ N/m^2$. The sound pressure level is defined as (SPL):

$$SPL = 20 \log_{10} (p'/p_o). \tag{23}$$

In Equations (1) through (3), the atmospheric pressure is chosen as the reference. Hence, the dimensional sound pressure level is related to the non-dimensional one through the following formula:

$$SPL = 10 \log_{10} (\pi \overline{\Phi_n \Phi_n^*}) + 193.6\ dB. \tag{24}$$

In the present calculation, sound radiation from a unit slice of jet is computed. The radius of the slice is assumed to be L, and the length of the circular slice is also L. Hence, the total volume of such a unit slice is πL^3. The sound intensity at a given angle is calculated at a radial distance of $r = 100\ L$. In the present program, each slice of jet is further subdivided into nine annular segments of equal width. The sound emission from each segment is calculated in 26 directions:

from 5 to 90 degrees at 5 degree intervals; and from 90 to 170 degrees at 10 degree intervals. The total noise radiation from the slice is the sum of these nine segments. After the calculation of intensity, the total sound power is computed by integrating the sound intensity over a sphere with a radius of 100L.

It should be noted that L is the local dimension of the shear layer. For jet noise calculations, it is necessary to take the diameter of the nozzle exit as the reference dimension. Furthermore, the sound pressure level should be calculated for a convenient distance such as r = 100D instead of 100L. Also, the unit length of a slice of jet should be defined as D. Hence, it is necessary to adjust the computed nondimensional SPL by means of a numerical factor. Assuming that

$$L = \epsilon D,$$

the following relation can be obtained from the previous equations:

$$(SPL)_D = (SPL)_L + 10 \log_{10} (\epsilon^2) . \tag{25}$$

The power correction factor is given to the computer program as an input. It contains three components: the scale correction, the correction for turbulence intensity, and an empirical correction factor. That is

$$P_w = \epsilon^2 \ (v_o/0.160)^4 \ P_{em}, \tag{26}$$

where the empirical factor is given as P_{em}.

The computer output for the present calculation is set up in such a way as to reduce congestion over the printed page. In order to obtain the actual calculated SPL at 100D, 60 dB should be added to the output value. For the total sound power for a segment or for the entire slice, it is assumed that the diameter of the jet nozzle exit is 1.0 meter. In this case, the output value of PWL should be increased by 100 dB in order to obtain the actual sound power. The main reason for doing this is that the results can be printed with two digits before the decimal point instead of three, thus a wider blank space is available

between numbers to facilitate easy reading.

2.5 The layout of the computer program.

The present computer program is organized into two parts. The first part is the WKBJ transformation, and the second part is for the calculation of far field noise. In the general solutions to the convected wave equation, the WKBJ coordinates are carried implicitly. However, the closed form solutions for noise emission from small volumes of turbulence depend only on ordinary coordinates. The only factor which is related to the WKBJ transformation is the aero-acoustic attenuation factor in Equation (3), F(b)/F(o). The value of b is

$$b = \frac{2\sqrt{2}\, M\, W(y, \theta) \cos\theta}{\sqrt{\mu}\, L_t \left\{ (1 - M_c \cos\theta)^2 + \alpha^2 M_c^2 \cos\theta^2 \right\}^{1/2}}$$

where $W(y, \theta)$ is defined by Equation (7). The calculation for part one is therefore relatively easy, as the only quantities to be computed are the location of y_o and the integral $W(y, \theta)$. This part of the computation depends only on the mean flow properties. Since both the velocity and the speed of sound profiles are assumed, the only input parameters are the values of M_c and A at the centerline of the profile. For each given angle of far field noise emission, the transition point can be defined by the following formula:

$$M_c(y_o) + A(y_o) = \frac{1}{\cos\theta} \quad , \qquad (27)$$

In the computer program, the search for y_o is performed by numerical iteration. The velocity profile is represented by 200 points from $y=0$ to 1.0 and 20 points from $y = 1.0$ to 2.0. Such a subdivision is compatible with the angular subdivision as chosen in the present program. The results of this part of calculation is directly available for the noise calculation. In the present program, the option of data card output of values of $W(y, \theta)$ is also available. Since the WKBJ transformation depends only on the mean flow properties, it is not necessary to repeat the first part of the calculation if changes are made only

in the procedures of noise calculation, variations in source distribution, or turbulence structure. Hence, the data of $W(y, \theta)$ can be used with the second part of the present program, or any other modified program based on the general solutions of the Phillips theory.

In previous sections, the calculations of noise have been discussed in detail. In general, the computations are set up for the prediction of the far field noise radiated from a unit slice from a circular jet. The slice is subdivided into nine concentric annular segments with identical width in the radial direction. In each segment, the mean convection Mach number and the speed of sound ratio is represented by a single value. Based on experimental indications, the temporal and spatial scales of turbulence are assumed to be constant throughout the entire slice. In the computer output, noise radiation from each segment are given at 26 angles from 5 to 170 degrees. The first number is the sound pressure level, and the second number in the parenthesis is the band number which indicates the peak frequency of the Gaussian spectrum. At the end of each column, the total sound power from each slice is provided in decibels referring to 10^{-12} watt. The self noise and shear noise are printed on separate pages. The sum of the two are given on a page following the self and the shear noise output. It should be noted that the amplitude ratio of the self noise and the shear noise is assumed to be one.

The calculations are normalized according to the radius of the slice. If the sound pressure level is measured at 100 radii away from the center of the slice, the actual SPL is the value of SPL as shown in the computer output plus 60 db. If the radius of the slice is assumed to be 1 meter, the actual sound power level should be the printed value plus 100 db. If the diameter of the slice is different from the standard dimension, appropriate adjustments for frequency, SPL, and PWL can be given to the program via the scale factors s_f and P_w as defined as Eqs. (17) and (26), respectively.

Noise intensity according to Equation (2) is computed for a number of angles in the neighborhood of θ_2. The SPL is computed at five angles above and below the rounded off value of θ_2 at two degree intervals. The result is

printed on the same page as the self noise.

In this program, two types of turbulence intensity profiles are assumed:

$$v_o(y) = 0.16\ e^{2\sqrt{2}\,(y-0.5)^2} \tag{28}$$

$$v_o(y) = 0.16\ e^{0.707y^2} \tag{29}$$

Equation (27) indicates that the maximum turbulence intensity is located at $y = 0.5$. This profile is suitable for uses in the mixing region of the jet. The maximum turbulence intensity in Equation (28) is located at $y = 0$. Therefore, the latter case is applicable for the developed region of the exhaust flow. These two types of profiles are identified in the program via an input index.

The definition of variables in the computer program, and the arrangement of the input data will be given in Appendix B.

3.0 AN EXAMPLE AND DISCUSSION OF RESULT

3.1 The general trends of the computed results.

As discussions in the previous section have shown, the solution to the convected wave equation has a very complicated form. It is rather difficult to draw quantitative conclusions from Eqs. (1) through (3) by means of an order of magnitude analysis alone. After the construction of the present computer program, it becomes practical to evaluate accurately the dependence of sound emission on various mean flow and turbulence parameters.

Extensive calculation for noise radiation from a unit slice of jet has been undertaken. It appears that a single slice of jet just beyond the end of the mixing region can be highly representative of the overall jet noise radiation. In the mixing region, the turbulence intensity and convection Mach number can both be assumed constant. If the turbulence function is assumed to be Gaussian, the spatial scale of turbulence and the scale ratio α will be sufficient to specify the source function. Since the value of L_1 can be assumed to be a linear function of x/D and the value of α can be assumed constant in this region, the noise emission characteristics in this entire zone are numerically similar. In the transition region beyond the selected slice of jet, experimental evidences seem to indicate that both the mean flow and the turbulence are changing very slowly. It can be expected that the sound radiation characteristics can also be slow varying in this region. In a subsonic jet, the sound power per unit length is approximately constant from the nozzle exit to 10D. Beyond 10D, the sound power per unit length diminishes at a rate close to x^{-7}. In a supersonic jet, experimental evidences indicates that the noise emission strength is following a x^{-7} law from the jet exit to the end of the sonic core. In the subsequent subsonic region, the x^{-7} law holds. According to such source strength distribution, the calculated sound emission from the above chosen slice of jet may be typical of 50 to 70 percent of the overall sound power from the entire jet.

The total sound power as a function of M_j is shown in Fig. 3. In this set of computation, the values of α and A are assumed to be constants. The spatial scale of the turbulence is constant in the subsonic range, while it is proportional to the convection Mach number in the supersonic range. That is:

$$\alpha = 0.55$$

$$A = 1.00$$

$$L_1 = 0.72 \qquad M_j \leq 1,$$

$$L_1 = 0.72\, M_j, \quad M_j > 1.$$

The U^8 law for sound power dependence is precisely observed for M_j less than 2.0. The U^3 law is established for convection Mach numbers of greater than 3.5. A smooth transition exists between the U^8 and the U^3 regions. By comparing the current result with the Lighthill theory, it is interesting to note that the approach to U^3 law in the supersonic region is much slower for the Phillips solution. One of the reasons may be the coupled effect of refraction and convection. The influence of the convection factor is significantly weakened by the coupled effect of refraction and convection.

The apparent success in reproducing the U^8 and the U^3 laws in the present theory is unfortunately compounded with a failure in the prediction of absolute sound power. The appropriate Lighthill parameter for jet noise prediction is given by:

$$W = \eta \rho U^8 / c_o^5 \qquad (30)$$

$$\eta = 3 \times 10^{-5}$$

The current prediction according to Eqs. (1) through (3) produces a coefficient which is approximately 15 db too high. This puzzling factor can be compared with a previous study by Pao and Lowson, (Reference 6). The value of α in Reference 6 was chosen to be $\alpha = 0.167$. This value is based on the direct measurements in a low speed round jet, (Reference 1). Since the sound power of low speed jets depends on the α^4 in both the Lighthill and the Phillips theory, an increase in the value of α will change the value of η. By substituting $\alpha = 0.55$ into the results of Reference 6 , the value of η would have increased by approximately 22 dB. In the Phillips solution, sound is attenuated as it passes through the shear flow. An overall increase in sound

power in the order of 15 dB can be expected. In the high speed range, however, the convection factor contains a component of α^{-5}, which compensates for the direct influence of α^4. The dependence of sound power on α is small. Other variables such as the density of the jet and the spatial scale of turbulence will have more direct influence on sound power in the supersonic range. In the present computed results, the overall sound power is arbitrarily adjusted by 15 dB.

The computed self noise and shear noise have different directivity patterns in the downstream direction. In the classical analysis, the shear noise has an apparent dipole pattern with the axis of the loops in the direction of the flow. In the present solution, the aerodynamic attenuation factor is different for self and shear noise. A typical example is given in Figure 4. In the directions close to the axis of the jet, shear noise clearly dominates the noise output. This may be one of the important factors for the observed behavior of jet noise in the downstream direction such that the frequency is much lower than its expected value if both self noise and shear noise are important in this region.

The Phillips solution predicts the peak angle of noise radiation to be in the neighborhood of 40 to 70 degrees from the flow direction. In the classical calculations, the basic Lighthill solution indicates that the maximum noise radiation occurs at the axis of the jet for $M_c \leq 1.0$. Hence, it is necessary to provide independent refraction corrections to account for the "dip" near the axis of the jet. In the Phillips solution, there are two factors which contribute to the decrease in sound intensity near the axis. The first one is the refraction factor q_∞/q_o; and the second one is the aerodynamical attenuation factor $F(b)/F(0)$. Calculations have shown that the latter factor is as important as than the first one.

The prediction of directivity in upstream directions is drastically different from previous theoretical results. The coupling of refraction and convection has reduced the convection factor to a constant in Equation (1). In the Phillips

solution, the directional pattern is determined entirely by refraction and Doppler shift. The directional factor, designated as $D(\theta)$ for convenience, can be given as

$$D(\theta) = \frac{A \sin\theta}{(1-M_c\cos\theta)^2 - A^2\cos^2\theta}^{1/2} \cdot \frac{A}{(1-M_c\cos\theta)}$$

For convection Mach numbers in the transonic and supersonic range, the above factor behaves as $(1 - M_c \cos\theta)^{-2} \sin\theta$. This factor should compare favorably with observations where the upstream directivity is thought to behave as $(1 - M_c \cos\theta)^{-3}$. In the high convection Mach number regime, such as rocket noise radiation, the Phillips solution provides directional patterns which agree very well with experimental measurements.

For noise emission calculations throughout the transonic and low supersonic range, the peak frequency of noise radiation remains in the neighborhood of $St = 0.25$. As discussed in the previous section, the mechanism which governs the frequency undergoes a change from the time scale to the spatial scale of the turbulence. In the high supersonic range, the frequency is determined by the convection velocity and the spatial scale of the turbulence. The calculations have shown that it is necessary to assume that the scale should increase linearly with the convection Mach number.

3.2 The input parameters for the F-1 rocket engine noise prediction.

The basic computer program for noise prediction from a single slice of jet can be effectively used for noise prediction for an entire rocket exhaust flow. In the present report, the F-1 engine is chosen as an example. It is necessary to provide both the mean flow and turbulence parameters at selected stations along the flow.

It is assumed here that the exhaust flow is expanded in the atmosphere at sea level condition, and surface impingement is not considered. The mixing properties of the flow is calculated according to the mixing model as given by Donaldson and Gray (Reference 2). Results of such a calculation were reported

previously in Reference 3. The convection Mach number M_c, and the speed of sound ratio A, along the centerline are given in Figure 5 . The geometry of the exhaust flow and the boundaries of the core, the supersonic region, and the region of M_c 1 are shown in Figure 6 . In the present case, the boundary of the flow is defined as twice the radial coordinate of the half velocity point for the portion of flow beyond the core. In the core region, the jet boundary is the coordinate of the half velocity point plus the distance from this point to the boundary of the core. Generally, the exhaust flow is bounded within a cone with a half angle of 10 degrees. Thirteen stations from $x/D = 5$ to 100 are chosen as representative locations for the noise calculations. At $x/D = 100$, the convection Mach number at the centerline of the flow is slightly below 0.5. According to the limitations of the present theory, noise prediction for $M_c < 0.6$ will be relatively inaccurate. Therefore, noise prediction for x/D greater than 100 will not be attempted.

The structure of the turbulence can be defined by the spatial scale L_1 and the scale ratio α. Since experimental results of turbulence structure in a supersonic jet is lacking, it is necessary to make simple assumptions concerning the values of these two quantities.

The spatial integral scale of turbulence as chosen in the present analytical model is different from previous definition adopted in Reference 6. In the present case, L_1 is related to the experimental integral scale via:

$$L_1 = \frac{2}{\sqrt{\pi}} \int_0^\infty R(x)\, dx$$

Therefore, the proper range of L_1 should be 0.4 to 0.9 for low speed subsonic jets. The value of L_1 for this numerical example is chosen as follows:

$$L_1 = 0.72 \qquad \text{for } M_c \leq 1;$$

$$L_1 = 0.72\, M_c \qquad \text{for } M_c > 1.$$

Although these conditions are empirical, the second formula appears to be

necessary for the correct prediction of rocket noise frequency. The values of the turbulence parameters are given in Table 3 and 4. It can be seen from this table that the value of L_1 can be six times the local thickness of the mixing layer, which is indeed a substantial correlation length.

The input value of α requires some explanation. In the computer program, the input value of α_o is modified through a formula:

$$\alpha_{mod} = \alpha_o \, A^{0.75} / (a + bA)^{1.75} \tag{33}$$

The modified value of the scale ratio is used in the noise calculation. For some analysis in the transonic and low supersonic velocity range, it was found that the above formula, with a constant value of α_o, can automatically duplicate the trends of sound power as a function of jet density as reported by Hoch et al. (Reference 7). However, the rocket flow velocity is far beyond this speed range. In the present calculation, the above formula is by-passed by assuming a variable value for α_o such that the modified value α_{mod} is the desired value to be used in the computation. Both the assumed value of α_o and α_{mod} are shown in Table 3.

In order to place the noise calculation for individual slices upon the same reference unit, it is necessary to supply as input parameters a frequency scale and a sound power adjustment factor. The frequency scale is defined by Eq. (17). The power adjustment contains three factors: the geometrical factor, the adjustment for the turbulence intensity, and an arbitrary factor. The detailed break-down of the power adjustment factor is given in Table 4. The basis for the arbitrary power adjustment will be discussed in the next section.

3.3 Discussion of results.

The computed results are given in Appendix A. The computed output for each slice contains a table for the WKBJ transformation function, the far field SPL and Strouhal number band for self and shear noise, and a table for the sum of self and shear noise. Since both the mean flow and the turbulence are given in terms of simple mathematical models, it is advantageous to have the output in its present form such that one can keep track of the contribution to noise from various parts of the jet. Any irregularity in the computation can also be detected.

Table 3: Run Parameters for F-1 Engine Noise

X/D	A_{max}	M_{max}	α_o	α(mod)	L/D	L_1	SF	10 $\log_{10}$ Pw
5	2.4	8.6	1.75	0.729	0.30	6.15	3.370	-21.26
10	2.4	8.6	1.75	0.729	0.60	6.15	1.685	-18.26
20	2.4	8.6	1.75	0.729	1.20	6.15	0.843	-15.26
25	2.5	7.0	1.75	0.701	1.50	5.00	0.500	-12.24
30	2.6	5.4	1.75	0.674	1.80	3.85	0.346	- 9.41
35	2.6	4.3	1.60	0.619	2.25	3.08	0.225	- 7.04
40	2.5	3.25	1.60	0.652	2.72	2.30	0.141	- 4.72
50	2.1	2.1	1.30	0.675	3.81	1.50	0.065	- 0.76
60	2.0	1.4	0.80	0.553	5.17	1.00	0.032	5.04
70	1.85	1.2	0.60	0.507	6.68	0.80	0.021	5.80
80	1.70	1.0	0.50	0.518	8.23	0.80	0.014	6.11
90	1.60	0.75	0.40	0.498	9.95	0.80	0.010	8.93
100	1.50	0.50	0.40	0.529	11.65	0.8	0.008	10.626

Table 4. The Correction Factors for Sound Power

X/D	Geometrical	$(v_o/0.16)^4$	Empirical	Total (dB)
5	0.74	-12.00	-10.00	-21.26
10	0.74	-12.00	- 7.00	-18.26
20	0.74	-12.00	- 4.00	-15.26
25	1.76	-12.00	- 2.00	-12.24
30	2.59	-11.00	--	- 9.41
35	3.46	-10.50	--	- 7.04
40	4.28	- 9.00	--	- 4.72
50	5.74	- 2.00	--	- 0.76
60	7.04	- 2.00	--	5.04
70	8.19	- 1.40	--	5.80
80	9.11	- 1.00	--	8.11
90	9.93	- 1.00	--	8.93
100	10.63	0.00	--	10.63

$$PWDB = 10 \log_{10} P_{Geo} \cdot (v_o/0.16)^4 \cdot P_{em}$$

In other words, the present program is designed as a tool for selecting the best assumptions of the mean flow and turbulence structure for direct prediction of rocket noise.

The most encouraging result is the prediction of directivity. In Figure the directivity of sound emission from Segment 5 of each selected slice is shown. The directivity patterns are normalized with respect to the SPL at the 90 degree direction. If these directivity patterns are compared directly with rocket noise data, it can be seen that the peak to 90-degree difference in SPL is too high. However, the boundary of the jet of the actual exhaust flow has a divergence of approximately ten degrees. The unsteadiness of the boundary as well as the turbulent scattering in the flow itself will produce additional fluctuations in the sound radiation direction. In the current theory, the shear layer is assumed to be parallel to the axis of the jet. If it is assumed that the combined effect of jet boundary divergence and scattering provides a directional difference of 15 degrees, the directional patterns as given by Figure 7 should be modified. With this correction, the measured 90 degree direction will correspond to the 75 degree point in Figure 7 . As a result of this simple correction, the agreement with experimental data for all angles are very close (references 8, 9). It is very important to point out here that the agreement of directivity in the upstream directions is very important. The predicted values of SPL as based on the classical Lighthill results will be much lower in such directions. As a result, the basic directivity curves for rocket noise prediction are empirical and very conservative in most of the methods as recommended for engineering purposes. Another important feature of the current noise prediction is the accurate determination of the direction of maximum noise intensity. For noise radiations in the high velocity sections, the angle of maximum radiation is between 55 to 75 degrees from the axis of the flow. For the low speed slices, the maximum angle is approximately 45 degrees. Such angular variations can not be predicted accurately in the classical methods.

For each slice of the jet, the Strouhal number band for the maximum radiation intensity can be obtained from the computed output. These characteristic frequencies are plotted against the location of the slice along the exhaust flow Figure 8 . On the same figure, the measurements of apparent sound source location as a function

of frequency is also shown. After correcting the difference in distance between the actual source location and the estimated point of emergence at the boundary of the jet, the agreement between the measured and the calculated sound source location is very close. However, both the definition of the so called sound source location and the comparison of results as discussed above can be misleading. The sound source for the emission of sound at any given frequency is widely distributed instead of concentrated. As the direction of emission is changed, the foot print of the source location is also changed. For example, the sound source locations for St = 0.01 (Band 10) at 45 degrees and 135 degrees are shown in Figure 9 . The source location for other Strouhal numbers can be obtained from the numerical results as given in Appendix A. It can be seen clearly that the sound source for ST = 0.01 at 45 degrees extends from 20D to nearly 70D. For sound emission at the same Strouhal number at 135 degrees, the sound source location extends from 10D to 50D. Since the location of sound source is very important for noise prediction in the geometrical near field and mid-field, these results of the present computation may have important engineering applications.

The prediction of the absolute value of sound power was found to be the most difficult. The power dependence on M_c is adjusted arbitrarily by -15 dB vertically for all values of M_c. This factor is written in the computer program as a constant element. From Table 4 , one can find an additional item of empirical adjustment of sound power for some of the slices in the mixing region. The latter empirical adjustment is based on experimental observations of sound source strength in the mixing region of a supersonic jet. In the Phillips theory, the dimensional analysis of sound power indicates that the sound source strength per unit length of the flow is a constant. However, experimental evidences indicate that the source strength follows an x^1 law. It is easy to provide a physically convincing argument for the x^1 law. For a small volume of turbulence convected at supersonic speeds, the sound power radiation is proportional to the kinetic energy in the turbulence, (the U^3-law.) In the mixing region, the volume of the turbulent region increases as x^1, while the turbulence intensity remains approximately constant throughout this region. Therefore, the sound power from a unit length of the jet should also follow x^1. Yet, this argument is hardly useful for any analytical

investigation of jet and rocket noise. Further analytical work is definitely required on this subject. The x^1 law has been observed to hold from a short distance from the nozzle exit to the end of the core region with convection velocities greater than the ambient speed of sound. Based on this observation, empirical power adjustments have been given to slices at $x/D = 5$, 10, 20, and 25.

There are several possible ways to resolve the fifteen dB over-prediction of sound power.

(a) In the present model the local mean speed of the exhaust flow is taken as the convection velocity of the turbulence. According to experimental evidences, the convection speed for a volume of turbulence is generally lower than the local mean speed. If the difference is 20 per cent, the predicted sound power will be at least 8 dB lower than the currently predicted value before any arbitrary correction is made.

(b) The assumed values of α_{mod} is between 0.49 and 0.73, with the higher values given to slices with higher convection speeds. Lower values of α_{mod} may change the overall sound power by two to four dB.

(c) For a Gaussian spectrum, the lower frequencies contain most of the turbulent kinetic energy. If the turbulence spectrum is assumed to decay according to a power law, part of the kinetic energy will be shifted from the lower frequencies to the higher frequencies. According to the Phillips theory, the high frequency noise radiation is highly attenuated. The overall noise radiation is contributed mainly through the energy content in the low frequency range. Hence, the total sound power emission from a power law spectrum should be somewhat lower.

In summary, the discrepancy in sound power prediction has its origin in the definition of source function. Other than the major items as listed above, factors such as the non-isotropic nature of the turbulence, the variation of L_1

Table 5: Contribution to Total Sound Power From Various Annular Segments in a Slice of F-1 Rocket Exhaust With Unit Length $\Delta X = D$.

X/D Segment	10	20	25	30	35	40	50	60	70	80	90	100
9	171.58	174.58	175.12	175.00	173.88	171.71	165.48	159.07	154.25	149.09	141.64	130.59
8	174.66	177.66	177.77	177.48	176.35	174.35	166.47	159.94	155.69	150.46	142.51	131.52
7	177.07	180.07	179.42	179.26	177.83	175.88	167.39	160.88	156.54	151.44	143.91	132.20
6	175.50	178.50	180.64	178.85	178.44	175.96	168.09	161.68	157.29	152.26	144.68	133.27
5	171.97	174.97	178.58	179.08	176.99	178.39	168.42	162.17	158.15	152.78	145.15	133.66
4	173.96	176.96	175.21	176.13	175.78	173.02	168.17	161.76	158.03	153.28	145.22	133.54
3	166.98	169.98	174.19	171.74	171.99	169.85	167.01	161.32	157.68	152.46	144.95	133.04
2	162.23	165.23	168.62	165.98	166.40	164.59	164.99	159.53	155.28	151.07	143.31	130.87
1	155.32	158.32	160.92	161.46	158.59	156.95	161.28	155.94	151.64	146.63	140.13	128.36

and L_t across the shear layer, etc., should also be examined.

The sound source strength distribution for x/D less than 100 is shown in Figure 10 and Table 5 . Since empirical corrections are involved in their calculation, the result has little or no analytical significance.

Since the Gaussian turbulence structure has relatively poor spectral characteristics, the construction of a computed spectrum is not attempted in the present report. However, it takes only a minor modification to the present program in order to include such calculations. Discussion of the procedure was given previously in Section 2.3.

The present numerical example has demonstrated that the Phillips theory can predict correctly the quality of the sound field as produced by a rocket exhaust flow. If some empirical assumptions are made regarding the strength of the sound source, an accurate modeling of the actual sound field of rocket motors can be accomplished.

REFERENCES

1. Davies, P.O.A.L. et al., "The characteristics of the turbulence in the mixing region of a round jet," J. Fluid Mech., Vol. 15, 337-367; Corrigendum, 559, 1963.

2. Donaldson, C.DuP. and Gray, K. E., "Theoretical and experimental investigation of the compressible free mixing of two dissimilar gases," AIAA J., vol. 4, 2017-2025, 1966.

3. Pao, S. P., "Effects of high combustion chamber pressure on rocket noise environment," Wyle Laboratories Research Report WR 72-6, April 1972.

4. Pao, S. P., "Applications of the generalized jet noise theory," Wyle Laboratories Research Report WR 72-5, March 1972.

5. Lush, P. A., "Measurements of subsonic jet noise and comparison with theory," J. Fluid Mech., Vol. 46, 477-500, 1971.

6. Pao, S. P. and Lowson, M. V., "Some applications of jet noise theory," AIAA Paper 70-233, AIAA 8th Aerospace Sciences Meeting, January 1970.

7. Hoch, R. C., Cocking, B. J., et al., "Study of the influence of density on jet noise," SNECMA-NGTE paper presented at the First International Symposium on Air Breathing Engines, Marseille, June 1972.

8. Smith, E. B., "Acoustic scale-model tests of high speed flows," Contract Report CR-66-13, Martin-Marietta Corp., Denver, 1966.

9. Cole, J. N. et al., "Noise radiation from fourteen types of rockets in the 1000 to 130,000 pound-thrust range," WADC TR 57-354, December 1957.

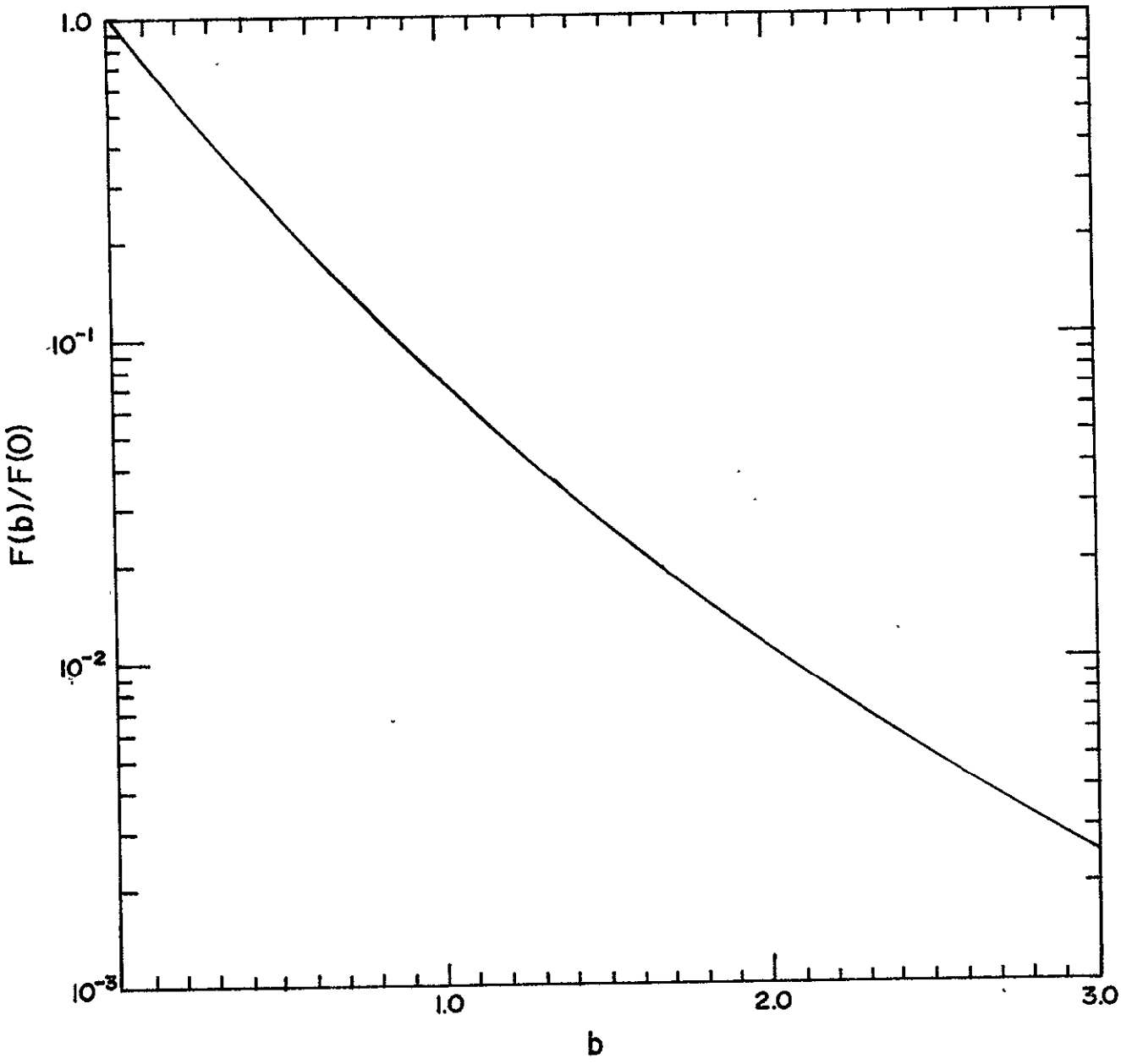

Figure 1: The value of $F(b)/F(0)$.

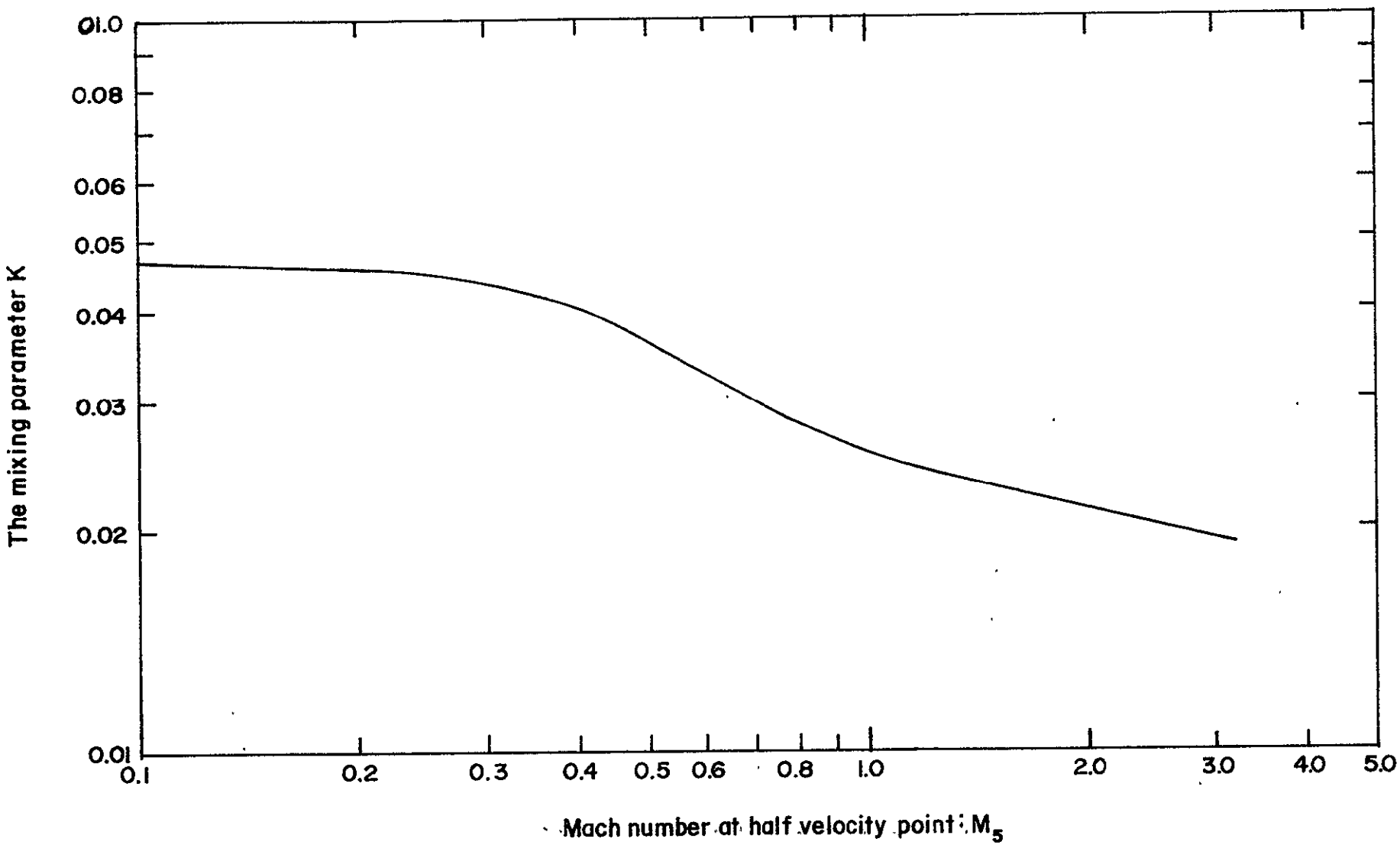

Figure 2: The mixing parameter versus Mach number at the half velocity point.

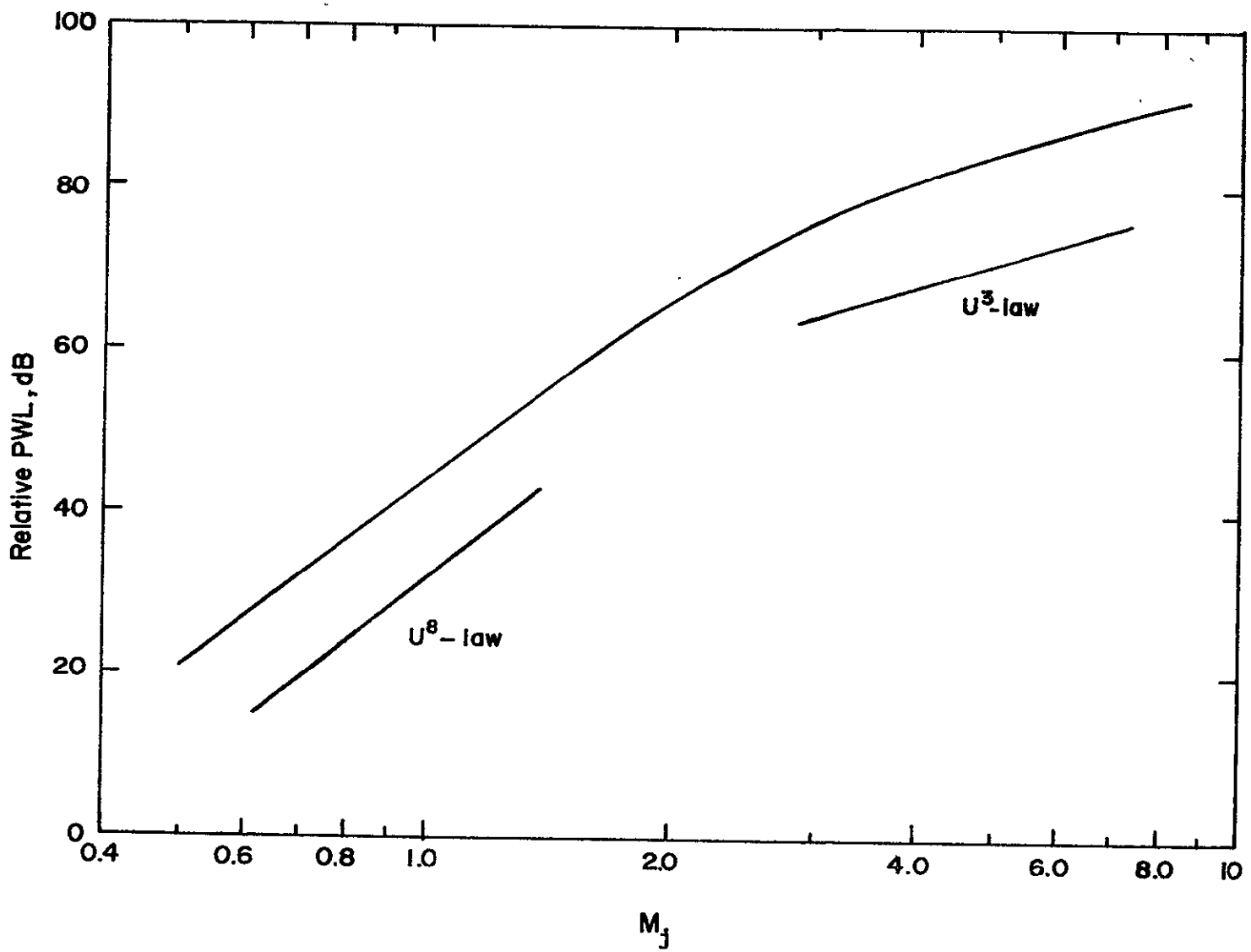

Figure 3. Dependence of sound power on jet velocity fatio, $U/_{co}$.

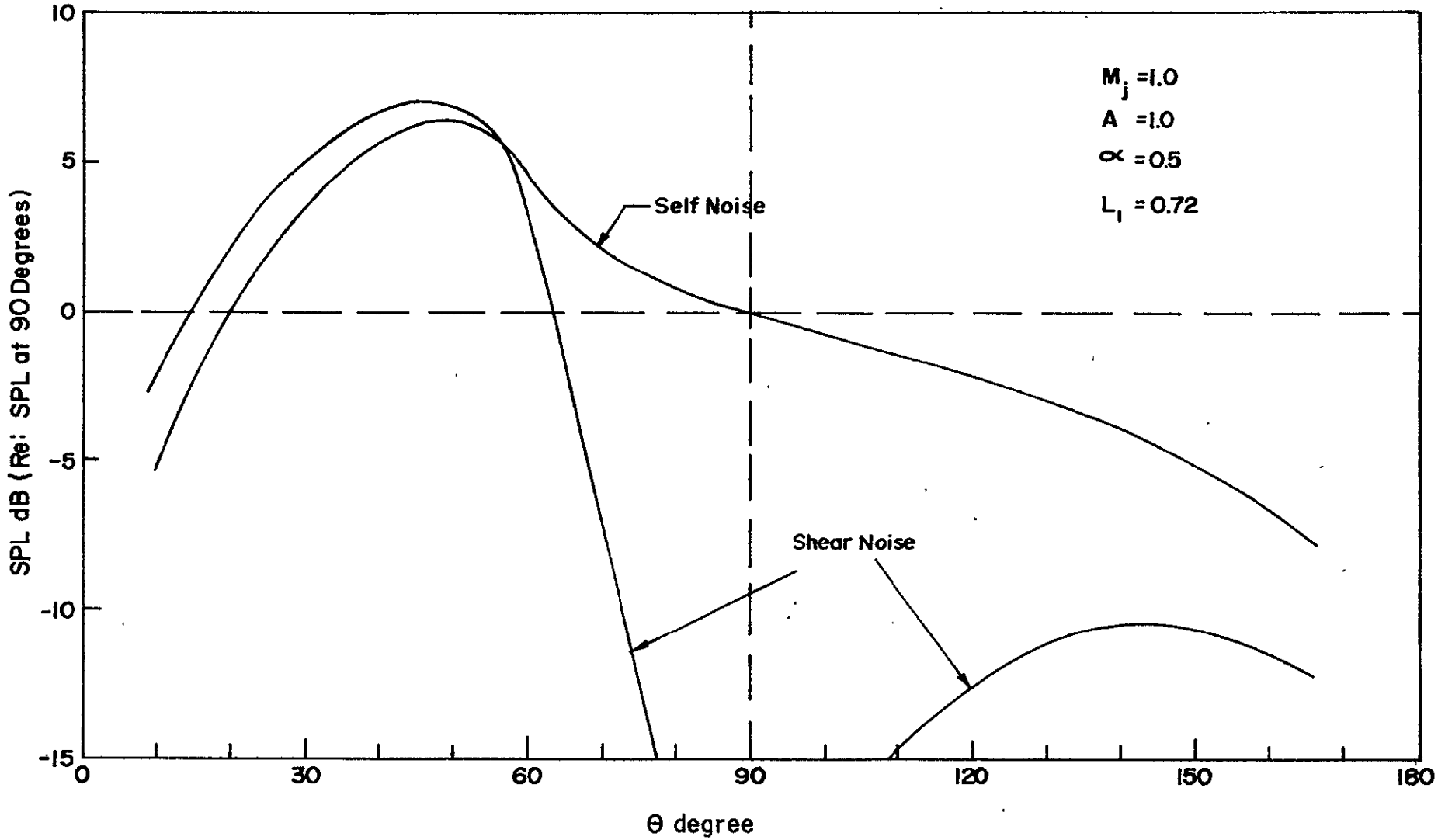

Figure 4: Directivity Pattern for Self and Shear Noise.

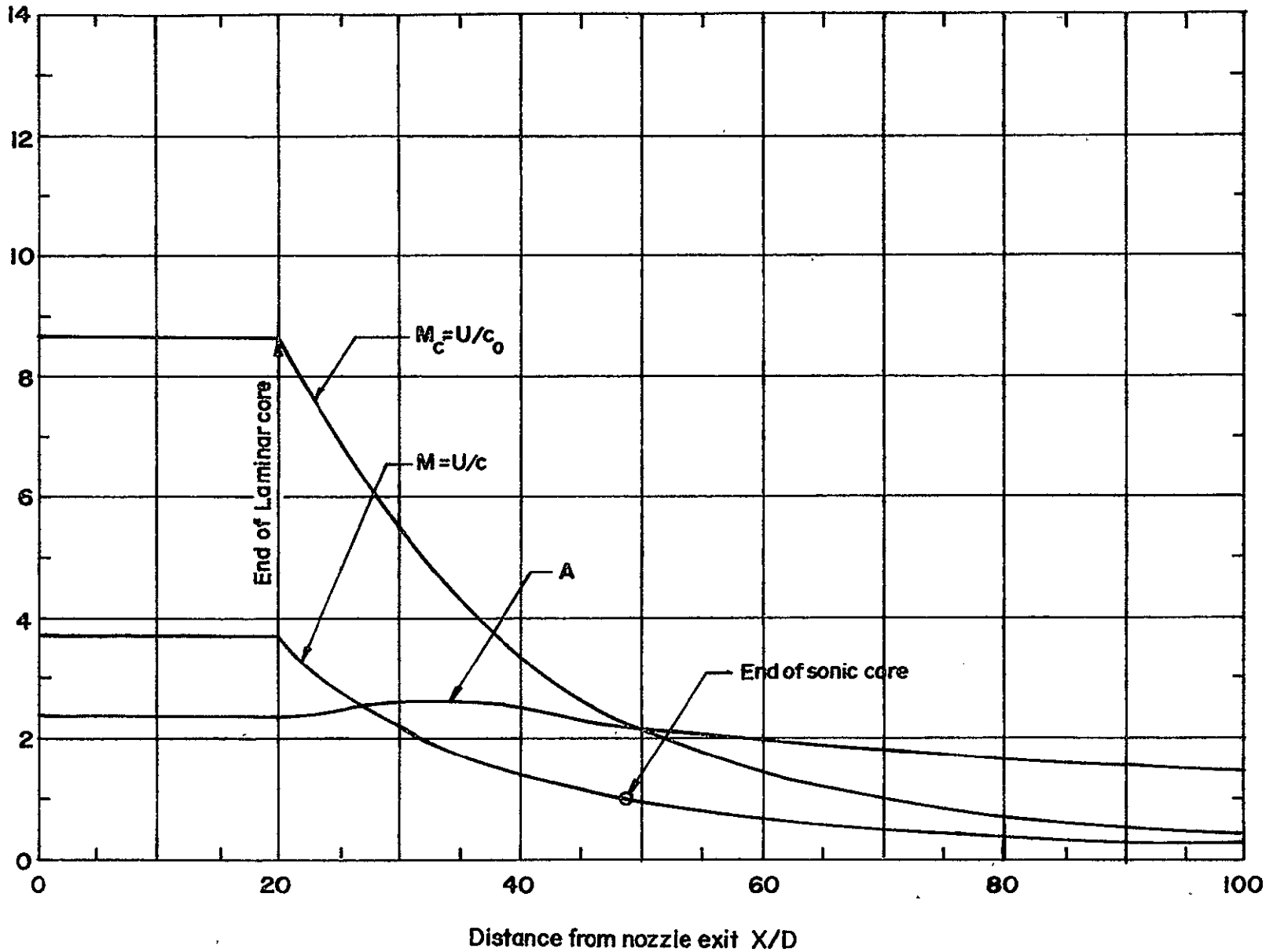

Figure 5. Important Flow Parameters for the F_1 Engine.

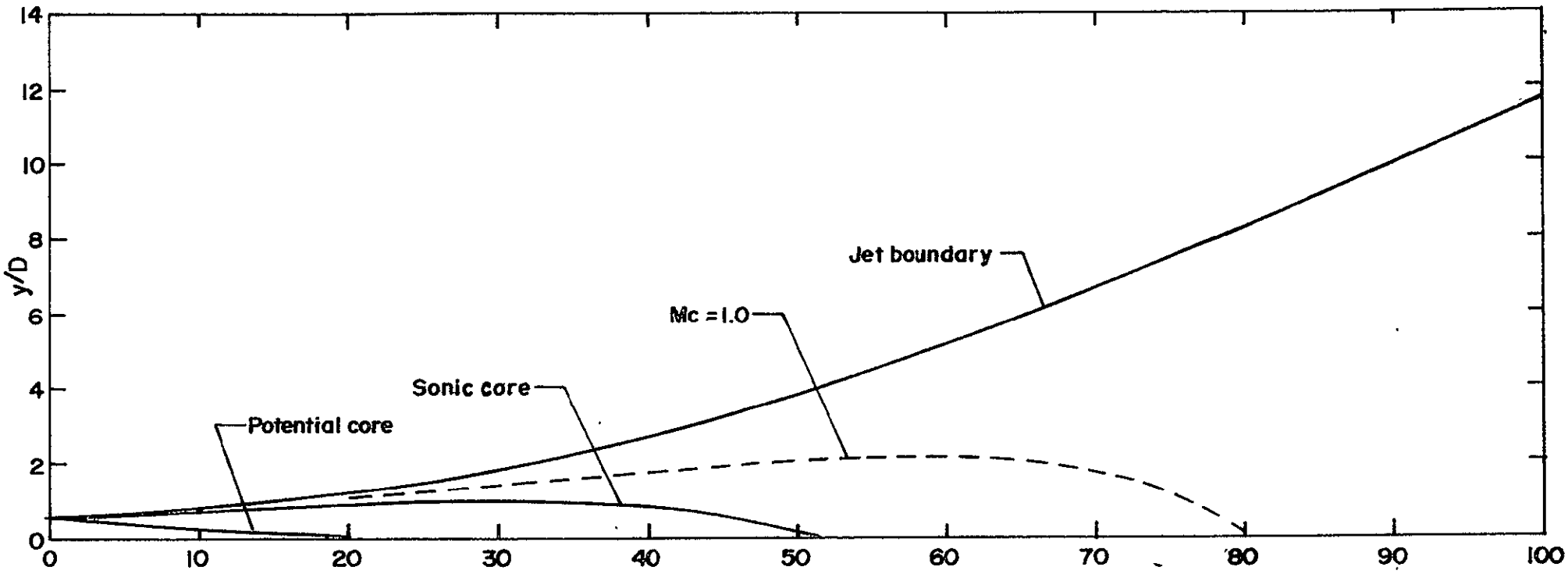

Figure 6. Exhaust plume geometry of the F-1 rocket engine.

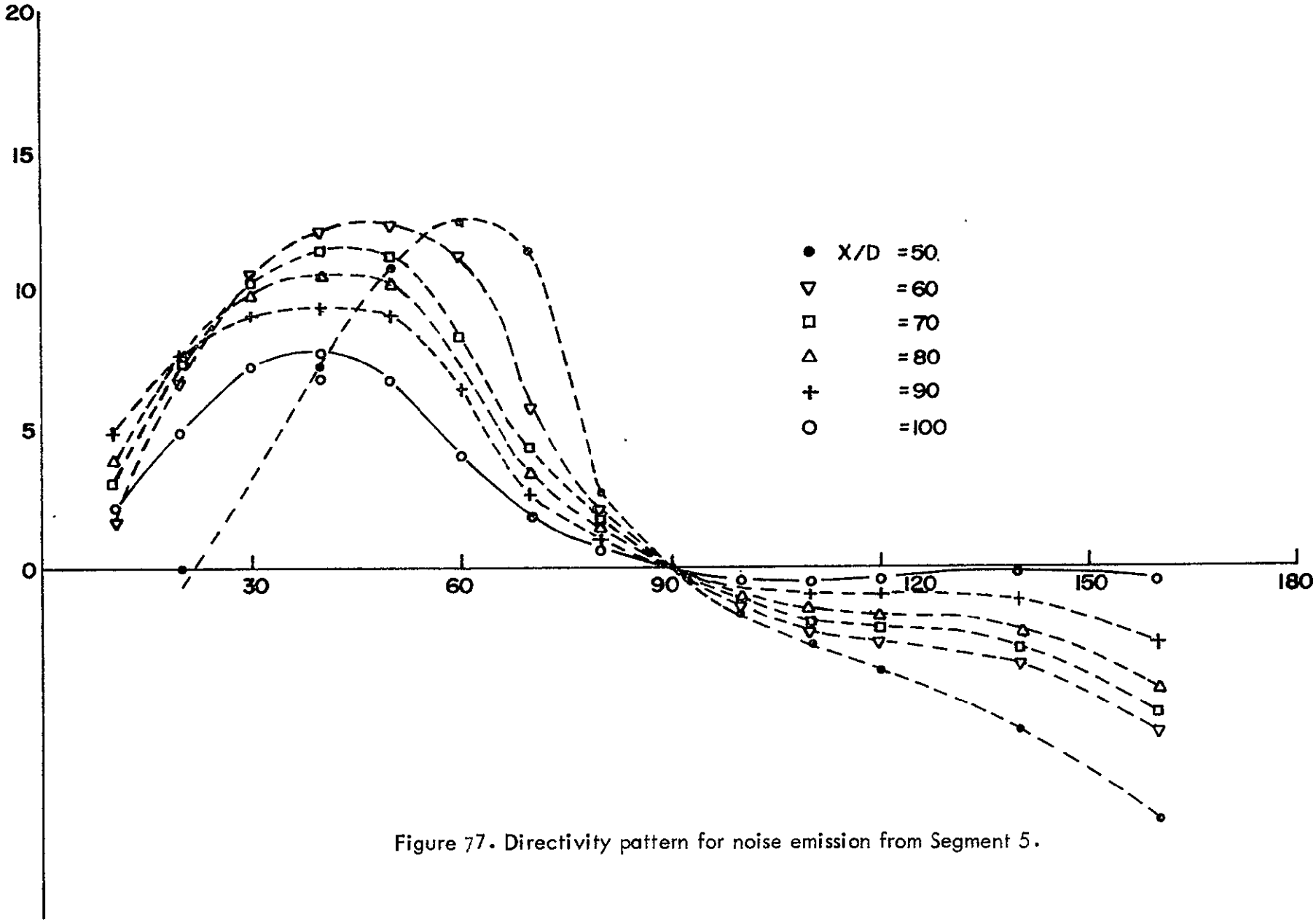

Figure 77. Directivity pattern for noise emission from Segment 5.

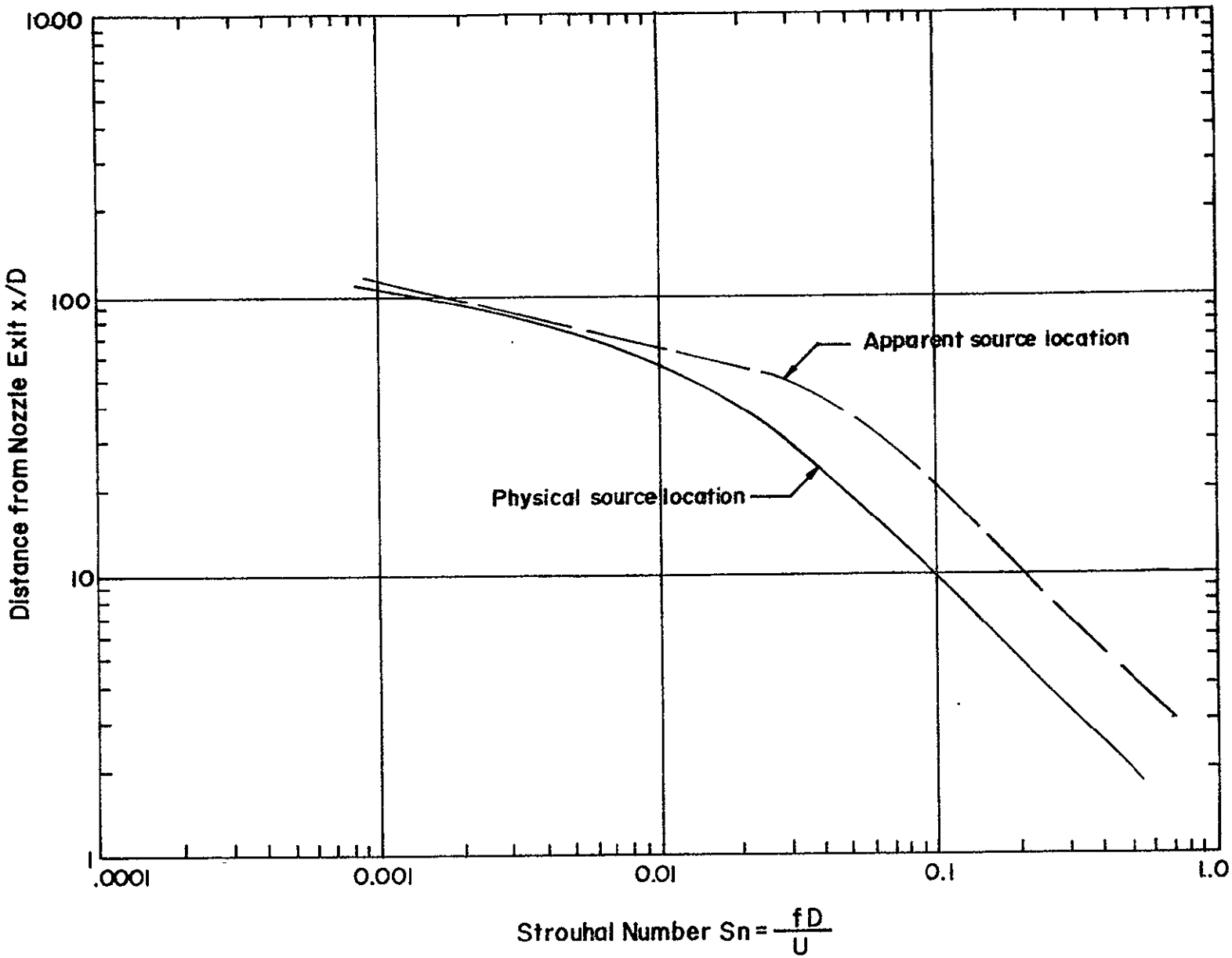

Figure 8. Peak Strouhal number at various axial stations.

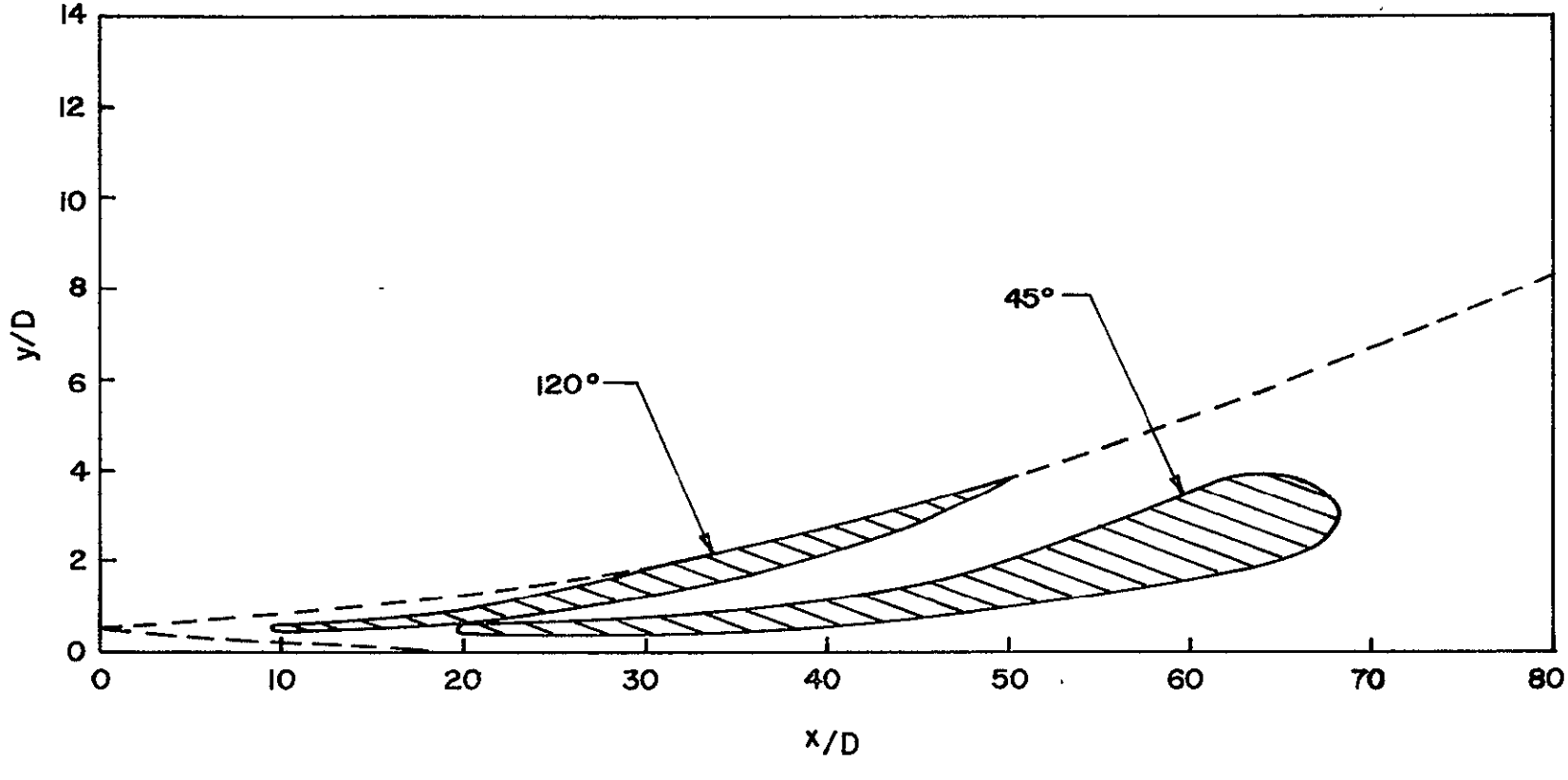

Figure 9. Sound Source Location for Noise Radiation at St = 0.01 in two different directions: 45° and 120°.

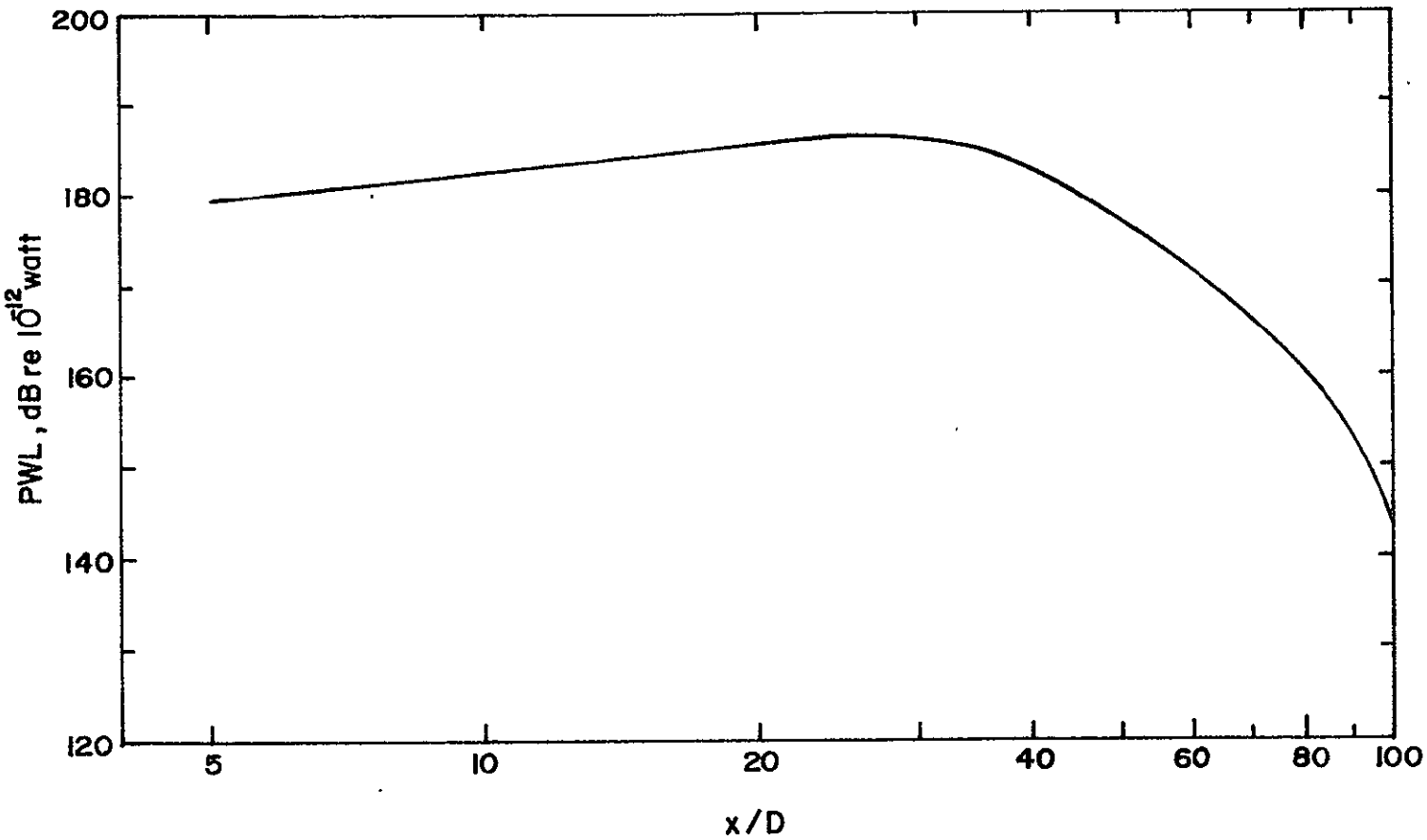

Figure 10. Sound power per unit length of one F-1 Rocket engine, $\Delta x = D$.

APPENDIX B

The Input Information

The input for this computer program contains two groups of input cards. Group I contains two cards which carry the general information for each run. Group II is the data for each slice of the jet. There are one data card for the mean flow information, one data card for the turbulence information, and optional data cards for the WKBJ transformation function $W(y, \theta)$, if any. Group II data can be repeated as many times as necessary, depending on the number of individual slices.

Group I

Card 1: The read statement is in Subroutine INITAL.

13A6	TITLE(13)	Title for each run. The total length of the title should not be more than 78 characters.

Card 2: The read statement is in Subroutine INITAL.

F10.1	THET	The first computed angle of sound radiation. THET = 0. degree.
F10.1	DTHET	Angular increments between 0 to 90 degrees. DTHET = 5. degrees.
F10.1	DELY1	Grid size for $0.0 \leq y \leq 1.0$: DELY1 = 0.005.
F10.1	DELY2	Grid size for $1.0 \leq y \leq 2.0$: DELY2 = 0.050.

Group II

Card 3: The read statement is in Subroutine RSTART.

F10.3	AMAX	Maximum value of the speed of sound ratio in a slice of jet.
F10.3	XMMAX	The maximum convection Mach number in the slice.
10 X	- - -	
I5	IPCH	Code for the card punch output for $W(y, \theta)$. IPCH = 0: no punch output; = 1: punch card output.

Card 4: The read statement is in Subroutine SETUP

I5	IRD	Read code for the punch card output for $W(y, \theta)$. IRD = 0: no data; $W(y, \theta)$ is generated in the program. IRD = 1: Read data for $W(y, \theta)$.
I5	ICODE	Turbulence intensity profile code: ICODE = 1: profile for the mixing zone; = 2: profile for the developed zone.
I5	IPRT	IPRT = 0: regular computed output for noise; = 1: detailed output information for the noise computation of each segment. This option is for debugging only.
5X	--	
F10.0	ALPHA	The scale ratio. Recommended input value: $0.3 \leq$ ALPHA ≤ 0.80.
F10.0	XL	The reference scale of the slice: XL = 1.0.
F10.0	XL1	The spatial scale of turbulence: XL1 ≥ 0.40.
F10.0	SF	The frequency scale s_f.
F10.0	PWDB	The power adjustment factor in decibels: PWDB = $10 \log_{10} (P_W)$.

Optional cards for the WKBJ transformation function: The read statements are in Subroutine SETUP.

ERRATA

APPENDIX C

1. Equation (79): the function $W(y_o, \theta)$ should read $W(y, \theta)$.

2. A multiplicative factor of γ^2 should be included in the following equations: Eqs. (67), (68), (70), (72), (73), (75), (78), (82), (83), (84), and (85).

3. The coefficient Equation (83) should read:

$$\frac{21\ \gamma^2\ \pi^2\ v_o^4\ M^8\ Pa^2(0)\ \alpha^{9/2}\ \tan\theta}{2^{3/4}\ r^2\ A^2\ L_1^{3/2}\ \Omega^{1/2}}\ \Gamma(3/4)\ \text{-----}$$

4. The coefficient of Equation (84) should read:

$$\frac{160 \times 2^{2/3} \times \gamma^2 \times \pi^2\ v_o^4\ M^8\ Ai^2(0)\ \alpha^{13/3}\ \tan\theta}{9\ r^2\ A^2\ L^{4/3}\ \Omega^{1/3}}\ \Gamma(3/2)\ \text{----}$$

5. The factor $F(b)$ in Equation (85) should be replaced by $F(b)/F(0)$.

6. The function $W(y_o, \theta)$ in Equation (87) should read $W(y, \theta)$.

APPENDIX A

NOISE PREDICTION FOR THE F-1 ROCKET ENGINE

TABLE A-1A: THE WKBJ INTEGRAL AND RUN PARAMETERS AT X/D=5.

CONVECTION MACH NUMBER = 8.6

THETA(RAD)	S(21)	S(41)	S(61)	S(81)	S(101)	S(121)	S(141)	S(161)	S(181)
.00	.24801+01	.21273+01	.17845+01	.14670+01	.11887+01	.96054+00	.79203+00	.69644+00	.63946+00
5.00	.24627+01	.21101+01	.17674+01	.14502+01	.11721+01	.94430+00	.77614+00	.68158+00	.62377+00
10.00	.24168+01	.20648+01	.17229+01	.14064+01	.11291+01	.90217+00	.73507+00	.64183+00	.58362+00
15.00	.23680+01	.20171+01	.16783+01	.13610+01	.10851+01	.85971+00	.69444+00	.60362+00	.54378+00
20.00	.23140+01	.19647+01	.16285+01	.13121+01	.10382+01	.81499+00	.65239+00	.56668+00	.50306+00
25.00	.22518+01	.19046+01	.15677+01	.12567+01	.98547+00	.76535+00	.60640+00	.52663+00	.45859+00
30.00	.21903+01	.18458+01	.15119+01	.12042+01	.93647+00	.72035+00	.56621+00	.49404+00	.41958+00
35.00	.21177+01	.17769+01	.14468+01	.11432+01	.88006+00	.66912+00	.52128+00	.45661+00	.37530+00
40.00	.20306+01	.16944+01	.13692+01	.10709+01	.81367+00	.60939+00	.46978+00	.41199+00	.32381+00
45.00	.19433+01	.16129+01	.12941+01	.10027+01	.75299+00	.55737+00	.42867+00	.37449+00	.27922+00
50.00	.18407+01	.15180+01	.12074+01	.92502+00	.68525+00	.50105+00	.38733+00	.33253+00	.23042+00
55.00	.17171+01	.14046+01	.11050+01	.83456+00	.60808+00	.43934+00	.34800+00	.28255+00	.17460+00
60.00	.15601+01	.12617+01	.97724+00	.72325+00	.51519+00	.36642+00	.30580+00	.21722+00	.10627+00
65.00	.13755+01	.10973+01	.83459+00	.60443+00	.42338+00	.31087+00	.25900+00	.14897+00	.43140-01
70.00	.11338+01	.88682+00	.65780+00	.46496+00	.32777+00	.26494+00	.17496+00	.65005-01	.24860-02
75.00	.80195+00	.60934+00	.43979+00	.31564+00	.26054+00	.16594+00	.56378-01	.79713-02	.13369+00
80.00	.38687+00	.33209+00	.28397+00	.19805+00	.72217-01	.00000	.10242+00	.32159+00	.64912+00

CARD INPUT FOR MMAX, A, MC, THETA, AND W? NO
DETAILED PRINTOUT? NO

ALPHA	L	L1	SF	PW(DB)
1.750	1.000	6.150	3.370	-21.266

MODIFIED ALPHA IS: .7294

TABLE A-1B: THE SELF NOISE INTENSITY AND FREQUENCY AT X/D = 5.

CONVECTION MACH NUMBER = 8.6

DATE 090573

CONVECTION MACH NO.= 8.600 SPEED OF SOUND RATIO= 2.40 VO CODE= 1

SELF NOISE INTENSITY(DECIBELS) WITH FREQUENCY BAND NUMBERS

ANGLE (DEG)	SEGMENT 1	SEGMENT 2	SEGMENT 3	SEGMENT 4	SEGMENT 5	SEGMENT 6	SEGMENT 7	SEGMENT 8	SEGMENT 9	TOTAL
	MC 8.42971	7.93880	7.18332	6.24488	5.21616	4.18607	3.22768	2.39412	1.70193	
	A 2.26000	2.12000	1.98000	1.84000	1.70000	1.56000	1.42000	1.28000	1.14000	
5.0	-5.24(11)	3.45(12)	10.37(12)	16.20(13)	21.16(14)	25.41(15)	29.29(16)	35.16(18)	31.73(19)	37.89
10.0	-1.85(11)	6.84(12)	13.75(12)	19.58(13)	24.55(14)	28.80(15)	32.69(16)	38.79(18)	35.00(19)	41.39
15.0	.43(12)	9.12(12)	16.02(12)	21.84(13)	26.80(14)	31.05(15)	34.97(16)	41.53(18)	37.07(19)	43.88
20.0	2.36(12)	11.03(12)	17.91(12)	23.72(13)	28.66(14)	32.92(15)	36.88(16)	44.41(18)	38.67(20)	46.32
25.0	4.18(12)	12.82(12)	19.68(13)	25.46(13)	30.39(14)	34.64(15)	38.66(17)	39.79(18)	40.07(20)	44.99
30.0	5.95(12)	14.56(12)	21.38(13)	27.13(14)	32.03(15)	36.30(16)	40.40(17)	47.43(19)	41.32(20)	49.87
35.0	7.79(12)	16.35(13)	23.13(13)	28.83(14)	33.72(15)	37.99(16)	42.23(17)	46.86(19)	42.55(21)	49.68
40.0	9.73(13)	18.24(13)	24.96(14)	30.63(14)	35.49(15)	39.79(16)	44.24(18)	47.13(19)	43.82(21)	50.88
45.0	11.76(13)	20.21(13)	26.88(14)	32.50(15)	37.34(16)	41.69(17)	46.51(18)	47.72(20)	45.10(22)	52.01
50.0	13.97(14)	22.34(14)	28.95(14)	34.52(15)	39.36(16)	43.82(17)	49.40(19)	48.61(20)	46.49(22)	53.82
55.0	16.40(14)	24.70(15)	31.24(15)	36.77(16)	41.64(17)	46.31(18)	44.86(19)	49.79(21)	48.08(23)	54.05
60.0	19.15(15)	27.36(15)	33.84(16)	39.37(17)	44.34(18)	49.48(19)	53.75(20)	51.35(22)	50.00(24)	57.79
65.0	22.29(16)	30.43(16)	36.88(17)	42.46(18)	47.71(19)	54.36(20)	54.20(21)	53.31(23)	52.52(24)	60.05
70.0	26.14(17)	34.23(17)	40.73(18)	46.56(19)	52.73(20)	58.46(21)	56.20(23)	56.00(24)	55.46(24)	60.68
75.0	31.41(19)	39.57(19)	46.44(20)	46.64(20)	49.57(21)	58.80(23)	59.60(24)	49.50(24)	50.97(23)	63.17
80.0	34.40(21)	41.91(21)	47.30(22)	58.99(23)	53.19(24)	63.79(24)	53.03(23)	51.26(22)	48.52(22)	62.35
85.0	39.94(23)	46.46(22)	50.38(22)	52.47(21)	53.95(21)	53.42(20)	51.94(20)	49.56(21)	46.77(21)	60.32
90.0	33.47(17)	40.33(17)	44.93(17)	48.00(18)	49.77(18)	50.36(18)	49.80(19)	48.13(20)	46.37(20)	57.04
100.0	26.31(13)	33.45(13)	38.53(14)	42.26(14)	44.82(15)	46.27(16)	46.59(17)	45.77(18)	43.10(19)	53.08
110.0	22.36(11)	29.58(12)	34.81(12)	38.75(13)	41.60(13)	43.41(15)	44.17(16)	43.82(17)	41.25(18)	50.47
120.0	19.53(10)	26.79(10)	32.09(11)	36.13(11)	39.13(12)	41.14(14)	42.15(15)	42.10(16)	39.61(17)	48.10
130.0	17.25(9)	24.53(9)	29.86(10)	33.97(11)	37.85(12)	39.18(13)	40.34(14)	40.50(16)	38.07(17)	46.59
140.0	15.21(9)	22.50(9)	27.86(9)	32.01(10)	35.14(11)	37.35(12)	38.62(14)	38.91(15)	36.54(17)	44.87
150.0	13.21(8)	20.51(8)	25.88(9)	30.05(10)	33.23(11)	35.48(12)	36.82(13)	37.21(15)	34.86(16)	43.07
160.0	10.95(8)	18.25(8)	23.63(8)	27.82(9)	31.01(10)	33.30(11)	34.68(13)	35.13(14)	32.81(16)	40.94
170.0	7.65(8)	14.95(8)	20.34(8)	24.53(9)	27.74(10)	30.04(11)	31.45(13)	31.94(14)	29.63(16)	37.72
	40.01	46.99	51.87	58.19	57.53	60.26	61.42	59.22	56.46	67.13

A2	84.63	84.29	83.73	82.90	81.69	79.98	77.58	74.19	69.40
	27.83	35.59	40.69	44.55	47.16	48.02	47.71	46.00	43.02
	29.65	37.37	42.26	45.90	48.30	48.91	48.40	46.52	43.35
	31.82	39.46	44.07	47.44	49.57	49.89	49.17	47.09	43.73
	34.40	41.91	46.16	49.17	50.97	50.97	50.00	47.71	44.16
	37.35	44.61	48.47	51.05	52.46	52.12	50.89	48.40	44.64
	39.85	46.66	50.51	52.79	53.86	53.27	51.81	49.13	45.17
	38.11	44.44	50.38	53.38	54.58	54.22	52.67	49.88	45.75
	25.40	31.98	43.61	50.11	53.12	54.41	53.27	50.59	46.37
	-99.00	-99.00	23.59	38.60	46.53	52.59	53.10	51.13	47.01
	-99.00	-99.00	-99.00	-99.00	28.26	46.28	51.11	51.19	47.63
	-99.00	-99.00	-99.00	-99.00	-99.00	28.86	45.10	50.15	48.13

TABLE A-1c: THE SHEAR NOISE INTENSITY AND FREQUENCY AT X/D = 5.

CONVECTION MACH NUMBER = 8.6

DATE 090573

CONVECTION MACH NO.= 8.600 SPEED OF SOUND RATIO= 2.40 VO CODE= 1

SHEAR NOISE INTENSITY(DECIBELS) WITH FREQUENCY BAND NUMBERS

ANGLE (DEG)	SEGMENT 1	SEGMENT 2	SEGMENT 3	SEGMENT 4	SEGMENT 5	SEGMENT 6	SEGMENT 7	SEGMENT 8	SEGMENT 9	TOTAL
	MC 8.42971	7.93880	7.18332	6.24488	5.21616	4.18607	3.22768	2.39112	1.70193	
	A 2.26000	2.12000	1.99000	1.84000	1.70000	1.56000	1.42000	1.28000	1.14000	
5.0	-15.32(10)	-6.88(10)	.17(10)	6.55(11)	12.57(12)	18.52(13)	25.03(14)	35.17(16)	32.73(17)	37.46
10.0	-11.99(10)	-3.54(10)	3.50(11)	9.89(11)	15.91(12)	21.88(13)	28.43(14)	38.84(16)	35.95(17)	40.97
15.0	-9.76(10)	-1.32(10)	5.72(11)	12.10(11)	18.13(12)	24.12(13)	30.73(15)	41.70(16)	37.95(18)	43.53
20.0	-7.89(10)	.53(10)	7.56(11)	13.94(11)	19.97(12)	25.99(13)	32.71(15)	44.78(16)	39.49(18)	46.16
25.0	-6.16(10)	2.25(10)	9.26(11)	15.63(12)	21.68(13)	27.75(14)	34.61(15)	39.79(16)	40.82(18)	44.83
30.0	-4.46(10)	3.92(11)	10.92(11)	17.28(12)	23.35(13)	29.48(14)	36.54(15)	48.21(17)	42.01(18)	49.43
35.0	-2.70(11)	5.65(11)	12.62(12)	18.98(12)	25.07(13)	31.30(14)	38.65(16)	47.59(17)	43.17(19)	49.91
40.0	-.84(11)	7.48(11)	14.43(12)	20.79(13)	26.93(14)	33.29(15)	41.06(16)	47.79(18)	44.37(19)	50.13
45.0	1.14(11)	9.42(12)	16.35(12)	22.73(13)	28.93(14)	35.49(15)	43.94(17)	48.33(18)	45.57(20)	51.26
50.0	3.32(12)	11.56(12)	18.48(13)	24.89(14)	31.21(15)	38.08(16)	47.73(17)	49.16(19)	46.89(21)	52.98
55.0	5.78(12)	13.99(13)	20.91(13)	27.38(14)	33.90(15)	41.29(16)	44.86(18)	50.26(19)	48.38(21)	53.47
60.0	8.64(13)	16.83(14)	23.79(14)	30.40(15)	37.26(16)	45.62(17)	54.25(19)	51.72(20)	50.19(22)	57.50
65.0	12.10(14)	20.29(14)	27.36(15)	34.25(16)	41.81(17)	52.61(18)	54.63(20)	53.56(21)	52.60(22)	59.54

70.0	16.64(15)	24.91(16)	32.25(16)	39.83(17)	49.20(18)	48.46(19)	56.50(21)	56.11(22)	45.46(22)	60.24
75.0	23.55(17)	32.16(17)	40.43(18)	46.64(19)	49.57(20)	59.08(21)	59.70(22)	49.50(22)	43.46(21)	63.82
80.0	34.40(19)	41.91(20)	47.30(20)	59.31(21)	53.19(22)	53.79(23)	53.03(24)	40.44(20)	34.82(20)	62.81
85.0	39.94(21)	46.46(21)	50.38(20)	52.47(19)	39.93(19)	37.21(19)	33.78(19)	29.61(19)	25.16(19)	55.35
90.0	*99.00(16)	*99.00(16)	*99.00(16)	*99.00(16)	-99.00(16)	*99.00(17)	*99.00(17)	-99.00(18)	*99.00(19)	-89.96
100.0	7.45(12)	14.34(12)	19.32(12)	23.06(13)	25.72(14)	27.27(15)	27.67(16)	26.79(17)	23.87(17)	34.04
110.0	5.49(10)	12.54(10)	17.80(10)	21.96(11)	25.17(12)	27.43(13)	28.65(14)	28.69(15)	26.33(17)	34.80
120.0	3.44(9)	10.55(9)	15.95(9)	20.31(10)	23.80(11)	26.43(12)	28.13(13)	28.74(15)	26.76(16)	34.33
130.0	1.55(8)	8.70(8)	14.17(8)	18.65(9)	22.30(10)	25.16(11)	27.15(13)	28.14(14)	26.44(15)	33.46
140.0	-.26(7)	6.93(7)	12.44(8)	16.98(8)	20.74(9)	23.74(11)	25.93(12)	27.18(14)	25.68(15)	32.34
150.0	-2.11(7)	5.08(7)	10.62(7)	15.21(8)	19.04(9)	22.13(10)	24.45(12)	25.88(13)	24.52(15)	30.94
160.0	-4.29(6)	2.91(6)	8.47(7)	13.09(8)	16.96(9)	20.11(10)	22.51(11)	24.05(13)	22.79(14)	29.86
170.0	-7.54(6)	-.33(6)	5.24(7)	9.87(8)	13.76(9)	16.95(10)	19.39(11)	21.00(13)	19.78(14)	25.97
	38.48	45.29	49.82	57.71	53.48	58.57	60.66	57.98	54.24	65.71

TABLE A-1D: THE TOTAL NOISE INTENSITY AT X/D = 5.

CONVECTION MACH NUMBER = 8.6

DATE 090573

CONVECTION MACH NO.= 8.600 SPEED OF SOUND RATIO= 2.40 VO CODE= 1

TOTAL NOISE INTENSITY(DECIBELS)

ANGLE (DEG)	SEGMENT 1	SEGMENT 2	SEGMENT 3	SEGMENT 4	SEGMENT 5	SEGMENT 6	SEGMENT 7	SEGMENT 8	SEGMENT 9	TOTAL
MC	8.42971	7.93880	7.18332	6.24488	5.21616	4.18607	3.22788	2.39112	1.70193	
*	2.26000	2.12000	1.98000	1.84000	1.70000	1.56000	1.42080	1.28000	1.14000	
5.0	-4.84	3.84	10.76	16.65	21.73	26.22	30.67	38.18	35.26	40.69
10.0	-1.45	7.22	14.15	20.03	25.10	29.60	34.08	41.83	38.51	44.19
15.0	.83	9.49	16.41	22.28	27.35	31.85	36.36	44.63	40.54	46.72
20.0	2.75	11.40	18.30	24.15	29.21	33.72	38.29	47.61	42.11	49.25
25.0	4.56	13.18	20.05	25.89	30.93	35.45	40.10	48.80	43.47	47.55
30.0	6.33	14.92	21.75	27.56	32.58	37.12	41.90	50.05	44.69	52.41
35.0	8.16	16.70	23.50	29.26	34.27	38.83	43.81	50.25	45.88	52.56
40.0	10.09	18.59	25.33	31.06	36.06	40.67	45.95	50.49	47.13	53.42
45.0	12.12	20.56	27.24	32.93	37.92	42.62	48.42	51.05	48.35	54.66
50.0	14.33	22.69	29.32	34.97	39.98	44.84	51.65	51.90	49.71	56.43
55.0	16.76	25.05	31.62	37.25	42.31	47.50	47.87	53.05	51.24	56.78

60.0	19.52	27.73	34.25	39.89	45.11	50.98	57.02	54.55	53.11	60.46
65.0	22.69	30.83	37.34	43.07	48.70	56.58	57.43	56.45	55.57	62.81
70.0	26.60	34.71	41.30	47.39	54.33	51.47	59.37	59.07	48.47	63.42
75.0	32.07	40.30	47.41	49.65	52.58	61.95	62.66	52.51	51.68	66.10
80.0	37.41	44.92	50.31	62.17	56.21	56.80	56.04	51.61	48.70	65.20
85.0	42.95	49.47	53.39	55.48	54.12	53.52	52.01	49.60	46.80	61.65
90.0	33.47	40.33	44.93	48.00	49.77	50.36	49.80	48.13	45.37	57.84
100.0	26.37	33.51	38.59	42.31	44.87	46.32	46.65	45.82	43.15	53.13
110.0	22.44	29.66	34.89	38.84	41.70	43.52	44.29	43.95	41.39	50.59
120.0	19.64	26.89	32.19	36.25	39.26	41.28	42.32	42.30	39.83	48.57
130.0	17.36	24.64	29.98	34.09	37.19	39.35	40.55	40.75	38.36	46.80
140.0	15.33	22.62	27.98	32.14	35.30	37.53	38.85	39.20	36.88	45.10
150.0	13.34	20.63	26.01	30.19	33.39	35.67	37.06	37.52	35.25	43.33
160.0	11.07	18.38	23.76	27.96	31.18	33.50	34.94	35.46	33.23	41.21
170.0	7.78	15.08	20.47	24.68	27.91	30.25	31.71	32.27	30.06	38.80
	42.32	49.23	53.98	60.96	58.97	62.50	64.07	61.66	58.50	69.49

TABLE A-2A: THE WKBJ INTEGRAL AND RUN PARAMETERS AT X/D = 10.

THETA(RAD)	S(21)	S(41)	S(61)	S(81)	S(101)	S(121)	S(141)	S(161)	S(181)
.00	.24801+01	.21273+01	.17845+01	.14670+01	.11887+01	.96054+00	.79203+00	.69644+00	.63946+00
5.00	.24627+01	.21101+01	.17674+01	.14502+01	.11721+01	.94430+00	.77614+00	.68108+00	.62377+00
10.00	.24168+01	.20648+01	.17229+01	.14064+01	.11291+01	.90217+00	.73507+00	.64183+00	.58362+00
15.00	.23680+01	.20171+01	.16763+01	.13610+01	.10851+01	.85971+00	.69444+00	.60382+00	.54378+00
20.00	.23140+01	.19647+01	.16255+01	.13121+01	.10382+01	.81499+00	.65239+00	.56608+00	.50306+00
25.00	.22518+01	.19046+01	.15677+01	.12567+01	.98547+00	.76535+00	.60640+00	.52653+00	.45859+00
30.00	.21903+01	.18458+01	.15119+01	.12042+01	.93647+00	.72035+00	.56621+00	.49404+00	.41958+00
35.00	.21177+01	.17769+01	.14468+01	.11432+01	.88006+00	.66912+00	.52128+00	.45681+00	.37530+00
40.00	.20306+01	.16944+01	.13692+01	.10709+01	.81367+00	.60939+00	.46978+00	.41199+00	.32381+00
45.00	.19433+01	.16129+01	.12941+01	.10027+01	.75299+00	.55737+00	.42867+00	.37449+00	.27922+00
50.00	.18407+01	.15180+01	.12074+01	.92502+00	.68525+00	.50105+00	.38733+00	.33263+00	.23042+00
55.00	.17171+01	.14046+01	.11050+01	.83456+00	.60808+00	.43934+00	.34800+00	.28255+00	.17460+00
60.00	.15601+01	.12617+01	.97724+00	.72325+00	.51519+00	.36842+00	.30580+00	.21722+00	.10827+00
65.00	.13755+01	.10973+01	.83459+00	.60443+00	.42338+00	.31087+00	.25400+00	.14897+00	.43540-01
70.00	.11338+01	.88682+00	.65780+00	.46496+00	.32777+00	.26894+00	.17496+00	.65005-01	.24860-02
75.00	.80195+00	.60934+00	.43929+00	.31564+00	.26054+00	.16594+00	.56378-01	.79713-02	.13369+00
80.00	.38687+00	.33209+00	.28397+00	.18805+00	.77217-01	.00000	.10242+00	.32159+00	.64912+00

CARD INPUT FOR MMAX, A, MC, THETA, AND W? NO
DETAILED PRINTOUT? NO

ALPHA	L	LI	SF	PW(DB)
1.750	1.000	6.150	1.685	-18.266

MODIFIED ALPHA IS: .7294

TABLE A-2B: THE SELF NOISE INTENSITY AND FREQUENCY AT X/D = 10.

DATE 090573

CONVECTION MACH NO.= 0.600 SPEED OF SOUND RATIO= 2.40 VO CODE= 1

SELF NOISE INTENSITY(DECIBELS) WITH FREQUENCY BAND NUMBERS

ANGLE (DEG)	SEGMENT 1	SEGMENT 2	SEGMENT 3	SEGMENT 4	SEGMENT 5	SEGMENT 6	SEGMENT 7	SEGMENT 8	SEGMENT 9	TOTAL
	MC 8.42971	7.93880	7.19332	6.24488	5.21616	4.18607	3.22768	2.39112	1.70193	
	A 2.26000	2.12000	1.98000	1.84000	1.70000	1.56000	1.42000	1.28000	1.14000	
5.0	-2.24(8)	6.45(9)	13.37(9)	19.20(10)	24.16(11)	28.41(12)	32.29(13)	38.16(15)	34.73(16)	40.89
10.0	1.15(8)	9.84(9)	16.75(9)	22.58(10)	27.55(11)	31.80(12)	35.69(13)	41.79(15)	38.00(16)	44.89
15.0	3.43(9)	12.12(9)	19.02(9)	24.84(10)	29.80(11)	34.05(12)	37.97(13)	44.53(15)	40.07(16)	46.88
20.0	5.36(9)	14.03(9)	20.91(10)	26.72(10)	31.66(11)	35.92(12)	39.88(13)	47.41(15)	41.67(17)	49.32
25.0	7.18(9)	15.82(9)	22.68(10)	28.46(10)	33.39(11)	37.64(12)	41.66(14)	42.79(15)	43.07(17)	47.99
30.0	8.95(9)	17.56(9)	24.38(10)	30.13(11)	35.03(12)	39.30(13)	43.40(14)	50.43(16)	44.32(17)	52.37
35.0	10.79(9)	19.35(10)	26.13(10)	31.83(11)	36.72(12)	40.99(13)	45.23(14)	49.86(16)	85.55(18)	52.88
40.0	12.73(10)	21.24(10)	27.96(11)	33.63(11)	38.49(12)	42.79(13)	47.24(15)	50.13(16)	46.82(18)	53.68
45.0	14.76(10)	23.21(10)	29.88(11)	35.50(12)	40.34(13)	44.69(14)	49.51(15)	50.72(17)	48.10(19)	55.81
50.0	16.97(11)	25.34(11)	31.95(11)	37.52(12)	42.36(13)	46.82(14)	52.40(16)	51.61(17)	49.49(19)	56.82
55.0	19.40(11)	27.70(12)	34.24(12)	39.77(13)	44.64(14)	49.31(15)	47.86(16)	52.79(18)	51.08(20)	57.05
60.0	22.15(12)	30.36(12)	36.84(13)	42.37(14)	47.34(15)	52.48(16)	56.75(17)	54.35(19)	53.00(21)	60.79
65.0	25.29(13)	33.43(13)	39.88(14)	45.46(15)	50.71(16)	57.36(17)	57.20(18)	56.31(20)	55.52(21)	63.05
70.0	29.14(14)	37.23(14)	43.73(15)	49.56(16)	55.73(17)	51.46(18)	59.20(20)	59.00(21)	48.46(21)	63.88
75.0	34.41(16)	42.57(16)	49.44(17)	49.64(17)	52.57(18)	61.80(20)	62.60(21)	52.50(21)	53.97(20)	66.17
80.0	37.40(18)	44.91(18)	50.30(19)	61.99(20)	56.19(21)	56.79(21)	56.03(20)	54.26(19)	51.52(19)	65.35
85.0	42.94(20)	49.46(19)	53.38(19)	55.47(18)	56.95(18)	56.42(17)	54.94(17)	52.56(18)	49.77(18)	63.42

90.0	36.47(14)	43.33(14)	47.93(14)	51.00(15)	52.77(15)	53.36(15)	52.80(16)	51.13(17)	48.37(17)	60.04
100.0	29.31(10)	36.45(10)	41.53(11)	45.26(11)	47.82(12)	49.27(13)	49.59(14)	48.77(15)	46.10(16)	56.08
110.0	25.36(8)	32.58(9)	37.81(9)	41.75(10)	44.60(10)	46.41(12)	47.17(13)	46.82(14)	44.25(15)	53.47
120.0	22.53(7)	29.79(7)	35.09(8)	39.13(8)	42.13(9)	44.14(11)	45.15(12)	45.10(13)	42.61(14)	51.40
130.0	20.25(6)	27.53(6)	32.86(7)	36.97(8)	40.05(9)	42.18(10)	43.34(11)	43.50(13)	41.07(14)	49.59
140.0	18.21(6)	25.50(6)	30.86(8)	35.01(7)	38.14(8)	40.35(9)	41.62(11)	41.91(12)	39.54(14)	47.87
150.0	16.21(5)	23.51(5)	28.88(6)	33.05(7)	36.23(8)	38.48(9)	39.82(10)	40.21(12)	37.86(13)	46.07
160.0	13.95(5)	21.25(5)	26.63(5)	30.82(6)	34.01(7)	36.30(8)	37.68(10)	38.13(11)	35.81(13)	43.94
170.0	10.65(5)	17.95(5)	23.34(5)	27.53(6)	30.74(7)	33.04(8)	34.45(10)	34.94(11)	32.63(13)	40.72
	43.01	49.99	54.87	61.19	60.53	63.26	64.42	62.22	59.46	70.13
A_2	84.63	84.29	83.73	82.90	81.69	79.98	77.58	74.19	69.40	
	30.83	38.59	43.69	47.55	50.16	51.02	50.71	49.00	46.02	
	32.65	40.37	45.26	48.90	51.30	51.91	51.40	49.52	46.35	
	34.82	42.46	47.07	50.44	52.57	52.89	52.17	50.09	46.73	
	37.40	44.91	49.16	52.17	53.97	53.97	53.00	50.71	47.16	
	40.35	47.61	51.47	54.05	55.46	55.12	53.89	51.40	47.64	
	42.85	49.66	53.51	55.79	56.86	56.27	54.81	52.13	48.17	
	41.11	47.44	53.38	56.38	57.58	57.22	55.67	52.88	48.75	
	28.40	34.98	46.61	53.11	56.12	57.41	56.27	53.59	49.37	
	-99.00	-99.00	26.59	41.60	49.53	55.59	56.10	54.13	50.01	
	-99.00	-99.00	-99.00	-99.00	31.26	49.28	54.11	54.19	50.63	
	-99.00	-99.00	-99.00	-99.00	-99.00	31.86	48.10	53.15	51.13	

TABLE A-2c: THE SHEAR NOISE INTENSITY AND FREQUENCY AT X/D - 10.

DATE 090573

CONVECTION MACH NO.= 8.600 SPEED OF SOUND RATIO= 2.40 VO CODE= 1

SHEAR NOISE INTENSITY(DECIBELS) WITH FREQUENCY BAND NUMBERS

ANGLE (DEG)		SEGMENT 1	SEGMENT 2	SEGMENT 3	SEGMENT 4	SEGMENT 5	SEGMENT 6	SEGMENT 7	SEGMENT 8	SEGMENT 9	TOTAL
	MC	8.42971	7.93880	7.18332	6.24488	5.21616	4.18607	3.22788	2.39112	1.70193	
	A	2.26000	2.12000	1.98000	1.84000	1.70000	1.56000	1.42000	1.28000	1.14000	
5.0		-12.32(7)	-3.88(7)	3.17(7)	9.55(8)	15.57(9)	21.52(10)	28.03(11)	36.17(13)	35.73(14)	40.46
10.0		-8.99(7)	-.54(7)	6.50(8)	12.89(8)	18.91(9)	24.88(10)	31.43(11)	41.84(13)	38.95(14)	43.97

15.0	-6.76(7)	1.68(7)	8.72(8)	15.10(8)	21.13(9)	27.12(10)	33.73(12)	44.70(13)	40.95(15)	46.53
20.0	-4.89(7)	3.53(7)	10.56(8)	16.94(8)	22.97(9)	28.99(10)	35.71(12)	47.78(13)	42.49(15)	49.16
25.0	-3.16(7)	5.25(7)	12.26(8)	18.63(9)	24.68(10)	30.75(11)	37.61(12)	42.79(13)	43.82(15)	47.03
30.0	-1.46(7)	6.92(8)	13.92(8)	20.28(9)	26.35(10)	32.48(11)	39.54(12)	51.21(14)	45.01(15)	52.93
35.0	.30(8)	8.65(8)	15.62(9)	21.98(9)	28.07(10)	34.30(11)	41.65(13)	50.59(14)	46.17(16)	52.91
40.0	2.16(8)	10.48(8)	17.43(9)	23.79(10)	29.93(11)	36.29(12)	44.06(13)	50.79(15)	47.37(16)	53.13
45.0	4.14(8)	12.42(9)	19.35(9)	25.73(10)	31.93(11)	38.49(12)	46.94(14)	51.33(15)	48.57(17)	54.26
50.0	6.32(9)	14.56(9)	21.48(10)	27.89(11)	34.21(12)	41.08(13)	50.73(14)	52.16(16)	49.89(18)	55.98
55.0	8.78(9)	16.99(10)	23.91(10)	30.38(11)	36.90(12)	44.29(13)	47.86(15)	53.26(16)	51.38(18)	56.47
60.0	11.64(10)	19.83(11)	26.79(11)	33.40(12)	40.26(13)	48.82(14)	57.25(16)	54.72(17)	53.19(19)	60.50
65.0	15.10(11)	23.29(11)	30.36(12)	37.25(13)	44.81(14)	55.61(15)	57.63(17)	56.56(18)	55.60(19)	62.54
70.0	19.64(12)	27.91(13)	35.25(13)	42.83(14)	52.20(15)	61.46(16)	59.50(18)	59.11(19)	48.46(19)	63.24
75.0	26.55(14)	35.16(14)	43.43(15)	49.64(16)	52.57(17)	62.08(18)	62.70(19)	52.50(19)	46.46(18)	66.02
80.0	37.40(16)	44.91(17)	50.30(17)	62.31(18)	56.19(19)	56.79(20)	56.03(18)	43.44(17)	37.82(17)	65.01
85.0	42.94(18)	49.46(18)	53.38(17)	55.47(16)	42.93(16)	40.21(16)	36.78(16)	32.61(16)	28.16(16)	58.55
90.0	-99.00(13)	-99.00(13)	-99.00(13)	-99.00(13)	-99.00(13)	-99.00(14)	-99.00(14)	-99.00(15)	-99.00(16)	-89.96
100.0	10.45(9)	17.34(9)	22.32(9)	26.06(10)	28.72(11)	30.27(12)	30.67(13)	29.79(14)	26.87(14)	37.84
110.0	-8.49(7)	15.54(7)	20.80(7)	24.96(8)	28.17(9)	30.43(10)	31.65(11)	31.69(12)	29.33(14)	37.80
120.0	6.44(6)	13.55(6)	18.95(6)	23.31(7)	26.80(8)	29.43(9)	31.13(10)	31.74(12)	29.76(13)	37.33
130.0	4.55(5)	11.70(5)	17.17(5)	21.65(6)	25.30(7)	28.16(8)	30.15(10)	31.14(11)	29.44(12)	36.46
140.0	2.74(4)	9.93(4)	15.44(5)	19.98(5)	23.74(6)	26.74(8)	28.93(9)	30.18(11)	28.68(12)	35.54
150.0	.89(4)	8.08(4)	13.62(4)	18.21(5)	22.04(6)	25.13(7)	27.45(9)	28.88(10)	27.52(12)	33.94
160.0	-1.29(3)	5.91(3)	11.47(4)	16.09(5)	19.96(6)	23.11(7)	25.51(8)	27.05(10)	25.79(11)	32.06
170.0	-4.54(3)	2.67(3)	8.24(4)	12.87(5)	16.76(6)	19.95(7)	22.39(8)	24.00(10)	22.78(11)	28.97
	41.48	48.29	52.82	60.71	56.48	61.57	63.66	60.98	57.24	68.71

TABLE A-2D: THE TOTAL NOISE INTENSITY AT X/D = 10.

DATE 080573

CONVECTION MACH NO.= 0.600 SPEED OF SOUND RATIO= 2.40 VO CODE= 1

TOTAL NOISE INTENSITY(DECIBELS)

ANGLE	SEGMENT 1	SEGMENT 2	SEGMENT 3	SEGMENT 4	SEGMENT 5	SEGMENT 6	SEGMENT 7	SEGMENT 8	SEGMENT 9	TOTAL
(DEG) MC	8.42971	7.93880	7.18332	6.24488	5.21616	4.18607	3.22768	2.39112	1.70193	
A	2.26000	2.12000	1.98000	1.84000	1.70000	1.56000	1.42000	1.28000	1.14000	
5.0	-1.84	6.84	13.76	19.65	24.73	29.22	33.67	41.18	38.26	43.89
10.0	1.55	10.22	17.15	23.03	28.10	32.60	37.08	44.83	41.51	47.19
15.0	3.83	12.49	19.41	25.28	30.35	34.85	39.36	47.63	43.54	49.72
20.0	5.75	14.40	21.30	27.15	32.21	36.72	41.29	50.61	45.11	52.25

25•0	7•56	16•18	23•05	28•89	33•93	38•45	43•10	45•80	46•47	50•55
30•0	9•33	17•92	24•75	30•56	35•58	40•12	44•90	53•85	47•69	55•41
35•0	11•16	19•70	26•50	32•26	37•27	41•83	46•81	53•25	48•88	55•56
40•0	13•09	21•59	28•33	34•06	39•06	43•67	48•95	53•49	50•11	56•42
45•0	15•12	23•56	30•24	35•93	40•92	45•62	51•42	54•05	51•35	57•66
50•0	17•33	25•69	32•32	37•97	42•98	47•84	54•65	54•90	52•71	59•43
55•0	19•76	28•05	34•62	40•25	45•31	50•50	50•87	56•05	54•24	59•78
60•0	22•52	30•73	37•25	42•89	48•11	53•98	60•02	57•55	56•11	63•86
65•0	25•69	33•83	40•34	46•07	51•70	59•58	60•43	59•45	58•57	65•81
70•0	29•60	37•71	44•30	50•39	57•33	54•47	62•37	62•07	51•47	66•47
75•0	35•07	43•30	53•41	52•65	55•58	64•95	65•66	55•51	54•66	67•10
80•0	40•41	47•92	53•31	65•17	59•21	59•80	59•04	54•61	51•70	68•20
85•0	45•95	52•47	56•39	58•48	57•12	56•52	55•01	52•60	49•80	64•85
90•0	36•47	43•33	47•93	51•00	52•77	53•36	52•80	51•13	48•37	60•84
100•0	29•37	36•51	41•59	45•31	47•87	49•32	49•85	48•82	46•15	56•73
110•0	25•44	32•66	37•89	41•84	44•70	46•52	47•29	46•95	44•39	53•59
120•0	22•64	29•89	35•19	39•25	42•26	44•28	45•32	45•30	42•83	51•57
130•0	20•36	27•64	32•98	37•09	40•19	42•35	43•55	43•75	41•36	49•60
140•0	18•33	25•62	30•98	35•14	38•30	40•53	41•85	42•20	39•88	48•10
150•0	16•34	23•63	29•01	33•19	36•39	38•67	40•06	40•52	38•25	46•33
160•0	14•07	21•38	26•76	30•96	34•18	36•50	37•94	38•46	36•23	44•21
170•0	10•78	18•08	23•47	27•68	30•91	33•25	34•71	35•27	33•06	41•80
	45•32	52•23	56•98	63•96	61•97	65•50	67•07	64•66	61•50	72•49

TABLE A-3A: THE WKBJ INTEGRAL AND RUN PARAMETERS AT x/D = 20.

THETA(RAD)	S(21)	S(41)	S(61)	S(81)	S(101)	S(121)	S(141)	S(161)	S(181)
.00	.24801+01	.21273+01	.17845+01	.14670+01	.11887+01	.96054+00	.79203+00	.69644+00	.63946+00
5.00	.24627+01	.21101+01	.17674+01	.14502+01	.11721+01	.94430+00	.77614+00	.68108+00	.62377+00
10.00	.24168+01	.20648+01	.17229+01	.14064+01	.11291+01	.90217+00	.73607+00	.64183+00	.58362+00
15.00	.23680+01	.20171+01	.16763+01	.13610+01	.10851+01	.85971+00	.69444+00	.60382+00	.54378+00
20.00	.23140+01	.19647+01	.16255+01	.13121+01	.10382+01	.81499+00	.65239+00	.56608+00	.50306+00
25.00	.22518+01	.19046+01	.15677+01	.12567+01	.98547+00	.76535+00	.60640+00	.52653+00	.45859+00
30.00	.21903+01	.18458+01	.15119+01	.12042+01	.93647+00	.72035+00	.56621+00	.49484+00	.41958+00
35.00	.21177+01	.17769+01	.14468+01	.11432+01	.88006+00	.66912+00	.52128+00	.45651+00	.37530+00
40.00	.20306+01	.16944+01	.13692+01	.10709+01	.81367+00	.60939+00	.46978+00	.41199+00	.32381+00
45.00	.19433+01	.16129+01	.12941+01	.10027+01	.75299+00	.55737+00	.42867+00	.37449+00	.27922+00
50.00	.18407+01	.15180+01	.12074+01	.92502+00	.68525+00	.50105+00	.38733+00	.33253+00	.23042+00
55.00	.17171+01	.14046+01	.11050+01	.83456+00	.60808+00	.43934+00	.34800+00	.28255+00	.17460+00
60.00	.15601+01	.12617+01	.97724+00	.72325+00	.51519+00	.36642+00	.30980+00	.21722+00	.10627+00
65.00	.13756+01	.11973+01	.83459+00	.60443+00	.42338+00	.31087+00	.25400+00	.14897+00	.43140-01
70.00	.11338+01	.88682+00	.65780+00	.46496+00	.32777+00	.26894+00	.17496+00	.65005-01	.24860-02
75.00	.80195+00	.63934+00	.43979+00	.31564+00	.28054+00	.16594+00	.56378-01	.79713-02	.13369+00
80.00	.38687+00	.33209+00	.28397+00	.18805+00	.77217-01	.00000	.10242+00	.32169+00	.64912+00

CARD INPUT FOR MMAX, A, MC, THETA, AND W? NO
DETAILED PRINTOUT? NO

ALPHA	L	L1	SF	PW(DB)
1.750	1.000	6.150	.843	-15.266

MODIFIED ALPHA IS: .7294

TABLE A-3B: THE SELF NOISE INTENSITY AND FREQUENCY AT X/D = 20.

DATE 090573

CONVECTION MACH NO.= 0.600 SPEED OF SOUND RATIO= 2.40 VO CODE= 1

SELF NOISE INTENSITY(DECIBELS) WITH FREQUENCY BAND NUMBERS

ANGLE		SEGMENT 1	SEGMENT 2	SEGMENT 3	SEGMENT 4	SEGMENT 5	SEGMENT 6	SEGMENT 7	SEGMENT 8	SEGMENT 9	TOTAL
(DEG)	MC	8.42971	7.93880	7.18332	6.24488	5.21616	4.18607	3.22768	2.39112	1.70193	
	A	2.26000	2.12000	1.98000	1.84000	1.70000	1.56000	1.42000	1.28000	1.14000	
5.0		.76(5)	9.45(6)	16.37(6)	22.20(7)	27.16(8)	31.41(9)	35.29(10)	41.16(12)	37.73(13)	43.89
10.0		4.15(5)	12.84(6)	19.75(6)	25.58(7)	30.55(8)	34.80(9)	38.69(10)	44.79(12)	41.00(13)	47.39
15.0		6.43(6)	15.12(6)	22.02(6)	27.84(7)	32.80(8)	37.05(9)	40.97(10)	47.53(12)	43.07(13)	49.88
20.0		8.36(6)	17.03(6)	23.91(7)	29.72(7)	34.66(8)	38.92(9)	42.88(11)	50.41(12)	44.67(14)	52.32
25.0		10.18(6)	18.82(6)	25.68(7)	31.46(7)	36.39(8)	40.64(9)	44.66(11)	45.79(12)	46.07(14)	50.99
30.0		11.95(6)	20.56(6)	27.38(7)	33.13(8)	38.03(9)	42.30(10)	46.40(11)	53.43(13)	47.32(14)	55.37
35.0		13.79(6)	22.35(7)	29.13(7)	34.83(8)	39.72(9)	43.99(10)	48.23(11)	52.86(13)	48.55(15)	55.88
40.0		15.73(7)	24.24(7)	30.96(8)	36.63(8)	41.49(9)	45.79(10)	50.24(12)	53.13(13)	49.82(15)	56.68
45.0		17.76(7)	26.21(7)	32.88(8)	38.50(9)	43.34(10)	47.69(11)	52.51(12)	53.72(14)	51.10(16)	58.01
50.0		19.97(8)	28.34(8)	34.95(8)	40.52(9)	45.36(10)	49.82(11)	55.40(13)	54.61(14)	52.49(16)	59.62
55.0		22.40(8)	30.70(9)	37.24(9)	42.77(10)	47.64(11)	52.31(12)	50.86(13)	55.79(15)	54.08(17)	60.85
60.0		25.15(9)	33.36(9)	39.84(10)	45.37(11)	50.34(12)	55.48(13)	59.75(14)	57.35(16)	56.00(18)	63.79
65.0		28.29(10)	36.43(10)	42.88(11)	48.46(12)	53.71(13)	60.36(14)	60.20(15)	59.31(17)	58.52(18)	66.85
70.0		32.14(11)	40.23(11)	46.73(12)	52.56(13)	58.73(14)	64.46(15)	62.20(17)	62.00(18)	61.46(18)	66.88
75.0		37.41(13)	45.57(13)	52.44(14)	52.64(14)	55.57(15)	64.80(17)	65.60(18)	65.50(18)	56.97(17)	69.17
80.0		40.40(15)	47.91(15)	53.30(16)	64.99(17)	59.19(18)	59.79(18)	59.03(17)	57.26(16)	54.52(16)	68.35
85.0		45.94(17)	52.46(16)	56.38(16)	58.47(15)	59.95(15)	59.42(14)	57.94(14)	55.56(15)	52.77(15)	66.92
90.0		39.47(11)	46.33(11)	50.93(11)	54.00(12)	55.77(12)	56.36(12)	55.80(13)	54.13(14)	51.37(14)	63.04

100.0	32.31(7)	39.45(7)	44.53(8)	48.26(8)	50.82(9)	52.27(10)	52.59(10)	51.77(12)	49.10(13)	59.88
110.0	28.36(5)	35.58(6)	40.81(6)	44.75(7)	47.60(7)	49.41(9)	50.17(10)	49.82(11)	47.25(12)	56.47
120.0	25.53(4)	32.79(4)	38.09(5)	42.13(5)	45.13(6)	47.14(8)	48.15(9)	48.10(10)	45.61(11)	54.90
130.0	23.25(3)	30.53(3)	35.86(4)	39.97(5)	43.05(6)	45.18(7)	46.34(8)	46.50(10)	44.07(11)	52.59
140.0	21.21(3)	28.50(3)	33.86(3)	38.01(4)	41.14(5)	43.35(6)	44.62(8)	44.91(9)	42.54(11)	50.87
150.0	19.21(2)	26.51(2)	31.88(3)	36.05(4)	39.23(5)	41.48(6)	42.82(7)	43.21(9)	40.86(10)	49.87
160.0	16.95(2)	24.25(2)	29.63(2)	33.82(3)	37.01(4)	39.30(5)	40.68(7)	41.13(8)	38.81(10)	46.94
170.0	13.66(2)	20.95(2)	26.34(2)	30.53(3)	33.74(4)	36.04(5)	37.45(7)	37.94(8)	35.63(10)	43.72
	46.01	52.99	57.87	64.19	63.53	66.26	67.42	65.22	62.46	73.13
A2	84.63	84.29	83.73	82.90	81.69	79.98	77.58	74.19	69.40	
	33.83	41.59	46.69	50.55	53.16	54.02	53.71	52.00	49.02	
	35.65	43.37	48.26	51.90	54.30	54.91	54.40	52.52	49.35	
	37.82	45.46	50.07	53.44	55.57	55.89	55.17	53.09	49.73	
	40.40	47.91	52.16	55.17	56.97	56.97	56.00	53.71	50.16	
	43.35	50.61	54.47	57.05	58.46	58.12	56.89	54.40	50.64	
	45.85	52.66	56.51	58.79	59.86	59.27	57.81	55.13	51.17	
	44.11	50.44	56.38	59.38	60.58	60.22	58.67	55.88	51.75	
	31.40	37.98	49.61	56.11	59.12	60.41	59.27	56.59	52.37	
	-99.00	-99.00	29.59	44.60	52.53	58.59	59.10	57.13	53.01	
	-99.00	-99.00	-99.00	-99.00	34.26	52.28	57.11	57.19	53.63	
	-99.00	-99.00	-99.00	-99.00	-99.00	34.86	51.10	56.15	54.13	

TABLE A-3c: THE SHEAR NOISE INTENSITY AND FREQUENCY AT X/D = 20

DATE 090573

CONVECTION MACH NO.= 0.605 SPEED OF SOUND RATIO= 2.40 VO CODE= 1

SHEAR NOISE INTENSITY(DECIBELS) WITH FREQUENCY BAND NUMBERS

ANGLE (DEG)		SEGMENT 1	SEGMENT 2	SEGMENT 3	SEGMENT 4	SEGMENT 5	SEGMENT 6	SEGMENT 7	SEGMENT 8	SEGMENT 9	TOTAL
	VC	8.42971	7.93880	7.18332	6.24488	5.21616	4.18607	3.22768	2.39112	1.70193	
	A	2.26000	2.12000	1.98000	1.84000	1.70000	1.56000	1.42000	1.28000	1.14000	
5.0		-9.32(4)	-.88(4)	6.17(4)	12.55(5)	18.57(6)	24.52(7)	31.03(8)	41.17(10)	38.73(11)	43.46
10.0		-5.99(4)	2.46(4)	9.50(5)	15.89(5)	21.91(6)	27.88(7)	34.43(8)	44.84(10)	41.95(11)	46.97
15.0		-3.76(4)	4.68(4)	11.72(5)	18.10(5)	24.13(6)	30.12(7)	36.73(9)	47.70(10)	43.95(12)	49.53
20.0		-1.89(4)	6.53(4)	13.56(5)	19.94(6)	25.97(6)	31.99(7)	38.71(9)	50.78(10)	45.49(12)	52.16
25.0		-.16(4)	8.25(4)	15.26(5)	21.63(6)	27.68(7)	33.75(8)	40.61(9)	45.79(10)	46.82(12)	50.03
30.0		1.54(4)	9.92(5)	16.92(5)	23.28(6)	29.35(7)	35.48(8)	42.54(9)	54.21(11)	48.01(12)	55.43

SEGMENT 4	SEGMENT 5	SEGMENT 6	SEGMENT 7	SEGMENT 8	SEGMENT 9	TOTAL
[illegible](6)	31.[illegible]7(7)	37.30(8)	44.65(10)	53.59(11)	49.17(13)	55.41
[illegible](7)	32.93(8)	39.29(9)	47.06(10)	53.79(12)	50.37(13)	56.13
[illegible](7)	34.93(8)	41.49(9)	49.94(11)	54.33(12)	51.57(14)	57.26
[illegible](8)	37.21(9)	44.08(10)	53.73(11)	55.16(13)	52.89(15)	58.98
[illegible](8)	39.90(9)	47.29(10)	50.86(12)	56.26(13)	54.38(15)	59.47
[illegible](9)	43.26(10)	51.62(11)	60.25(13)	57.72(14)	56.19(16)	63.50
[illegible](10)	47.81(11)	58.61(12)	60.63(14)	59.56(15)	58.60(16)	65.54
[illegible](11)	55.20(12)	54.46(13)	62.50(15)	62.11(16)	51.46(16)	66.24
[illegible](13)	55.57(14)	65.08(15)	65.70(16)	55.50(16)	49.46(15)	69.02
[illegible](15)	59.19(16)	59.79(17)	59.03(15)	46.44(14)	40.82(14)	68.01
[illegible](13)	45.93(13)	43.21(13)	39.78(13)	35.61(13)	31.16(13)	61.55
[illegible](10)	-99.00(10)	-99.00(11)	-99.00(11)	-99.00(12)	-99.00(13)	-89.46
[illegible](7)	31.72(8)	33.27(9)	33.67(10)	32.79(11)	29.87(11)	40.04
[illegible](5)	31.17(6)	33.43(7)	34.65(8)	34.69(9)	32.33(11)	40.80
[illegible](4)	29.80(5)	32.43(6)	34.13(7)	34.74(9)	32.76(10)	40.33
[illegible](3)	28.30(4)	31.16(5)	33.15(7)	34.14(8)	32.44(9)	39.46
[illegible](2)	26.74(3)	29.74(5)	31.93(6)	33.18(8)	31.68(9)	38.34
[illegible](2)	25.04(3)	28.13(4)	30.45(6)	31.88(7)	30.52(9)	36.94
[illegible](2)	22.96(3)	26.11(4)	28.51(5)	30.05(7)	28.79(8)	35.06
[illegible](2)	19.76(3)	22.95(4)	25.39(5)	27.00(7)	25.78(8)	31.27
[illegible]	59.48	64.57	66.66	63.98	60.24	71.71

TOTAL NOISE INTENSITY AT X/D = 20

TABLE A-3D

DATE 090573

SPEED OF SOUND RATIO= 2.40 VO CODE= 1

NOZZLE EXIT MACH NO.= 0.60

TOTAL NOISE INTENSITY (DECIBELS)

ANGLE (DEG)		SEGMENT 1	SEGMENT 2	SEGMENT 3	SEGMENT 4	SEGMENT 5	SEGMENT 6	SEGMENT 7	SEGMENT 8	SEGMENT 9	TOTAL
	MC	[illegible]	7.95880	[illegible]	6.[illegible]4488	5.21616	4.18607	3.22768	2.39112	1.70193	
	A	[illegible]	2.12000	1.94000	1.[illegible]4000	1.70000	1.56000	1.42000	1.28000	1.14000	
5.0		[illegible]	[illegible]	16.76	[illegible]2.65	27.73	32.22	36.67	44.18	41.26	46.89
10.0		[illegible]	[illegible]	2[illegible].15	26.03	31.10	35.60	40.08	47.83	44.51	50.19
15.0		[illegible]	[illegible]	22.41	28.28	33.35	37.85	42.36	50.63	46.54	52.72
20.0		[illegible]	[illegible]	24.30	30.15	35.21	39.72	44.29	53.61	48.11	55.25
25.0		[illegible]	[illegible]	26.05	31.89	36.93	41.45	46.10	48.80	49.47	53.55
30.0		12.33	[illegible]	27.75	33.56	38.58	43.12	47.90	56.85	50.69	58.41
35.0		14.[illegible]	[illegible]	29.50	35.26	40.27	44.83	49.81	56.25	51.88	58.66

40.0	16.09	24.59	31.33	37.06	42.06	46.67	51.95	56.49	53.11	59.42
45.0	18.12	26.56	33.24	38.93	43.92	48.62	54.42	57.05	54.35	60.66
50.0	20.33	28.69	35.32	40.97	45.98	50.84	57.65	57.90	55.71	62.43
55.0	22.76	31.05	37.62	43.25	48.31	53.50	53.87	59.05	57.24	62.78
60.0	25.52	33.73	40.25	45.89	51.11	56.98	63.02	60.55	59.17	66.86
65.0	28.69	36.83	43.34	49.07	54.70	62.58	63.43	62.45	61.57	68.81
70.0	32.60	40.71	47.30	53.39	60.33	57.47	65.37	65.07	64.47	69.47
75.0	38.07	46.30	53.41	55.65	58.58	67.95	68.66	58.51	57.68	72.10
80.0	43.41	50.92	56.31	68.17	62.21	62.80	62.04	57.61	54.70	71.20
85.0	48.95	55.47	59.39	61.48	60.12	59.52	58.01	55.60	52.80	67.65
90.0	39.47	46.33	50.93	54.00	55.77	56.36	55.80	54.13	51.37	63.04
100.0	32.37	39.51	44.59	48.31	50.87	52.32	52.65	51.82	49.15	59.13
110.0	28.44	35.66	40.89	44.84	47.70	49.52	50.29	49.95	47.39	56.59
120.0	25.64	32.89	38.19	42.25	45.26	47.28	48.32	48.30	45.83	54.57
130.0	23.36	30.64	35.98	40.09	43.19	45.35	46.55	46.75	44.36	52.80
140.0	21.33	28.62	33.98	38.14	41.30	43.53	44.85	45.20	42.88	51.10
150.0	19.34	26.63	32.01	36.19	39.39	41.67	43.06	43.52	41.25	49.33
160.0	17.07	24.38	29.76	33.96	37.18	39.50	40.94	41.46	39.23	47.21
170.0	13.78	21.08	26.47	30.68	33.91	36.25	37.71	38.27	36.06	44.00
	48.32	55.23	59.98	66.96	64.97	68.50	70.07	67.66	64.50	75.49

TABLE A-4A: THE WKBJ INTEGRAL AND RUN PARAMETERS AT X/D = 25.

THETA(RAD)	S(21)	S(41)	S(61)	S(81)	S(101)	S(121)	S(141)	S(161)	S(181)
.00	.19285+01	.16711+01	.14218+01	.11935+01	.99811+00	.84643+00	.75214+00	.70386+00	.60932+00
5.00	.19080+01	.16507+01	.14017+01	.11736+01	.97848+00	.82713+00	.73329+00	.68482+00	.59025+00
10.00	.18613+01	.16047+01	.13563+01	.11290+01	.93469+00	.78432+00	.69188+00	.64282+00	.54739+00
15.00	.18144+01	.15589+01	.13117+01	.10856+01	.89274+00	.74404+00	.65405+00	.60405+00	.50771+00
20.00	.17610+01	.15071+01	.12615+01	.10373+01	.84650+00	.70026+00	.61392+00	.56196+00	.46410+00
25.00	.17051+01	.14532+01	.12100+01	.98829+00	.80027+00	.65739+00	.57625+00	.52076+00	.42099+00
30.00	.16427+01	.13937+01	.11534+01	.93502+00	.75071+00	.61228+00	.53863+00	.47784+00	.37563+00
35.00	.15780+01	.13325+01	.10961+01	.88201+00	.70250+00	.56990+00	.50599+00	.43698+00	.33197+00
40.00	.15012+01	.12604+01	.10290+01	.82030+00	.64700+00	.52204+00	.46662+00	.38870+00	.28159+00
45.00	.14134+01	.11785+01	.95364+00	.75196+00	.58675+00	.47197+00	.42253+00	.33616+00	.22663+00
50.00	.13237+01	.10966+01	.88001+00	.68773+00	.53324+00	.43254+00	.38381+00	.28901+00	.17778+00
55.00	.12177+01	.10010+01	.79570+00	.61595+00	.47612+00	.39674+00	.33839+00	.23569+00	.12450+00
60.00	.10839+01	.88158+00	.69195+00	.52975+00	.41112+00	.35857+00	.27592+00	.16668+00	.60353-01
65.00	.93207+00	.75082+00	.58418+00	.44825+00	.34444+00	.31073+00	.20977+00	.98740-01	.10664-01
70.00	.73710+00	.58933+00	.45992+00	.36957+00	.28311+00	.22936+00	.11822+00	.21695-01	.35338-01
75.00	.49988+00	.41801+00	.37324+00	.31023+00	.21005+00	.98814-01	.92525-02	.57346-01	.22559+00
80.00	.41899+00	.31621+00	.29613+00	.95688-01	.88241-02	.57178-01	.22515+00	.48689+00	.84643+00

CARD INPUT FOR MMAX, A, MC, THETA, AND W? NO
DETAILED PRINTOUT? NO

ALPHA	L	L1	SF	PWL(DB)
1.750	1.000	5.000	.1500	-12.239

MODIFIED ALPHA IS: .7006

TABLE A-4B: THE SELF NOISE INTENSITY AND FREQUENCY AT X/D = 25.

DATE 090573

CONVECTION MACH NO.= 7.000 SPEED OF SOUND RATIO= 2.50 VO CODE= 1

SELF NOISE INTENSITY(DECIBELS) WITH FREQUENCY BAND NUMBERS

ANGLE	SEGMENT 1	SEGMENT 2	SEGMENT 3	SEGMENT 4	SEGMENT 5	SEGMENT 6	SEGMENT 7	SEGMENT 8	SEGMENT 9	TOTAL
(DEG) MC	6.86139	6.46181	5.84689	5.08304	4.24571	3.40727	2.62718	1.94626	1.38529	
A	2.35000	2.20000	2.05000	1.90000	1.75000	1.60000	1.45000	1.30000	1.15000	
5.0	3.67(5)	12.31(5)	19.20(6)	25.05(6)	30.19(7)	34.75(8)	40.43(10)	39.89(11)	37.90(13)	44.97
10.0	7.09(5)	15.72(5)	22.62(6)	28.47(6)	33.57(7)	38.20(8)	44.00(10)	43.21(11)	41.27(13)	48.41
15.0	9.38(5)	18.02(5)	24.90(6)	30.76(7)	35.86(8)	40.52(9)	46.55(10)	45.29(11)	43.43(13)	50.71
20.0	11.33(5)	19.95(6)	26.83(6)	32.68(7)	37.78(8)	42.47(9)	48.93(10)	46.93(12)	45.16(13)	52.70
25.0	13.14(5)	21.74(6)	28.60(6)	34.44(7)	39.54(8)	44.29(9)	51.56(10)	48.34(12)	46.67(14)	54.73
30.0	14.93(6)	23.50(6)	30.34(6)	36.16(7)	41.27(8)	46.09(9)	48.49(11)	49.65(12)	48.08(14)	54.68
35.0	16.75(6)	25.29(6)	32.09(7)	37.90(8)	43.02(8)	47.95(10)	55.41(11)	50.91(13)	49.45(14)	58.13
40.0	18.67(6)	27.17(7)	33.94(7)	39.73(8)	44.87(9)	50.00(10)	54.66(11)	52.22(13)	50.87(15)	58.80
45.0	20.72(7)	29.17(7)	35.91(8)	41.69(8)	46.88(9)	52.34(10)	55.05(12)	53.61(14)	52.36(15)	59.83
50.0	22.91(7)	31.31(8)	38.01(8)	43.79(9)	49.09(10)	55.23(11)	55.88(12)	55.06(14)	53.90(16)	61.46
55.0	25.33(8)	33.68(8)	40.36(9)	46.17(9)	51.68(10)	52.03(12)	57.12(13)	56.69(15)	55.62(16)	62.32
60.0	28.11(9)	36.41(9)	43.09(9)	49.01(10)	55.04(11)	59.47(13)	58.82(14)	58.60(16)	57.73(17)	65.30
65.0	31.37(9)	39.64(10)	46.39(10)	52.64(11)	52.68(12)	60.25(14)	60.92(15)	60.78(16)	51.83(17)	66.10
70.0	35.56(11)	43.89(11)	50.97(12)	51.74(13)	61.70(14)	62.71(15)	63.57(18)	55.31(17)	59.29(16)	68.90
75.0	37.37(12)	45.09(13)	50.82(13)	61.10(14)	64.31(15)	66.18(16)	58.29(17)	62.08(16)	56.44(15)	70.42
80.0	48.23(15)	56.40(15)	62.35(16)	58.68(16)	60.27(17)	63.36(16)	59.81(15)	58.59(14)	54.68(14)	68.50
85.0	43.86(15)	50.18(14)	53.86(14)	57.88(14)	58.97(13)	58.94(13)	57.88(13)	56.45(13)	53.33(14)	65.83
90.0	38.90(11)	45.95(11)	50.73(11)	53.98(11)	55.94(11)	56.70(12)	56.31(12)	54.81(13)	52.21(13)	63.37
100.0	32.90(7)	40.18(7)	45.40(8)	49.24(8)	51.89(9)	53.41(10)	53.79(11)	52.28(11)	50.32(12)	60.09
110.0	29.29(5)	36.67(6)	42.03(6)	46.10(7)	49.05(7)	50.94(8)	51.74(9)	50.27(10)	48.73(11)	57.76
120.0	26.64(4)	34.05(4)	39.49(5)	43.68(6)	46.79(6)	48.89(7)	49.96(9)	48.53(10)	47.28(11)	55.85
130.0	24.45(3)	31.88(4)	37.37(4)	41.62(5)	44.84(6)	47.08(7)	48.32(8)	46.93(9)	45.88(10)	54.14

140.0	22.47(3)	29.92(3)	35.44(3)	39.74(4)	43.02(5)	45.34(6)	46.70(7)	45.34(9)	44.44(10)	52.48
150.0	20.51(2)	27.97(3)	33.50(3)	37.83(4)	41.15(5)	43.53(6)	44.97(7)	43.64(8)	42.85(10)	50.73
160.0	18.27(2)	25.73(2)	31.28(3)	35.62(3)	38.97(4)	41.39(6)	42.88(7)	41.57(8)	40.85(9)	48.63
170.0	14.98(2)	22.45(2)	28.00(3)	32.35(3)	35.72(4)	38.16(5)	39.68(7)	38.37(8)	37.69(9)	45.43
	48.02	55.73	61.36	62.97	66.07	67.96	67.01	65.80	63.33	73.99
A2	83.77	83.37	82.72	81.77	80.40	78.48	75.80	72.06	66.77	
	35.58	43.36	48.48	52.33	54.91	55.73	55.08	53.43	50.47	
	37.37	45.09	50.00	53.61	55.95	56.52	55.65	53.84	50.71	
	39.45	47.07	51.70	55.03	57.08	57.38	56.27	54.30	50.98	
	41.81	49.26	53.56	56.54	58.26	58.27	56.93	54.79	51.29	
	44.27	51.43	55.42	58.04	59.41	59.16	57.62	55.31	51.64	
	45.89	52.59	56.72	59.16	60.27	59.93	58.29	55.85	52.03	
	43.86	50.16	55.89	58.98	60.32	60.36	58.87	56.37	52.45	
	34.54	41.02	50.32	55.78	58.47	59.97	59.21	56.83	52.89	
	13.60	20.50	37.32	47.31	53.08	57.90	59.00	57.12	53.33	
	-99.00	-99.00	-99.00	28.18	41.43	52.75	57.72	57.05	53.75	
	-99.00	-99.00	-99.00	-99.00	-99.00	41.76	54.42	56.26	54.09	

TABLE A-4C: THE SHEAR NOISE INTENSITY AND FREQUENCY AT X/D = 25.

DATE 090573

CONVECTION MACH NO.= 7.000 SPEED OF SOUND RATIO= 2.50 VO CODE= 1

SHEAR NOISE INTENSITY(DECIBELS) WITH FREQUENCY BAND NUMBERS

ANGLE	SEGMENT 1	SEGMENT 2	SEGMENT 3	SEGMENT 4	SEGMENT 5	SEGMENT 6	SEGMENT 7	SEGMENT 8	SEGMENT 9	TOTAL
(DEG) MC	6.86139	6.46181	5.84689	5.08304	4.24571	3.40727	2.62718	1.94626	1.38529	
A	2.35000	2.20000	2.05000	1.90000	1.75000	1.60000	1.45000	1.30000	1.15000	
5.0	-4.04(3)	4.41(3)	11.53(4)	18.10(5)	24.48(6)	31.21(7)	40.27(8)	41.17(9)	39.06(11)	45.25
10.0	-.68(3)	7.77(4)	14.90(4)	21.47(5)	27.87(6)	34.63(7)	43.86(8)	44.42(9)	42.36(11)	48.62
15.0	1.57(3)	10.01(4)	17.14(4)	23.72(5)	30.14(6)	36.96(7)	46.48(8)	46.44(9)	44.44(11)	50.88
20.0	3.45(3)	11.89(4)	19.01(4)	25.61(5)	32.06(6)	38.96(7)	49.00(8)	48.01(10)	46.09(11)	52.86
25.0	5.20(4)	13.63(4)	20.75(5)	27.35(5)	33.85(6)	40.87(7)	51.86(9)	49.35(10)	47.52(12)	54.93
30.0	6.94(4)	15.35(4)	22.47(5)	29.09(6)	35.64(6)	42.83(8)	48.49(9)	50.58(10)	48.85(12)	54.56
35.0	8.71(4)	17.10(5)	24.22(6)	30.87(6)	37.50(7)	44.93(8)	56.34(9)	51.77(11)	50.13(12)	58.58
40.0	10.60(5)	18.98(5)	26.10(5)	32.78(6)	39.54(7)	47.32(8)	55.52(10)	52.99(11)	51.45(13)	58.91
45.0	12.65(5)	21.02(5)	28.15(6)	34.90(7)	41.83(8)	50.19(9)	55.85(10)	54.29(12)	52.83(14)	59.86

50.0	14.91(5)	23.25(6)	30.41(6)	37.27(7)	44.49(8)	53.89(9)	56.62(11)	55.65(12)	54.27(14)	61.38
55.0	17.49(6)	25.83(6)	33.05(7)	40.09(8)	47.79(9)	52.03(10)	57.79(13)	57.18(13)	56.88(15)	62.41
60.0	20.56(7)	28.93(7)	36.28(8)	43.66(9)	52.30(10)	60.14(11)	59.38(12)	58.96(14)	57.86(15)	65.43
65.0	24.41(8)	32.86(8)	40.50(9)	48.59(10)	52.68(11)	60.86(12)	61.36(13)	60.99(15)	51.83(15)	66.30
70.0	29.80(9)	38.52(9)	46.89(10)	51.74(11)	61.71(12)	63.18(13)	63.82(14)	55.31(15)	55.68(14)	68.38
75.0	37.37(11)	45.09(11)	50.82(12)	61.70(13)	64.74(14)	66.38(15)	58.29(15)	57.34(14)	47.60(14)	70.10
80.0	49.23(13)	57.04(14)	62.78(14)	58.68(15)	60.27(15)	60.36(14)	50.95(13)	46.72(13)	40.36(13)	67.45
85.0	43.86(13)	50.18(13)	53.86(12)	44.70(12)	43.89(12)	42.05(12)	39.28(12)	36.22(12)	31.52(12)	56.59
90.0	-99.00(9)	-99.00(9)	-99.00(9)	-99.00(10)	-99.00(10)	-99.00(10)	-99.00(11)	-99.00(11)	-99.00(12)	-89.46
100.0	15.43(6)	22.42(6)	27.46(8)	31.23(7)	33.87(7)	35.37(8)	35.66(9)	33.93(10)	31.56(11)	41.92
110.0	14.14(4)	21.29(4)	26.63(5)	30.83(5)	34.04(6)	36.25(7)	37.36(8)	36.09(9)	34.54(10)	43.21
120.0	12.39(3)	19.62(3)	25.11(3)	29.54(4)	33.06(5)	35.67(6)	37.28(7)	36.32(8)	35.36(9)	43.04
130.0	10.68(2)	17.96(2)	23.53(3)	28.09(3)	31.80(4)	34.66(5)	36.60(6)	35.87(8)	35.33(9)	42.36
140.0	8.99(1)	16.29(1)	21.92(2)	26.56(3)	30.39(4)	33.42(5)	35.58(6)	35.01(7)	34.78(8)	41.38
150.0	7.20(1)	14.52(1)	20.18(1)	24.88(2)	28.78(3)	31.92(4)	34.23(6)	33.78(7)	33.76(8)	40.08
160.0	5.06(1)	12.40(1)	18.08(1)	22.81(2)	26.77(3)	29.98(4)	32.38(5)	32.00(7)	32.13(8)	38.26
170.0	1.83(0)	9.17(1)	14.87(1)	19.62(2)	23.60(3)	26.85(4)	29.31(5)	28.98(7)	29.19(8)	35.21
	47.79	55.48	60.99	61.26	65.81	67.27	65.72	63.40	60.41	72.68

TABLE A-46: THE TOTAL NOISE INTENSITY AT X/D = 25.

DATE 090573

CONVECTION MACH NO.= 7.000 SPEED OF SOUND RATIO= 2.50 VO CODE= 1

TOTAL NOISE INTENSITY(DECIBELS)

ANGLE		SEGMENT 1	SEGMENT 2	SEGMENT 3	SEGMENT 4	SEGMENT 5	SEGMENT 6	SEGMENT 7	SEGMENT 8	SEGMENT 9	TOTAL
(DEG)	MC	6.86139	6.46181	5.84689	5.08304	4.24571	3.40727	2.62718	1.94626	1.38529	
	A	2.35000	2.20000	2.05000	1.90000	1.75000	1.60000	1.45000	1.30000	1.15000	
5.0		4.35	12.96	19.88	25.85	31.18	36.34	43.36	43.58	41.53	48.12
10.0		7.76	16.37	23.29	29.26	34.60	39.79	46.94	46.86	44.86	51.53
15.0		10.05	18.66	25.57	31.54	36.89	42.10	49.63	48.91	46.97	53.81
20.0		11.99	20.58	27.49	33.45	38.81	44.07	51.97	50.51	48.66	55.79
25.0		13.79	22.36	29.26	35.21	40.57	45.92	54.72	51.88	50.12	57.84
30.0		15.57	24.12	31.80	36.94	42.32	47.77	51.80	53.15	51.49	57.58
35.0		17.38	25.90	32.75	38.68	44.09	49.71	58.91	54.37	52.81	61.37
40.0		19.30	27.78	34.60	40.53	45.99	51.87	58.12	55.63	54.18	61.72
45.0		21.35	29.79	36.58	42.51	48.06	54.40	58.48	56.97	55.61	62.86
50.0		23.55	31.94	38.71	44.66	50.38	57.62	59.28	58.38	57.10	64.43
55.0		25.99	34.34	41.10	47.13	53.17	55.04	60.48	59.95	58.76	65.88

60.0	28.81	37.13	43.91	50.12	56.89	62.83	62.12	61.79	60.81	68.88
65.0	32.16	40.47	47.38	54.08	55.69	63.58	64.16	63.90	54.84	69.21
70.0	36.58	45.00	52.41	54.75	64.43	65.96	66.71	58.32	60.86	71.40
75.0	40.38	48.10	53.83	64.42	67.54	69.29	61.30	63.34	56.97	73.28
80.0	51.65	59.74	65.58	61.69	63.28	63.37	60.34	58.87	54.84	71.02
85.0	46.87	53.19	56.87	58.09	59.10	59.03	57.94	56.49	53.38	66.32
90.0	38.90	45.95	50.73	53.98	55.94	56.70	56.31	54.81	52.21	63.37
100.0	32.97	40.26	45.47	49.31	51.96	53.48	53.85	52.34	50.38	60.15
110.0	29.42	36.79	42.16	46.23	49.19	51.08	51.90	50.43	48.89	57.91
120.0	26.80	34.21	39.65	43.84	46.97	49.10	50.19	48.79	47.55	56.87
130.0	24.63	32.06	37.55	41.81	45.05	47.32	48.60	47.25	46.24	54.41
140.0	22.66	30.11	35.63	39.94	43.25	45.61	47.02	45.73	44.89	52.81
150.0	20.70	28.16	33.70	38.04	41.39	43.82	45.32	44.07	43.35	51.09
160.0	18.47	25.93	31.48	35.84	39.22	41.69	43.25	42.02	41.39	49.01
170.0	15.18	22.65	28.21	32.58	35.98	38.47	40.06	38.85	38.27	45.82
	50.92	58.62	64.19	65.21	68.58	70.64	69.42	67.77	65.12	76.39

TABLE A-5A: THE WKBJ INTEGRAL AND RUN PARAMETERS AT X/D = 30.

THETA(RAD)	S(21)	S(41)	S(61)	S(81)	S(101)	S(121)	S(141)	S(161)	S(181)
.00	.14402+01	.12772+01	.11285+01	.98434+00	.87768+00	.82193+00	.76473+00	.67096+00	.56117+00
5.00	.14179+01	.12552+01	.10997+01	.96283+00	.85651+00	.80137+00	.74363+00	.64916+00	.53980+00
10.00	.13735+01	.12115+01	.10567+01	.92067+00	.81537+00	.76201+00	.70272+00	.60766+00	.49807+00
15.00	.13238+01	.11629+01	.10094+01	.87476+00	.77123+00	.72059+00	.65884+00	.56280+00	.45285+00
20.00	.12724+01	.11132+01	.96157+00	.82902+00	.72809+00	.68028+00	.61526+00	.51786+00	.40749+00
25.00	.12216+01	.10646+01	.91561+00	.78582+00	.68848+00	.64396+00	.57495+00	.47582+00	.36487+00
30.00	.11619+01	.10080+01	.86216+00	.73625+00	.64375+00	.60231+00	.52865+00	.42745+00	.31598+00
35.00	.11038+01	.95385+00	.81234+00	.69138+00	.60536+00	.56531+00	.48639+00	.38285+00	.27099+00
40.00	.10271+01	.88215+00	.74623+00	.63176+00	.55461+00	.51363+00	.42892+00	.32283+00	.21097+00
45.00	.96186+00	.82358+00	.69498+00	.58914+00	.52489+00	.47696+00	.38599+00	.27736+00	.16628+00
50.00	.88835+00	.75889+00	.64010+00	.54611+00	.50032+00	.43598+00	.33845+00	.22764+00	.11895+00
55.00	.79786+00	.68053+00	.57538+00	.49883+00	.46074+00	.38128+00	.27727+00	.16543+00	.62511-01
60.00	.70805+00	.60837+00	.52371+00	.47844+00	.42140+00	.32808+00	.21854+00	.10868+00	.19636-01
65.00	.60569+00	.53511+00	.48902+00	.44545+00	.36108+00	.25571+00	.14400+00	.44349-01	.27145-02
70.00	.55564+00	.51923+00	.45753+00	.37106+00	.26646+00	.15464+00	.52302-01	.41222-02	.10042+00
75.00	.53771+00	.44351+00	.34084+00	.23039+00	.11972+00	.26386-01	.24429-01	.14949+00	.35584+00
80.00	.28335+00	.17478+00	.75189-01	.41706-02	.55481-01	.20006+00	.42066+00	.72191+00	.11128+01

CARD INPUT FOR MMAX, A, MC, THETA, AND W? NO
DETAILED PRINTOUT? NO

ALPHA	L	L1	SF	PW(DB)
1.750	1.000	3.850	.346	-9.411

MODIFIED ALPHA IS: .6747

TABLE A-5B: THE SELF NOISE INTENSITY AND FREQUENCY AT X/D = 30.

DATE 090573

CONVECTION MACH NO.= 5.400 SPEED OF SOUND RATIO= 2.60 VO CODE= 1

SELF NOISE INTENSITY(DECIBELS) WITH FREQUENCY BAND NUMBERS

ANGLE (DEG)	SEGMENT 1	SEGMENT 2	SEGMENT 3	SEGMENT 4	SEGMENT 5	SEGMENT 6	SEGMENT 7	SEGMENT 8	SEGMENT 9	TOTAL
MC	5.29307	4.98483	4.51046	3.92120	3.27527	2.62846	2.02688	1.50140	1.06865	
A	2.44000	2.28000	2.12000	1.96000	1.80000	1.64000	1.48000	1.32000	1.16000	
5.0	5.71(6)	14.28(6)	21.19(6)	27.23(7)	32.95(8)	43.54(9)	38.70(10)	38.61(12)	37.73(13)	46.61
10.0	9.15(6)	17.72(6)	24.64(7)	30.69(7)	36.45(8)	45.72(9)	42.09(10)	42.05(12)	41.18(13)	49.48
15.0	11.49(6)	20.07(6)	26.99(7)	33.06(7)	38.87(8)	46.79(9)	44.31(11)	44.32(12)	43.47(14)	51.28
20.0	13.46(6)	22.03(6)	28.96(7)	35.04(8)	40.94(8)	47.59(9)	46.08(11)	46.15(12)	45.32(14)	52.78
25.0	15.27(6)	23.83(6)	30.76(7)	36.87(8)	42.89(9)	48.34(10)	47.61(11)	47.75(13)	46.93(14)	54.16
30.0	17.08(6)	25.64(7)	32.57(7)	38.71(8)	44.91(9)	49.18(10)	49.10(11)	49.31(13)	48.48(15)	55.57
35.0	18.91(7)	27.44(7)	34.38(8)	40.57(8)	47.08(9)	50.09(10)	50.53(12)	50.79(13)	49.96(15)	56.99
40.0	20.88(7)	29.41(7)	36.35(8)	42.63(9)	49.75(10)	51.23(11)	52.12(12)	52.42(14)	51.57(15)	58.64
45.0	22.92(7)	31.42(8)	38.39(8)	44.82(9)	49.43(10)	52.44(11)	53.65(13)	53.96(14)	53.06(16)	59.94
50.0	25.17(8)	33.66(8)	40.69(9)	47.41(10)	54.01(11)	53.90(12)	55.34(13)	55.59(15)	54.65(16)	61.94
55.0	27.75(9)	36.25(9)	43.42(10)	50.93(10)	53.82(11)	56.74(13)	57.27(14)	57.39(15)	56.48(16)	63.81
60.0	30.80(9)	39.36(10)	46.93(10)	49.39(11)	55.23(12)	57.88(13)	59.31(15)	59.22(16)	58.86(16)	65.50
65.0	34.94(10)	43.84(11)	46.71(11)	54.08(12)	57.71(13)	80.50(14)	61.54(16)	61.36(16)	52.48(16)	67.00
70.0	35.89(12)	43.70(12)	52.06(13)	57.16(13)	61.22(15)	63.39(16)	63.88(16)	55.74(16)	56.58(15)	68.74
75.0	41.76(13)	50.34(14)	57.05(14)	62.03(15)	64.80(16)	59.14(16)	58.17(18)	59.07(15)	54.89(14)	68.94
80.0	49.34(15)	51.38(16)	55.72(16)	58.16(16)	59.01(15)	58.74(15)	57.54(14)	56.91(14)	53.67(14)	66.11
85.0	37.90(14)	47.13(14)	51.73(13)	54.72(13)	56.40(13)	56.93(13)	56.38(13)	55.38(13)	52.68(13)	63.80
90.0	36.26(11)	43.56(11)	48.60(11)	52.14(11)	54.38(12)	55.44(12)	55.35(12)	54.14(13)	51.82(13)	62.15
100.0	31.58(8)	39.08(8)	44.49(9)	48.52(9)	51.35(10)	53.03(10)	53.55(11)	52.13(12)	50.34(12)	59.75

110.0	28.48(7)	36.06(7)	41.63(7)	45.88(8)	49.61(8)	51.05(9)	51.98(10)	50.47(11)	49.03(12)	57.88
120.0	26.07(6)	33.70(6)	39.36(6)	43.74(7)	47.05(7)	49.32(8)	50.52(9)	48.98(10)	47.81(11)	56.87
130.0	24.03(5)	31.69(5)	37.39(5)	41.87(6)	45.29(7)	47.72(8)	49.11(9)	47.56(10)	46.59(11)	54.77
140.0	22.15(4)	29.82(4)	35.57(5)	40.09(5)	43.60(6)	46.12(7)	47.66(8)	46.11(9)	45.30(10)	53.26
150.0	20.25(4)	27.93(4)	33.70(4)	38.26(5)	41.81(6)	44.42(7)	46.04(8)	44.51(9)	43.81(10)	51.82
160.0	18.05(3)	25.74(4)	31.52(4)	36.10(5)	39.69(6)	42.34(7)	44.03(8)	42.50(9)	41.88(10)	49.59
170.0	14.78(3)	22.47(3)	28.26(4)	32.86(5)	36.47(5)	39.14(6)	40.87(8)	39.35(9)	38.78(10)	46.92
	48.31	53.46	59.05	63.34	66.23	66.32	66.74	65.32	63.06	73.90
A2	82.57	82.09	81.33	80.21	78.64	76.45	73.43	69.24	63.34	
	37.44	45.18	50.23	53.93	55.87	56.61	55.93	54.11	51.34	
	39.18	46.81	51.62	55.06	56.71	57.22	56.35	54.38	51.46	
	41.07	48.54	53.07	56.21	57.57	57.84	56.78	54.67	51.62	
	42.99	50.22	54.48	57.29	58.39	58.43	57.21	54.97	51.80	
	44.51	51.38	55.52	58.08	59.07	58.95	57.63	55.29	52.01	
	44.52	51.00	55.54	58.16	59.39	59.28	57.97	55.60	52.24	
	41.25	47.53	53.42	56.81	59.01	59.24	58.17	55.87	52.48	
	33.32	39.79	48.00	53.09	57.35	58.54	58.10	56.06	52.72	
	19.44	26.25	38.19	46.04	53.68	56.73	57.57	56.11	52.95	
	99.00	99.00	18.91	33.59	47.06	53.20	56.28	55.90	53.13	
	*99.00	*99.00	*99.00	*99.00	35.22	47.01	53.77	55.27	53.24	

TABLE A-5c: THE SHEAR NOISE INTENSITY AND FREQUENCY AT X/D = 30.

DATE 090573

CONVECTION MACH NO.= 5.400 SPEED OF SOUND RATIO= 2.60 VO CODE= 1

SHEAR NOISE INTENSITY(DECIBELS) WITH FREQUENCY BAND NUMBERS

ANGLE		SEGMENT 1	SEGMENT 2	SEGMENT 3	SEGMENT 4	SEGMENT 5	SEGMENT 6	SEGMENT 7	SEGMENT 8	SEGMENT 9	TOTAL
(DEG)	MC	5.293907	4.98483	4.51046	3.92120	3.27527	2.62846	2.02688	1.50140	1.06866	
	A	2.44000	2.28000	2.12000	1.96000	1.80000	1.64000	1.48000	1.32000	1.16000	
5.0		1.24(4)	9.73(4)	17.06(5)	24.13(5)	31.67(6)	45.13(7)	40.37(8)	40.19(10)	39.10(11)	48.05
10.0		4.62(4)	13.12(4)	20.47(5)	27.56(5)	35.14(6)	47.25(7)	43.68(8)	43.53(10)	42.45(11)	50.81
15.0		6.92(4)	15.42(4)	22.78(5)	29.90(6)	37.57(6)	48.25(7)	45.81(9)	45.71(10)	44.64(12)	52.91
20.0		8.84(4)	17.35(5)	24.73(5)	31.90(6)	39.69(7)	48.99(8)	47.50(9)	47.45(10)	46.37(12)	53.90
25.0		10.64(4)	19.14(5)	26.55(5)	33.77(6)	41.75(7)	49.68(8)	48.95(9)	48.95(11)	47.88(12)	55.18
30.0		12.44(5)	20.95(5)	28.39(6)	35.70(6)	43.95(7)	50.46(8)	50.35(10)	50.40(11)	49.31(13)	56.47
35.0		14.29(5)	22.81(5)	30.29(6)	37.71(7)	46.40(8)	51.31(9)	51.70(10)	51.78(12)	50.68(13)	57.79
40.0		16.32(5)	24.85(6)	32.40(6)	40.00(7)	49.46(8)	52.37(9)	53.17(10)	53.27(12)	52.13(14)	59.33

45.0	18.50(6)	27.05(6)	34.69(7)	42.57(7)	49.43(8)	53.52(10)	54.62(11)	54.70(13)	53.51(14)	60.58
50.0	20.99(6)	29.59(7)	37.38(7)	45.73(8)	55.04(9)	54.92(10)	56.21(12)	56.20(13)	54.97(14)	62.80
55.0	23.98(7)	32.65(7)	40.73(8)	50.16(9)	54.81(10)	56.66(11)	58.00(12)	57.84(14)	56.65(14)	64.13
60.0	27.73(8)	36.58(8)	45.30(9)	49.39(10)	56.18(11)	58.71(12)	59.90(13)	59.51(14)	58.91(14)	65.95
65.0	33.10(9)	42.50(9)	46.71(10)	55.03(11)	58.59(12)	61.17(13)	61.92(14)	61.48(15)	52.48(14)	67.45
70.0	35.89(10)	43.70(10)	53.03(11)	58.05(12)	61.92(13)	63.80(14)	64.02(15)	55.74(14)	50.92(13)	68.94
75.0	42.92(12)	51.37(12)	57.91(13)	62.64(13)	65.11(14)	59.14(15)	58.17(14)	52.19(13)	44.93(13)	68.77
80.0	50.08(14)	51.38(14)	55.72(14)	58.16(15)	59.01(14)	51.17(13)	47.13(13)	44.13(12)	38.79(12)	63.58
85.0	37.90(12)	35.54(12)	38.78(12)	40.28(12)	40.43(12)	39.43(12)	37.37(12)	34.88(12)	30.67(12)	47.59
90.0	-99.00(10)	-99.00(10)	-99.00(10)	-99.00(10)	-99.00(10)	-99.00(10)	-99.00(11)	-99.00(11)	-99.00(11)	-89.96
100.0	15.65(7)	22.79(7)	27.96(7)	31.81(8)	34.49(8)	36.00(9)	36.28(10)	34.46(10)	32.05(11)	42.51
110.0	15.29(5)	22.59(5)	28.06(6)	32.35(6)	35.61(7)	37.81(8)	38.85(9)	37.32(9)	35.64(10)	44.82
120.0	14.01(4)	21.40(4)	27.04(5)	31.58(5)	35.18(6)	37.81(7)	39.37(8)	38.08(9)	36.93(10)	44.98
130.0	12.58(3)	20.02(3)	25.75(4)	30.45(4)	34.27(5)	37.19(6)	39.10(7)	38.00(8)	37.26(9)	44.67
140.0	11.06(3)	18.53(3)	24.33(3)	29.13(4)	33.10(5)	36.21(6)	38.38(7)	37.42(8)	37.00(9)	43.94
150.0	9.38(2)	16.88(2)	22.72(3)	27.59(3)	31.64(4)	34.89(5)	37.24(6)	36.38(8)	36.19(9)	42.83
160.0	7.32(2)	14.83(2)	20.69(3)	25.61(3)	29.73(4)	33.06(5)	35.52(6)	34.74(7)	34.71(8)	41.13
170.0	4.13(2)	11.65(2)	17.53(2)	22.46(3)	26.62(4)	30.00(5)	32.53(6)	31.79(7)	31.85(8)	38.15
	48.59	52.41	58.38	62.89	65.90	65.30	65.69	63.42	60.56	72.36

TABLE A-5D: THE TOTAL NOISE INTENSITY AT X/D = 30.

DATE 090573

CONVECTION MACH NO.= 5.400 SPEED OF SOUND RATIO= 2.60 VO CODE= 1

TOTAL NOISE INTENSITY(DECIBELS)

ANGLE (DEG)	SEGMENT 1	SEGMENT 2	SEGMENT 3	SEGMENT 4	SEGMENT 5	SEGMENT 6	SEGMENT 7	SEGMENT 8	SEGMENT 9	TOTAL
MC	5.29307	4.98483	4.51046	3.92120	3.27527	2.62846	2.02668	1.50140	1.06865	
A	2.44080	2.28300	2.12000	1.96000	1.80000	1.64000	1.48000	1.32000	1.16000	
5.0	7.04	15.59	22.61	28.96	35.37	47.42	42.62	42.48	41.48	50.40
10.0	10.46	19.01	26.05	32.41	38.85	49.56	45.97	45.86	44.87	53.20
15.0	12.79	21.35	28.39	34.77	41.28	50.59	48.14	48.08	47.11	54.95
20.0	14.75	23.30	30.35	36.76	43.37	51.36	49.85	49.86	48.89	56.39
25.0	16.55	25.10	32.16	38.60	45.36	52.08	51.34	51.40	50.44	57.71
30.0	18.36	26.91	33.97	40.47	47.47	52.88	52.78	52.90	51.93	59.05
35.0	20.19	28.73	35.81	42.39	49.76	53.75	54.17	54.33	53.34	60.42
40.0	22.18	30.71	37.82	44.52	52.62	54.85	55.69	55.88	54.87	62.01

45.0	24.26	32.78	39.94	46.85	52.44	56.03	57.18	57.35	56.30	63.28
50.0	26.57	35.09	42.35	49.66	57.56	57.45	58.80	58.91	57.83	65.29
55.0	29.27	37.83	45.29	53.58	57.35	59.23	60.66	60.63	59.58	66.88
60.0	32.54	41.20	49.21	52.40	58.74	61.33	62.83	62.38	61.89	68.74
65.0	37.13	46.23	49.72	57.59	61.19	63.86	64.75	64.43	55.49	70.24
70.0	38.90	46.71	55.58	60.63	64.59	66.61	66.96	58.75	57.62	71.85
75.0	45.39	53.90	60.51	65.36	67.97	62.15	61.18	59.88	55.31	71.87
80.0	52.73	54.39	58.73	61.17	62.02	59.44	57.92	57.14	53.81	68.84
85.0	40.91	47.42	51.95	54.88	56.51	57.00	56.43	56.42	52.71	63.90
90.0	36.26	43.56	48.60	52.14	54.38	55.44	55.35	54.14	51.82	62.15
100.0	31.69	39.18	44.58	48.61	51.43	53.11	53.44	52.21	50.40	59.83
110.0	28.68	36.25	41.81	46.07	49.21	51.25	52.49	50.68	49.23	58.08
120.0	26.34	33.95	39.60	44.00	47.33	49.62	50.84	49.32	48.15	56.58
130.0	24.33	31.97	37.68	42.17	45.62	48.08	49.52	48.02	47.07	55.17
140.0	22.48	30.13	35.88	40.43	43.97	46.55	48.14	46.66	45.90	53.74
150.0	20.59	28.26	34.03	38.62	42.21	44.88	46.58	45.13	44.50	52.15
160.0	18.40	26.08	31.86	36.47	40.11	42.82	44.60	43.18	42.64	50.16
170.0	15.14	22.82	28.61	33.24	36.89	39.64	41.87	40.05	39.58	47.02
	51.46	55.98	61.74	66.13	69.08	68.85	69.26	67.48	65.00	75.92

TABLE A-6A: THE WKBJ INTEGRAL AND RUN PARAMETERS AT X/D = 35.

THETA(RAD)	S(21)	S(41)	S(61)	S(81)	S(101)	S(121)	S(141)	S(161)	S(181)
.00	.11804+01	.10843+01	.99683+00	.93206+00	.89936+00	.83009+00	.73591+00	.62830+00	.51616+00
5.00	.11561+01	.10603+01	.97311+00	.90878+00	.87619+00	.80659+00	.71224+00	.60453+00	.49240+00
10.00	.11318+01	.10169+01	.93070+00	.86770+00	.83478+00	.76421+00	.66933+00	.56186+00	.44922+00
15.00	.10614+01	.96791+00	.88393+00	.82276+00	.78936+00	.71718+00	.62141+00	.51300+00	.40090+00
20.00	.10114+01	.92012+00	.83613+00	.78102+00	.74632+00	.67192+00	.57490+00	.46581+00	.35389+00
25.00	.96737+00	.87904+00	.80052+00	.74862+00	.71097+00	.63373+00	.53512+00	.42542+00	.31363+00
30.00	.91094+00	.82664+00	.75283+00	.70891+00	.66498+00	.58431+00	.48378+00	.37329+00	.26197+00
35.00	.86112+00	.78219+00	.71478+00	.68007+00	.62694+00	.54227+00	.43952+00	.32825+00	.21784+00
40.00	.79396+00	.72230+00	.66386+00	.63429+00	.57229+00	.48309+00	.37788+00	.26599+00	.15723+00
45.00	.74617+00	.68472+00	.63799+00	.60738+00	.53635+00	.44212+00	.33434+00	.22228+00	.11652+00
50.00	.70100+00	.65532+00	.63027+00	.57883+00	.49845+00	.39884+00	.28865+00	.17741+00	.77172-01
55.00	.65778+00	.64310+00	.60248+00	.53429+00	.44426+00	.33919+00	.22734+00	.11903+00	.29591-01
60.00	.68527+00	.63432+00	.56897+00	.48535+00	.38569+00	.27582+00	.16439+00	.63924-01	.53344-03
65.00	.67383+00	.59770+00	.51193+00	.41385+00	.30563+00	.19357+00	.88328-01	.97140-02	.42580-01
70.00	.61650+00	.51906+00	.41568+00	.30597+00	.19390+00	.88711-01	.98123-02	.42758-01	.17367+00
75.00	.47195+00	.36006+00	.24778+00	.13916+00	.44938-01	.46719-02	.94690-01	.25739+00	.48988+00
80.00	.12459+00	.44899-01	.63961-02	.67227-01	.19814+00	.39045+00	.64887+00	.98067+00	.13961+01

CARD INPUT FOR MMAX, A, MC, THETA, AND W? NO
DETAILED PRINTOUT? NO

ALPHA	L	L1	SF	PW(DB)
1.600	1.000	3.080	.225	-7.038

MODIFIED ALPHA IS: .6190

TABLE A-6B: THE SELF NOISE INTENSITY AND FREQUENCY AT X/D = 35.

DATE 090573

CONVECTION MACH NO.= 4.300 SPEED OF SOUND RATIO= 2.60 VO CODE= 1

SELF NOISE INTENSITY(DECIBELS) WITH FREQUENCY BAND NUMBERS

ANGLE	SEGMENT 1	SEGMENT 2	SEGMENT 3	SEGMENT 4	SEGMENT 5	SEGMENT 6	SEGMENT 7	SEGMENT 8	SEGMENT 9	TOTAL
(DEG) MC	4.21485	3.96940	3.59166	3.12244	2.60808	2.09303	1.61384	1.19556	.85096	
A	2.44000	2.28000	2.12000	1.96000	1.80000	1.64000	1.48000	1.32000	1.16000	
5.0	6.95(6)	15.48(6)	22.66(6)	30.11(7)	34.73(8)	35.98(9)	37.83(10)	38.50(12)	37.81(13)	44.31
10.0	10.41(6)	18.95(6)	26.16(7)	33.72(7)	37.46(8)	39.44(9)	41.34(11)	42.04(12)	41.35(13)	47.82
15.0	12.80(6)	21.35(6)	28.59(7)	36.38(7)	39.60(8)	41.76(9)	43.73(11)	44.45(12)	43.75(13)	50.19
20.0	14.81(6)	23.37(6)	30.67(7)	38.87(8)	41.27(8)	43.64(10)	45.68(11)	46.40(13)	45.68(14)	52.13
25.0	16.65(6)	25.23(7)	32.60(7)	41.69(8)	42.68(9)	45.28(10)	47.38(11)	48.08(13)	47.32(14)	53.84
30.0	18.55(6)	27.15(7)	34.64(7)	39.83(8)	44.11(9)	46.95(10)	49.10(12)	49.78(13)	48.96(14)	55.36
35.0	20.49(7)	29.11(7)	36.81(8)	44.41(8)	45.49(9)	48.56(11)	50.75(12)	51.35(14)	50.44(14)	57.04
40.0	22.66(7)	31.34(8)	39.49(8)	44.35(9)	47.10(10)	50.40(11)	52.59(13)	53.08(14)	52.07(15)	58.72
45.0	25.04(8)	33.84(8)	41.21(9)	45.07(9)	48.71(10)	52.19(12)	54.30(13)	54.59(14)	53.46(15)	60.28
50.0	28.06(8)	37.30(9)	43.36(9)	46.33(10)	50.58(11)	54.14(12)	56.06(14)	56.08(15)	54.86(15)	61.93
55.0	29.98(9)	38.15(9)	43.38(10)	48.24(11)	52.90(12)	56.43(13)	57.99(14)	57.64(15)	56.61(15)	63.80
60.0	31.01(10)	38.93(10)	45.14(11)	50.80(11)	55.66(13)	58.84(14)	59.78(15)	59.09(15)	57.16(14)	65.08
65.0	32.73(11)	41.31(11)	48.29(12)	54.33(12)	58.93(14)	61.23(15)	61.33(15)	55.18(15)	56.05(14)	66.58
70.0	36.91(12)	45.86(12)	53.11(13)	58.76(14)	62.04(15)	62.85(15)	57.37(15)	58.84(14)	54.22(13)	67.86
75.0	43.87(14)	52.47(14)	58.40(18)	61.70(15)	58.63(15)	58.24(15)	59.27(14)	56.31(13)	53.05(13)	67.20
80.0	43.58(15)	49.95(15)	53.61(15)	55.40(14)	54.98(14)	55.43(13)	56.58(13)	54.78(13)	52.14(13)	63.58
85.0	35.40(13)	42.74(13)	47.73(12)	51.15(12)	53.29(12)	54.27(12)	54.84(12)	53.61(12)	51.37(12)	61.35
90.0	32.75(11)	40.26(11)	45.55(11)	49.35(11)	51.88(11)	53.25(11)	53.49(12)	52.64(12)	50.69(12)	60.11
100.0	29.09(8)	36.76(8)	42.36(9)	46.57(9)	49.59(9)	51.48(10)	51.37(10)	51.01(11)	49.49(11)	58.14
110.0	26.45(7)	34.20(7)	39.95(7)	44.39(8)	47.70(8)	49.93(9)	49.65(10)	49.63(10)	48.41(11)	56.54
120.0	24.31(6)	32.11(6)	37.95(6)	42.53(7)	46.03(7)	48.49(8)	48.13(9)	48.35(10)	47.38(10)	55.12

130.0	22.43(5)	30.26(5)	36.16(6)	40.83(6)	44.46(7)	47.09(8)	46.69(8)	47.10(9)	46.31(10)	53.75
140.0	20.66(4)	28.50(5)	34.44(5)	39.18(6)	42.90(6)	45.65(7)	45.23(8)	45.78(9)	45.15(10)	52.36
150.0	18.82(4)	26.68(4)	32.65(5)	37.43(5)	41.21(6)	44.05(7)	43.62(8)	44.28(9)	43.77(10)	50.80
160.0	16.67(4)	24.53(4)	30.52(4)	35.32(5)	39.15(6)	42.04(7)	41.61(8)	42.34(9)	41.92(9)	48.82
170.0	13.42(4)	21.30(4)	27.29(4)	32.11(5)	35.96(6)	38.89(6)	38.46(7)	39.23(8)	38.86(9)	45.69
	45.45	53.26	58.86	62.72	64.15	65.67	65.42	64.25	62.06	72.29
A2	81.36	80.79	79.92	78.65	76.89	74.46	71.14	66.58	60.18	
	39.41	46.36	51.41	55.05	56.90	57.48	56.66	54.69	51.95	
	41.02	47.79	52.60	55.94	57.52	57.86	56.88	54.80	51.96	
	42.59	49.20	53.73	56.75	58.07	58.20	57.09	54.92	51.99	
	43.82	50.36	54.65	57.36	58.50	58.46	57.26	55.03	52.03	
	44.09	50.84	55.05	57.57	58.68	58.57	57.36	55.14	52.09	
	42.48	49.95	54.47	57.05	58.46	58.43	57.35	55.21	52.16	
	38.19	46.91	52.29	55.40	57.58	57.92	57.15	55.24	52.22	
	30.98	41.28	48.03	52.20	55.74	56.85	56.68	55.17	52.27	
	20.35	32.79	41.36	47.07	52.63	54.97	55.80	54.96	52.28	
	.95	19.61	31.43	39.45	47.84	52.01	54.34	54.55	52.24	
	-99.00	-99.00	12.68	27.17	40.70	47.56	52.07	53.84	52.12	

TABLE A-6c: THE SHEAR NOISE INTENSITY AND FREQUENCY AT X/D = 35.

DATE 090573

CONVECTION MACH NO.= 4.300 SPEED OF SOUND RATIO= 2.60 VO CODE= 1

SHEAR NOISE INTENSITY(DECIBELS) WITH FREQUENCY BAND NUMBERS

ANGLE (DEG)	SEGMENT 1	SEGMENT 2	SEGMENT 3	SEGMENT 4	SEGMENT 5	SEGMENT 6	SEGMENT 7	SEGMENT 8	SEGMENT 9	TOTAL
	MC 4.21485	3.96940	3.59166	3.12244	2.60808	2.09303	1.61384	1.19556	.85098	
	A 2.44000	2.28000	2.12000	1.96000	1.80000	1.64000	1.48000	1.32000	1.16000	
5.0	5.45(4)	14.05(4)	21.93(5)	30.86(5)	36.01(6)	37.97(7)	39.82(8)	40.32(10)	39.34(11)	46.09
10.0	8.87(4)	17.49(4)	26.40(5)	34.46(5)	39.27(6)	41.35(7)	43.24(8)	43.75(10)	42.76(11)	49.49
15.0	11.23(4)	19.86(4)	27.83(5)	37.14(6)	41.33(6)	43.58(7)	45.51(9)	46.03(10)	45.02(11)	51.75
20.0	13.24(4)	21.89(5)	29.94(5)	39.70(6)	42.93(7)	45.38(8)	47.36(9)	47.86(10)	46.81(12)	53.58
25.0	15.12(4)	23.81(5)	31.96(5)	42.67(6)	44.29(7)	46.94(8)	48.96(9)	49.42(11)	48.33(12)	55.20
30.0	17.09(5)	25.81(5)	34.13(6)	39.83(6)	45.65(7)	48.52(8)	50.56(10)	50.97(11)	49.80(12)	56.58
35.0	19.16(5)	27.94(5)	36.52(6)	45.79(7)	46.98(8)	50.05(9)	52.10(10)	52.41(12)	51.15(13)	58.20
40.0	21.52(5)	30.40(6)	39.52(6)	45.68(7)	48.60(8)	51.77(9)	53.78(11)	53.95(12)	52.58(13)	59.72

45.0	24.24(6)	33.30(6)	41.21(7)	46.39(8)	50.67(9)	53.48(10)	55.37(11)	55.32(13)	53.83(13)	61.17
50.0	27.77(6)	37.37(7)	44.60(7)	47.65(8)	51.90(9)	55.35(10)	57.01(12)	56.66(13)	55.10(13)	62.74
55.0	29.98(7)	38.15(7)	44.64(8)	49.53(9)	54.15(10)	57.50(11)	58.74(13)	58.02(13)	56.70(13)	64.47
60.0	32.29(8)	40.21(8)	46.43(9)	52.07(10)	56.82(11)	59.75(12)	60.32(13)	59.29(13)	52.16(13)	65.72
65.0	34.12(9)	42.65(9)	49.58(10)	55.53(11)	59.92(12)	61.87(13)	61.60(13)	55.18(13)	52.72(12)	66.95
70.0	38.42(10)	47.24(11)	54.34(11)	59.75(12)	62.68(13)	63.12(13)	57.37(13)	56.48(13)	47.35(12)	67.88
75.0	45.32(12)	53.63(12)	59.21(13)	62.13(13)	58.63(14)	58.24(13)	54.19(12)	48.14(12)	42.35(12)	66.50
80.0	43.58(14)	49.95(14)	53.61(14)	55.40(13)	48.34(12)	46.22(12)	45.15(11)	41.35(11)	36.83(11)	59.34
85.0	23.39(11)	29.77(11)	33.62(11)	35.79(11)	36.60(11)	36.24(11)	35.46(11)	32.85(11)	29.17(11)	43.48
90.0	-99.00(9)	-99.00(9)	-99.00(9)	-99.00(9)	-99.00(10)	-99.00(10)	-99.00(10)	-99.00(10)	-99.00(10)	-89.46
100.0	14.10(7)	21.38(7)	26.67(7)	30.64(8)	33.43(8)	35.05(8)	34.59(9)	33.72(9)	31.50(10)	41.41
110.0	14.59(5)	22.03(6)	27.62(6)	32.03(6)	35.38(7)	37.64(7)	37.35(8)	37.16(9)	35.55(9)	44.12
120.0	13.80(4)	21.33(4)	27.09(5)	31.77(5)	35.47(6)	38.18(7)	38.04(8)	38.34(8)	37.22(9)	44.88
130.0	12.66(4)	20.24(4)	26.12(4)	30.97(5)	34.91(5)	37.93(6)	37.92(7)	38.61(8)	37.87(9)	44.87
140.0	11.33(3)	18.95(3)	24.90(4)	29.87(4)	33.98(5)	37.22(6)	37.31(7)	38.29(7)	37.86(8)	44.37
150.0	9.78(3)	17.42(3)	23.43(3)	28.47(4)	32.69(4)	36.09(5)	36.26(6)	37.45(7)	37.25(8)	43.43
160.0	7.79(2)	15.45(2)	21.49(3)	26.58(3)	30.88(4)	34.38(5)	34.61(6)	35.94(7)	35.91(8)	41.65
170.0	4.65(2)	12.32(2)	18.37(3)	23.49(3)	27.83(4)	31.39(5)	31.65(6)	33.07(7)	33.14(8)	38.94
	45.70	53.52	59.09	62.83	63.80	65.17	64.12	62.18	59.23	71.88

TABLE A-6D: THE TOTAL NOISE INTENSITY AT X/D = 35.

DATE 090573

CONVECTION MACH NO.= 4.300 SPEED OF SOUND RATIO= 2.60 VO CODE= 1

TOTAL NOISE INTENSITY(DECIBELS)

ANGLE	SEGMENT 1	SEGMENT 2	SEGMENT 3	SEGMENT 4	SEGMENT 5	SEGMENT 6	SEGMENT 7	SEGMENT 8	SEGMENT 9	TOTAL
(DEG) MC	4.21485	3.96940	3.59166	3.12244	2.60808	2.09303	1.61384	1.19556	.85096	
A	2.44000	2.28000	2.12000	1.96000	1.80000	1.64000	1.48000	1.32000	1.16000	
5.0	9.27	17.83	25.32	33.51	38.18	40.10	41.95	42.52	41.65	48.30
10.0	12.72	21.29	28.81	37.12	41.47	43.51	45.40	45.99	45.12	51.74
15.0	15.09	23.68	31.24	39.79	43.56	45.78	47.72	48.32	47.44	54.05
20.0	17.10	25.71	33.33	42.32	45.19	47.61	49.81	50.20	49.29	55.93
25.0	18.97	27.59	35.30	45.21	46.57	49.20	51.25	51.81	50.86	57.58
30.0	20.89	29.54	37.40	42.84	47.96	50.82	52.90	53.43	52.41	59.02
35.0	22.88	31.58	39.68	48.17	49.31	52.38	54.48	54.92	53.82	60.87
40.0	25.14	33.91	42.52	48.08	50.86	54.15	56.24	56.55	55.34	62.26
45.0	27.67	36.59	44.22	48.79	52.46	55.89	57.88	57.98	56.66	63.76

50.0	30.93	40.35	47.04	50.05	54.30	57.80	59.57	59.39	57.99	65.37
55.0	32.99	41.16	47.07	51.94	56.58	60.01	61.39	60.85	59.67	67.16
60.0	34.71	42.63	48.84	54.49	59.29	62.33	63.07	62.20	55.17	68.92
65.0	36.49	45.04	52.00	57.98	62.46	64.57	64.48	58.19	57.71	69.78
70.0	40.74	49.61	56.78	62.30	65.38	66.00	60.38	60.49	55.03	70.68
75.0	47.66	56.10	61.84	64.93	61.64	61.25	60.44	56.93	53.40	69.87
80.0	46.59	52.96	56.62	58.41	55.83	55.92	56.88	54.98	52.26	64.97
85.0	35.67	42.96	47.90	51.28	53.38	54.34	54.89	53.65	51.39	61.42
90.0	32.75	40.26	45.55	49.35	51.88	53.25	53.49	52.64	50.69	60.11
100.0	29.22	36.89	42.47	46.68	49.70	51.58	51.46	51.09	49.50	58.23
110.0	26.72	34.46	40.20	44.63	47.95	50.17	49.90	49.87	48.63	56.78
120.0	24.68	32.45	38.29	42.88	46.40	48.87	48.54	48.76	47.78	55.51
130.0	22.86	30.67	36.57	41.26	44.92	47.59	47.23	47.67	46.90	54.26
140.0	21.14	28.96	34.90	39.66	43.43	46.23	45.88	46.49	45.89	53.00
150.0	19.33	27.17	33.14	37.95	41.79	44.69	44.35	45.10	44.64	51.53
160.0	17.19	25.04	31.03	35.87	39.75	42.73	42.40	43.24	42.89	49.62
170.0	13.97	21.81	27.81	32.67	36.58	39.60	39.28	40.17	39.89	46.52
	48.59	56.40	61.99	65.78	66.99	68.44	67.83	66.35	63.88	74.87

TABLE A-7A: THE WKBJ INTEGRAL AND RUN PARAMETERS AT X/D = 40.

THETA(RAD)	S(21)	S(41)	S(61)	S(81)	S(101)	S(121)	S(141)	S(161)	S(181)
.00	.11457+01	.11027+01	.10487+01	.97843+00	.89198+00	.79233+00	.68385+00	.57167+00	.46557+00
5.00	.11203+01	.10768+01	.10225+01	.95193+00	.86528+00	.76550+00	.65695+00	.54476+00	.43473+00
10.00	.10803+01	.10355+01	.98003+00	.90866+00	.82142+00	.72124+00	.61246+00	.50034+00	.39044+00
15.00	.10427+01	.99562+00	.93856+00	.86563+00	.77741+00	.67656+00	.56742+00	.45518+00	.34578+00
20.00	.10048+01	.95475+00	.89497+00	.82033+00	.73073+00	.62895+00	.51932+00	.40708+00	.29833+00
25.00	.97122+00	.91746+00	.85448+00	.77739+00	.68601+00	.58304+00	.47282+00	.36075+00	.25291+00
30.00	.93466+00	.87647+00	.80963+00	.72954+00	.63598+00	.53158+00	.42069+00	.30878+00	.20254+00
35.00	.90535+00	.84207+00	.77073+00	.68710+00	.59094+00	.48489+00	.37335+00	.26199+00	.15805+00
40.00	.86959+00	.80055+00	.72407+00	.63633+00	.53721+00	.42935+00	.31729+00	.20704+00	.10666+00
45.00	.84859+00	.77313+00	.69086+00	.59850+00	.49608+00	.38637+00	.27415+00	.16600+00	.71360-01
50.00	.81698+00	.73444+00	.64578+00	.54831+00	.44239+00	.33105+00	.21950+00	.11529+00	.30535-01
55.00	.78363+00	.69337+00	.59777+00	.49490+00	.38559+00	.27335+00	.16425+00	.67628-01	.28591-02
60.00	.73457+00	.63613+00	.53336+00	.42523+00	.31337+00	.20224+00	.99584-01	.19470-01	.22995-01
65.00	.65914+00	.55268+00	.44334+00	.33141+00	.21986+00	.11518+00	.29714-01	.13062-01	.10616+00
70.00	.53682+00	.42469+00	.31233+00	.20221+00	.10042+00	.20456-01	.22124-01	.12452+00	.28719+00
75.00	.32207+00	.21618+00	.11723+00	.34645-01	.73871-02	.89591-01	.23218+00	.43222+00	.69327+00

CARD INPUT FOR MMAX, A, MC, THETA, AND W? NO

DETAILED PRINTOUT? NO

ALPHA	L	L1	SF	PW(DB)
1.600	1.000	2.300	.141	-4.724

MODIFIED ALPHA IS: .6514

TABLE A-7B: THE SELF NOISE INTENSITY AND FREQUENCY AT X/D = 40.

DATE 090573

CONVECTION MACH NO.= 3.250 SPEED OF SOUND RATIO= 2.50 VO CODE= 1

SELF NOISE INTENSITY(DECIBELS) WITH FREQUENCY BAND NUMBERS

ANGLE (DEG)		SEGMENT 1	SEGMENT 2	SEGMENT 3	SEGMENT 4	SEGMENT 5	SEGMENT 6	SEGMENT 7	SEGMENT 8	SEGMENT 9	TOTAL
	MC	3.18565	3.00013	2.71463	2.35998	1.97122	1.58194	1.21976	.90362	.64317	
	A	2.35000	2.20000	2.05000	1.90000	1.75000	1.60000	1.45000	1.30000	1.15000	
5.0		8.74(6)	16.51(6)	22.07(7)	26.87(8)	31.10(9)	34.47(10)	36.57(11)	37.14(12)	36.33(13)	42.74
10.0		12.02(6)	19.84(7)	25.48(7)	30.36(8)	34.66(9)	38.10(10)	40.23(11)	40.81(12)	39.99(13)	46.39
15.0		14.05(6)	21.94(7)	27.71(7)	32.69(8)	37.07(9)	40.58(10)	42.73(11)	43.30(12)	42.45(13)	48.86
20.0		15.63(7)	23.60(7)	29.51(7)	34.62(8)	39.10(9)	42.67(10)	44.84(12)	45.37(13)	44.48(13)	50.92
25.0		16.97(7)	25.04(7)	31.11(8)	36.35(8)	40.95(9)	44.57(10)	46.73(12)	47.19(13)	46.23(13)	52.75
30.0		18.26(7)	26.44(7)	32.69(8)	38.09(9)	42.80(10)	46.48(11)	48.59(12)	48.95(13)	47.91(14)	54.55
35.0		19.53(7)	27.81(8)	34.24(8)	39.81(9)	44.64(10)	48.32(11)	50.34(13)	50.55(14)	49.40(14)	56.22
40.0		20.95(8)	29.35(8)	35.97(9)	41.72(9)	46.66(11)	50.33(12)	52.17(13)	52.17(14)	50.92(14)	57.98
45.0		22.42(8)	30.95(9)	37.76(9)	43.68(10)	48.67(11)	52.21(12)	53.77(13)	53.50(14)	52.19(14)	59.63
50.0		24.25(9)	32.92(9)	39.93(10)	46.01(11)	51.00(12)	54.27(13)	55.41(14)	54.83(14)	53.70(14)	61.24
55.0		26.49(9)	35.31(10)	42.52(10)	48.69(11)	53.50(12)	56.26(13)	56.82(14)	56.99(14)	55.07(14)	62.43
60.0		29.46(10)	38.46(11)	45.81(11)	51.90(12)	56.76(13)	58.06(14)	57.98(14)	57.53(14)	54.02(13)	64.31
65.0		33.54(11)	42.67(12)	49.93(12)	55.39(13)	58.45(14)	59.23(14)	59.06(14)	58.72(14)	52.13(13)	65.06
70.0		38.94(13)	47.77(13)	54.04(14)	57.79(14)	59.28(14)	56.93(14)	55.38(14)	54.35(13)	51.05(13)	64.78
75.0		42.73(14)	50.15(14)	54.55(14)	55.35(14)	55.84(14)	56.38(13)	54.83(13)	52.88(13)	50.25(12)	63.37
80.0		38.67(14)	44.90(14)	48.48(13)	48.78(13)	53.06(13)	53.55(12)	53.14(12)	51.83(12)	49.60(12)	60.27
85.0		31.10(12)	38.59(12)	43.79(12)	47.45(12)	50.56(12)	51.81(12)	51.91(12)	50.98(12)	49.03(12)	58.55
90.0		29.41(11)	37.01(11)	42.39(11)	46.30(11)	48.97(11)	50.49(11)	50.90(11)	50.25(11)	48.52(12)	57.46
100.0		26.79(9)	34.51(9)	40.13(9)	44.37(9)	46.46(10)	48.42(10)	49.26(10)	49.00(11)	47.61(11)	55.75

110.0	24.72(7)	32.51(8)	38.27(8)	42.72(8)	44.52(9)	46.75(9)	47.89(10)	47.91(10)	46.77(11)	54.38
120.0	22.94(6)	30.76(7)	36.63(7)	41.22(7)	42.85(8)	45.28(9)	46.64(9)	46.87(10)	45.93(10)	53.14
130.0	21.30(6)	29.15(6)	35.08(6)	39.78(7)	41.32(7)	43.89(8)	45.41(9)	45.82(9)	45.06(10)	51.95
140.0	19.68(5)	27.56(5)	33.53(6)	38.31(6)	39.78(7)	42.47(8)	44.12(8)	44.68(9)	44.06(10)	50.20
150.0	17.96(5)	25.85(5)	31.86(5)	36.68(6)	38.12(7)	40.89(7)	42.65(8)	43.32(9)	42.81(10)	49.26
160.0	15.88(5)	23.77(5)	29.80(5)	34.66(6)	36.08(6)	38.90(7)	40.73(8)	41.49(9)	41.07(10)	47.38
170.0	12.68(4)	20.58(5)	26.62(5)	31.50(6)	32.91(6)	35.76(7)	37.63(8)	38.45(9)	38.08(9)	44.31
	43.50.	51.23	56.58	59.91	62.40	63.26	63.32	62.14	59.96	70.10
A2	79.59	78.91	77.88	76.42	74.41	71.68	68.00	63.01	56.11	
	40.77	47.62	52.36	55.52	57.60	57.12	56.12	54.12	51.36	
	41.78	48.50	53.03	55.93	57.23	57.23	56.14	54.09	51.28	
	42.53	49.18	53.51	56.18	57.35	57.28	56.13	54.06	51.21	
	42.77	49.46	53.68	56.17	57.30	57.24	56.08	54.02	51.15	
	42.13	49.06	53.32	55.76	57.00	57.08	55.96	53.96	51.10	
	40.21	47.64	52.18	54.77	56.35	56.72	55.74	53.86	51.05	
	36.72	44.90	50.02	53.02	55.20	56.10	55.38	53.72	50.99	
	31.55	40.67	46.62	50.32	53.42	55.12	54.83	53.50	50.92	
	24.50	34.80	41.83	46.46	50.82	53.67	54.00	53.16	50.82	
	14.60	26.76	35.28	41.19	47.22	51.60	52.81	52.68	50.68	
	3.91	14.35	25.90	33.83	42.28	48.73	51.15	51.99	50.47	

TABLE A-7C: THE SHEAR NOISE INTENSITY AND FREQUENCY AT X/D = 40.

DATE 090573

CONVECTION MACH NO.= 3.250 SPEED OF SOUND RATIO= 2.50 VO CODE= 1

SHEAR NOISE INTENSITY(DECIBELS) WITH FREQUENCY BAND NUMBERS

ANGLE (DEG)	SEGMENT 1	SEGMENT 2	SEGMENT 3	SEGMENT 4	SEGMENT 5	SEGMENT 6	SEGMENT 7	SEGMENT 8	SEGMENT 9	TOTAL
MC	3.18565	3.00013	2.71463	2.35998	1.97122	1.58194	1.21976	.90362	.64317	
A	2.35000	2.20000	2.05000	1.90000	1.75000	1.60000	1.45000	1.30000	1.15000	
5.0	10.96(4)	18.77(5)	24.43(5)	29.36(6)	33.70(7)	37.09(8)	39.04(9)	39.28(10)	38.05(10)	44.99
10.0	14.18(4)	22.04(5)	27.78(5)	32.77(6)	37.17(7)	40.61(8)	42.57(9)	42.80(10)	41.55(11)	48.50
15.0	16.16(5)	24.09(5)	29.93(5)	35.02(6)	39.49(7)	42.97(8)	44.94(9)	45.13(10)	43.85(11)	50.63
20.0	17.69(5)	25.69(5)	31.67(6)	36.87(6)	41.42(7)	44.94(8)	46.89(9)	47.03(11)	45.69(11)	52.75
25.0	19.00(5)	27.08(5)	33.21(6)	38.54(6)	43.17(7)	46.72(9)	48.63(10)	48.68(11)	47.27(11)	54.43
30.0	20.26(5)	28.44(6)	34.73(6)	40.20(7)	44.92(8)	48.49(9)	50.31(10)	50.24(11)	48.74(12)	56.06
35.0	21.51(6)	29.78(6)	36.25(6)	41.86(7)	46.67(8)	50.21(9)	51.89(11)	51.65(12)	50.05(12)	57.59

40.0	32.91(6)	31.29(6)	37.93(7)	43.69(8)	48.58(9)	52.85(10)	53.52(11)	53.04(12)	51.35(12)	59.17
45.0	24.42(6)	32.90(7)	39.71(7)	45.61(8)	50.51(9)	53.80(10)	54.94(12)	54.19(12)	52.47(12)	60.61
50.0	26.27(7)	34.87(7)	41.86(8)	47.88(9)	52.72(10)	55.67(11)	56.34(12)	55.29(12)	53.81(12)	62.16
55.0	28.56(8)	37.30(8)	44.44(9)	50.51(10)	55.08(11)	57.43(12)	57.50(12)	56.25(12)	54.07(12)	63.29
60.0	31.59(9)	40.46(9)	47.69(10)	53.98(10)	57.49(11)	58.91(12)	58.37(13)	57.60(12)	54.93(12)	64.85
65.0	35.72(10)	44.65(10)	51.68(11)	54.78(11)	59.38(12)	59.68(13)	59.16(13)	57.72(12)	47.21(11)	65.52
70.0	41.02(11)	49.51(11)	55.35(12)	58.61(12)	59.85(13)	56.93(13)	55.38(12)	49.02(12)	43.08(11)	64.82
75.0	43.95(12)	50.95(13)	54.95(13)	55.35(13)	55.84(12)	52.82(12)	47.74(11)	43.49(11)	38.82(11)	61.58
80.0	38.67(13)	44.90(12)	48.48(12)	41.90(12)	44.19(11)	42.80(11)	40.64(11)	37.67(11)	33.84(11)	52.78
85.0	17.48(10)	24.15(10)	28.39(10)	31.00(10)	33.10(10)	33.89(10)	31.99(10)	29.83(10)	26.59(10)	39.71
90.0	-99.00(9)	-99.00(9)	-99.00(9)	-99.00(9)	-99.00(9)	-99.00(10)	-99.00(10)	-99.00(10)	-99.00(10)	-89.46
100.0	12.46(7)	19.77(7)	25.05(7)	28.98(8)	30.76(8)	32.38(9)	32.79(9)	31.96(9)	29.83(10)	39.33
110.0	14.01(6)	21.45(6)	27.01(6)	31.36(7)	33.10(7)	35.26(8)	36.26(8)	35.99(9)	34.35(9)	42.64
120.0	13.86(5)	21.39(5)	27.13(5)	31.75(6)	33.50(6)	36.06(7)	37.50(8)	37.67(8)	36.45(9)	43.86
130.0	13.14(4)	20.73(4)	26.59(5)	31.41(5)	33.17(6)	36.03(7)	37.81(7)	38.35(8)	37.47(9)	44.24
140.0	12.10(4)	19.72(4)	25.68(4)	30.62(5)	32.42(5)	35.49(6)	37.53(7)	38.36(8)	37.76(8)	44.05
150.0	10.74(3)	18.39(4)	24.40(4)	29.44(4)	31.26(5)	34.49(6)	36.73(7)	37.78(7)	37.41(8)	43.34
160.0	8.88(3)	16.55(3)	22.60(4)	27.70(4)	29.53(5)	32.88(6)	35.25(6)	36.46(7)	36.25(8)	41.95
170.0	5.80(3)	13.48(3)	19.55(4)	24.69(4)	26.54(5)	29.94(6)	32.39(6)	33.70(7)	33.60(8)	39.14
	44.33	51.90	57.09	60.11	62.37	62.61	62.36	60.36	56.90	69.33

TABLE A-7D: THE TOTAL NOISE INTENSITY AT X/D = 40.

DATE 090573

CONVECTION MACH NO.= 3.250 SPEED OF SOUND RATIO= 2.50 VO CODE= 1

TOTAL NOISE INTENSITY(DECIBELS)

ANGLE	SEGMENT 1	SEGMENT 2	SEGMENT 3	SEGMENT 4	SEGMENT 5	SEGMENT 6	SEGMENT 7	SEGMENT 8	SEGMENT 9	TOTAL
(DEG) MC	3.18565	3.00013	2.71463	2.35998	1.97122	1.58194	1.21976	.90362	.64317	
λ	2.35000	2.20000	2.05000	1.90000	1.75000	1.60000	1.45000	1.30000	1.15000	
5.0	13.00	20.80	26.42	31.30	35.60	38.99	40.99	41.35	40.29	47.02
10.0	16.24	24.09	29.79	34.74	39.10	42.54	44.57	44.93	43.85	50.58
15.0	18.25	26.15	31.97	37.02	41.46	44.95	46.98	47.32	46.21	52.97
20.0	19.79	27.78	33.74	38.90	43.42	46.96	49.00	49.29	48.14	54.94
25.0	21.11	29.19	35.30	40.59	45.21	48.79	50.79	51.01	49.79	56.68
30.0	22.39	30.56	36.84	42.28	47.00	50.61	52.55	52.66	51.35	58.38
35.0	23.64	31.92	38.37	43.96	48.78	52.38	54.20	54.14	52.75	59.97

40.0	25.05	33.43	40.07	45.83	50.74	54.28	56.91	55.64	54.15	61.62
45.0	26.54	35.04	41.85	47.76	52.70	56.08	57.40	56.87	55.34	63.11
50.0	28.39	37.01	44.01	50.06	54.95	58.03	58.91	58.08	56.77	64.74
55.0	30.66	39.43	46.59	52.70	57.37	59.89	60.19	59.13	54.08	65.89
60.0	33.66	42.58	49.86	55.83	59.89	61.51	61.19	60.58	56.11	67.60
65.0	37.78	46.78	53.90	59.15	61.95	62.47	62.12	56.73	53.35	68.91
70.0	43.12	51.74	57.75	61.23	62.48	59.94	58.39	55.47	51.69	67.81
75.0	46.39	53.58	57.76	58.36	58.85	57.74	55.60	53.35	50.55	65.57
80.0	41.68	47.92	51.50	49.59	53.59	53.90	53.38	51.99	49.71	60.98
85.0	31.29	38.75	43.91	47.54	50.74	51.87	51.95	51.01	49.08	58.81
90.0	29.41	37.01	42.39	46.30	48.97	50.49	50.90	50.25	48.52	57.46
100.0	26.95	34.65	40.27	44.50	46.57	48.52	49.36	49.09	47.68	55.85
110.0	25.07	32.83	38.59	43.03	44.82	47.06	48.18	48.18	47.01	54.66
120.0	23.44	31.24	37.09	41.69	43.33	45.77	47.14	47.36	46.40	53.63
130.0	21.91	29.73	35.85	40.37	41.94	44.55	46.11	46.54	45.75	52.63
140.0	20.38	28.22	34.19	38.99	40.52	43.26	44.98	45.59	44.97	51.55
150.0	18.72	26.57	32.57	37.43	38.94	41.78	43.64	44.39	43.91	50.25
160.0	16.67	24.53	30.56	35.46	36.95	39.87	41.81	42.68	42.31	48.47
170.0	13.49	21.35	27.40	32.32	33.81	36.77	38.77	39.70	39.41	45.46
	46.95	54.59	59.85	63.02	65.39	65.96	65.88	64.35	61.71	72.74

TABLE A-8A: THE WKBJ INTEGRAL AND RUN PARAMETERS AT X/D = 50.

YMETA(NA0)	S(21)	S(41)	S(61)	S(81)	S(101)	S(121)	S(141)	S(161)	S(181)
.00	.12251+01	.11290+01	.10294+01	.92512+00	.81622+00	.70436+00	.59231+00	.48359+00	.38252+00
5.00	.11953+01	.10990+01	.99937+00	.89496+00	.78599+00	.67411+00	.56207+00	.45345+00	.35256+00
10.00	.11509+01	.10541+01	.95410+00	.84939+00	.74022+00	.62826+00	.51630+00	.40745+00	.30762+00
15.00	.11090+01	.10066+01	.90594+00	.80073+00	.69122+00	.57915+00	.46734+00	.35949+00	.26016+00
20.00	.10582+01	.95985+00	.85632+00	.75242+00	.64247+00	.53025+00	.41871+00	.31184+00	.21384+00
25.00	.10107+01	.91113+00	.80848+00	.70170+00	.59120+00	.47887+00	.36775+00	.26166+00	.16632+00
30.00	.96037+00	.85928+00	.75528+00	.64744+00	.53633+00	.42397+00	.31357+00	.20940+00	.11714+00
35.00	.91984+00	.81697+00	.71138+00	.60236+00	.49064+00	.37844+00	.26919+00	.16759+00	.80670-01
40.00	.87295+00	.76803+00	.66068+00	.55040+00	.43820+00	.32651+00	.21916+00	.12146+00	.41436-01
45.00	.82846+00	.72131+00	.61209+00	.50064+00	.38826+00	.27779+00	.17360+00	.82065-01	.14303-01
50.00	.77305+00	.66362+00	.55262+00	.44033+00	.32851+00	.22057+00	.12183+00	.40787-01	.15872+02
55.00	.70215+00	.59068+00	.47841+00	.36621+00	.25653+00	.15374+00	.65053-01	.48791-02	.36934-01
60.00	.60850+00	.49602+00	.38396+00	.27409+00	.17006+00	.78285-01	.11327-01	.26514-01	.11761+00
65.00	.47974+00	.36927+00	.26148+00	.15977+00	.70540-01	.73627-02	.33045-01	.12935+00	.27032+00
70.00	.29334+00	.19447+00	.10379+00	.29899-01	.67698-02	.77694-01	.19671+00	.35908+00	.56459+00
75.00	.27052-01	.24038-02	.53074-01	.14517+00	.27586+00	.44833+00	.65872+00	.91571+00	.12207+01

CARD INPUT FOR MMAX, A, MC, THETA, AND W? NO
DETAILED PRINTOUT? NO

ALPHA	L	L1	SF	PW(DB)
1.300	1.000	1.500	.4065	-.760

MODIFIED ALPHA IS: .6749

TABLE A-8B: THE SELF NOISE INTENSITY AND FREQUENCY AT X/D = 50.

DATE 090573

CONVECTION MACH NO.= 2.100 SPEED OF SOUND RATIO= 2.10 VO CODE= 2

SELF NOISE INTENSITY(DECIBELS) WITH FREQUENCY BAND NUMBERS

ANGLE (DEG)	SEGMENT 1	SEGMENT 2	SEGMENT 3	SEGMENT 4	SEGMENT 5	SEGMENT 6	SEGMENT 7	SEGMENT 8	SEGMENT 9	TOTAL
MC	2.05842	1.93854	1.75407	1.52491	1.27371	1.02218	.78815	.58388	.41559	
A	1.99000	1.88000	1.77000	1.66000	1.55000	1.44000	1.33000	1.22000	1.11000	
5.0	12.36(6)	17.07(7)	20.74(7)	24.03(8)	26.96(9)	29.24(10)	30.64(11)	31.26(11)	31.44(11)	37.53
10.0	15.95(7)	20.71(7)	24.44(7)	27.81(8)	30.80(9)	33.12(10)	34.51(11)	35.10(11)	35.24(11)	41.36
15.0	18.43(7)	23.24(7)	27.04(8)	30.48(8)	33.54(9)	35.87(10)	37.23(11)	37.76(11)	37.85(11)	44.85
20.0	20.49(7)	25.36(7)	29.24(8)	32.76(9)	35.97(10)	38.19(11)	39.47(11)	39.91(12)	39.94(12)	46.25
25.0	22.43(7)	27.37(8)	31.33(8)	34.93(9)	38.07(10)	40.33(11)	41.49(12)	41.80(12)	41.75(12)	48.23
30.0	24.37(8)	29.39(8)	33.45(9)	37.13(9)	40.27(10)	42.40(11)	43.38(12)	43.53(12)	43.41(12)	50.12
35.0	26.26(8)	31.36(8)	35.50(9)	39.21(10)	42.26(11)	44.18(12)	44.90(12)	44.87(12)	44.72(12)	51.70
40.0	28.35(8)	33.55(9)	37.76(9)	41.47(10)	44.34(11)	45.93(12)	46.33(12)	46.10(12)	46.05(12)	53.29
45.0	30.61(9)	35.89(9)	40.14(10)	43.73(11)	46.26(11)	47.39(12)	47.42(12)	47.06(12)	47.63(12)	54.77
50.0	33.26(9)	38.62(10)	42.83(10)	46.13(11)	48.09(12)	48.64(12)	48.32(12)	48.06(12)	46.57(12)	55.85
55.0	36.41(10)	41.78(11)	45.75(11)	48.44(12)	49.61(12)	49.55(13)	49.05(12)	48.22(12)	46.40(12)	56.98
60.0	40.01(11)	45.16(11)	48.48(12)	50.19(12)	50.47(13)	50.01(13)	49.55(12)	47.86(12)	45.16(11)	57.88
65.0	43.28(12)	47.76(12)	50.01(12)	50.69(13)	50.51(13)	50.30(12)	48.30(12)	45.95(12)	44.40(11)	58.15
70.0	44.37(13)	47.99(13)	49.48(13)	51.25(13)	49.91(12)	47.52(12)	46.04(12)	44.90(11)	43.83(11)	57.50
75.0	45.12(13)	47.42(13)	47.83(12)	46.27(12)	45.85(12)	45.36(11)	44.80(11)	44.14(11)	43.37(11)	55.33
80.0	34.95(12)	40.92(11)	42.60(11)	43.51(11)	43.94(11)	44.04(11)	43.89(11)	43.53(11)	42.98(11)	52.38
85.0	33.99(10)	38.49(10)	40.53(10)	41.82(10)	42.62(10)	43.04(10)	43.15(10)	43.01(11)	42.62(11)	51.25
90.0	33.14(10)	36.82(10)	39.04(10)	40.54(10)	41.56(10)	42.20(10)	42.52(10)	42.54(10)	42.30(10)	50.41
100.0	31.65(8)	34.36(8)	36.78(9)	38.55(9)	39.86(9)	40.82(9)	41.43(10)	41.72(10)	41.70(10)	49.11
110.0	30.32(7)	32.48(7)	35.02(8)	36.95(8)	38.47(8)	39.64(9)	40.47(9)	40.97(9)	41.13(10)	48.85
120.0	29.06(7)	30.87(7)	33.49(7)	35.54(7)	37.21(8)	38.55(8)	39.57(9)	40.24(9)	40.55(10)	47.09

130.0	27.80(6)	29.37(6)	32.05(6)	34.19(7)	35.98(7)	37.47(8)	38.65(8)	39.47(9)	39.91(9)	46.15
140.0	26.47(6)	27.88(6)	30.60(6)	32.81(6)	34.70(7)	36.31(8)	37.62(8)	38.59(9)	39.14(9)	45.13
150.0	24.95(5)	26.25(5)	29.00(6)	31.27(6)	33.23(7)	34.93(7)	36.36(8)	37.45(9)	38.12(9)	43.88
160.0	23.00(5)	24.23(5)	27.01(5)	29.31(6)	31.32(7)	33.10(7)	34.62(8)	35.81(8)	36.57(9)	42.16
170.0	19.88(5)	21.07(5)	23.86(5)	26.18(6)	28.23(6)	30.05(7)	31.63(8)	32.89(8)	33.71(9)	39.20
	47.72	51.48	53.58	54.98	55.39	55.38	55.04	54.48	53.81	63.57
A2	75.70	74.82	73.52	71.70	69.26	66.04	61.83	56.33	49.04	
	50.01	52.79	53.83	53.93	53.27	52.15	50.83	49.15	47.32	
	49.90	52.65	53.60	53.66	52.96	51.86	50.60	48.97	47.20	
	49.44	52.23	53.14	53.24	52.56	51.52	50.35	48.77	47.08	
	48.55	51.45	52.40	52.63	52.03	51.11	50.06	48.57	46.95	
	47.13	50.23	51.31	51.78	51.34	50.60	49.74	48.34	46.81	
	45.12	48.50	49.80	50.63	50.44	49.96	49.35	48.09	46.66	
	42.45	46.20	47.83	49.14	49.30	49.17	48.89	47.80	46.49	
	39.09	43.27	45.32	47.24	47.87	48.19	48.33	47.46	46.30	
	34.97	39.66	42.22	44.88	46.08	46.98	47.64	47.06	46.09	
	29.91	35.23	38.40	41.95	43.87	45.47	46.81	46.58	45.85	
	23.48	29.70	33.67	38.36	41.14	43.62	45.78	45.99	45.56	

TABLE A-8C: THE SHEAR NOISE INTENSITY AND FREQUENCY AT X/D = 50.

DATE 090573

CONVECTION MACH NO.= 2.100 SPEED OF SOUND RATIO= 2.10 VO CODE= 2

SHEAR NOISE INTENSITY(DECIBELS) WITH FREQUENCY BAND NUMBERS

ANGLE	SEGMENT 1	SEGMENT 2	SEGMENT 3	SEGMENT 4	SEGMENT 5	SEGMENT 6	SEGMENT 7	SEGMENT 8	SEGMENT 9	TOTAL
(DEG) MC	2.05842	1.93854	1.75407	1.52491	1.27371	1.02218	.78815	.58388	.41559	
	1.99000	1.88000	1.77000	1.66000	1.55000	1.44000	1.33000	1.22000	1.11000	
5.0	16.13(4)	20.81(5)	24.51(5)	27.84(6)	30.72(7)	32.74(7)	33.65(8)	33.66(9)	33.25(9)	40.36
10.0	19.65(4)	24.37(5)	28.11(5)	31.50(6)	34.42(7)	36.45(8)	37.32(9)	37.29(9)	36.84(9)	44.01
15.0	22.05(5)	26.81(5)	30.61(6)	34.06(6)	37.01(7)	39.02(8)	39.83(9)	39.72(9)	39.22(9)	46.50
20.0	24.06(5)	28.86(5)	32.72(6)	36.22(7)	39.19(7)	41.13(8)	41.83(9)	41.62(10)	41.07(10)	48.50
25.0	25.94(5)	30.79(6)	34.72(6)	38.27(7)	41.22(8)	43.05(9)	43.58(9)	43.24(10)	42.63(10)	50.29
30.0	27.83(5)	32.75(6)	36.75(6)	40.34(7)	43.22(8)	44.86(9)	45.18(10)	44.68(10)	44.02(10)	51.96
35.0	29.71(6)	34.69(6)	38.74(7)	42.31(8)	45.04(9)	46.40(9)	46.44(10)	45.77(10)	45.13(10)	53.39
40.0	31.79(6)	36.84(7)	40.93(7)	44.43(8)	46.68(9)	47.85(10)	47.56(10)	46.74(10)	46.26(10)	54.81
45.0	34.06(7)	39.17(7)	43.24(8)	46.54(9)	48.54(10)	48.99(10)	48.36(11)	47.48(11)	47.70(10)	56.14

50.0	36.73(7)	41.87(8)	45.81(9)	48.68(9)	50.02(10)	49.87(11)	48.95(11)	48.25(11)	46.57(10)	57.16
55.0	39.86(8)	44.91(9)	48.47(9)	50.59(10)	51.06(11)	50.34(11)	49.36(11)	48.22(11)	44.13(10)	58.06
60.0	43.26(9)	47.95(10)	50.69(10)	51.72(11)	51.35(11)	50.37(11)	49.55(11)	45.97(10)	40.79(10)	58.67
65.0	45.88(10)	49.78(10)	51.39(11)	51.47(11)	50.81(11)	50.30(11)	46.14(10)	41.32(10)	37.71(10)	58.45
70.0	46.71(11)	48.86(11)	49.91(11)	51.25(11)	49.41(11)	44.06(10)	40.34(10)	37.28(10)	34.52(10)	56.88
75.0	45.12(11)	47.42(11)	47.83(11)	42.05(10)	39.71(10)	37.44(10)	35.25(10)	33.10(9)	30.94(9)	52.69
80.0	27.66(10)	32.69(10)	33.27(10)	32.98(10)	32.19(9)	31.07(9)	29.73(9)	28.20(9)	26.50(9)	40.62
85.0	17.67(9)	21.55(9)	22.87(9)	23.38(9)	23.34(9)	22.89(9)	22.11(9)	21.04(9)	19.69(9)	31.48
90.0	-99.00(8)	-99.00(8)	-99.00(8)	-99.00(8)	-99.00(8)	-99.00(9)	-99.00(9)	-99.00(9)	-99.00(9)	-89.96
100.0	17.03(7)	19.36(7)	21.45(7)	22.91(7)	23.53(8)	24.54(8)	24.75(8)	24.55(8)	23.92(9)	32.63
110.0	19.98(6)	21.82(6)	24.15(6)	25.94(6)	27.36(7)	28.41(7)	29.07(8)	29.29(8)	29.00(8)	36.82
120.0	20.79(5)	22.33(5)	24.82(5)	26.85(6)	28.58(6)	29.99(7)	31.02(7)	31.59(8)	31.61(8)	38.92
130.0	20.76(4)	22.08(5)	24.70(5)	26.92(5)	28.88(6)	30.58(6)	31.93(7)	32.81(7)	33.11(8)	39.29
140.0	20.20(4)	21.39(4)	24.09(5)	26.45(5)	28.60(5)	30.53(6)	32.14(7)	33.29(7)	33.84(8)	39.84
150.0	19.19(4)	20.28(4)	23.05(4)	25.51(5)	27.80(5)	29.91(6)	31.73(6)	33.10(7)	33.86(8)	39.19
160.0	17.56(3)	18.59(4)	21.40(4)	23.93(4)	26.32(5)	28.56(6)	30.54(6)	32.09(7)	33.00(7)	38.06
170.0	14.62(3)	15.61(4)	18.45(4)	21.02(4)	23.47(5)	25.78(6)	27.86(6)	29.52(7)	30.54(7)	35.44
	48.75	52.43	54.38	55.33	55.44	54.76	53.59	52.12	50.54	63.05

TABLE A-8D: THE TOTAL NOISE INTENSITY AT X/D = 50.

DATE 090573

CONVECTION MACH NO.= 2.100 SPEED OF SOUND RATIO= 2.10 VO CODE= 2

TOTAL NOISE INTENSITY(DECIBELS)

ANGLE		SEGMENT 1	SEGMENT 2	SEGMENT 3	SEGMENT 4	SEGMENT 5	SEGMENT 6	SEGMENT 7	SEGMENT 8	SEGMENT 9	TOTAL
(DEG)	MC	2.05842	1.93854	1.75407	1.52491	1.27371	1.02218	.78815	.58388	.41559	
	B	1.99000	1.88000	1.77000	1.66000	1.55000	1.44000	1.33000	1.22000	1.11000	
5.0		17.65	22.34	26.03	29.35	32.25	34.34	35.41	35.63	35.45	42.18
10.0		21.20	25.92	29.66	33.04	35.99	38.10	39.15	39.34	39.13	45.90
15.0		23.62	28.39	32.19	35.64	38.62	40.73	41.73	41.86	41.60	48.45
20.0		25.64	30.46	34.33	37.84	40.85	42.91	43.82	43.86	43.55	50.53
25.0		27.54	32.42	36.36	39.93	42.93	44.91	45.87	45.59	45.23	52.39
30.0		29.45	34.40	38.41	42.03	45.00	46.81	47.38	47.15	46.74	54.15
35.0		31.33	36.35	40.43	44.04	46.88	48.44	48.75	48.35	47.94	55.64
40.0		33.41	38.51	42.64	46.21	48.81	50.01	50.00	49.45	49.17	57.13
45.0		35.68	40.85	44.97	48.37	50.56	51.27	50.93	50.28	50.67	58.52
50.0		38.34	43.55	47.58	50.60	52.17	52.31	51.66	51.16	49.58	59.56
55.0		41.48	46.63	50.33	52.66	53.41	52.97	52.22	51.23	48.42	60.56
60.0		44.94	49.78	52.73	54.03	53.94	53.20	52.56	50.03	46.51	61.80

65.0	47.79	51.90	53.74	54.10	53.47	53.31	50.86	47.24	45.24	61.31
70.0	48.10	51.46	52.71	54.26	52.92	49.13	47.08	45.59	44.31	60.21
75.0	48.13	50.43	50.84	47.66	46.79	46.01	45.26	44.47	43.61	57.22
80.0	35.69	41.53	43.08	43.88	44.22	44.26	44.06	43.66	43.07	52.66
85.0	34.09	38.58	40.61	41.88	42.67	43.08	43.19	43.04	42.64	51.30
90.0	33.14	36.82	39.04	40.54	41.56	42.20	42.82	42.54	42.30	50.41
100.0	31.80	34.50	36.91	38.66	39.97	40.92	41.52	41.80	41.77	49.20
110.0	30.70	32.84	35.36	37.28	38.79	39.96	40.78	41.26	41.38	48.35
120.0	29.66	31.44	34.04	36.09	37.76	39.12	40.14	40.80	41.07	47.65
130.0	28.58	30.12	32.79	34.94	36.75	38.28	39.48	40.32	40.73	46.96
140.0	27.39	28.76	31.48	33.72	35.65	37.33	38.70	39.71	40.27	46.18
150.0	25.97	27.23	29.99	32.29	34.32	36.12	37.65	38.81	39.59	45.15
160.0	24.09	25.28	28.06	30.41	32.51	34.41	36.05	37.35	38.15	43.59
170.0	21.01	22.15	24.96	27.33	29.48	31.43	33.15	34.53	35.42	40.72
	51.28	54.99	57.01	58.17	58.42	58.09	57.39	56.47	55.48	66.33

TABLE A-9A: THE WKBJ INTEGRAL AND RUN PARAMETERS AT X/D = 60.

THETA(RAD)	S(21)	S(41)	S(61)	S(81)	S(101)	S(121)	S(141)	S(161)	S(181)
.00	.11761+01	.10655+01	.95401+00	.84173+00	.72940+00	.61650+00	.51117+00	.41016+00	.31903+00
5.00	.11430+01	.10323+01	.92083+00	.80853+00	.69622+00	.58537+00	.47814+00	.37780+00	.28844+00
10.00	.10948+01	.98396+00	.87235+00	.76001+00	.64774+00	.53705+00	.43013+00	.32981+00	.23980+00
15.00	.10454+01	.93441+00	.82265+00	.71026+00	.59807+00	.48767+00	.38130+00	.28191+00	.19340+00
20.00	.99134+00	.88006+00	.76810+00	.65566+00	.54384+00	.43369+00	.32819+00	.23022+00	.14401+00
25.00	.93934+00	.82774+00	.71557+00	.60311+00	.49137+00	.38212+00	.27788+00	.18200+00	.99181-01
30.00	.88577+00	.77381+00	.66145+00	.54907+00	.43781+00	.32961+00	.22721+00	.13433+00	.56472-01
35.00	.84467+00	.73239+00	.61992+00	.50781+00	.39736+00	.29075+00	.19104+00	.10253+00	.32132-01
40.00	.79531+00	.68283+00	.57045+00	.45894+00	.34985+00	.24568+00	.14999+00	.68080-01	.98801-02
45.00	.73464+00	.62226+00	.51039+00	.40011+00	.29331+00	.19299+00	.10356+00	.32260-01	.29847-02
50.00	.65963+00	.54795+00	.43782+00	.32951+00	.22668+00	.13274+00	.53772-01	.26272-02	.35775-01
55.00	.56584+00	.45614+00	.34859+00	.24530+00	.14968+00	.67220-01	.86886-02	.24946-01	.10452+00
60.00	.44617+00	.34121+00	.24049+00	.14639+00	.65272-01	.79126-02	.26145-01	.10718+00	.22525+00
65.00	.28847+00	.19512+00	.10980+00	.38517-01	.41275-03	.50898-01	.14509+00	.27443+00	.43905+00
70.00	.82272-01	.25014-01	.38116-02	.56235-01	.14642+00	.27028+00	.42751+00	.61895+00	.84618+00

CARD INPUT FOR MMAX, A, MC, THETA, AND W? NO
DETAILED PRINTOUT? NO

ALPHA	L	L1	SF	PW(DB)
.800	1.000	1.000	.032	5.041

MODIFIED ALPHA IS: .5533

TABLE A-9B: THE SELF NOISE INTENSITY AND FREQUENCY AT X/D = 60.

DATE 090573

CONVECTION MACH NO.= 1.400 SPEED OF SOUND RATIO= 2.00 VO CODE= 2

SELF NOISE INTENSITY(DECIBELS) WITH FREQUENCY BAND NUMBERS

ANGLE	SEGMENT 1	SEGMENT 2	SEGMENT 3	SEGMENT 4	SEGMENT 5	SEGMENT 6	SEGMENT 7	SEGMENT 8	SEGMENT 9	TOTAL
(DEG) MC	1.37228	1.29236	1.16938	1.01661	.84914	.68145	.52544	.38925	.27706	
K	1.90000	1.80000	1.70000	1.60000	1.50000	1.40000	1.30000	1.20000	1.10000	
5.0	11.77(6)	16.95(7)	20.97(7)	24.26(8)	26.58(9)	27.73(9)	27.95(9)	27.68(9)	27.31(9)	35.12
10.0	15.63(7)	20.87(7)	24.96(8)	28.31(8)	30.61(9)	31.70(9)	31.84(9)	31.50(9)	31.08(9)	39.03
15.0	18.37(7)	23.68(7)	27.84(8)	31.21(9)	33.46(9)	34.43(9)	34.46(9)	34.03(9)	33.57(9)	41.71
20.0	20.82(7)	26.21(8)	30.43(8)	33.78(9)	35.90(9)	86.70(10)	36.57(10)	36.04(9)	35.54(9)	43.93
25.0	23.11(7)	28.57(8)	32.81(8)	36.06(9)	37.98(10)	38.54(10)	38.24(10)	37.61(10)	37.10(9)	45.78
30.0	25.40(8)	30.92(8)	35.13(9)	38.19(9)	39.80(10)	40.07(10)	39.58(10)	38.86(10)	38.41(9)	47.39
35.0	27.50(8)	33.01(9)	37.07(9)	39.80(10)	41.80(10)	40.98(10)	40.33(10)	39.58(10)	39.38(9)	48.50
40.0	29.75(9)	35.19(9)	38.96(10)	41.22(10)	41.97(10)	41.65(10)	40.88(10)	40.20(10)	40.92(9)	49.56
45.0	32.09(9)	37.35(10)	40.67(10)	42.35(10)	42.63(10)	42.06(10)	41.24(10)	40.91(10)	41.46(9)	50.41
50.0	34.32(10)	39.22(10)	41.94(10)	43.01(10)	42.89(10)	42.18(10)	41.55(10)	43.34(10)	39.26(9)	51.04
55.0	35.97(10)	40.36(10)	42.45(11)	43.02(11)	42.68(10)	42.10(10)	44.71(10)	40.42(9)	38.23(9)	51.29
60.0	36.52(10)	40.39(11)	42.00(11)	42.35(11)	42.17(10)	95.31(10)	40.77(10)	38.76(9)	37.60(9)	50.94
65.0	35.76(11)	39.27(11)	40.77(11)	41.59(10)	44.71(10)	40.05(10)	38.74(9)	37.88(9)	37.15(9)	49.87
70.0	40.38(11)	42.60(10)	42.92(10)	39.12(10)	38.50(10)	38.09(9)	37.70(9)	37.27(9)	86.80(9)	49.36
75.0	30.93(10)	33.98(10)	35.51(10)	36.36(9)	36.81(9)	36.98(9)	36.97(9)	36.80(9)	36.50(9)	45.52
80.0	28.13(9)	31.65(9)	33.66(9)	34.92(9)	35.72(9)	36.18(9)	36.39(9)	36.40(9)	36.24(9)	44.53
85.0	26.55(9)	30.22(9)	32.41(9)	33.88(8)	34.88(8)	35.53(8)	35.91(8)	36.06(8)	36.01(8)	43.85
90.0	25.38(8)	29.13(8)	31.43(8)	33.04(8)	34.19(8)	34.98(8)	35.49(8)	35.75(8)	35.79(8)	43.31
100.0	23.62(7)	27.45(7)	29.89(7)	31.68(7)	33.04(8)	34.05(8)	34.76(8)	35.20(8)	35.39(8)	42.44
110.0	22.24(6)	26.11(6)	28.65(7)	30.57(7)	32.07(7)	33.25(7)	34.12(8)	34.70(8)	35.01(8)	41.72
120.0	21.05(6)	24.94(6)	27.54(6)	29.56(6)	31.19(7)	32.50(7)	33.51(7)	34.21(7)	34.62(8)	41.07
130.0	19.92(5)	23.82(5)	26.48(6)	28.58(6)	30.32(6)	81.75(7)	32.88(7)	33.69(7)	34.18(8)	40.40
140.0	18.74(5)	22.65(5)	25.34(5)	27.52(6)	29.35(6)	30.90(6)	32.16(7)	33.08(7)	33.63(7)	39.66
150.0	17.38(5)	21.28(5)	24.01(5)	26.24(5)	28.17(6)	29.83(6)	31.20(7)	32.23(7)	32.85(7)	38.69
160.0	15.56(4)	19.46(5)	22.21(5)	24.50(5)	26.50(6)	28.26(6)	29.74(6)	30.87(7)	81.55(7)	37.23
170.0	12.53(4)	16.43(4)	19.19(5)	21.51(5)	23.57(5)	25.40(6)	26.97(8)	28.17(7)	28.89(7)	34.45
	42.05	45.63	47.53	48.20	49.00	48.92	48.52	47.97	47.42	57.17

A2	72.21	71.13	69.60	67.53	64.81	61.29	56.78	51.01	43.43
	47.45	50.09	51.13	50.82	49.95	48.36	46.66	44.37	41.47
	46.01	48.76	50.00	49.86	49.20	47.79	46.31	44.22	41.60
	44.35	47.25	48.72	48.79	48.38	47.18	45.92	44.02	41.67
	42.48	45.55	47.29	47.61	47.47	46.49	45.48	43.79	41.69
	40.38	43.64	45.68	46.28	46.45	45.73	44.98	43.50	41.66
	38.09	41.50	43.89	44.81	45.32	44.87	44.43	43.17	41.58
	35.44	39.13	41.89	43.16	44.06	43.92	43.80	42.78	41.46
	32.54	36.49	39.66	41.32	42.65	42.85	43.10	42.34	41.29
	29.30	33.54	37.17	39.26	41.06	41.65	42.30	41.83	41.07
	25.61	30.18	34.36	36.93	39.28	40.30	41.40	41.25	40.80
	21.30	26.31	31.15	34.29	37.26	38.77	40.38	40.58	40.48

TABLE A-9c: THE SHEAR NOISE INTENSITY AND FREQUENCY AT X/D=60.

DATE 090573

CONVECTION MACH NO.= 1.40 SPEED OF SOUND RATIO= 2.00 VO CODE= 2

SHEAR NOISE INTENSITY(DECIBELS) WITH FREQUENCY BAND NUMBERS

ANGLE (DEG)	SEGMENT 1	SEGMENT 2	SEGMENT 3	SEGMENT 4	SEGMENT 5	SEGMENT 6	SEGMENT 7	SEGMENT 8	SEGMENT 9	TOTAL
	MC 1.37228	1.29236	1.16938	1.01661	.84914	.68145	.52644	.38925	.27706	
	λ 1.90000	1.80000	1.70000	1.60000	1.50000	1.40000	1.30000	1.20000	1.10000	
5.0	17.00(4)	22.12(5)	26.11(5)	29.23(6)	31.04(6)	31.40(7)	30.78(7)	29.77(7)	28.80(7)	38.46
10.0	20.78(4)	25.95(5)	29.99(5)	33.12(6)	34.88(7)	35.14(7)	34.42(7)	33.35(7)	32.35(7)	42.19
15.0	23.46(4)	28.68(5)	32.76(6)	35.85(6)	37.48(7)	37.59(7)	36.76(7)	35.61(7)	34.59(7)	44.87
20.0	25.85(5)	31.12(5)	35.20(6)	38.20(7)	39.63(7)	39.53(8)	38.55(8)	37.33(8)	36.29(8)	46.88
25.0	28.09(5)	33.41(6)	37.44(6)	40.25(7)	41.38(7)	41.03(8)	39.90(8)	38.61(8)	37.40(8)	48.34
30.0	30.36(5)	35.68(6)	39.59(7)	42.08(7)	42.83(8)	42.18(8)	40.90(8)	39.58(8)	38.69(8)	49.76
35.0	32.46(6)	37.71(6)	41.35(7)	43.38(8)	43.68(8)	42.77(8)	41.39(8)	40.11(8)	39.54(8)	50.73
40.0	34.65(6)	39.73(7)	42.95(7)	44.39(8)	44.22(8)	43.08(8)	41.66(8)	40.52(8)	40.96(8)	51.60
45.0	36.81(7)	41.58(7)	44.19(8)	44.99(8)	44.39(9)	43.10(8)	41.75(8)	41.05(8)	41.46(8)	52.21
50.0	38.60(7)	42.87(8)	44.78(8)	45.00(9)	44.12(9)	42.83(9)	41.78(8)	43.34(8)	37.35(8)	52.44
55.0	39.44(8)	43.15(8)	44.47(9)	44.32(9)	43.40(9)	42.39(9)	44.71(8)	38.88(8)	34.66(8)	52.15
60.0	38.89(9)	42.16(9)	43.17(9)	43.00(9)	42.44(9)	45.31(8)	39.17(8)	35.11(8)	32.18(7)	51.12
65.0	36.98(9)	40.06(9)	41.18(9)	41.72(9)	44.71(9)	37.71(8)	34.47(8)	31.90(8)	29.63(7)	49.24
70.0	40.38(9)	42.60(9)	42.92(9)	36.90(8)	34.50(8)	32.42(8)	30.48(8)	28.65(7)	26.85(7)	47.82
75.0	27.56(8)	29.60(8)	29.96(8)	29.54(8)	28.70(8)	27.61(8)	26.38(7)	25.04(7)	23.62(7)	37.54

80.0	18.60(8)	21.40(8)	22.58(8)	22.94(7)	22.80(7)	22.30(7)	21.55(7)	20.59(7)	19.45(7)	31.12
85.0	9.18(7)	12.29(7)	13.86(7)	14.66(7)	14.95(7)	14.86(7)	14.45(7)	13.79(7)	12.89(7)	23.26
90.0	-99.00(7)	-99.00(7)	-99.00(7)	-99.00(7)	-99.00(7)	-99.00(7)	-99.00(7)	-99.00(7)	-99.00(7)	-89.46
100.0	9.42(6)	12.85(6)	14.93(6)	16.37(6)	17.37(6)	17.98(6)	18.25(6)	18.16(6)	17.74(7)	26.14
110.0	12.92(5)	16.44(5)	18.70(5)	20.39(5)	21.69(6)	22.63(6)	23.21(6)	23.40(6)	23.21(6)	30.85
120.0	14.25(4)	17.82(4)	20.22(5)	22.12(5)	23.67(5)	24.89(5)	25.75(6)	26.20(6)	26.20(6)	33.23
130.0	14.68(4)	18.29(4)	20.79(4)	22.86(4)	24.63(5)	26.10(5)	27.21(5)	27.89(6)	28.07(6)	34.61
140.0	14.52(3)	18.16(4)	20.75(4)	22.96(4)	24.91(4)	26.60(5)	27.94(5)	28.83(6)	29.18(6)	35.31
150.0	13.84(3)	17.48(3)	20.14(4)	22.46(4)	24.58(4)	26.46(5)	28.00(5)	29.08(6)	29.57(6)	35.36
160.0	12.45(3)	16.11(3)	18.82(3)	21.22(4)	23.46(4)	25.49(5)	27.21(5)	28.45(5)	29.05(6)	34.58
170.0	9.67(3)	13.32(3)	16.06(3)	18.52(4)	20.83(4)	22.97(4)	24.81(5)	26.17(5)	26.85(6)	32.21
	43.66	47.25	48.98	49.24	49.32	48.40	47.10	45.57	44.04	57.05

TABLE A-9D: THE TOTAL NOISE INTENSITY AT X/D = 60.

DATE 090573

CONVECTION MACH NO.= 1.40 SPEED OF SOUND RATIO= 2.00 VD CODE= 2

TOTAL NOISE INTENSITY(DECIBELS)

ANGLE	SEGMENT 1	SEGMENT 2	SEGMENT 3	SEGMENT 4	SEGMENT 5	SEGMENT 6	SEGMENT 7	SEGMENT 8	SEGMENT 9	TOTAL
(DEG) AC	1.37228	1.29236	1.16938	1.01661	.84914	.68145	.52544	.38925	.27708	
A	1.90000	1.80000	1.70000	1.60000	1.50000	1.40000	1.30000	1.20000	1.10000	
5.0	18.14	23.27	27.27	30.43	32.37	32.95	32.60	31.86	31.13	40.11
10.0	21.93	27.12	31.17	34.36	36.26	36.76	36.33	35.53	34.77	43.90
15.0	24.63	29.88	33.97	37.13	38.93	39.30	38.77	37.90	37.12	46.45
20.0	27.03	32.34	36.45	39.54	41.17	41.35	40.68	39.74	38.94	48.53
25.0	29.29	34.64	38.73	41.65	43.02	42.97	42.15	41.15	40.37	50.25
30.0	31.56	36.93	40.92	43.57	44.58	44.27	43.30	42.25	41.56	51.74
35.0	33.66	38.98	42.73	44.96	45.55	44.98	43.90	42.86	42.47	52.77
40.0	35.86	41.04	44.41	46.10	46.25	45.43	44.30	43.37	43.95	53.72
45.0	38.07	42.97	45.79	46.88	46.61	45.62	44.51	43.99	44.47	54.42
50.0	39.98	44.43	46.60	47.13	46.56	45.53	44.68	46.35	41.42	54.81
55.0	41.06	44.98	46.59	46.73	46.06	45.26	47.72	42.73	39.81	54.75
60.0	40.88	44.37	45.63	45.69	45.32	48.32	43.05	40.32	38.70	54.84
65.0	39.42	42.69	43.99	44.66	47.72	42.05	40.12	38.86	37.86	52.67
70.0	43.39	45.61	45.93	41.16	39.96	39.13	38.45	37.83	37.22	51.87
75.0	32.58	35.33	36.58	37.18	37.43	37.46	37.33	37.08	36.72	46.16
80.0	28.59	32.04	33.98	35.19	35.93	36.36	36.53	36.52	36.33	44.72

90.0	26.43	30.29	32.47	33.93	34.92	35.57	35.94	36.08	36.03	43.89
100.0	25.38	29.13	31.43	33.04	34.19	34.98	35.49	35.75	35.79	43.31
110.0	23.78	27.60	30.03	31.81	33.16	34.16	34.86	35.29	35.47	42.54
120.0	22.72	26.56	29.07	30.97	32.45	33.61	34.46	35.01	35.29	42.07
130.0	21.87	25.71	28.28	30.28	31.90	33.20	34.18	34.85	35.20	41.73
140.0	21.06	24.89	27.51	29.61	31.35	32.79	33.92	34.71	35.13	41.42
150.0	20.14	23.97	26.64	28.82	30.69	32.28	33.55	34.46	34.96	41.02
160.0	18.97	22.80	25.50	27.76	29.75	31.48	32.90	33.94	34.52	40.35
170.0	17.29	21.11	23.85	26.17	28.25	30.10	31.67	32.84	33.49	39.11
180.0	14.34	18.16	20.91	23.28	25.42	27.36	29.03	30.30	31.00	36.48
	45.94	49.53	51.32	51.76	52.17	51.68	50.88	49.94	49.02	60.12

TABLE A-10A: THE WKBJ INTEGRAL AND RUN PARAMETERS AT X/D = 70.

THETA(RAD)	S(21)	S(41)	S(61)	S(81)	S(101)	S(121)	S(141)	S(161)	S(181)
.00	.11418+01	.10297+01	.91724+00	.80487+00	.69350+00	.58467+00	.48046+00	.38346+00	.29694+00
5.00	.11063+01	.99418+00	.88176+00	.76940+00	.65806+00	.54931+00	.44524+00	.34845+00	.26225+00
10.00	.10583+01	.94613+00	.83368+00	.72136+00	.61016+00	.50166+00	.39801+00	.30167+00	.21666+00
15.00	.10067+01	.89441+00	.78194+00	.66970+00	.55874+00	.45069+00	.34779+00	.25279+00	.16934+00
20.00	.95504+00	.84267+00	.73019+00	.61811+00	.50753+00	.40020+00	.29843+00	.20520+00	.12446+00
25.00	.90229+00	.78983+00	.67739+00	.56559+00	.45561+00	.34933+00	.24923+00	.15887+00	.81849-01
30.00	.85346+00	.74097+00	.62870+00	.51735+00	.40829+00	.30365+00	.20587+00	.11862+00	.48152-01
35.00	.80196+00	.68958+00	.57767+00	.46712+00	.35946+00	.25899+00	.16282+00	.81318-01	.19742-01
40.00	.74562+00	.63362+00	.52246+00	.41323+00	.30775+00	.20869+00	.11976+00	.46607-01	.13584-02
45.00	.67708+00	.56598+00	.45623+00	.34925+00	.24725+00	.15350+00	.72614-01	.13732-01	.15508-01
50.00	.59314+00	.48391+00	.37881+00	.27372+00	.17752+00	.92553-01	.26128-01	.55384-02	.63122-01
55.00	.48922+00	.38377+00	.28171+00	.18571+00	.99901-01	.31265-01	.27556-02	.57001-01	.14914+00
60.00	.35783+00	.26023+00	.16840+00	.86657-01	.25743-01	.77707-02	.69136-01	.16782+00	.29593+00
65.00	.18914+00	.10995+00	.42772-01	.85732-03	.37697-01	.11917+00	.23326+00	.37763+00	.55239+00
70.00	.13714-02	.25194-04	.86113-01	.17546+00	.29290+00	.43905+00	.61476+00	.82103+00	.10591+01

CARD INPUT FOR MMAX, A, MC, THETA, AND W? NO
DETAILED PRINTOUT? NO

ALPHA	I	L1	SF	PW(DB)
.600	1.000	.800	.021	5.795

MODIFIED ALPHA IS: .5070

TABLE A-10B: THE SELF NOISE INTENSITY AND FREQUENCY AT X/D = 70.

DATE 090573

CONVECTION MACH NO.= 1.200 SPEED OF SOUND RATIO= 1.85 VO CODE= 2

SELF NOISE INTENSITY(DECIBELS) WITH FREQUENCY BAND NUMBERS

ANGLE. (DEG)	SEGMENT 1	SEGMENT 2	SEGMENT 3	SEGMENT 4	SEGMENT 5	SEGMENT 6	SEGMENT 7	SEGMENT 8	SEGMENT 9	TOTAL
MC	1.17624	1.10774	1.00232	.87138	.72784	.58410	.45037	.33364	.23748	
K	1.76500	1.68000	1.59500	1.51000	1.42500	1.34000	1.25500	1.17000	1.08500	
5.0	9.79(6)	15.00(6)	18.87(7)	21.76(7)	23.52(8)	24.21(8)	24.17(8)	23.78(8)	23.34(8)	31.68
10.0	13.73(6)	19.00(7)	22.93(7)	25.83(8)	27.55(8)	28.15(8)	28.02(8)	27.57(8)	27.09(8)	35.59
15.0	16.59(6)	21.94(7)	25.90(7)	28.77(8)	30.38(8)	30.85(8)	30.62(8)	30.09(8)	29.58(8)	38.28
20.0	19.07(7)	24.47(7)	28.43(8)	31.20(8)	32.64(8)	32.95(9)	32.59(8)	31.99(8)	31.47(8)	40.41
25.0	21.40(7)	26.84(7)	30.74(8)	33.33(8)	34.53(9)	34.84(9)	34.15(8)	33.47(8)	32.99(8)	42.18
30.0	23.56(7)	28.98(8)	32.73(8)	35.05(9)	35.96(9)	35.86(9)	35.25(9)	34.54(8)	34.20(8)	43.56
35.0	25.68(8)	31.01(8)	34.51(9)	36.46(9)	37.05(9)	36.74(9)	36.04(9)	35.36(8)	35.49(8)	44.72
40.0	27.71(8)	32.85(9)	35.97(9)	37.50(9)	37.78(9)	37.30(9)	36.55(9)	36.07(8)	36.54(8)	45.29
45.0	29.59(9)	34.44(9)	37.11(9)	38.21(9)	38.20(9)	37.61(9)	36.96(9)	37.32(8)	35.79(8)	46.23
50.0	31.08(9)	35.54(9)	37.74(9)	38.47(9)	38.28(9)	37.72(9)	37.61(9)	39.02(8)	34.31(8)	46.72
55.0	31.88(9)	35.92(9)	37.73(9)	38.23(9)	38.05(9)	38.01(9)	40.28(8)	35.18(8)	33.57(8)	46.72
60.0	31.80(9)	35.48(9)	37.06(9)	37.62(9)	42.72(9)	40.68(9)	35.45(8)	34.10(8)	33.08(8)	47.86
65.0	30.96(9)	34.49(9)	42.11(9)	41.23(9)	36.29(9)	34.99(8)	34.16(8)	33.44(8)	32.72(8)	46.78
70.0	34.86(9)	37.16(9)	33.81(9)	33.91(9)	33.86(8)	33.68(8)	33.37(8)	32.95(8)	32.42(8)	43.76
75.0	26.24(9)	29.47(8)	31.17(8)	32.12(8)	32.63(8)	32.82(8)	32.78(8)	32.56(8)	32.18(7)	41.25
80.0	24.28(8)	27.77(8)	29.75(8)	30.99(8)	31.75(8)	32.16(8)	32.30(7)	32.22(7)	31.96(7)	40.47
85.0	23.00(7)	26.60(7)	28.73(7)	30.13(7)	31.05(7)	31.62(7)	31.90(7)	31.93(7)	31.76(7)	39.90
90.0	22.01(7)	25.68(7)	27.90(7)	29.41(7)	30.46(7)	31.15(7)	31.54(7)	31.67(7)	31.57(7)	39.43
100.0	20.48(6)	24.22(6)	26.56(6)	28.24(6)	29.47(7)	30.34(7)	30.91(7)	31.20(7)	31.23(7)	38.66
110.0	19.25(5)	23.03(6)	25.46(6)	27.25(6)	28.62(6)	29.64(6)	30.35(6)	30.76(7)	30.90(7)	38.01
120.0	18.17(5)	21.98(5)	24.47(5)	26.35(5)	27.83(6)	28.98(6)	29.81(6)	30.33(6)	30.55(7)	37.41
130.0	17.14(4)	20.95(5)	23.49(5)	25.46(5)	27.04(5)	28.30(6)	29.25(8)	29.87(6)	30.17(7)	36.80
140.0	16.04(4)	19.86(4)	22.44(4)	24.48(5)	26.16(5)	27.54(5)	28.60(6)	29.32(6)	29.68(6)	36.11
150.0	14.75(4)	18.57(4)	21.18(4)	23.28(5)	25.05(5)	26.54(5)	27.72(8)	28.54(6)	28.97(6)	35.20
160.0	12.99(4)	16.80(4)	19.44(4)	21.60(4)	23.45(5)	25.04(5)	26.33(6)	27.26(6)	27.74(6)	33.80
170.0	10.00(4)	13.81(4)	16.46(4)	18.65(4)	20.56(5)	22.23(5)	23.61(8)	24.63(6)	25.15(6)	31.07

	37.69	41.37	44.09	44.66	45.17	44.66	44.29	43.77	42.82	53.15
A2	70.12	68.98	67.36	65.17	62.32	58.69	54.10	48.31	40.87	
	44.04	47.28	47.60	47.17	46.20	44.72	42.59	40.07	36.49	
	42.49	45.92	46.39	46.17	45.44	44.21	42.30	40.04	36.80	
	40.81	44.45	45.08	45.09	44.62	43.65	41.96	39.94	37.03	
	38.99	42.84	43.66	43.92	43.71	43.01	41.55	39.80	37.19	
	37.01	41.10	42.11	42.63	42.72	42.31	41.09	39.59	37.28	
	34.86	39.21	40.43	41.23	41.64	41.54	40.57	39.33	37.32	
	32.53	37.16	38.59	39.70	40.44	40.68	39.98	39.02	37.29	
	29.98	34.92	36.58	38.02	39.13	39.72	39.31	38.64	37.21	
	27.18	32.46	34.37	36.16	37.68	38.66	38.56	38.21	37.08	
	24.06	29.75	31.92	34.11	36.06	37.48	37.71	37.70	36.88	
	20.50	26.71	29.18	31.81	34.27	36.17	36.77	37.12	36.63	

TABLE A-10c: THE SHEAR NOISE INTENSITY AND FREQUENCY AT X/D = 70.

DATE 090573

CONVECTION MACH NO.= 1.200 SPEED OF SOUND RATIO= 1.85 VO CODE= 2

SHEAR NOISE INTENSITY(DECIBELS) WITH FREQUENCY BAND NUMBERS

ANGLE (DEG)	SEGMENT 1	SEGMENT 2	SEGMENT 3	SEGMENT 4	SEGMENT 5	SEGMENT 6	SEGMENT 7	SEGMENT 8	SEGMENT 9	TOTAL
	MC 1.17624	1.10774	1.00232	.87138	.72784	.58410	.45037	.33364	.23748	
	A 1.76500	1.68000	1.59500	1.51000	1.42500	1.34000	1.25500	1.17000	1.08500	
5.0	15.75(3)	20.87(4)	24.56(4)	27.00(5)	27.98(5)	27.73(6)	26.82(6)	25.72(6)	24.72(6)	35.21
10.0	19.62(4)	24.78(4)	28.50(5)	30.89(5)	31.77(6)	31.42(6)	30.42(6)	29.26(6)	28.24(6)	38.94
15.0	22.42(4)	27.62(4)	31.32(5)	33.60(5)	34.31(6)	33.82(6)	32.73(6)	31.51(6)	30.48(6)	41.44
20.0	24.84(4)	30.05(5)	33.66(5)	35.76(6)	36.24(6)	35.58(6)	34.39(6)	33.13(6)	32.12(6)	43.36
25.0	27.10(5)	32.28(5)	35.73(6)	37.54(6)	37.75(7)	36.91(7)	35.62(7)	34.34(7)	33.41(6)	44.92
30.0	29.18(5)	34.26(5)	37.43(6)	38.87(6)	38.78(7)	37.77(7)	36.43(7)	35.17(7)	34.44(6)	46.10
35.0	31.14(5)	36.03(6)	38.81(6)	39.82(7)	39.43(7)	38.29(7)	36.93(7)	35.77(7)	35.58(7)	47.02
40.0	32.88(6)	37.45(6)	39.76(7)	40.33(7)	39.70(7)	38.47(7)	37.17(7)	36.29(7)	36.54(7)	47.43
45.0	34.24(6)	38.41(7)	40.22(7)	40.42(7)	39.62(7)	38.40(7)	37.30(7)	37.38(7)	34.74(6)	47.86
50.0	34.93(7)	38.67(7)	40.07(7)	40.03(8)	39.19(7)	38.15(7)	37.72(7)	39.02(7)	31.85(6)	47.85
55.0	34.70(7)	38.09(8)	39.23(8)	39.14(8)	38.49(7)	38.14(7)	40.28(7)	32.83(7)	29.52(6)	47.25
60.0	33.52(8)	36.70(8)	37.81(8)	37.98(8)	42.72(7)	40.68(7)	32.79(7)	29.76(6)	27.25(6)	47.25

65.0	31.68(8)	34.90(8)	42.11(8)	41.23(7)	38.52(7)	31.45(7)	29.03(7)	26.87(6)	24.86(6)	46.01
70.0	34.86(8)	37.16(7)	31.46(7)	30.11(7)	28.62(7)	27.06(7)	25.46(6)	23.84(6)	22.20(6)	41.03
75.0	21.14(7)	23.54(7)	24.25(7)	24.16(7)	23.58(6)	22.70(6)	21.63(6)	20.41(6)	19.06(6)	32.13
80.0	13.58(6)	16.45(6)	17.72(6)	18.17(6)	18.12(6)	17.70(6)	17.00(6)	16.09(6)	14.98(6)	26.41
85.0	4.80(6)	7.90(6)	9.47(6)	10.28(6)	10.57(6)	10.48(6)	10.07(6)	9.40(6)	8.48(6)	18.87
90.0	-99.00(5)	-99.00(5)	-99.00(5)	-99.00(5)	-99.00(6)	-99.00(6)	-99.00(8)	-99.00(6)	-99.00(6)	-89.96
100.0	5.85(5)	9.23(5)	11.24(5)	12.60(5)	13.50(5)	14.02(5)	14.18(5)	14.01(5)	13.51(5)	22.18
110.0	9.66(4)	13.12(4)	15.29(4)	16.88(4)	18.05(5)	18.86(5)	19.31(5)	19.38(5)	19.08(5)	27.04
120.0	11.23(3)	14.74(4)	17.04(4)	18.82(4)	20.23(4)	21.30(4)	22.00(5)	22.30(5)	22.17(5)	29.66
130.0	11.85(3)	15.40(3)	17.80(3)	19.75(4)	21.36(4)	22.66(4)	23.60(4)	24.11(5)	24.15(5)	31.05
140.0	11.85(3)	15.42(3)	17.92(3)	20.00(3)	21.80(4)	23.31(4)	24.46(4)	25.17(5)	25.36(5)	31.85
150.0	11.29(2)	14.88(3)	17.44(3)	19.64(3)	21.59(3)	23.29(4)	24.64(4)	25.53(5)	25.85(5)	31.99
160.0	10.01(2)	13.60(2)	16.21(3)	18.49(3)	20.58(3)	22.43(4)	23.96(4)	25.01(4)	25.44(5)	31.30
170.0	7.28(2)	10.87(2)	13.52(2)	15.86(3)	18.02(3)	19.99(4)	21.64(4)	22.82(4)	23.32(5)	29.00
	39.40	43.02	45.19	45.35	45.11	43.85	42.61	41.21	38.72	52.83

TABLE A-10D: THE TOTAL NOISE INTENSITY AT X/D = 70.

DATE 090573

CONVECTION MACH NO.= 1.200 SPEED OF SOUND RATIO= 1.85 VO CODE= 2

TOTAL NOISE INTENSITY(DECIBELS)

ANGLE	SEGMENT 1	SEGMENT 2	SEGMENT 3	SEGMENT 4	SEGMENT 5	SEGMENT 6	SEGMENT 7	SEGMENT 8	SEGMENT 9	TOTAL
(DEG) MC	1.17624	1.10774	1.00232	.87138	.72784	.58410	.46037	.33364	.23748	
A	1.76500	1.68000	1.59500	1.51000	1.42500	1.34000	1.26500	1.17000	1.08500	
5.0	16.73	21.87	25.60	28.14	29.31	29.33	28.70	27.86	27.09	36.80
10.0	20.62	25.80	29.56	32.07	33.16	33.09	32.40	31.51	30.71	40.69
15.0	23.43	28.66	32.41	34.84	35.79	35.59	34.81	33.87	33.07	43.15
20.0	25.86	31.11	34.80	37.06	37.82	37.47	36.59	35.61	34.82	45.14
25.0	28.13	33.37	36.93	38.94	39.44	38.93	37.96	36.94	36.21	46.77
30.0	30.23	35.39	38.70	40.38	40.61	39.93	38.89	37.88	37.33	48.03
35.0	32.23	37.22	40.18	41.47	41.41	40.59	39.51	38.58	38.54	49.03
40.0	34.03	38.75	41.27	42.15	41.85	40.93	39.88	39.20	39.58	49.60
45.0	35.52	39.88	41.95	42.46	41.98	41.04	40.14	40.36	38.31	50.13
50.0	36.43	40.39	42.07	42.33	41.77	40.95	40.68	42.03	36.26	50.33

55.0	36.52	40.15	41.55	41.72	41.29	41.08	43.29	37.17	35.01	50.00
60.0	35.75	39.14	40.46	40.81	45.73	43.69	37.33	35.47	34.09	50.31
65.0	34.35	37.71	45.12	44.24	38.51	36.58	35.32	34.30	33.37	49.43
70.0	37.87	40.17	36.80	35.42	35.00	34.53	34.02	33.45	32.82	45.62
75.0	27.41	30.46	31.97	32.77	33.14	33.22	33.10	32.81	32.38	41.75
80.0	24.64	28.08	30.02	31.21	31.93	32.31	32.43	32.33	32.04	40.64
85.0	23.07	26.66	28.78	30.17	31.09	31.65	31.93	31.96	31.78	39.93
90.0	22.01	25.68	27.90	29.41	30.46	31.15	31.54	31.67	31.57	39.43
100.0	20.63	24.35	26.69	28.36	29.58	30.44	31.00	31.28	31.30	38.75
110.0	19.70	23.45	25.86	27.63	28.98	29.99	30.68	31.07	31.17	38.34
120.0	18.97	22.73	25.19	27.06	28.53	29.66	30.48	30.97	31.14	38.07
130.0	18.26	22.02	24.53	26.49	28.08	29.35	30.30	30.90	31.14	37.82
140.0	17.45	21.20	23.75	25.80	27.52	28.93	30.01	30.73	31.06	37.49
150.0	16.37	20.11	22.71	24.84	26.67	28.22	29.46	30.30	30.69	36.90
160.0	14.76	18.50	21.13	23.33	25.26	26.94	28.32	29.29	29.75	35.74
170.0	11.86	15.59	18.24	20.48	22.48	24.26	25.75	26.83	27.34	33.17
	41.64	45.28	47.68	48.03	48.15	47.29	46.54	45.69	44.25	56.00

TABLE A-11A: THE WKBJ INTEGRAL AND RUN PARAMETERS AT X/D = 80.

THETA(RAD)	S(21)	S(41)	S(61)	S(81)	S(101)	S(121)	S(141)	S(161)	S(181)
.00	.10955+01	.98307+00	.87094+00	.75976+00	.65065+00	.54519+00	.44534+00	.35348+00	.27249+00
5.00	.10598+01	.94732+00	.83521+00	.72407+00	.61504+00	.50970+00	.41003+00	.31843+00	.23782+00
10.00	.10078+01	.89534+00	.78330+00	.67231+00	.56352+00	.45856+00	.35945+00	.26885+00	.18922+00
15.00	.95422+00	.84187+00	.72998+00	.61925+00	.51090+00	.40660+00	.30848+00	.21911+00	.14176+00
20.00	.90234+00	.79012+00	.67846+00	.56816+00	.46049+00	.35722+00	.26062+00	.17383+00	.99345-01
25.00	.84898+00	.73699+00	.62572+00	.51606+00	.40941+00	.30766+00	.21326+00	.12929+00	.60067-01
30.00	.79627+00	.68467+00	.57403+00	.46536+00	.36019+00	.26063+00	.16941+00	.90120-01	.28266-01
35.00	.74309+00	.63219+00	.52255+00	.41537+00	.31240+00	.21604+00	.12945+00	.57132-01	.73091-02
40.00	.67863+00	.56891+00	.46090+00	.35603+00	.25637+00	.16476+00	.85174-01	.23936-01	.48266-02
45.00	.60096+00	.49326+00	.38792+00	.28672+00	.19221+00	.10804+00	.39771-01	.31291-03	.38224-01
50.00	.50669+00	.40253+00	.30172+00	.20661+00	.12063+00	.49985-01	.28535-02	.30277-01	.10317+00
55.00	.39115+00	.29345+00	.20078+00	.11660+00	.46367-01	.18275-02	.33285-01	.10882+00	.21891+00
60.00	.24789+00	.16305+00	.86846-01	.25948-01	.38122-02	.55538-01	.14158+00	.25581+00	.39539+00
65.00	.73887-01	.21987-01	.36326-02	.50846-01	.13043+00	.23781+00	.37162+00	.53124+00	.71648+00

CARD INPUT FOR MMAX, A, MC, THETA, AND W? NO
DETAILED PRINTOUT? NO

ALPHA	L	L1	SF	PW(DB)
.500	1.000	.800	.014	6.112

MODIFIED ALPHA IS: .5179

TABLE A-11B: THE SELF NOISE INTENSITY AND FREQUENCY AT X/D = 80.

DATE 090573

CONVECTION MACH NO.= 1.000 SPEED OF SOUND RATIO= 1.70 VO CODE= 2

SELF NOISE INTENSITY(DECIBELS) WITH FREQUENCY BAND NUMBERS

ANGLE (DEG)	SEGMENT 1	SEGMENT 2	SEGMENT 3	SEGMENT 4	SEGMENT 5	SEGMENT 6	SEGMENT 7	SEGMENT 8	SEGMENT 9	TOTAL
MC	.98020	.92312	.83527	.72615	.60653	.48675	.37531	.27804	.19790	
A	1.63000	1.56000	1.49000	1.42000	1.35000	1.28000	1.21000	1.14000	1.07000	
5.0	9.42(5)	14.37(6)	17.65(6)	19.68(6)	20.58(6)	20.53(6)	20.18(6)	19.53(6)	18.89(6)	28.38
10.0	13.43(5)	18.42(6)	21.70(6)	23.68(6)	24.50(7)	24.46(7)	23.94(8)	23.24(6)	22.58(6)	32.24
15.0	16.28(6)	21.29(6)	24.53(6)	26.41(7)	27.11(7)	26.97(7)	26.37(7)	25.62(6)	24.96(6)	34.81
20.0	18.64(6)	23.63(6)	26.78(7)	28.51(7)	29.06(7)	28.81(7)	28.13(7)	27.35(6)	26.72(6)	36.74
25.0	20.75(6)	25.69(6)	28.68(7)	30.22(7)	30.59(7)	30.21(7)	29.47(7)	28.67(6)	28.16(6)	38.29
30.0	22.61(6)	27.43(7)	30.21(7)	31.51(7)	31.70(7)	31.21(7)	30.42(7)	29.66(6)	29.45(6)	39.50
35.0	24.18(7)	28.81(7)	31.33(7)	32.39(7)	32.41(7)	31.83(7)	31.09(7)	30.44(6)	31.35(6)	40.46
40.0	25.57(7)	29.96(7)	32.19(7)	33.00(7)	32.87(7)	32.25(7)	31.55(7)	31.46(6)	26.61(6)	40.76
45.0	26.62(7)	30.75(7)	32.69(7)	33.29(7)	33.08(7)	32.50(7)	32.15(7)	33.92(6)	29.55(6)	41.60
50.0	27.22(7)	31.07(8)	32.77(8)	33.24(7)	33.04(7)	32.79(7)	35.64(7)	30.82(6)	28.64(6)	41.85
55.0	27.25(8)	30.85(8)	32.40(8)	32.89(7)	33.08(7)	86.57(7)	31.42(6)	29.48(6)	28.11(6)	41.74
60.0	26.74(8)	30.19(8)	31.82(7)	37.91(7)	36.43(7)	31.18(7)	29.81(6)	28.75(6)	27.74(6)	42.86
65.0	26.37(7)	35.05(7)	35.40(7)	30.97(7)	30.19(7)	89.58(6)	28.95(6)	28.24(6)	27.45(6)	40.90
70.0	24.07(7)	26.78(7)	28.02(7)	28.59(7)	28.77(6)	28.66(6)	28.35(6)	27.86(6)	27.22(6)	37.32
75.0	21.39(7)	24.66(6)	26.39(6)	27.36(6)	27.86(6)	28.01(6)	27.89(6)	27.55(6)	27.01(6)	36.87
80.0	19.98(6)	23.41(6)	25.32(6)	26.49(6)	27.17(6)	27.48(6)	27.50(6)	27.28(6)	26.83(6)	35.76
85.0	18.97(6)	22.48(6)	24.50(6)	25.80(6)	26.61(6)	27.04(6)	27.17(6)	27.04(6)	26.67(6)	35.28
90.0	18.16(5)	21.72(5)	23.82(5)	25.21(5)	26.12(5)	26.65(5)	26.87(5)	26.82(5)	26.51(5)	34.88
100.0	16.86(5)	20.48(5)	22.69(5)	24.22(5)	25.28(5)	25.97(5)	26.34(5)	26.42(5)	26.23(5)	34.20
110.0	15.79(4)	19.46(4)	21.74(4)	23.37(4)	24.55(5)	25.37(5)	25.87(5)	26.05(5)	25.95(5)	33.63
120.0	14.84(4)	18.53(4)	20.87(4)	22.58(4)	23.87(4)	24.80(4)	25.41(5)	25.69(5)	25.66(5)	33.09

130.0	13.91(3)	17.61(3)	20.00(3)	21.79(4)	23.17(4)	24.21(4)	24.92(5)	25.29(5)	25.33(5)	32.84
140.0	12.92(3)	16.62(3)	19.04(3)	20.90(3)	22.38(4)	23.53(4)	24.34(4)	24.81(5)	24.90(5)	31.91
150.0	11.71(3)	15.41(3)	17.87(3)	19.79(3)	21.36(4)	22.62(4)	23.55(4)	24.11(5)	24.26(5)	31.06
160.0	10.02(2)	13.71(3)	16.20(3)	18.19(3)	19.84(3)	21.20(4)	22.25(4)	22.92(4)	23.13(5)	29.72
170.0	7.08(2)	10.76(3)	13.27(3)	15.29(3)	17.01(3)	18.46(4)	19.61(4)	20.37(4)	20.63(5)	27.06
	32.77	37.49	39.06	40.22	40.04	39.86	39.37	38.70	37.71	48.31
A2	67.47	66.25	64.53	62.23	59.26	55.53	50.89	45.15	37.94	
	38.75	41.27	42.16	41.70	40.65	39.07	36.88	34.01	29.85	
	37.42	40.06	41.13	40.86	40.04	38.69	36.75	34.12	30.35	
	36.00	38.75	40.02	39.96	39.37	38.26	36.56	34.16	30.75	
	34.47	37.35	38.83	38.97	38.63	37.76	36.31	34.15	31.07	
	32.83	35.84	37.54	37.91	37.81	37.20	36.01	34.07	31.32	
	31.06	34.22	36.14	36.74	36.91	36.57	35.64	33.92	31.49	
	29.15	32.46	34.63	35.47	35.92	35.87	35.21	33.72	31.59	
	27.09	30.55	32.98	34.08	34.83	35.08	34.70	33.46	31.63	
	24.83	28.46	31.18	32.56	33.63	34.20	34.13	33.13	31.60	
	22.34	26.17	29.20	30.89	32.30	33.23	33.48	32.74	31.52	
	19.58	23.62	27.01	29.03	30.83	32.14	32.75	32.28	31.37	

TABLE A-11c: THE SHEAR NOISE INTENSITY AND FREQUENCY AT X/D = 80.

DATE 090573

CONVECTION MACH NO.= 1.000 SPEED OF SOUND RATIO= 1.70 VO CODE= 2

SHEAR NOISE INTENSITY(DECIBELS) WITH FREQUENCY BAND NUMBERS

ANGLE	SEGMENT 1	SEGMENT 2	SEGMENT 3	SEGMENT 4	SEGMENT 5	SEGMENT 6	SEGMENT 7	SEGMENT 8	SEGMENT 9	TOTAL
(DEG) MC	.98020	.92312	.83527	.72615	.60653	.48675	.37531	.27804	.19790	
A	1.63000	1.56000	1.49000	1.42000	1.35000	1.28000	1.21000	1.14000	1.07000	
5.0	15.49(3)	20.15(3)	22.93(4)	24.21(4)	24.22(4)	23.43(4)	22.27(4)	21.05(4)	19.97(4)	31.70
10.0	19.39(3)	24.05(3)	26.78(4)	27.97(4)	27.89(4)	27.01(5)	25.79(5)	24.53(4)	23.44(4)	35.87
15.0	22.11(3)	26.74(4)	29.37(4)	30.42(4)	30.20(5)	29.23(5)	27.96(5)	26.67(5)	25.61(4)	37.74
20.0	24.31(3)	28.86(4)	31.33(4)	32.19(5)	31.83(5)	30.77(5)	29.45(5)	28.16(5)	27.16(5)	39.46
25.0	26.20(4)	30.62(4)	32.87(5)	33.51(5)	33.00(5)	31.86(5)	30.52(5)	29.26(5)	28.42(5)	40.77
30.0	27.76(4)	31.99(4)	33.98(5)	34.39(5)	33.75(5)	32.55(5)	31.22(5)	30.06(5)	29.57(5)	41.72

35.0	28.92(4)	32.92(5)	34.63(5)	34.83(5)	34.09(5)	32.89(5)	31.62(5)	30.68(5)	31.38(5)	42.85
40.0	29.74(5)	33.47(5)	34.92(5)	34.96(6)	34.16(6)	33.01(5)	31.91(5)	31.55(5)	26.61(5)	42.42
45.0	30.07(5)	33.56(5)	34.79(6)	34.73(6)	33.96(6)	32.96(5)	32.31(5)	33.92(5)	27.91(5)	42.68
50.0	29.84(6)	33.11(6)	34.22(6)	34.16(6)	33.54(6)	32.97(5)	35.64(5)	29.37(5)	25.66(5)	42.90
55.0	29.00(6)	32.13(6)	33.23(6)	33.34(6)	33.25(6)	86.57(-5)	29.85(5)	26.34(5)	23.61(4)	41.75
60.0	27.66(6)	30.78(6)	32.12(6)	32.91(6)	36.43(5)	29.06(5)	26.16(5)	23.73(5)	21.51(4)	41.92
65.0	26.59(6)	35.05(6)	35.40(6)	29.14(5)	26.89(5)	24.89(5)	22.98(8)	21.11(5)	19.25(4)	39.61
70.0	21.85(6)	23.67(5)	23.86(5)	23.30(5)	22.33(5)	21.12(5)	19.75(5)	18.28(4)	16.71(4)	31.81
75.0	14.63(5)	17.22(5)	18.16(5)	18.28(5)	17.89(5)	17.15(4)	16.17(4)	15.00(4)	13.66(4)	26.27
80.0	8.11(5)	11.00(5)	12.31(4)	12.83(4)	12.82(4)	12.43(4)	11.74(4)	10.81(4)	9.67(4)	21.08
85.0	-.11(4)	2.96(4)	4.50(4)	5.28(4)	5.55(4)	5.42(4)	4.96(4)	4.23(4)	3.24(4)	13.82
90.0	-99.00(4)	-99.00(4)	-99.00(4)	-99.00(4)	-99.00(4)	-99.00(4)	-99.00(4)	-99.00(4)	-99.00(4)	-89.46
100.0	1.77(3)	5.07(3)	6.98(3)	8.22(3)	8.99(3)	9.37(4)	9.40(4)	9.08(4)	8.44(4)	17.54
110.0	5.89(3)	9.27(3)	11.33(3)	12.77(3)	13.79(3)	14.42(3)	14.69(3)	14.59(4)	14.12(4)	22.56
120.0	7.73(2)	11.15(2)	13.33(2)	14.95(3)	16.18(3)	17.05(3)	17.54(3)	17.64(3)	17.32(4)	25.22
130.0	8.57(2)	12.03(2)	14.31(2)	16.08(2)	17.50(2)	18.58(3)	19.29(3)	19.57(3)	19.40(3)	26.83
140.0	8.76(1)	12.24(1)	14.60(2)	16.51(2)	18.11(2)	19.39(3)	20.29(3)	20.76(3)	20.72(3)	27.73
150.0	8.36(1)	11.85(1)	14.28(1)	16.30(2)	18.05(2)	19.81(2)	20.61(3)	21.25(3)	21.33(3)	27.99
160.0	7.18(1)	10.69(1)	13.17(1)	15.28(2)	17.16(2)	18.78(2)	20.05(8)	20.85(3)	21.04(3)	27.39
170.0	4.53(1)	8.03(1)	10.55(1)	12.72(2)	14.59(2)	16.43(2)	17.84(3)	18.76(3)	19.03(3)	25.16
	34.33	38.57	39.81	40.31	39.49	38.54	37.23	35.68	33.44	47.59

TABLE A-11D: THE TOTAL NOISE INTENSITY AT X/D = 80.

DATE 090573

CONVECTION MACH NO.= 1.000 SPEED OF SOUND RATIO= 1.70 VO CODE= 2

TOTAL NOISE INTENSITY(DECIBELS)

ANGLE (DEG)		SEGMENT 1	SEGMENT 2	SEGMENT 3	SEGMENT 4	SEGMENT 5	SEGMENT 6	SEGMENT 7	SEGMENT 8	SEGMENT 9	TOTAL
	MC	.98020	.92312	.83527	.72615	.60653	.48675	.37581	.27804	.19790	
	A	1.63000	1.56000	1.49000	1.42000	1.35000	1.28000	1.21000	1.14000	1.07000	
5.0		16.45	21.17	24.06	25.52	25.79	25.26	24.56	23.36	22.47	33.36
10.0		20.37	25.10	27.96	29.34	29.52	28.93	27.97	26.94	26.04	37.09
15.0		23.12	27.83	30.60	31.87	31.94	31.26	30.25	29.19	28.31	39.53
20.0		25.35	30.00	32.64	33.74	33.67	32.91	31.85	30.78	29.96	41.32
25.0		27.29	31.83	34.27	35.18	34.97	34.13	33.03	31.99	31.30	42.72
30.0		28.92	33.29	35.50	36.20	35.85	34.94	33.85	32.87	32.52	43.76
35.0		30.18	34.34	36.29	36.79	36.34	35.40	34.35	33.57	34.38	44.52
40.0		31.14	35.07	36.77	37.10	36.57	35.66	34.75	34.51	29.62	44.68

45.0	31.69	35.39	36.88	37.08	36.55	35.75	35.24	36.93	31.82	45.18
50.0	31.73	35.22	36.56	36.73	36.31	35.89	38.65	33.17	30.42	45.15
55.0	31.22	34.55	35.84	36.14	36.18	39.58	33.72	31.20	29.43	44.76
60.0	30.24	33.50	34.98	40.92	39.44	33.26	31.87	29.94	28.67	45.16
65.0	29.49	38.06	38.41	33.16	31.85	30.85	29.93	29.01	28.09	43.32
70.0	26.11	28.51	29.43	29.72	29.66	29.37	28.91	28.31	27.59	38.29
75.0	22.22	25.38	27.00	27.87	28.28	28.35	28.17	27.78	27.21	36.78
80.0	20.25	23.65	25.54	26.68	27.33	27.62	27.62	27.37	26.92	35.90
85.0	19.02	22.53	24.55	25.84	26.64	27.07	27.20	27.06	26.69	35.31
90.0	18.16	21.72	23.82	25.21	26.12	26.65	26.87	26.82	26.51	34.88
100.0	16.99	20.61	22.81	24.33	25.38	26.07	26.43	26.50	26.30	34.30
110.0	16.22	19.85	22.12	23.73	24.90	25.71	26.19	26.35	26.22	33.95
120.0	15.61	19.25	21.57	23.27	24.55	25.48	26.06	26.32	26.25	33.75
130.0	15.03	18.67	21.04	22.82	24.21	25.26	25.97	26.32	26.32	33.57
140.0	14.33	17.97	20.38	22.25	23.76	24.94	25.79	26.25	26.31	33.31
150.0	13.36	16.99	19.45	21.40	23.03	24.35	25.83	25.92	26.08	32.80
160.0	11.84	15.47	17.96	19.98	21.71	23.17	24.30	25.01	25.22	31.72
170.0	9.00	12.62	15.13	17.21	19.01	20.57	21.82	22.65	22.91	29.23
	36.63	41.07	42.46	43.28	42.78	42.26	41.44	40.46	39.09	50.98

TABLE A-12A: THE WKBJ INTEGRAL AND RUN PARAMETERS AT X/D=90.

THETA(RAD)	S(21)	S(41)	S(61)	S(81)	S(101)	S(121)	S(141)	S(161)	S(181)
.00	.10200+01	.90953+00	.80018+00	.69283+00	.58867+00	.48918+00	.39614+00	.31189+00	.23811+00
5.00	.98204+00	.87162+00	.76234+00	.65509+00	.55106+00	.45175+00	.35895+00	.27474+00	.20971+00
10.00	.92854+00	.81829+00	.71924+00	.60229+00	.49887+00	.39992+00	.30787+00	.22467+00	.15808+00
15.00	.87406+00	.76412+00	.65547+00	.54906+00	.44616+00	.34640+00	.25767+00	.17629+00	.10728+00
20.00	.82028+00	.71083+00	.60280+00	.49722+00	.39545+00	.29918+00	.21050+00	.13142+00	.66960-01
25.00	.76525+00	.65654+00	.54945+00	.44509+00	.34494+00	.25087+00	.16516+00	.90736-01	.31975-01
30.00	.71453+00	.60691+00	.50118+00	.39859+00	.30079+00	.20987+00	.12847+00	.60196-01	.11329-01
35.00	.65278+00	.54679+00	.44307+00	.34306+00	.24885+00	.16231+00	.87273-01	.28530-01	.99660-03
40.00	.57879+00	.47525+00	.37454+00	.27837+00	.18902+00	.10956+00	.44448-01	.27256-02	.25956-01
45.00	.49020+00	.39050+00	.29446+00	.20422+00	.12276+00	.54362-01	.70133-02	.18937-01	.78721-01
50.00	.38452+00	.29109+00	.20268+00	.12226+00	.54241-01	.69243-02	.19537-01	.80697-01	.16753+00
55.00	.25766+00	.17533+00	.10068+00	.38769-01	.82519-03	.32373-01	.10118+00	.19568+00	.31098+00
60.00	.10751+00	.48582-01	.63198-02	.18119-01	.76157-01	.16065+00	.26847+00	.39814+00	.54879+00

CARD INPUT FOR MMAX, A, MC, THETA, AND W? NO
DETAILED PRINTOUT? NO

ALPHA	L	L1	SF	PW(DB)
.400	1.000	.800	.010	8.934

MODIFIED ALPHA IS: .4977

TABLE A-12B: THE SELF NOISE INTENSITY AND FREQUENCY AT X/D = 90.

DATE 090573

CONVECTION MACH NO.= .750 SPEED OF SOUND RATIO= 1.60 VO CODE= 2

SELF NOISE INTENSITY(DECIBELS) WITH FREQUENCY BAND NUMBERS

ANGLE (DEG)		SEGMENT 1 .73515	SEGMENT 2 .69234	SEGMENT 3 .62645	SEGMENT 4 .54461	SEGMENT 5 .45490	SEGMENT 6 .36506	SEGMENT 7 .28148	SEGMENT 8 .20853	SEGMENT 9 .14842	TOTAL
	MC	1.54000	1.48000	1.42000	1.36000	1.30000	1.24000	1.18000	1.12000	1.06000	
	A										
5.0		8.47(5)	12.59(5)	14.71(5)	15.58(5)	15.58(5)	15.05(5)	14.24(5)	13.36(4)	12.57(4)	23.93
10.0		12.25(5)	16.35(5)	18.43(5)	19.23(5)	19.18(5)	18.59(6)	17.75(5)	16.85(5)	16.07(4)	27.13
15.0		14.73(5)	18.78(5)	20.79(5)	21.52(5)	21.40(5)	20.77(5)	19.90(5)	18.99(5)	18.26(4)	29.89
20.0		16.57(5)	20.56(5)	22.48(5)	23.13(5)	22.94(5)	22.27(5)	21.39(5)	20.51(5)	19.89(4)	30.98
25.0		17.99(5)	21.89(6)	23.70(6)	24.26(6)	24.02(5)	23.33(5)	22.46(5)	21.65(5)	21.31(4)	32.16
30.0		18.95(6)	22.73(6)	24.44(6)	24.93(6)	24.65(5)	23.96(5)	23.15(5)	22.51(5)	22.98(4)	32.96
35.0		19.65(6)	23.32(6)	24.92(6)	25.35(6)	25.06(5)	24.41(5)	23.72(5)	23.52(5)	18.83(4)	33.21
40.0		20.09(6)	23.63(6)	25.14(6)	25.52(6)	25.25(5)	24.72(5)	24.37(5)	20.50(5)	22.37(4)	33.43
45.0		20.21(6)	23.63(6)	25.07(6)	25.46(6)	25.30(5)	25.08(5)	27.79(5)	23.89(5)	21.35(4)	34.24
50.0		19.99(6)	23.31(6)	24.74(6)	25.24(5)	25.44(5)	29.07(5)	24.68(5)	22.34(4)	20.80(4)	34.30
55.0		19.48(6)	22.77(6)	24.34(6)	25.37(5)	29.37(5)	24.53(5)	22.82(5)	21.59(4)	20.44(4)	33.96
60.0		19.06(6)	22.69(6)	28.88(5)	28.40(5)	23.61(5)	22.74(5)	21.95(5)	21.11(4)	20.17(4)	34.05
65.0		22.72(5)	25.15(5)	21.83(5)	22.12(5)	22.10(5)	21.84(5)	21.38(4)	20.75(4)	19.97(4)	31.76
70.0		15.42(5)	18.51(5)	20.07(5)	20.88(5)	21.23(5)	21.23(4)	20.96(4)	20.48(4)	19.79(4)	29.87
75.0		13.98(5)	17.28(5)	19.05(5)	20.07(4)	20.60(4)	20.76(4)	20.63(4)	20.24(4)	19.64(4)	29.87
80.0		13.03(4)	16.42(4)	18.31(4)	19.45(4)	20.10(4)	20.38(4)	20.34(4)	20.04(4)	19.51(4)	28.63
85.0		12.30(4)	15.74(4)	17.71(4)	18.95(4)	19.69(4)	20.05(4)	20.09(4)	19.86(4)	19.38(4)	28.27
90.0		11.69(4)	15.18(4)	17.20(4)	18.51(4)	19.32(4)	19.76(4)	19.87(4)	19.70(4)	19.27(4)	27.97
100.0		10.71(3)	14.24(3)	16.35(3)	17.76(3)	18.69(3)	19.25(4)	19.47(4)	19.40(4)	19.05(4)	27.45
110.0		9.90(3)	13.46(3)	15.62(3)	17.11(3)	18.14(3)	18.80(3)	19.12(4)	19.13(4)	18.84(4)	27.00
120.0		9.18(2)	12.75(2)	14.96(3)	16.52(3)	17.63(3)	18.37(3)	18.78(3)	18.86(3)	18.63(4)	26.58
130.0		8.48(2)	12.06(2)	14.30(2)	15.92(3)	17.11(3)	17.94(3)	18.42(3)	18.57(3)	18.38(3)	26.16
140.0		7.72(2)	11.29(2)	13.57(2)	15.25(2)	16.52(3)	17.43(3)	18.00(3)	18.21(3)	18.06(3)	25.67
150.0		6.77(2)	10.32(2)	12.62(2)	14.36(2)	15.72(2)	16.74(3)	17.41(3)	17.69(3)	17.56(3)	25.80
160.0		5.34(1)	8.85(2)	11.18(2)	12.98(2)	14.43(2)	15.57(3)	16.35(3)	16.72(3)	16.61(3)	23.87
170.0		2.59(1)	6.08(2)	8.42(2)	10.27(2)	11.81(2)	13.06(3)	13.96(3)	14.42(3)	14.32(3)	21.41
		26.76	30.08	31.98	32.50	32.72	32.53	32.04	31.03	30.36	40.96
	A_2	63.93	62.59	60.75	58.33	55.26	51.46	46.82	41.17	34.15	
		29.99	32.51	33.37	32.98	31.95	30.30	27.93	24.83	20.28	

28.99	31.60	32.62	32.40	31.58	30.15	28.03	25.17	21.02
27.91	30.62	31.81	31.76	31.13	29.92	28.05	25.43	21.65
26.75	29.57	30.91	31.04	30.62	29.63	28.00	25.62	22.17
25.51	28.42	29.94	30.24	30.03	29.27	27.88	25.73	22.59
24.17	27.19	28.88	29.36	29.37	28.85	27.69	25.77	22.94
22.72	25.85	27.73	28.40	28.63	28.35	27.44	25.74	23.20
21.16	24.41	26.48	27.34	27.81	27.77	27.12	25.64	23.38
19.46	22.83	25.11	26.18	26.89	27.12	26.72	25.47	23.50
17.61	21.11	23.61	24.91	25.88	26.38	26.26	25.24	23.54
15.57	19.22	21.96	23.50	24.75	25.55	25.72	24.94	23.52

TABLE A-12c: THE SHEAR NOISE INTENSITY AND FREQUENCY AT X/D = 90.

DATE 090573

CONVECTION MACH NO.= .75 SPEED OF SOUND RATIO= 1.60 VO CODE= 2

SHEAR NOISE INTENSITY(DECIBELS) WITH FREQUENCY BAND NUMBERS

ANGLE	SEGMENT 1	SEGMENT 2	SEGMENT 3	SEGMENT 4	SEGMENT 5	SEGMENT 6	SEGMENT 7	SEGMENT 8	SEGMENT 9	TOTAL
(DEG) MC	.73515	.69234	.62645	.54461	.45490	.36506	.28148	.20853	.14842	
A	1.54000	1.48000	1.42000	1.36000	1.30000	1.24000	1.18000	1.12000	1.06000	
5.0	13.38(2)	16.97(3)	18.42(3)	18.58(3)	17.92(3)	16.82(3)	15.55(3)	14.31(3)	13.23(3)	26.10
10.0	16.96(3)	20.51(3)	21.91(3)	22.00(3)	21.30(3)	20.16(3)	18.88(3)	17.62(3)	16.57(3)	29.52
15.0	19.17(3)	22.67(3)	24.00(3)	24.03(3)	23.28(3)	22.12(3)	20.83(3)	19.60(3)	18.61(3)	31.56
20.0	20.71(3)	24.13(3)	25.38(3)	25.36(4)	24.57(3)	23.41(3)	22.13(3)	20.95(3)	20.11(3)	32.92
25.0	21.76(3)	25.09(3)	26.26(4)	26.20(4)	25.40(4)	24.25(3)	23.02(3)	21.94(3)	21.41(3)	33.84
30.0	22.31(3)	25.55(4)	26.66(4)	26.57(4)	25.80(4)	24.70(3)	23.57(8)	22.70(3)	23.01(3)	34.37
35.0	22.54(4)	25.70(4)	26.76(4)	26.68(4)	25.95(4)	24.95(4)	23.99(3)	23.60(3)	18.83(3)	34.40
40.0	22.45(4)	25.53(4)	26.57(4)	26.52(4)	25.88(4)	25.05(4)	24.50(3)	20.50(3)	21.24(3)	34.27
45.0	22.02(4)	25.04(4)	26.09(4)	26.12(4)	25.67(4)	25.23(4)	27.79(3)	22.94(3)	19.11(3)	34.59
50.0	21.24(4)	24.24(4)	25.36(4)	25.59(4)	25.58(4)	29.07(3)	23.69(3)	20.01(3)	17.28(3)	34.25
55.0	20.20(4)	23.25(4)	24.60(4)	25.46(4)	29.37(4)	23.17(3)	20.13(3)	17.70(3)	15.47(3)	33.48
60.0	19.32(4)	22.80(4)	28.88(4)	28.40(4)	21.42(3)	19.30(3)	17.35(3)	15.45(3)	13.55(3)	33.17
65.0	22.72(4)	25.15(4)	19.27(4)	18.50(3)	17.39(3)	16.08(3)	14.63(3)	13.08(3)	11.44(3)	29.18
70.0	11.11(4)	13.52(3)	14.29(3)	14.24(3)	13.71(3)	12.84(3)	11.74(3)	10.46(3)	9.01(3)	22.19
75.0	5.75(3)	8.50(3)	9.65(3)	9.99(3)	9.81(3)	9.25(3)	8.42(3)	7.35(3)	6.08(3)	18.09

80.0	.14(3)	3.08(3)	4.46(3)	5.06(3)	5.13(3)	4.82(3)	4.19(3)	3.30(3)	2.18(2)	13.38
85.0	-7.49(3)	-4.43(3)	-2.89(3)	-2.10(3)	-1.83(2)	-1.95(2)	-2.41(2)	-3.16(2)	-4.16(2)	-6.44
90.0	-99.00(2)	-99.00(2)	-99.00(2)	-99.00(2)	-99.00(2)	-99.00(2)	-99.00(2)	-99.00(2)	-99.00(2)	-89.46
100.0	-4.66(2)	-1.33(2)	.49(2)	1.62(2)	2.28(2)	2.54(2)	2.44(2)	2.01(2)	1.26(2)	10.73
110.0	.08(1)	3.36(1)	5.30(1)	6.59(2)	7.44(2)	7.89(2)	7.98(2)	7.71(2)	7.08(2)	16.03
120.0	2.37(1)	5.69(1)	7.72(1)	9.16(1)	10.17(1)	10.81(2)	11.07(2)	10.94(2)	10.43(2)	18.94
130.0	3.64(1)	6.98(1)	9.09(1)	10.66(1)	11.83(1)	12.64(1)	13.07(2)	13.08(2)	12.67(2)	20.78
140.0	4.23(0)	7.58(0)	9.76(1)	11.44(1)	12.76(1)	13.74(1)	14.33(2)	14.48(2)	14.16(2)	21.92
150.0	4.20(0)	7.54(0)	9.78(0)	11.57(1)	13.04(1)	14.18(1)	14.93(1)	15.21(2)	14.96(2)	22.41
160.0	3.36(0)	6.69(0)	8.97(0)	10.85(1)	12.46(1)	13.76(1)	14.68(1)	15.09(2)	14.90(2)	22.06
170.0	.95(0)	4.26(0)	6.57(0)	8.52(0)	10.24(1)	11.68(1)	12.75(1)	13.28(2)	13.12(2)	20.06
	27.45	30.51	31.89	31.89	31.47	30.69	29.36	27.11	25.70	39.58

TABLE A-12D: THE TOTAL NOISE INTENSITY AT X/D = 90.

DATE 090573

CONVECTION MACH NO.= .750 SPEED OF SOUND RATIO= 1.60 VO CODE= 2

TOTAL NOISE INTENSITY(DECIBELS)

ANGLE	SEGMENT 1	SEGMENT 2	SEGMENT 3	SEGMENT 4	SEGMENT 5	SEGMENT 6	SEGMENT 7	SEGMENT 8	SEGMENT 9	TOTAL
(DEG) MC	.73515	.69234	.62645	.54461	.45490	.36506	.28148	.20853	.14842	
A	1.54000	1.48000	1.42000	1.36000	1.30000	1.24000	1.18000	1.12000	1.06000	
5.0	14.59	18.32	19.96	20.34	19.92	19.03	17.96	16.87	15.92	28.01
10.0	18.22	21.92	23.52	23.85	23.37	22.46	21.36	20.26	19.34	31.50
15.0	20.51	24.16	25.69	25.97	25.45	24.51	23.40	22.32	21.48	33.62
20.0	22.12	25.71	27.17	27.39	26.84	25.89	24.79	23.74	23.01	35.07
25.0	23.28	26.79	28.18	28.35	27.78	26.83	25.76	24.81	24.37	36.09
30.0	23.95	27.38	28.70	28.84	28.27	27.36	26.37	25.61	26.00	36.73
35.0	24.35	27.68	28.95	29.07	28.53	27.69	26.87	26.57	21.84	36.85
40.0	24.44	27.69	28.92	29.06	28.59	27.90	27.44	23.51	24.85	36.88
45.0	24.22	27.40	28.62	28.82	28.50	28.17	30.80	26.46	23.38	37.43
50.0	23.67	26.81	28.07	28.43	28.52	32.08	27.22	24.34	22.40	37.28
55.0	22.87	26.02	27.48	28.43	32.38	26.91	24.69	23.07	21.64	36.73
60.0	22.20	25.72	31.89	31.41	25.66	24.36	23.24	22.15	21.03	36.64
65.0	25.73	28.16	23.75	23.69	23.36	22.86	22.21	21.44	20.54	33.67
70.0	16.79	19.71	21.09	21.74	21.93	21.81	21.45	20.89	20.14	30.88
75.0	14.59	17.82	19.52	20.48	20.95	21.06	20.88	20.46	19.83	29.41
80.0	13.24	16.62	18.48	19.61	20.24	20.50	20.45	20.13	19.59	28.76

80.0	12.34	15.79	17.75	18.98	19.72	20.08	20.12	19.88	19.40	28.30
90.0	11.69	15.18	17.20	18.51	19.32	19.76	19.87	19.70	19.27	27.97
100.0	10.84	14.36	16.46	17.86	18.79	19.34	19.56	19.48	19.12	27.64
110.0	10.33	13.87	16.01	17.48	18.50	19.14	19.44	19.43	19.12	27.33
120.0	10.00	13.53	15.71	17.25	18.35	19.07	19.46	19.51	19.24	27.27
130.0	9.71	13.23	15.45	17.05	18.24	19.06	19.53	19.65	19.41	27.27
140.0	9.33	12.83	15.08	16.76	18.04	18.98	19.55	19.75	19.54	27.20
150.0	8.68	12.16	14.44	16.19	17.59	18.66	19.85	19.63	19.46	26.91
160.0	7.47	10.91	13.22	15.05	16.57	17.77	18.61	18.99	18.85	26.07
170.0	4.86	8.27	10.60	12.50	14.10	15.43	16.41	16.89	16.77	23.80
	30.13	33.31	34.95	35.22	35.15	34.68	33.91	32.51	31.64	43.33

TABLE A-13A: THE WKBJ INTEGRAL AND RUN PARAMETERS AT X/D = 100.

THETA(RAD)	S(2)	S(4)	S(6)	S(8)	S(10)	S(12)	S(14)	S(16)	S(18)
.00	.91270+00	.80807+00	.70534+00	.60548+00	.50967+00	.41924+00	.33568+00	.26076+00	.19670+00
5.00	.87230+00	.76778+00	.66519+00	.56551+00	.46991+00	.37973+00	.29651+00	.22202+00	.15854+00
10.00	.81836+00	.71420+00	.61204+00	.51288+00	.41752+00	.32856+00	.24636+00	.17341+00	.11156+00
15.00	.76148+00	.65799+00	.55660+00	.45836+00	.36454+00	.27660+00	.19622+00	.12586+00	.67128-01
20.00	.70935+00	.60687+00	.50664+00	.40982+00	.31774+00	.23198+00	.15442+00	.87405-01	.34434-01
25.00	.66716+00	.56613+00	.46761+00	.37283+00	.28328+00	.19972+00	.11732+00	.55976-01	.11697-01
30.00	.59728+00	.49834+00	.40226+00	.31042+00	.22450+00	.14659+00	.79337-01	.26806-01	.29527-03
35.00	.52486+00	.42893+00	.33636+00	.24876+00	.16815+00	.97107-01	.39371-01	.24804-02	.22132-01
40.00	.43940+00	.34790+00	.26052+00	.17924+00	.10666+00	.46474-01	.56056-02	.17319-01	.69553-01
45.00	.33884+00	.25415+00	.17482+00	.10354+00	.44244-01	.44469-02	.19521-01	.73888-01	.14942+00
50.00	.22176+00	.14833+00	.82699-01	.29488-01	.00000	.32813-01	.94253-01	.17621+00	.27593+00
55.00	.89640-01	.38285-01	.32742-02	.19594-01	.72230-04	.14665+00	.24007+00	.35098+00	.47843+00
60.00	.20262-01	.62236-01	.12214+00	.19945+00	.29399+00	.40563+00	.53416+00	.67952+00	.84085+00

CARD INPUT FOR MMAX, A, MC, THETA, AND W? NO
DETAILED PRINTOUT? NO

ALPHA	L	LI	SF	PW(DB)
.400	1.000	.800	.008	10.626

MODIFIED ALPHA IS: .5288

TABLE A-13B: THE SELF NOISE INTENSITY AND FREQUENCY AT X/D = 100.

DATE 090573

CONVECTION MACH NO.= .500 SPEED OF SOUND RATIO= 1.50 VO CODE= 2

SELF NOISE INTENSITY(DECIBELS) WITH FREQUENCY BAND NUMBERS

ANGLE (DEG)	SEGMENT 1	SEGMENT 2	SEGMENT 3	SEGMENT 4	SEGMENT 5	SEGMENT 6	SEGMENT 7	SEGMENT 8	SEGMENT 9	TOTAL
MC	.49010	.46156	.41764	.36307	.30327	.24338	.18766	.13902	.09895	
A	1.46000	1.40000	1.35000	1.30000	1.25000	1.20000	1.15000	1.10000	1.05000	
5.0	-.53(4)	2.91(4)	4.48(4)	5.02(4)	4.92(4)	4.41(4)	3.69(3)	2.90(3)	2.20(3)	13.15
10.0	2.87(4)	6.30(4)	7.84(4)	8.37(4)	8.24(4)	7.73(4)	7.00(3)	6.22(3)	5.57(3)	16.49
15.0	4.93(4)	8.33(4)	9.85(4)	10.35(4)	10.22(4)	9.70(4)	8.98(3)	8.24(3)	7.71(3)	18.50
20.0	6.27(4)	9.64(4)	11.14(4)	11.63(4)	11.49(4)	10.98(4)	10.30(3)	9.65(3)	9.38(3)	19.83
25.0	7.16(4)	10.49(4)	11.97(4)	12.45(4)	12.32(4)	11.85(4)	11.25(3)	10.77(3)	11.25(3)	20.82
30.0	7.75(4)	11.04(4)	12.50(4)	12.99(4)	12.89(4)	12.48(4)	12.03(3)	12.01(3)	7.18(3)	21.16
35.0	8.10(4)	11.36(4)	12.81(4)	13.31(4)	13.28(4)	13.02(4)	12.94(4)	8.88(3)	11.22(3)	21.54
40.0	8.23(4)	11.46(4)	12.91(4)	13.48(4)	13.59(4)	13.69(4)	10.09(3)	12.79(3)	10.21(3)	21.72
45.0	8.16(4)	11.37(4)	12.88(4)	13.61(4)	14.14(4)	17.02(4)	13.59(3)	11.31(3)	9.69(3)	22.66
50.0	7.97(4)	11.23(4)	12.95(4)	14.33(4)	17.64(4)	13.54(4)	11.89(3)	10.61(3)	9.37(3)	22.62
55.0	8.07(4)	11.81(4)	17.35(4)	17.17(4)	12.81(4)	11.95(3)	11.11(3)	10.19(3)	9.14(3)	22.88
60.0	11.99(4)	10.63(4)	11.32(4)	11.55(4)	11.48(4)	11.16(3)	10.62(3)	9.89(3)	8.97(3)	20.47
65.0	5.32(4)	8.30(4)	9.76(4)	10.48(4)	10.74(3)	10.64(3)	10.27(3)	9.66(3)	8.83(3)	19.13
70.0	4.03(4)	7.22(4)	8.89(3)	9.81(3)	10.22(3)	10.26(3)	10.00(3)	9.48(3)	8.72(3)	18.61
75.0	3.23(3)	6.51(3)	8.28(3)	9.31(3)	9.82(3)	9.96(3)	9.78(3)	9.32(3)	8.62(3)	18.24
80.0	2.64(3)	5.97(3)	7.81(3)	8.91(3)	9.50(3)	9.70(3)	9.59(3)	9.18(3)	8.53(3)	17.95
85.0	2.16(3)	5.53(3)	7.42(3)	8.57(3)	9.22(3)	9.49(3)	9.42(3)	9.06(3)	8.44(3)	17.71
90.0	1.76(3)	5.15(3)	7.08(3)	8.28(3)	8.98(3)	9.29(3)	9.27(3)	8.95(3)	8.37(3)	17.50
100.0	1.10(2)	4.53(2)	6.51(2)	7.78(3)	8.56(3)	8.95(3)	9.01(3)	8.76(3)	8.22(3)	17.14
110.0	.57(2)	4.02(2)	6.04(2)	7.36(2)	8.20(2)	8.66(2)	8.78(3)	8.58(3)	8.09(3)	16.84
120.0	.13(2)	3.57(2)	5.62(2)	6.99(2)	7.88(2)	8.40(2)	8.57(2)	8.41(3)	7.95(3)	16.57
130.0	-.26(2)	3.17(2)	5.23(2)	6.63(2)	7.58(2)	8.15(2)	8.36(2)	8.24(2)	7.79(3)	16.31
140.0	-.64(1)	2.75(1)	4.82(2)	6.25(2)	7.25(2)	7.88(2)	8.14(2)	8.04(2)	7.59(3)	16.03
150.0	-1.06(1)	2.24(1)	4.29(1)	5.76(2)	6.83(2)	7.52(2)	7.83(2)	7.74(2)	7.27(2)	15.65
160.0	-1.76(1)	1.37(1)	3.39(1)	4.91(2)	6.06(2)	6.85(2)	7.23(2)	7.15(2)	6.60(2)	14.95
170.0	-3.56(1)	-.74(1)	1.23(1)	2.80(1)	4.07(2)	5.02(2)	5.51(2)	5.41(2)	4.70(2)	13.06
	15.65	18.36	20.56	21.26	21.53	21.42	20.68	20.16	19.39	29.74

A2	58.97	57.51	55.55	53.04	49.92	46.15	41.62	36.19	29.50
	16.43	19.00	19.87	19.65	18.70	17.01	14.45	11.04	5.58
	15.89	18.52	19.52	19.42	18.67	17.14	14.82	11.69	6.73
	15.26	17.97	19.09	19.11	18.57	17.20	15.12	12.24	7.72
	14.57	17.34	18.58	18.74	18.39	17.18	15.33	12.69	8.57
	13.79	16.64	18.00	18.29	18.14	17.09	15.46	13.05	9.30
	12.93	15.85	17.35	17.77	17.82	16.93	15.52	13.34	9.92
	11.99	14.98	16.61	17.17	17.43	16.69	15.50	13.54	10.44
	10.95	14.02	15.79	16.48	16.97	16.39	15.42	13.67	10.87
	9.80	12.96	14.87	15.72	16.42	16.01	15.26	13.72	11.21
	8.54	11.79	13.86	14.86	15.80	15.56	15.04	13.71	11.48
	7.15	10.50	12.74	13.90	15.08	15.03	14.74	13.62	11.67

TABLE A-13c: THE SHEAR NOISE INTENSITY AND FREQUENCY AT X/D = 100.

DATE 050573

CONVECTION MACH NO.= .500 SPEED OF SOUND RATIO= 1.50 VO CODE= 2

SHEAR NOISE INTENSITY(DECIBELS) WITH FREQUENCY BAND NUMBERS

ANGLE (DEG)	SEGMENT 1	SEGMENT 2	SEGMENT 3	SEGMENT 4	SEGMENT 5	SEGMENT 6	SEGMENT 7	SEGMENT 8	SEGMENT 9	TOTAL
	MC .49010	.46156	.41764	.36307	.30327	.24338	.18766	.13902	.09895	
	A 1.45000	1.40000	1.35000	1.30000	1.25000	1.20000	1.15000	1.10000	1.05000	
5.0	2.23(2)	5.31(2)	6.49(2)	6.65(2)	6.20(2)	5.40(2)	4.42(2)	3.43(2)	2.57(2)	14.56
10.0	5.46(2)	8.53(2)	9.69(2)	9.84(2)	9.38(2)	8.58(2)	7.61(2)	6.63(2)	5.83(2)	17.76
15.0	7.31(2)	10.36(2)	11.51(2)	11.65(2)	11.19(2)	10.40(2)	9.46(2)	8.53(2)	7.86(2)	19.60
20.0	8.43(2)	11.46(2)	12.61(2)	12.76(2)	12.32(2)	11.55(2)	10.67(2)	9.85(2)	9.46(2)	20.78
25.0	9.08(2)	12.10(2)	13.25(2)	13.42(2)	13.01(2)	12.31(2)	11.52(2)	10.90(2)	11.28(2)	21.59
30.0	9.41(2)	12.41(2)	13.57(2)	13.77(2)	13.43(2)	12.82(2)	12.21(2)	12.07(2)	7.18(2)	21.81
35.0	9.47(2)	12.46(3)	13.64(2)	13.90(2)	13.66(2)	13.23(2)	13.02(2)	8.88(2)	10.37(2)	21.96
40.0	9.29(3)	12.28(3)	13.51(3)	13.87(2)	13.82(2)	13.76(2)	10.09(2)	12.04(2)	8.44(2)	21.86
45.0	8.90(3)	11.92(3)	13.25(3)	13.82(2)	14.23(2)	17.02(2)	12.76(2)	9.43(2)	6.87(2)	22.50
50.0	8.40(3)	11.52(3)	13.11(3)	14.38(2)	17.64(2)	12.39(2)	9.70(2)	7.46(2)	5.33(2)	22.11
55.0	8.22(3)	11.87(3)	17.35(2)	17.17(2)	11.01(2)	9.15(2)	7.37(2)	5.57(2)	3.72(2)	22.06
60.0	11.99(2)	9.42(2)	9.30(2)	8.67(2)	7.70(2)	6.50(2)	5.13(2)	3.61(2)	1.96(2)	17.63
65.0	2.11(2)	4.49(2)	5.26(2)	5.24(2)	4.73(2)	3.88(2)	2.78(2)	1.47(2)	.02(2)	13.19
70.0	-2.15(2)	.53(2)	1.61(2)	1.90(2)	1.67(2)	1.06(2)	.17(2)	-.97(2)	-2.33(1)	9.96

75.0	-6.38(2)	-3.53(2)	-2.25(2)	-1.75(2)	-1.77(2)	-2.19(2)	-2.92(2)	-3.92(1)	-5.16(1)	6.46
80.0	-11.26(2)	-8.31(2)	-6.88(2)	-6.22(2)	-6.09(2)	-6.35(1)	-6.95(1)	-7.83(1)	-8.97(1)	2.14
85.0	-18.36(1)	-15.33(1)	-13.79(1)	-13.02(1)	-12.76(1)	-12.90(1)	-13.38(1)	-14.17(1)	-15.23(1)	-4.51
90.0	-99.00(1)	-99.00(1)	-99.00(1)	-99.00(1)	-99.00(1)	-99.00(1)	-99.00(1)	-99.00(1)	-99.00(1)	-89.46
100.0	-14.37(1)	-11.22(1)	-9.50(1)	-8.50(1)	-7.98(1)	-7.87(1)	-8.11(1)	-8.69(1)	-9.58(1)	.86
110.0	-9.15(1)	-5.98(1)	-4.19(1)	-3.08(1)	-2.44(1)	-2.20(1)	-2.32(1)	-2.80(1)	-3.61(1)	5.99
120.0	-6.31(0)	-3.12(0)	-1.27(0)	-.07(1)	.69(1)	1.05(1)	1.03(1)	.64(1)	-.11(1)	9.19
130.0	-4.49(0)	-1.31(0)	.59(0)	1.88(0)	2.74(1)	3.22(1)	3.31(1)	3.00(1)	2.30(1)	11.33
140.0	-3.32(0)	-.17(0)	1.76(0)	3.14(0)	4.10(0)	4.69(1)	4.88(1)	4.65(1)	3.98(1)	12.79
150.0	-2.67(0)	.41(0)	2.35(0)	3.80(0)	4.87(0)	5.58(0)	5.86(1)	5.69(1)	5.02(1)	13.65
160.0	-2.65(0)	.27(0)	2.20(0)	3.71(0)	4.91(0)	5.75(0)	6.14(1)	6.00(1)	5.29(1)	13.79
170.0	-4.06(0)	-1.43(0)	.46(0)	2.04(0)	3.38(0)	4.40(0)	4.93(1)	4.79(1)	3.94(1)	12.80
	15.03	17.30	19.34	19.65	19.39	18.69	16.92	15.82	14.43	27.82

TABLE A-13D: THE TOTAL NOISE INTENSITY AT X/D = 100.

DATE 090573

CONVECTION MACH NO.= .500 SPEED OF SOUND RATIO= 1.50 VO CODE= 2

TOTAL NOISE INTENSITY(DECIBELS)

ANGLE	SEGMENT 1	SEGMENT 2	SEGMENT 3	SEGMENT 4	SEGMENT 5	SEGMENT 6	SEGMENT 7	SEGMENT 8	SEGMENT 9	TOTAL
(DEG) MC	.49010	.46156	.41764	.36307	.30327	.24338	.18766	.13902	.09895	
A	1.45000	1.40000	1.35000	1.30000	1.25000	1.20000	1.15000	1.10000	1.05000	
5.0	4.08	7.28	8.61	8.92	8.62	7.94	7.09	6.18	5.40	16.92
10.0	7.37	10.56	11.88	12.18	11.86	11.18	10.33	9.44	8.71	20.18
15.0	9.29	12.47	13.77	14.06	13.74	13.07	12.24	11.40	10.80	22.09
20.0	10.49	13.65	14.95	15.24	14.93	14.29	13.60	12.76	12.43	23.34
25.0	11.24	14.38	15.67	15.97	15.69	15.09	14.39	13.85	14.28	24.23
30.0	11.66	14.79	16.08	16.41	16.18	15.66	15.13	15.05	10.19	24.51
35.0	11.85	14.95	16.25	16.63	16.48	16.14	15.99	11.89	13.82	24.77
40.0	11.80	14.90	16.23	16.69	16.72	16.75	13.10	15.44	12.42	24.80
45.0	11.56	14.67	16.08	16.72	17.20	20.03	16.20	13.48	11.52	25.59
50.0	11.20	14.39	16.04	17.37	20.65	16.01	13.94	12.33	10.82	25.38
55.0	11.15	14.85	20.36	20.18	15.01	13.78	12.64	11.48	10.24	25.50
60.0	15.00	13.08	13.43	13.36	13.00	12.44	11.70	10.81	9.76	22.29
65.0	7.02	9.81	11.08	11.62	11.71	11.47	10.98	10.27	9.37	20.11
70.0	4.97	8.07	9.64	10.46	10.79	10.76	10.43	9.85	9.06	19.16

75+0	3+68	6+92	8+65	9+63	10+11	10+21	10+00	9+52	8+79	18+52
80+0	2+81	6+13	7+96	9+04	9+62	9+81	9+68	9+27	8+60	18+06
85+0	2+20	5+56	7+45	8+60	9+25	9+51	9+44	9+08	8+46	17+73
90+0	1+76	5+15	7+08	8+28	8+98	9+29	9+27	8+95	8+37	17+50
100+0	1+22	4+64	6+62	7+88	8+66	9+04	9+09	8+83	8+29	17+23
110+0	1+01	4+43	6+43	7+73	8+56	9+00	9+10	8+89	8+37	17+18
120+0	1+02	4+42	6+43	7+77	8+64	9+13	9+27	9+08	8+58	17+30
130+0	1+13	4+49	6+51	7+89	8+81	9+36	9+54	9+38	8+87	17+51
140+0	1+24	4+54	6+56	7+98	8+97	9+58	9+82	9+68	9+16	17+71
150+0	1+22	4+43	6+44	7+90	8+97	9+66	9+97	9+85	9+30	17+77
160+0	+83	3+86	5+85	7+36	8+53	9+35	9+73	9+62	9+00	17+42
170+0	+79	1+94	3+87	5+45	6+75	7+73	8+24	8+12	7+35	15+75
	18+36	20+87	23+01	23+54	23+60	23+27	22+20	21+52	20+59	31+71

APPENDIX B

THE LISTING OF THE COMPUTER PROGRAM

The Main Program

```
C      PROGRAM FOR CALCULATING NOISE INTENSITY FOR TURBULENCE IN JETS.
C
C      IL2 IDENTIFIES WHICH Y= I.
C      NYR IDENTIFIES WHICH Y= YR.
C      Y= HEIGHT OF THE JET FLOW(DIMENSIONLESS).
C
       CALL INITAL
777    CALL RSTART
       CALL ANGLE
C            CALLS XREF
C            CALLS INTEQ
       CALL NOISE($777)
C            CALLS SETUP
C            CALLS VORFLE
C            CALLS ANOISE
C                 CALLS FBAND
C                 CALLS EQ85
C                      CALLS INTEG
C                      CALLS PVAR
C                      CALLS PVARA
C                 CALLS EQ84
C                      CALLS PVAR
C                      CALLS PVARA
C                 CALLS EQ82
C                      CALLS PVAR
C                      CALLS PVARA
C            CALLS A2SELF
C                 CALLS EQ84
C                 CALLS PVAR
C            CALLS PRINT
C            CALLS OUTPUT
C            STOP
             END
```

Subroutine INITAL

```
       PARAMETER  MPTS= 221
C
       COMMON/BLOC1/ A(MPTS)  ,XMC(MPTS)  ,Y(MPTS)
       COMMON/BLOC2/ THETA ,DELTH1  ,THET2  ,THET  ,DTHET  ,IPCH
       COMMON/BLOC3/ DELY1  ,DELY2
       COMMON/BLOC11/IL2  ,NYR  ,LU
       COMMON/BLOC12/TITLE(13)
       DATA RAD1 /57.2957795/
C
       READ(5,500) (TITLE(I),I=1,13)
       READ(5,50)           THET ,DTHET ,DELY1,DELY2,
C
       DELTH1= DTHET /RAD1
C
C      0.<OR=Y <OR=1.
       IL2= 1./DELY1+1.E-04
       IF(IL2.GE.MPTS) GO TO 60
```

```
      DO 20 I=1,IL2
   20 Y(I)= (I-1)*DELY1
C
C     1. < Y <OR= 2.
      MP1= IL2+1
      LU= 1./DELY2+IL2
      IF(LU.GT.MPTS) GO TO 60
      DO 40 I=MP1,LU
   40 Y(I)= Y(I-1)+DELY2
C
      RETURN
C
   60 MP= MPTS
      WRITE(6,600) MP  ,IL2,LU
      STOP
C
  500 FORMAT(13A6)
  501 FORMAT(8F10.1)
  600 FORMAT(' ***** ERROR.  MPTS= ',I5,' IS TOO SMALL.  IL2= ',I5,'.  LU=
     1  ,I5)
      END
```

Subroutine RSTART

```
      PARAMETER  MPTS= 221
C
      COMMON/BLOC1/ A(MPTS)  ,XMC(MPTS)  ,Y(MPTS)
      COMMON/BLOC2/ THETA  ,DELTH1  ,THET2 ,THET  ,DTHET  ,IPCH
      COMMON/BLOC3/ DELY1  ,DELY2
      COMMON/BLOC4/ AMAX  ,XMMAX
      COMMON/BLOC5/ AMP  ,C3  ,C2  ,NPAS  ,AMM
      COMMON/BLOC11/IL2  ,NYR  ,LU
      COMMON/BLOC12/TITLE(13)
      DATA RAD1 /57.2957795/  C1 /4. /
C
      READ(5,503,END=777) AMAX,XMMAX,  IPCH
C
      NPAS= 1
      THETA= THET  /RAD1
      AMAX1= AMAX-1.
      AMP= AMAX+XMMAX
      AMM= AMAX-XMMAX
      THET2= ACOS(1./AMP)
      TEMP= C1*XMMAX
      C2= -4.*TEMP
      HC3= AMAX/TEMP
      IF(AMOD(HC3,DELY1).GT.0.) C3= AINT(HC3/DELY1)*DELY1+DELY1
C
      NYR= LU
      DO 20 I=1,IL2
      A(I)= AMAX1  *(1.-Y(I))+1.
   20 XMC(I)= XMMAX*EXP(-2.*Y(I)**2)
      MP1=IL2+1
      DO 40 I=MP1,LU
```

```
      A(I)= 1.
   40 XMC(I)= XNMAX*EXP(-2.*Y(I)**2)
C
      WRITE(6,601) (TITLE(I),I=1,13)
      WRITE(6,607) AMAX,XMMAX,C1
      WRITE(6,603) C2,HC3,C3
      WRITE(6,605) THET ,DTHET ,DELY1 ,DELY2
      WRITE(6,602)
      WRITE(6,600) (I,Y(I),XMC(I),A(I),I=1,153)
      WRITE(6,601)
      WRITE(6,602)
      WRITE(6,600) (I,Y(I),XMC(I),A(I),I=154,LU)
      IF(IPCH.EQ.0) RETURN


      WRITE(1,503)       XNMAX
      WRITE(1,604) (A   (I),I=21,181,20)
      WRITE(1,604) (XMC(I),I=21,181,20)
      RETURN
C
  777 WRITE(6,606)
      STOP
C
  503 FORMAT(2F10.3,10X,I5)
  600 FORMAT(( I4,'.',F8.3,2E14.7,2(I8,'.',F8.3,2E14.7)))
  601 FORMAT('1',13A6)
  602 FORMAT('0POINT',5X,'Y',10X,'MC',13X,'A',  2(8X,'POINT',5X,'Y',
     1 10X,'MC',13X,'A'))
  603 FORMAT('+', 76X, 'C2=',G8.2, 3X,'ORIG DY=',G11.5,3X,'MOD DY='
     1  ,G11.5)
  604 FORMAT(5E15.8)
  605 FORMAT(' INITIAL THETA(DEG)=',G8.2,5X,'DELTA THETA(DEG)=',G8.2 ,
     1  5X,'DELT Y1=',G10.3,10X,'DELT Y2=',G10.3)
  606 FORMAT('1END OF CARD INPUT')
  607 FORMAT('0SPEED OF SOUND RATIO=',G9.3,2X,'MAXIMUM MACH NO.=',G9.3
     1  ,4X,'C1=',G9.3)
      END
```

Subroutine ANGLE

```
      PARAMETER  NSP= 10  ,NTP= 18
C
      COMMON/BLOC2/ THETA  ,DELTH1  ,THET2 ,THET  ,DTHET  ,IPCH
      COMMON/BLOC7/ YR  ,DELY
      COMMON/BLOC8/ THETAD(NTP)  ,ES(NTP,NSP)  ,NT
      COMMON/BLOC11/IL2  ,NYR  ,LU
      DIMENSION  S(NSP)
      DATA RAD1 /57.2957795/
C
      WRITE(6,601)
      NT= 0
      THETAD(1 )= THETA
      DO 10 I=1,NTP
      DO 10 J=1,NSP
   10 ES(I,J)= 0.0
   20 NT= NT+1
```

```
      IF(NT.GT.1) THETAD(NT)= THETAD(NT-1)+DTHET
      COSAN= COS(THETA)
      XMF= 1./COSAN
      CALL YREF(XMF,NYR,THETA)
      WRITE(6,600) THETA,THETAD(NT),YR,NYR,DELY,COSAN,XMF,THET2
C
      IF(YR.LT.0.0) GO TO 180
      CALL INTEQ(S,XMF,NS)
      NSM1= NS+1
      DO 100 J= 1,NS
  100 ES(NT,J)= S(NSM1-J)
  180 THETA= THETA+DELTH
      IF(THETA.LE.THET2) GO TO 20
C
      WRITE(6,603)
      DO 300 I=1,NT
  300 WRITE(6,604)THETAD(I),(ES(I,J),J=1,NS)
      IF(IPCH.EQ.0) RETURN
      WRITE(1,602) NT
      WRITE(1,605) (THETAD(I),I=1,NT)
      DO 320 I=1,NT
  320 WRITE(1,606) (ES(I,J),J=1,9)
      RETURN
C
  600 FORMAT(F13.7,F12.2,F10.3,I9,4E17.7)
  601 FORMAT(  ,'THETA(RAD)',5X,'THETA(DEG)',6X,'YR',5X,'YR PT',4X,
     1 'ORIG DELT YN',6X,'COS(THETA)',6X,'1/COS(THETA)',6X,'THETA2(RAD)'
     2 )
  602 FORMAT(I5)
  603 FORMAT(////'0THETA(RAD)',6X,'S(21)',7X,'S(41)',7X,'S(61)',7X,'S(81)
     1',6X,'S(101)',6X,'S(12)',6X,'S(141)',6X,'S(161)',6X,'S(181)')
  604 FORMAT(F8.2,4X,9E12.5)
  605 FORMAT(8F10.2)
  606 FORMAT(5E15.8)
      END
```

Subroutine YREF

```
@FOR,1S YREF
      SUBROUTINE YREF(CTHETA,IL,THETA)
      PARAMETER  MPTS= 221
C
      COMMON/BLOC4/ A(MPTS)   ,XMC(MPTS)   ,Y(MPTS)
      COMMON/BLOC5/ AMP       ,C3          ,C2       ,NRAS    ,ANM
      COMMON/BLOC7/ YR        ,DELY
      COMMON/BLOC11/IL2       ,NYR         ,LU
      DATA HPI /1.57079633/
C
      DELTAY(A,B,C)= ABS(A/(B*C*EXP(-2.*C**2)))
```

```
C
C     THETA= 0.
      IF(ABS(THETA).GT.1.E-05) GO TO 20
      YR= 2.
      DELY= C3
      RETURN
C
C     THETA= 90. DEG.
   20 IF(ABS(THETA-HPI).GT.1.E-05) GO TO 40
      YR= -10.
      RETURN
C
C     THETA < 90. DEG.
   40 ISIGL= 1
      IF(THETA.GT.HPI) GO TO 100
      IF(CTHETA        .LE.AMP   ) GO TO 60
      YR= -10.
      RETURN
   60 L1= IL
      IF((XMC(L1)*A(L1)-CTHETA).LT.0.) ISIGL= -1
      L1= L1-1
      DO 80 I=L1,1,-1
      ISIG= 1
      IF((XMC(I)+A(I)-CTHETA).LT.0.) ISIG= -1
      IF(ISIG.EQ.ISIGL) GO TO 80
      ISIGL= ISIG
      IL= I+1
      YR= Y(IL)
      DELY= DELTAY(A(IL),C2,YR)
      RETURN
   80 CONTINUE
      GO TO 777
C
C     THETA > 90. DEG.
  100 IF(    AMM+CTHETA .GE.0.1) GO TO 120
      YR= -10.
      RETURN
  120 L2= IL
      IF(NPAS.NE.1) GO TO 125
      L2= IL2
      NPAS= 2
  125 IF((A(L2)-XMC(L2)+CTHETA ).LT.0.) ISIGL= -1
      L2= L2-1
      DO 140 I= L2,1,-1
      ISIG= 1
      IF((A(I)-XMC(I)+CTHETA).LT.0.) ISIG= -1
      IF(ISIG.EQ.ISIGL) GO TO 140
      ISIGL= ISIG
      IL= I+1
      YR= Y(IL)
      DELY= DELTAY(A(IL),C2,YR)
      RETURN
  140 CONTINUE
  777 WRITE(6,600) THETA
C
  600 FORMAT('0 *** ERROR:  NO YR FOR THETA=',G(5.8)
      END
```

Subroutine INTEQ

```
@FOR,1S INTEQ
      SUBROUTINE INTEQ(S,XMF,J)
C     CALCULATES THE INTEGRAL OF Q(Y)DY FROM YR TO Y.
C     SIMPSON'S 3/8 RULE FOR INTEGRATION.
C        INTEGRAL OF F(X)DX= 3H/8(F(A)+3F(A+H)+3F(A+2H)+...
C                                +3F(B-H)+F(B))
C
C     S= 0 AT YR
C     NYR SHOULD NEVER = 1.
C     NOTE***  ASSUMPTION:  MOD(IL2,MDF)= 1
C
      PARAMETER  MPTS= 224  ,NSP= 10
C
      COMMON/BLOC1/ A(MPTS)  ,XMC(MPTS)  ,Y(MPTS)
      COMMON/BLOC3/ DELY1  ,DELY2
      COMMON/BLOC11/IL2  ,NYR  ,IU
      DIMENSION S(1)  ,SS(NSP)
      DATA  ID, IU, MDF  /21, 181, 20  /
C
      FF(I)=SQRT(ABS(((XMC(I)-XMF)/A(I))**2  +1.))
C
C     3/8= .375
      DELH1= .375*DELY1
      DELH2= .375*DELY2
      SUM= FF(NYR)
      J= 0
C
      IF(NYR-IL2)  120,160,40
C     YR> 1.
   40 CALL SIMP38(NYR-1,IL2,-1,DELH2)
      IF(IL2-1.LT.ID) RETURN
      SUM= FF(IL2)
      CALL SIMP38(IL2-1,ID,-1,DELH1)
      RETURN
C
C     YR< 1.
  120 HOLD= SUM
      N1= NYR+1
      IF(N1.GT.IU) GO TO 130
      CALL SIMP38(N1,IU  ,1,DELH1)
      DO 125 I=1,J
  125 SS(J+1-I)= S(I)
      DO 126 I=1,J
  126 S(I)= SS(I)
  130 IF(MOD(NYR,MDF).NE.1) GO TO 140
      J= J+1
      S(J)= 0.0
  140 SUM= HOLD
C     YR < 1. AND Y= 1.
  160 IF(NYR-1.LT.ID) RETURN
      CALL SIMP38(NYR-1,ID,-1,DELH1)
      RETURN
C
```

```
      SUBROUTINE SIMP38(L1,L2,L3,DELH)
      DO 40 I=L1,L2,L3
        XLAST= FF(I)
        IF(I.GT.IL2) GO TO 40
        MD= MOD(I,MDF)
        IF(MD.NE.1) GO TO 40
        J= J+1
        S(J)= DELH*(SUM+XLAST)
   20   IF(I.EQ.NYR.OR.I.LE.IL2.OR.I.GE.IL2) GO TO 40
        S(J)= S(J)+S(1)
   40   SUM= SUM+ 3.*XLAST
        RETURN
C
        END
```

Subroutine NOISE

```
C          REFERENCE:  PAO,S.PAUL, AERODYNAMICAL NOISE
C          EMISSION FROM TURBULENT SHEAR LAYERS, P,S)
C
C          EQ.(82),(84)AND(85)
C
C     *** NOTE = ASSUMPTION:  RESULTS ARE FOR PTS. 21*18) IN STEPS
C                             OF 20.
C     A= THETA IN RADIANS.
C     AA= A(Y) IN PAO'S EQUATIONS.  SPEED OF SOUND RATIO.
C     AN= THETA IN DEGREES.
C     A1= THETA1 IN RADIANS FOR EACH SEGMENT)
C     A2= THETA2 IN RADIANS FOR EACH SEGMENT)
C     A3= THETA3 IN RADIANS FOR EACH SEGMENT)
C     DC= MC(Y) IN PAO'S EQUATIONS.
C     MNA= NUMBER OF ANGLES.
C     MSET= NUMBER OF SEGMENTS(PTS.)
C     THETAD(2-NT )= AM(1- NT*I)= ANGLES IN DEGREES.
C     XMMAX= D= MACH NUMBER= M= M MAX IN PAO'S EQUATIONS)
C
      PARAMETER  MPTS= 22)  ,MNAP= 27  ,MSETP= 9  ,NSP= 10
C
      COMMON/BLOC1/ AD(MPTS)  ,XMC(MPTS)  ,Y(MPTS)
      COMMON/BLOC2/ AA  ,AA2  ,ALPHA2  ,DL  ,FAC1  ,FAC2  ,FAC3  ,FAC4
      COMMON/BLOC10/GG(MNAP)  ,CB(MNAP)  ,OK(MNAP)  ,XY(MNAP)
      COMMON/BLOC13/MNA  ,AM(MNAP)
      COMMON/BLOC18/ DC, A84, A1, A2, A3, WT
      COMMON/BLOC19/CST ,CSTL ,CSTT ,CSTTL ,CSTS,CSTSL,IPLAG,IFLAG
      DIMENSION  SU(3,MNAP)  ,VO(NSP)  ,NII(MSETP,MNAP)
     1          ,N2(MSETP,MNAP)  ,TP(MSETP,3)  ,STP(3)  ,PTA2(MSETP)
      DATA  MSET  / 9 /
      FUN1(A)= 10.*ALOG10(A)
      FUN2(A)=FUN1(A) +94.
C
```

```
      IFLAG1= 0
      DO 10 J=1,3
      STP(J)= 0.0
      DO 10 I=1,MNA
   10 SU(J,I)= 0.0
      CALL SETUP (ICODE,IPRT)
      CALL VOPFLE(VO,MSET,ICODE)
C
C
C     CALCULATE NOISE INTENSITY(DECIBELS) FOR MNA ANGLES FOR EACH OF
C          MSET SEGMENTS.
      DO 100 I=1,MSET
      DO 15 J=1,3
   15 TP(I,J)= 0.0
      ITEM= I*20
      WT=I*0.06981372
      AA= AD(1+ITEM)
      AA2= AA**2
      DC= XMC(1+ITEM)
      TEMP= DC-AA
      IFLAG= 0
      A1= 0.0
      IF(TEMP.LT.1.) GO TO 20
      A1= ACOS(1./TEMP)
      IFLAG= 1
   20 A2= ACOS(1./(DC+AA))
      IF(TEMP.GE.-1.) GO TO 23

      A3= ACOS(1./TEMP)
      IFLAG1= 1
   23 CST=FAC1*VO(I)/AA2
      CSTS= FAC3*VO(I)/AA2
      CSTT= FAC4*VO(I)/AA2
      IF(IPRT.EQ.0) GO TO 24
      WRITE (6,21) DC    ,AA ,ICODE
      WRITE(6,22)
C

C     CALCULATE NOISE INTENSITY(DECIBELS) FOR MNA ANGLES.
   24 CALL ANOISE(I, IPRT,TP,SU,N1,N2)
C
      DO 80 J=1,3
      TP(I,J)= FUN2(TP(I,J))
   80 STP(J)= STP(J)+10.**((TP(I,J)-94.)*.1)
      VVL= FUN1(VO(I))
C
C     SELF NOISE INTENSITY FOR 5 ANGLES IN INCREMENTS OF 2 DEG ON EITHER
C          SIDE OF A2.
      CALL A2SELF(A2,DC,CSTT,I,IPRT,PTA2,CSTTL)
C
      IF(IPRT.EQ.5) CALL PRINT(CSTL,CSTSL,CSTTL,VVL,TP,DC,AA,ICODE,I)
  100 CONTINUE
C
```

```
      DO 160 J=1,3
      STP(J)= FUN2(STP(J))
      DO 160 M=1,MNA
  160 SU(J,M)= FUN2(SU(J,M))
C
      CALL OUTPUT(ICODE,N1,N2,SU,TP,STP,PTA2,MSET)
      RETURN
C
   21 FORMAT(1H1,15X,'CONVECTION MACH NO=',F10.8,10X,'SPEED OF SOUND RAT
     1IO=',F5.2 ,10X,'VO CODE=',I2//)
   22 FORMAT (1X,'ANGLE',5X,'SELFINT',          2X,'REFRACTION',5X,
     1'CON-REF',2X,'CONNECTION',9X,'F(B)',13X,'B',15X,'W',7X,'SELINTNO-F
     1B' //)
      END
```

END OF COMPILATION: NO DIAGNOSTICS.

Subroutine ANOISE

```
BFOR,IS ANOISE
      SUBROUTINE ANOISE( I ,IRRT,TP,SU,N1,N2)
C     CONS = 3./LN 2
C     DEG2= 2.45 DEGS =  0.0476056? RADIANS
C
      PARAMETER  MSETP=9 ,MNAP=27  ,NTP= 18  ,NSP= 10
      PARAMETER  MAP= MNAP+11
C
      COMMON/BLOC4/ AMAX, XMMAX
      COMMON/BLOC8/ THETAD(NTP) ,ES(NTP,NSP) ,NT
      COMMON/BLOC9/ AA  ,AA2  ,ALPHA2 ,BL  ,FAC1  ,FAC2  ,FAC3  ,FAC4
      COMMON/BLOC13/MNA  ,AM(MNAP)
      COMMON/BLOC14/C6  ,C7  ,SQR2  ,ZY  ,ZYY
      COMMON/BLOC15/AN  ,COSA  ,DCT  ,SINZY  ,P?3)
      COMMON/BLOC16/FAC5  ,XL  ,SFP
      COMMON/BLOC17/PP(MSETP,MAP) ,SHIN(MSETP,MNAP) ,DR(MSETP,MNAP)
      COMMON/BLOC18/  DC, A84, A1, A2, A3, WT
      COMMON/BLOC19/CST ,CSTL ,CSTT ,CSTIL ,CSTS,CSTSQ,IFLAG,IFLAG1
      DIMENSION  TP(MSETP,1)  ,SU(3,1)  ,N1(MSETP,1)  ,N2(MSETP,1)
      DATA  DEG2, CONS /0.0427605?  , 1.3280851? /
C
      DO 70 M=1,MNA
      AN=AM(M)
      W= ES(M+1,I)
C     CONVERT THETA FROM DEGREES TO RADIANS.
```

```
      A= AN*C7
      A84=A
      IF(A.GT.A2)  W=0.
      SINA= SIN(A)
      COSA= COS(A)
      SINZY= SINA*ZY
      DCT= 1.-DC*COSA
C
C     CALCULATE FREQUENCY BAND NUMBER FOR SELF NOISE(N1) AND
C          SHEAR NOISE(N2).
      IF(A.GT.A2) GO TO 20
      ABAND=FAC5*(DCT**2+ALPHA2*(DC*COSA)**2)
      GO TO 21
   20 ABAND=FAC5*DCT**2*(ALPHA2*(DC/AA)**2+1.)
   21 BBAND=W*COSA*XL*XMMAX
      CALL FBAND(ABAND,BBAND,CONS,SFP,N1,N2,I,M)
C
      IF(IFLAG.EQ.0) GO TO 30
      IF(ABS(A).LT.0.0001) GO TO 46
      IF(A.LT.A1-DEG2)  GO TO 50
      IF(ABS(A-A1).LT.DEG2) GO TO 40
   30 IF(ABS(A-A2).LT.DEG2) GO TO 40
      IF(A.GT. A2) GO TO 45
C
C     EQ (85):  FROM 0 DEG TO WITHIN 2 DEG OF THETA2(A2).
      CALL EQ85(SINA,CST ,CSTS,W,M,I,IPRT)
      GO TO 55

C     EQ (84):  WITHIN 2 DEG OF THETA2(A2).
   40 CALL EQ84(A,CSTT,CSTTL,M,I,IPRT,IDUM,DUM)
      GO TO 55
C     ACOUSTIC MODE:  EQ(82):  FROM WITHIN 2 DEG OF THETA2(A2) TO 180 DEG.
   45 IF(IFLAG1.EQ.0) GO TO 50
      IF(A.LE. A3) GO TO 50
   46 CONTINUE
      DO 48 J=1,3
   48 P(J)= 0.0
      PP(I,M)= -99.
      SHIN(I,M)= -99.
      DK(I,M)=  -99.
      GO TO 55
   50 CALL EQ82(SINA,CSTS,CSTSL,W,M,I,IPRT)
C
   55 DO 60 J=1,3
   60 TP(I,J)= TP(I,J)+P(J)
      SU(1,M)= SU(1,M) +10.**(.1*(PP(I,M)-94.))*.1)
      SU(2,M)= SU(2,M) +10.**(.1*(SHIN(I,M)-94.))*.1)
   70 SU(3,M)= SU(3,M) +10.**(.1*(DK  (I,M)-94.))*.1)
      RETURN
C
      END
```

Subroutine CONST

```
      BLOCK DATA
C     C4= 3.*SQRT(2)
C     C5= GAMMA(2/3)= 1.354117939
C     C6= 180./PI
C     C7= PI/180.
C     C8= SQRT(PI)
C     C9= 160.*SQRT(2)/9.
C     SQR2= SQRT(2)
C     ZY=2.*5.*3.14159265**2./180.
C     ZYY= 2.*ZY
C
      PARAMETER  MNAP= 27
C
      COMMON/BLOC6/ ALPHA  ,PI   ,XLI  ,RSQ  ,C4   ,C5   ,C8   ,C9   ,FO
     1             ,AI   ,OMEGA
      COMMON/BLOC3/MNA   ,AM(MNAP)
      COMMON/BLOC4/C6   ,C7   ,SQR2   ,ZY   ,ZYY
C
      DATA PI, ZY, ZYY /3.14159256,  .54831135, 1.0966227
     1     FO, RSQ     / .666667,  1.  /
     2     C4, C5, C6 / 4.242640687,  1.354117939,  57.29577795 /
     3     C7, C8, SQR2 / .17453292E-01,  1.77245385,  1.41421356 /
     4     C9          / 25.14159744 /
     5     AI, OMEGA   / .355028,  1. /
     6     MNA         / 26 /
C
      END
```

Subroutine SETUP

```
      SUBROUTINE SETUP (ICODE,IPRT)
      PARAMETER  NSP= 10  ,NTP= 18  ,MPTS= 221  ,MNAP= 27
C
      COMMON/BLOC5/ AD(MPTS)  ,XMC(MPTS)  ,Y(MPTS)
      COMMON/BLOC4/ AMAX  ,XMMAX
      COMMON/BLOC6/ ALPHA  ,PI   ,XLI  ,RSQ  ,C4   ,C5   ,C8   ,C9   ,FO
     1             ,AI   ,OMEGA
      COMMON/BLOC8/ THETAD(NTP)  ,ES(NTP,NSP)  ,NT
      COMMON/BLOC9/ AA  ,AA2  ,ALPHA2  ,DL  ,FAC1  ,FAC2  ,FAC3  ,FAC4
      COMMON/BLOC13/MNA  ,AM(MNAP)
      COMMON/BLOC16/FAC5  ,XL  ,SFP
```

```
C
C
      IPR= 'NO'
      READ(5,500,END=777) IRD,ICODE,IPRT,ALPHA,XL,XL1,SF,PWDB
      IF(IRD.EQ.0) GO TO 200
      READ(5,600)    D
      READ(5,601) (AD(I),I=21,181,20)
      READ(5,601) (XMC(I),I=21,181,20)
      READ(5,500) NT
      READ(5,600) (THETAD(I),I=1,NT)
      DO 180 I=1,NT
  180 READ(5,601) (ES(I,J),J=1,9)
      IR= 'YES'
      WRITE(6,604) (I,I=21,181,20)
      WRITE(6,605)  (THETAD(I),(ES(I,J),J=1,9),I=1,NT)
      GO TO 225
C
  200 D= XMMAX
      IR= 'NO'
  225 IF(IPRT.EQ.1) IPR= 'YES'
      WRITE(6,603) IR,IPR,ALPHA,XL,XL1,SF,PWDB
      DELTH= 5.
      DO 240 I=2,NT
  240 AM(I-1)= THETAD(I)
      DO 260 I=NT,MNA
      AM(I)= AM(I-1)+DELTH
      IF(ABS(AM(I)-90.).LT. 0.0001) DELTH= 10.
  260 CONTINUE
C
      SFP= SF/6.283853E-03
C
C     ALPHA IS MODIFIED ACCORDING TO MACH NUMBER AND SPEED RATIO.
C
      XM=XMMAX
      F1=XM**4/(2.5*XM**4)
      F2= 1.-F1
      ALPHA=ALPHA*AMAX**0.75/(F2+F1*AMAX**1.75)
      ALPHA2= ALPHA**2
      ALPHA4= ALPHA2**2
      WRITE(6,610) ALPHA
C
      DL=0.606*D
C     DEFINITION OF POWER FACTOR.
      PW=10.**(PWDB*0.1-2.2)
      BM=D
      FAC3= C4*PI**1.5*PW    *D**8*ALPHA4    *(DL/D)**4/(    XL1*RSQ)
      FAC1=FAC3
      FAC2=2.*ALPHA*DL/XLT
      FAC4= C9*PI**2*D**8*AI**2*ALPHA**4.333333*C5*(DL/D)**4.333
     1 *PW /(RSQ*    XL1**1.333333*OMEGA**.333333)
      XLT=XL1*D/ALPHA/DL
      FAC5= 0.125*XLT*XLT
      RETURN
```

```
C
  777 WRITE(6,602)
      STOP
C
  500 FORMAT(3I5,5X,5F10.0)
  600 FORMAT(8F10.3)
  601 FORMAT(5E15.8)
  602 FORMAT('1END OF CARD INPUT TO SUBROUTINE NOISE')
  603 FORMAT(///' CARD INPUT FOR MMAX, A, MC, THETA, AND W?',2X,A3/
     1 ' DETAILED PRINTOUT?',2X,A3//'0  ALPHA',9X,'L',12X,'L1',11X,'SF',
     2 11X, 'PW(DB)'/ F8.3,4F13.3)
  604 FORMAT(  '1THETA(RAD)' ,9 (6X,'S(',I3,')') )
  605 FORMAT( F8.2,4X,9E12.5)
  610 FORMAT(/5X,'MODIFIED ALPHA IS:', F10.4)
      END
```

END OF COMPILATION: NO DIAGNOSTICS.

Subroutine VOPFLE

```
@FOR,;S VOPFLE
      SUBROUTINE VOPFLE(V0,MSET,ICODE)
C     V0 PROFILE
C
      DIMENSION  V0(1)
C
      DO 66 I=1,MSET
      GO TO (20,40),ICODE
   20 X= -2.88*(I*.1-3.5)**2
      GO TO 66
   40 X= -0.707I*(I*.1)**2
   66 V0(I)=(0.16*EXP(X))**4
      RETURN
C
      END
```

Subroutine FBAND

```
@FOR,;S FBAND
      SUBROUTINE FBAND(ABAND,BBAND,CONS,SFP,N1,N2,I,M)
      PARAMETER  MSETP= 9
      DIMENSION N1(MSETP,1)  ,N2(MSETP,1)
C
      IF(ABS(ABAND).GE.1.E-05) GO TO 17
      WBAND1= 2./BBAND
      WBAND2= WBAND1
      GO TO 18
   17 BBSQ= BBAND**2
      TEMP= .5/ABAND
      WBAND1= TEMP*(-BBAND+SQRT(BBSQ+8.*ABAND))
      WBAND2= TEMP*(-BBAND+SQRT(BBSQ+4.*ABAND))
   18 N1(I,M)=CONS*ALOG(SFP*WBAND1)+0.5
      N2(I,M)=CONS*ALOG(SFP*WBAND2)+0.5
      RETURN
C
      END
```

Subroutine EQ85

```
@FOR,;S EQ85
      SUBROUTINE EQ85(SINA,CST,CSTL,W,M,I,IPRT)
      PARAMETER  MNAP= 27  ,MSETP= 9  ,MAP= MNAP+1
C
      COMMON/BLOC9/ AA  ,AA2  ,ALPHA2  ,DL  ,FAC1  ,FAC2  ,FAC3  ,FAC4
      COMMON/BLOC10/GG(MNAP)  ,CB(MNAP)          ,OK(MNAP)  ,XY(MNAP)
      COMMON/BLOC14/C6  ,C7  ,SQR2  ,ZY  ,ZYY
      COMMON/BLOC15/AN  ,COSA  ,DCT  ,SINZY  ,P(3)
      COMMON/BLOC17/ PP(MSETP,MAP),SHIN(MSETP,MNAP),DK(MSETP,MNAP)
C
      RF= SINA/SQRT(COSA**2+(DCT/AA)**2)
      CRI= COSA**4
      CO= DCT**2+ALPHA2*(DL*COSA)**2
      CALL PVAR (CO,RF,CRI,CST,QQP,RFL,CRIL,COVL ,CSTL)
C
      CB(M)= FAC2*W*COSA/SQRT(CO)
      B= CB(M)*SQR2
      CALL INTEG(B,FB,FBL)
      CALL INTEG(CB(M),FBC,GG(M))
      QQ= QQP*FB
      TT= QQP*FBC
      CALL PVARA (QQ,SINZY,P(1),PP(I,M))
      CALL PVARA (TT,SINZY,P(2),SHIN(I,M))
      CALL PVARA (QQ+TT,SINZY,P(3),DK(I,M))
      IF(IPRT.EQ.0) RETURN
      RR= PP(I,M)-FBL
      OK(M)=0.0
      XY(M)=1.0
      WRITE(6,23)AN,PP(I,M),RFL,CRIL,COVL,FBL,B,W,RR
      RETURN
C
   23 FORMAT (F6.1,5F12.3,7F15.8,F15.3)
      END
```

Subroutine INTEG

```
@FOR,;S INTEG
      SUBROUTINE INTEG(B,FB,FBL)
C     INTEGRAL FROM B TO U OF  EXP(B**2-U**2)*(U-B)**4*DU
C
      SUM=0.0
C
      DO 10 I=1,599
      H=0.005
      Q=I/1.
      X=B+H*Q
      Y=B**2-X**2
      Z=(X-B)**4
      F=EXP(Y)*Z
   10 SUM=SUM+F
C
      AF=B**2-(B+3.)**2
      FF=EXP(AF)*81.
      FC=0.005*(SUM+FF/2.)
      FB=FC/0.664667
      FBL=10.**ALOG10(FB)
      RETURN
      END
```

Subroutine EQ84

```
BFOR,IS EQ84
      SUBROUTINE EQ84(A,CSTT,CSTTL,M,I,IPRT,ISUB,R)
      PARAMETER  MNAP= 27  ,MSETP= 9  ,MAP= MNAP+11
C
      COMMON/BLOC9/ AA  ,AA2  ,ALPHA2  ,DL  ,FAC1  ,FAC2  ,FAC3  ,FAC4
      COMMON/BLOC10/GG(MNAP)  ,CB(MNAP)  ,OK(MNAP)  ,XY(MNAP)
      COMMON/BLOC15/AN  ,COSA  ,DCT  ,SINZY  ,P(3)
      COMMON/BLOC17/ PP(MSETP,MAP),SHIN(MSETP,MNAP),DK(MSETP,MNAP)
      COMMON/BLOC18/  DC, A84, A1, A2, A3, WT
      FUN2(A)= 10.*ALOG10(A)+94.
C
      PI=3.14159265
      RF= TAN(A)
      CO=DCT**2+ALPHA2*(DL*COSA)**2
      CRI= COSA**4.333
      IF(AN.LT.45.)   GO TO 10
      AX=2.*A-0.5*PI
      COSAX=COS(AX)
      RF=1./COSAX
      CRI= COSAX**4.333
      CO=DCT**2+ALPHA2*(DL*COSAX)**2
   10 CONTINUE
      TEMP= CSTT*CO**-0.16667
      CALL PVAR(CO,RF,CRI,TEMP,QQ  ,RFL,CRIL,COVL,CSTTL)
      IF(M.NE.0) GO TO 40
      PP(I,ISUB)= FUN2(QQ)
      IF(IPRT.EQ.1) WRITE(6,24) R   ,PP(I,ISUB),RFL,CRIL,COVL
      RETURN
C
   40 CALL PVARA (QQ,SINZY,P(1),PP(I,M))
      CALL PVARA (QQ+QQ,SINZY,P(3),DK(I,M))
      CALL PVARA (QQ,SINZY,P(2),SHIN(I,M))
      P(2)= P(1)
      SHIN(I,M)= PP(I,M)
      IF(IPRT.EQ.0) RETURN
      OK(M)=0.0
      XY(M)=1.0
      GG(M)= 0.0
      CB(M)= 0.0
      WRITE(6,24) AN,PP(I,M),RFL,CRIL,COVL,PP(I,M)
      RETURN
C
   24 FORMAT (F6.3,4F12.3,42X,F15.3)
      END
```

Subroutine EQ82

```
@FOR,IS EQ82
      SUBROUTINE EQ82(SINA,CSTS,CSTSL,W,M,I,IPRT)
C     ACOUSTIC MODE:  EQ(82):  FROM WITHIN 2 DEG OF THETA2(A2) TO 180 DEG.
C
      PARAMETER  MNAP= 27  ,MSETP= 9  ,MAP= MNAP+11
C
      COMMON/BLOC9/ AA  ,AA2  ,ALPHA2  ,DL  ,FAC1  ,FAC2  ,FAC3  ,FAC4
      COMMON/BLOC10/GG(MNAP)  ,CB(MNAP)          ,DK(MNAP)  ,XY(MNAP)
      COMMON/BLOC14/C6  ,C7  ,SQR2  ,ZY  ,ZYY
      COMMON/BLOC15/AN  ,COSA  ,DCT  ,SINZY  ,P(3)
      COMMON/BLOC17/ PP(MSETP,MAP),SHIN(MSETP,MAP),DK(MSETP,MNAP)
      COMMON/BLOC18/  DC, A84, A1, A2, A3, WT
C
      AO= ACOS(AA*COSA/DCT)
      RF= AA*SINA/(DCT*SIN(AO))
      RF=ABS(RF)
      CRI=ABS(AA/DCT)
      CO= AA2+ALPHA2*DL**2
      FB=1.
      FBC=1.
      IF(A84.GT.A1)  GO TO 10
      CB(M)=FAC2*W*COSA/SQRT(CO)
      B=CB(M)*SQR2
      CALL INTEG(B,FB,FBL)
      CALL INTEG(CB(M),FBC,GG(M))
      GO TO 12
   10 CONTINUE
      IF(DC.LT.2.)  GO TO 12
      DCMA=DC-0.5*AA
      CFI=(1.-DCMA*COSA)**2-0.25*(AA*COSA)**2
      RF=AA*SINA/SQRT(CFI)
      CRI=AA/(1.-DCMA*COSA)
   12 CONTINUE
      CALL PVAR(CO,RF,CRI,CSTS,QQP,RFL,CRIL,CQVL,CSTSL)
C
      SNEW= SINZY
      IF(AN.GT.90.) SNEW= SINA*ZYY
      ZO= COS(AO)**2
      XX= (ZO+ZO+ZO)**.5
      QQ=QQP*FB
      TT=QQP*XX*FBC
      CALL PVARA (QQ,SNEW,P(1),PP(I,M))
      CALL PVARA (TT,SNEW,P(2),SHIN(I,M))
      CALL PVARA (QQ+TT,SNEW,P(3),DK(I,M))
      IF(IPRT.EQ.0) RETURN
      DK(M)= AO*C6
      XY(M)= XX
      IF (XY(M) .LT. 1.E-43) XY(M)= 1.0
      GG(M)=0.0
      CB(M)=0.0
      WRITE(6,24) AN,PP(I,M),RFL,CRIL,CQVL
      RETURN
C
   24 FORMAT (F6.4,4F12.3,42X,F15.3)
      END
```

Subroutine PVAR

```
@FOR,;S PVAR
      SUBROUTINE PVAR (CO,RF,CRI,CST,QQP,RFL,CRIL,COVL,CSTL)
      COMMON/BLOC18/  DC, A84, A1, A2, A3, WT
C
      FUN1(A)= 10.*ALOG10(A)
      FUN2(A)=FUN1(A) +94.
C
      COV=CO**-2.5
      CSF= CST*WT
      CSTL= FUN1(CSF)
      CSTL= FUN1(CST)
      RFL= FUN1(RF)
      CRIL= FUN1(CRI)
      COVL= FUN1(COV)
      QQP= CSF*RF*CRI*COV
      RETURN
C
      ENTRY PVARA (QQ,SINZY,PX,PP)
C
      PX= QQ*SINZY
      IF(QQ.GE.1.E-16)  GO TO 60
      PP= -99.
      RETURN
   60 PP= FUN2(QQ)
      RETURN
C
      END
```

Subroutine A2SELF

```
@FOR,;S A2SELF
      SUBROUTINE A2SELF(A2,DC,CSTT,I,IPRT,PTA2,CSTTL)
      PARAMETER  MNAP= 27  ,MSETP= 9  ,MAP= MNAP+11
C
      COMMON/BLOC13/MNA  ,AM(MNAP)
      COMMON/BLOC14/C6  ,C7  ,SQR2  ,ZY  ,ZYY
      COMMON/BLOC15/AN  ,COSA  ,DCT  ,SINZY  ,P(3)
      COMMON/BLOC17/ PP(MSETP,MAP),SHIN(MSETP,MNAP),DK(MSETP,MNAP)
      DIMENSION  PTA2(1)  ,R(11)
C
      M= 0
      PTA2(I)= A2 *C6
      DO 90 N=1,11
      ISUB= MNA+N
      L= PTA2(I)
      R(N)= L-10.*2.*(N-1)
      IF(R(N).LT.90.) GO TO 40
      PP(I,ISUB)= -99.
      GO TO 90
   40 A= R(N)*C7
```

```
      COSA= COS(A)
      DCT= 1.-DC*COSA
      CALL FQ84(A,CSTT,CSTTL,M,I,IPRT,ISUB,R(N))
   80 CONTINUE
      RETURN
C
      END
```

Subroutine PRINT

```
@FOR,IS PRINT
      SUBROUTINE PRINT(CSTL,CSTSL,CSTTL,VVL,TP,DC,AA,ICODE,I)
      PARAMETER  MNAP= 27  ,MSETP= 9  ,MAP= MNAP+11
C
      COMMON/BLOC10/GG(MNAP)  ,CB(MNAP)  ,DK(MNAP)  ,XY(MNAP)
      COMMON/BLOC13/ MNA  ,AM(MNAP)
      COMMON/BLOC17/ PP(MSETP,MAP),SHIN(MSETP,MNAP),DK(MSETP,MNAP)
      DIMENSION TP(MSETP,1)
      WRITE (6,53) CSTL,CSTSL,CSTTL,VVL
      WRITE (6,69) TP(I,1)
      WRITE (6,21) DC   ,AA  ,ICODE
      WRITE(6,600)
      WRITE(6,601) (AM(M),SHIN(I,M),DK(M),XY(M),GG(M),CB(M),M=1,MNA)
      WRITE (6,69) TP(I,2)
      WRITE (6,99)
      WRITE (6,89) (AM(M),DK(I,M),M=1,MNA)
      WRITE (6,69) TP(I,3)
      RETURN
C
   21 FORMAT('1H',45X,'CONVECTION MACH NO.=',F10.6,10X,'SPEED OF SOUND RAT
     'IO=',F5.2 ,10X,'VO CODE=',I2//)
   53 FORMAT (5X,'CONSTANT FOR (S1)=',F10.3,5X,'CONSTANT FOR (SO)=',F10.3,
     '5X,'CONSTANT FOR (SP)=',F10.5,5X,'V0**4=',F10.3)
   69 FORMAT (// 15X,'TOTAL POWER=',F10.3)
   89 FORMAT (F6.1,F12.3)
   99 FORMAT (1X,'ANGLE',3X,'TOTAL-INT' //)
  600 FORMAT(    1X,'ANGLE',4X,'SHEARINT',6X,'AO',7X,'SH-SEL-RAT',7X,
     '1'F(BB)',15X,'(BB)' //)
  601 FORMAT (F6.1,3F12.3,2F15.8)
      END
```

Subroutine OUTPUT

```
@FOR,IS OUTPUT
      SUBROUTINE OUTPUT(ICODE,N1,N2,SU,TP,STP,PTA2,MSET)
      PARAMETER  MNAP= 27  ,MSETP= 9  ,MAP= MNAP+11  ,MPTS= 221
C
      COMMON/BLOC1/ AD(MPTS)  ,XMC(MPTS)  ,Y(MPTS)
      COMMON/BLOC4/ AMAX  ,XMMAX
      COMMON/BLOC13/MNA  ,AM(MNAP)
      COMMON/BLOC17/ PP(MSETP,MAP),SHIN(MSETP,MNAP),DK(MSETP,MNAP)
      DIMENSION  N1(MSETP,1)  ,N2(MSETP,1)  ,SU(3,1)  ,TP(MSETP,1)
```

```
     1          ,STP(1)   ,PTA2(1)
C
      WRITE (6,21) XMMAX,AMAX,ICODE
      WRITE(6,604) (I,I=1,9)
      WRITE(6,610) (XMC(I),I=21,181,20),TAD(I),I=21,181,20)
      WRITE(6,607) (AM(M),(PP(I,M),N1(I,M),I=1,MSET),SU(1,M),M=1,MNA)
      WRITE(6,608) (TP(I,1),I=1,MSET),STP(1)
      WRITE(6,611) (PTA2(I),I=1,MSET)
      WRITE(6,602) (     (PP(I,MNA+N)          ,I=1,MSET),N=1,11)
      WRITE (6,21) XMMAX,AMAX,ICODE
      WRITE(6,605) (I,I=1,9)
      WRITE(6,610) (XMC(I),I=21,181,20),TAD(I),I=21,181,20)
      WRITE(6,607) (AM(M),(SHIN(I,M),N2(I,M),I=1,MSET ),SU(2,M),M=1,MNA)
      WRITE(6,608) (TP(I,2),I=1,MSET),STP(2)
      WRITE (6,21) XMMAX,AMAX,ICODE
      WRITE(6,606) (I,I=1,9)
      WRITE(6,610) (XMC(I),I=21,181,20),TAD(I),I=21,181,20)
      WRITE(6,607) (AM(M),(DK(I,M),I=1,MSET),SU(3,M),M=1,MNA)
      WRITE(6,609) (TP(I,3),I=1,MSET),STP(3)
      RETURN
C
   21 FORMAT(1H1,45X,'CONVECTION MACH NO.='F6.3,14X ,'SPEED OF SOUND RAT
     1IO='F5.2 ,10X,'VO CODE=',I2//)
  602 FORMAT( 6X,F9.2,8F13.2)
  603 FORMAT(F6.1,9F13.2,F9.2)
  604 FORMAT( ' SELF NOISE INTENSITY(DECIBELS) WITH FREQUENCY BAND NUMB
     1ERS'  //   ' ANGLE',9(3X,'SEGMENT',I3),4X,'TOTAL')
  605 FORMAT( ' SHEAR NOISE INTENSITY(DECIBELS) WITH FREQUENCY BAND NUMB
     1ERS'  //   ' ANGLE',9(3X,'SEGMENT',I3),4X,'TOTAL')
  606 FORMAT(   ' TOTAL NOISE INTENSITY(DECIBELS)'
     1      //   ' ANGLE',9(3X,'SEGMENT',I3),4X,'TOTAL')
  607 FORMAT(1F6.1,9(F9.2,'(',I2,')'),F9.2)
  608 FORMAT(   / 6X,9(F9.2,4X),F9.2/   )
  609 FORMAT( / 6X,9F13.2,F9.2/)
  610 FORMAT(' (DEG) MC',F10.5,8F13.5/7X,'A',F15.5,8F13.5/)
  611 FORMAT(6X,'A2 ',F6.2,8F13.2/)
      END
```

APPENDIX C

AERODYNAMIC NOISE EMISSION FROM TURBULENT SHEAR LAYERS

J. Fluid Mech. (1973), *vol.* 59, *part* 3, *pp.* 451–470
Printed in Great Britain

Aerodynamic noise emission from turbulent shear layers

By S. P. PAO
University of Alabama, Huntsville

(Received 8 August 1972)

The Phillips (1960) convected wave equation is employed in this paper to study aerodynamic noise emission processes in subsonic and supersonic shear layers. The wave equation in three spatial dimensions is first reduced to an ordinary differential equation by Fourier transformation, then solved via the WKBJ method. Three typical solutions are required for discussions in this paper. The current results are different from the classical conclusions. The effects of refraction, convection, Mach-number dependence and temperature dependence of turbulent noise emission are analysed in the light of solutions to the Phillips equation. Owing to the inherent restrictions of the WKBJ transformation, the results of the present paper should be applied to wave radiation from shear layers whose thickness is no less than approximately one quarter of a wavelength. Such a condition is satisfied for turbulent round jets with an exit velocity greater than 0·6 times the ambient speed of sound.

1. Introduction

This analysis is based on the convected wave equation first introduced by Phillips in 1960. It is intended here to study the noise emission and propagation properties in shear layers with known turbulence structures. An effort has been made to keep the analysis in direct parallel with the classical theory of aerodynamic noise. However, no direct comparison with the Lighthill theory is made because some basic assumptions are different, and the implication of such differences has not been determined. The analytical results indicate several new aspects of noise radiation mechanisms which are not available in the classical results. Since the analysis and physical interpretation of this study are rather involved, the assumptions made at various points throughout this paper are summarized as follows.

The convected wave equation itself is derived through the basic principles of fluid mechanics, and it is a natural extension of the Lighthill equation of aerodynamic noise. The linearized version of the general equation has the form of a simple wave equation in Lagrangian co-ordinates. The right-hand side of this equation contains four terms: a turbulent quadrupole, shear flow and turbulence interaction, entropy fluctuation and viscous effect. If the flow domain is free of shocks, the acoustic pressure fluctuation can be assumed to be decoupled from the entropy fluctuations. It is tacitly assumed in the present analysis that all terms on the right-hand side of the wave equation are known quantities and the contributions of individual terms can be considered as in-

dependent of each other. Justification for such an assumption is a difficult fundamental question in the theories of aerodynamic noise.

The configuration of the flow field brings further restrictive assumptions to the convected wave equation such that it becomes mathematically manageable. The shear-layer profile and the turbulence structure are assumed to be homogeneous in time and in the two Cartesian co-ordinates in the plane of the shear layer. The mean flow velocity and temperature profiles are functions of the transverse spatial co-ordinate only. Under such conditions, the three-dimensional wave equation can be reduced to an ordinary differential equation by performing Fourier transformation in the three co-ordinates for which the flow properties are homogeneous. The unknown wave function now depends on only one independent variable, a spatial co-ordinate, together with two wavenumber components and frequency as parameters.

The ordinary differential equation thus obtained is a canonical Sturm–Liouville equation. In essence, this equation can be visualized as a simple wave equation with a variable wavenumber which takes both real and imaginary values. The point at which the wavenumber passes from one domain to another is called a transition point. In the present analysis, this one-dimensional wave equation is first transformed to a standard form by using a WKBJ transformation, and then solved by using the Green function and integral equation technique. Several transformations are employed as required for different numbers of transition points at different positions along the wave propagation path.

A crucial point to be discussed here is the inherent limitations introduced by the WKBJ method. According to Morse & Feshbach (1953), the WKBJ method is applicable only when the change in wavenumber in one wavelength is sufficiently small. In the present analysis, it means that the shear-layer thickness should be at least of the order of one wavelength. However, this comment applies mainly to cases where only the first approximation for the solution is taken. The accuracy of such a solution is therefore subject to an asymptotic condition where the solution is exact only if the wavenumber approaches infinity. In the present analysis, the WKBJ method is used in the transformation of the differential equation, while the equation is solved through the Green function and integral equation technique. Hence, for any given wavenumber the accuracy of the solution can be improved by taking higher terms of the iterations. For practical computations, the convergence rate should be sufficiently rapid as long as the shear-layer thickness is greater than one radian of the acoustic wavenumber, i.e. $kL > 1$, where k is the wavenumber and L is the shear-layer half-thickness. In the case of jet noise, the value of kL is directly proportional to the Strouhal number. It can be shown that the above restriction on wavenumber is satisfied for all noise radiation at frequencies higher than the peak of the noise spectrum if the jet exit velocity is greater than 0·6 times the ambient speed of sound. Hence, the above condition does not impose any significant limitation on the application of the present analysis in dealing with noise radiation from high-speed turbulent shear flows.

By solving the reduced wave equation through the WKBJ method, a solution for the wave function is obtained in mixed variables: one spatial co-ordinate,

two wavenumber components and frequency. In the far field, the pressure function approaches asymptotically a function harmonic in the transverse spatial co-ordinate. If the deviation from the harmonic function in the near field is ignored, the wave function can be transformed by Fourier analysis into a pure harmonic representation in wavenumber–frequency co-ordinates. However, neither of the above two representations is convenient for practical applications because it is much more important to know the noise spectrum and intensity at a given point in space. It is therefore necessary to transform the results back through an inverse Fourier transformation into physical co-ordinates. This has been accomplished in closed form. One assumption has been made here to simplify the mathematics: the shear layer is assumed to be symmetric in the transverse spatial co-ordinate. The noise radiation above and below the shear layer is the same at all times.

The key to this part of the analysis is that the process is actually a matching of solutions. First, the pressure field is computed through the Phillips wave equation. Second, it is assumed that in the far field the solution is matched by a pressure field which is governed by a simple wave equation throughout the entire space. Hence, the only differences between the two solutions are in the near field. As far as wave propagation in the far field is concerned, it really does not matter what has happened in the near field. The solution in the far field as obtained through the inverse transformation is indeed the correct solution to the Phillips equation. A by-product of this analysis is that an equivalent source function can be defined. After matching the solution of the Phillips equation in the far field with a solution which is governed by the simple wave equation, a source function in the framework of the simple wave equation can be identified among the formulae. Such an equivalent source function in the near field would provide the best indication of what effect the shear flow has conferred upon the radiation efficiency of the turbulent sound sources.

At this point, the main part of the analysis is complete. Since the non-homogeneous nature of the wave equation in the transverse direction precludes a clear description of the wave propagation process in common terminology of ray acoustics, it is necessary to make some further simplifying assumptions for the sake of interpretation of results. These assumptions include taking the high frequency limit, the definition of the turbulence structure as a Gaussian distribution, order-of-magnitude estimates of integrals, and others. These miscellaneous items will be discussed individually as they are needed later in this paper.

In a review by Laufer, Ffowcs Williams & Childress (1964), it was noted that the original Phillips solution contained a factor $\{M^2-k^2/Q^2\}^{-\frac{1}{4}}Q^{-\frac{1}{4}}$. If the angle ϕ between the x_1 axis and the projection of the wavenumber vector on the plane of the shear layer reaches a critical value such that $1-M_c\cos\phi = 0$, M^2-k^2/Q^2 vanishes. Therefore, the Phillips solution becomes singular. Furthermore, the spectrum of the radiated sound diverges as the factor Q approaches zero. It was on this basis that Laufer, Ffowcs Williams & Childress had strong reservations as to the validity of the Phillips solution.

Both of these singularities can be resolved as they are mathematical in nature.

The occurrence of the former singularity is a result of an assumption made in the analysis of the original Phillips solution. In Phillips (1960), the Mach number is assumed to be very large such that the distance between the pair of transition points is small compared with the thickness of the shear layer. However, the effective convection Mach number $M_c \cos\phi$ equals one at the critical angle. The separation between the transition points then equals the thickness of the shear layers, and the above assumption is violated. This point has been discussed in Pao (1972). In the present analysis, the position of the transition point and the proper form of the WKBJ transformation are determined without any mathematically restrictive assumption. Apart from the restrictions discussed earlier in this section, the solutions are uniformly valid for all wavenumbers at all Mach numbers.

The divergence of the spectrum is a mathematical problem associated with the spectral analysis of either the convected wave equation or the simple wave equation. The factor $(Mq)^{-\frac{1}{2}}$ in the spectral solution to the wave equation is an integrable singularity which appears to have no particular physical significance. In all practical applications, the solution to the wave equation should be written in terms of the space and time co-ordinates instead of the spectral co-ordinates. The former solution can be recovered from the latter by means of an inverse Fourier transformation as given in this paper. One finds that such a solution depends explicitly on $(Mq)^{\frac{1}{2}}$. The singular condition no longer exists.

Among the assumptions in this paper, there are two important differences from the Lighthill theory. In the Lighthill theory, it is assumed that the shear flow dimension is much smaller than the wavelength. In this analysis, the shear flow dimension should be at least of the same order as the wavelength. Second, the Lighthill theory was originally derived for convected turbulence at low Mach numbers while the Phillips theory was originally derived for shear flows with very high Mach numbers. Since the Lighthill theory has been subsequently extended by Ffowcs Williams (1963) to the high-speed regime, the second distinction is actually rather ambiguous. Nevertheless, these differences in the basic assumptions make it rather difficult to compare directly the results of the present analysis with the classical results. In view of such difficulties in comparison, the analysis in the present paper has been kept in direct parallel with the spectral analysis of classical aerodynamic noise theory. By comparing the analysis step by step, one can indeed gain much insight into the difference between these theories.

2. Formulation

By using the momentum equation, the continuity equation and the equation of state for a perfect gas, a convected wave equation can be derived (Phillips, 1960):

$$\frac{D^2}{Dt^2}\log\left(\frac{p}{p_0}\right)-\frac{\partial}{\partial x_i}\left\{c^2\frac{\partial}{\partial x_i}\log\left(\frac{p}{p_0}\right)\right\}=\gamma\frac{\partial u_i}{\partial x_j}\frac{\partial u_j}{\partial x_i}+\gamma\frac{D}{Dt}\left(\frac{1}{c_p}\frac{DS}{Dt}\right)$$
$$-\gamma\frac{\partial}{\partial x_i}\left\{\frac{1}{\rho}\frac{\partial}{\partial x_j}\mu\left(\frac{\partial u_i}{\partial x_j}+\frac{\partial u_j}{\partial x_i}-\frac{2}{3}\frac{\partial u_k}{\partial x_k}\delta_{ij}\right)\right\}, \quad (1)$$

where p is the pressure, S is the entropy, u_i denote the velocity components, t and x_i denote the time and three-dimensional Cartesian co-ordinates, and c_p, γ and μ are the specific heat at constant pressure, the specific heat ratio and the coefficient of viscosity, respectively. For sound radiation processes in a turbulent flow, both heat conduction and viscosity are likely to be unimportant. Furthermore, if the flow field is shock free, one can probably consider separately the effect of pressure fluctuations and the effect of entropy fluctuations. Under these circumstances, the last two terms of the right-hand side of (1) can be omitted.

In order to construct a solution to the convected wave equation, it is necessary to specify the flow field. A parallel shear flow has been chosen such that it has a characteristic thickness $2L$ and such that the mean flow properties and the turbulent structure are homogeneous in time and the spatial co-ordinates x_1 and x_2 in the plane of the shear layer. The mean flow velocity $\overline{u}_1$ and the local speed of sound a are functions of x_3 only. Although the foregoing assumption should be sufficient, further restrictions can reduce the bulk of the analysis without loss of generality. In Phillips (1960), an antisymmetric flow field is assumed. In the present analysis, the flow is restricted to symmetrical profiles. The fluid far from the shear layer is assumed to be stationary. Equation (1) can be further simplified if small terms are omitted. In a turbulent flow, the fluctuating velocity components are small in comparison with the mean velocity. However, the derivatives of the fluctuating velocity components cannot be assumed small. In the present study, terms depending on small quantities to second or higher orders are omitted. Equation (1) then becomes

$$\left\{\left(\frac{\partial}{\partial t}+\overline{u}_1\frac{\partial}{\partial x_1}\right)^2+\left(\frac{\partial}{\partial t}+\overline{u}_1\frac{\partial}{\partial x_1}\right)u_i'\frac{\partial}{\partial x_i}-\frac{\partial}{\partial x_i}c^2\frac{\partial}{\partial x_i}\right\}\log\left(\frac{p}{p_0}\right) = \gamma\left\{2\frac{\partial\overline{u}_1}{\partial x_2}\frac{\partial u_2'}{\partial x_1}+\frac{\partial u_i'}{\partial x_j}\frac{\partial u_j'}{\partial x_i}\right\}, \quad (2)$$

where u_i' denotes velocity fluctuations with zero mean and $\overline{u}_i$ the mean velocity. Equation (2) is different from the original equation given by Phillips in two respects.

(i) There are two source terms on the right-hand side of this equation. The first term is the shear noise and the second term is the self-noise.

(ii) An additional term $\{(\partial/\partial t+\overline{u}_1\,\partial/\partial x_1)\,u_i'\,\partial/\partial x_i\}\log(p/p_0)$ appears on the left-hand side. It can be regarded as a dispersion term. Both $\partial/\partial t$ and $\overline{u}_1\,\partial/\partial x_1$ of the fluctuating velocity components are large quantities. Fortunately, their combination represents the evolution of the turbulence in the moving frame of reference, which is known to be slow. The value of Du_i'/Dt is of the same order of magnitude as the acoustic radiation. Hence, the effect produced by this term may be compared to the diffraction of sound by sound, which is a second-order effect. After this term has been neglected the resulting equation has the same left-hand side as that given by Phillips.

In the present study, the right-hand side of (2) is assumed known, the same assumption as was made in the Lighthill theory. Such an assumption is made here strictly in the belief that the results of the analysis indeed represent the

first-order effects of turbulent noise radiation. Philosophically, the turbulent source function is a part of the dynamical process in the flow, and thus inseparable from the left-hand side of the differential equation. A rational discussion of the limitations of this assumption must be dealt with from a point of view quite different from the practical intentions of the present analysis, and thus lies beyond the scope of this paper.

The shear-layer half-thickness L and the maximum shear-layer velocity U can be chosen as the reference parameters to non-dimensionalize (2). Since the mean flow and turbulence are homogeneous in time and in the plane of the shear layer, a generalized Fourier transform in these co-ordinates is adopted to simplify the non-dimensional convected wave equation. The ordinary differential equation thus obtained can be written as

$$\frac{d^2}{dy^2}\Phi(y,k_1,k_2,\omega)+M^2q^2\Phi(y,k_1,k_2,\omega)=-\frac{M^2}{A^2(y)}\Gamma(y,k_1,k_2,\omega), \tag{3}$$

with

$$\left.\begin{aligned} q^2&=\left\{\frac{M\omega+k_1M_c(y)}{MA(y)}\right\}^2-\frac{k_1^2+k_2^2}{M^2},\\ v_i&=\frac{u_i'}{U},\quad y_i=\frac{x_i}{L},\quad \tau=\frac{tU}{L},\quad M=\frac{U}{c_0},\quad M_c(y)=\frac{\overline{u}_1(y)}{c_0}, \end{aligned}\right\} \tag{4}$$

where y is an abbreviation for y_3: M is the reference Mach number; k_i denotes the wavenumber components and ω stands for frequency. The functions A, Φ and Γ are defined by

$$\left.\begin{aligned} A(y)&=c(y)/c_0,\\ \zeta(\mathbf{y},\tau)&=\iiint\Phi(y,k_1,k_2,\omega)\exp i(k_1y_1+k_2y_2+\omega\tau)\,dk_1\,dk_2\,d\omega,\\ G(\mathbf{y},\tau)&=\iiint\Gamma(y,k_1,k_2,\omega)\exp i(k_1y_1+k_2y_2+\omega\tau)\,dk_1\,dk_2\,d\omega,\\ \zeta(y,\tau)&=A(y)\log\{p(\mathbf{y},\tau)/p_0\},\\ G(y,\tau)&=\gamma A(y)\left\{\frac{\partial v_i}{\partial y_j}\frac{\partial v_j}{\partial y_i}+\frac{2}{M}\frac{\partial M_c}{\partial y_2}\frac{\partial v_2}{\partial y_1}\right\}, \end{aligned}\right\} \tag{5}$$

where $G(\mathbf{y},\tau)$ represents both the self-noise and shear-noise source terms in the convected wave equation. Equation (5) will be the working equation for further analysis in this paper. Very few assumptions, apart from linearization and the choice of the flow model, have been adopted in the derivation of this equation. No significant restriction has been placed so far on the range of applicable Mach numbers of the flow as chosen for the convected wave equation.

The function Mq can be analytically identified with the wavenumber k_3. If the Lighthill wave equation is subjected to Fourier transformations in the y_1, y_2 and τ co-ordinates, an ordinary differential equation can be obtained:

$$\left.\begin{aligned} d^2p(y,k_1,k_2,\omega)/dy^2+k_3^2p(y,k_1,k_2,\omega)&=-M^2\Gamma(y,k_1,k_2,\omega),\\ k_3^2&=M^2\omega^2-(k_1^2+k_2^2). \end{aligned}\right\} \tag{6}$$

In the far field, the value of Mq approaches a constant. Hence, (3) and (6) are identical if the function Mq and the wavenumber component k_3 are assumed to

stand for the same quantity. Owing to the interaction of the shear flow and the wave propagation process, the function Mq becomes a variable in the near field. However, it can still be identified with the transverse wavenumber component in a limited sense.

The function M^2q^2 may vanish at certain points in the shear layer. Such a zero is called a transition point because the value of M^2q^2 changes sign across this point, and the reduced wave equation changes type either from hyperbolic to elliptic or vice versa. Hence, it is necessary to employ the WKBJ method to solve (3). There are three cases that need to be considered. In the first case, there is no transition point along the path between the sound source and the far field. In common practice, it is actually not necessary to use the WKBJ technique to solve (3) in this case. Here it is considered as a zeroth-order WKBJ transformation and is treated in the same manner as the other two cases. In the second case, there is one transition point located between the sound source and the far field. However, there should be no other transition point within approximately two radians of wavelength. Here the differential equation will be hyperbolic in the far field and elliptic near the source. The source oscillation which contributes to nose radiation is hydrodynamic in nature. For this case the WKBJ transformation for well-separated transition points will be employed. In the third case, there are two transition points near the sound source. The distance between these two transition points is less than two radians of wavelength. This case can be analysed by a WKBJ transformation for a transition point where M^2q^2 has a zero of second order.

The occurrence of transition points is mainly a function of the convection Mach number and the angle of radiation. The situation can be considered from two different points of view. If a small sound source volume is given in the shear layer, where the M_c can be regarded as constant, the number and position of transition points are determined by the angle of radiation. In order to describe completely the wave radiation in all directions, all of the above conditions for (3) will be encountered. From another point of view, one can consider wave radiation in a given direction with source contributions from all layers of the shear flow. In this case, the transition point will be fixed at a point of the shear layer where M_c is predetermined by the angle of radiation. Although the former point of view is the most practical for applications, the latter view is represented by the formulation of (3).

3. Solution to the convected wave equation

Through the Fourier analysis indicated in the previous section, the pressure field and the sound source function have been broken up into plane-wave elements. Since the Fourier transformation is performed in the stationary frame of reference, the frequency ω represents the frequency of a plane-wave element as measured at a fixed point in the far field. The projection of the wavenumber vector on the plane of the shear layer is represented by k_1 and k_2. These components remain constant throughout the entire space including the shear-layer flow domain if a plane-wave element has been chosen in the far field. However,

wave propagation is non-uniform in the direction normal to the plane of the shear layer and is governed by (3).

In the far field, a plane-wave element is determined by its frequency and wavenumber vector. In the present case, the frequency and two components of the wavenumber vector are known. Since the magnitudes of the wavenumber and frequency are related through the speed of sound, k_3 is also known. From the above indications, it is clear now that the role of (3) is to determine how a chosen plane-wave element in the far field is related to the turbulent sound sources in the near field, and how sound is propagated from the source through the shear layer into the far-field. The solutions to (3) given below for various cases will confirm the above-mentioned role of the reduced wave equation.

By using a WKBJ transformation, the one-dimensional wave equation can be transformed to the following standard form:

$$d^2\eta/d\xi^2 + \xi^n\eta = g_n(\xi)\,\eta + h_n(\xi) \quad (n = 0, 1, 2), \tag{7}$$

with

$$\left.\begin{aligned} g_n(\xi) &= \tfrac{1}{2}\psi'^{-2}\{\psi'''/\psi' - \tfrac{3}{2}(\psi''/\psi')^2\}, \\ h_n(\xi) &= -M^2\Gamma(\xi, k_1, k_2, \omega)/\psi'^{\frac{3}{2}}A^2, \end{aligned}\right\} \tag{8}$$

where the transformations of the independent and dependent variables are defined by

$$\left.\begin{aligned} \eta(\xi) &= \psi'(y)\,\Phi(y), \\ \xi = \psi(y) &= \left\{\frac{n+2}{2}\int_{y_0}^{y} Mq(y)\,dy\right\}^{2/(n+2)}, \\ \psi'(y) &= d\xi/dy = q(y)\,\xi^{-\frac{1}{2}n}. \end{aligned}\right\} \tag{9}$$

The value of n denotes the order of zero at the transition point, and the lower integral limit y_0 indicates the position of the transition point. For $n = 0$, there is actually no transition point throughout the path of integration. Therefore, y_0 can be conveniently chosen as $y_0 = 0$. The function $g_n(\xi)$ is a residue function arising from the WKBJ transformation. In the far field, $g_n(\xi)$ approaches zero as ξ^{-2}. In the neighbourhood of the transition point, the limiting values of ψ' and g_n remain finite as ξ approaches zero. In the remainder of this paper, the solutions will be identified by $S0$, $S1$ and $S2$ for cases with $n = 0$, 1 and 2, respectively.

Since the Green function, integral equation technique for solving (3) is essentially the same as that given in Phillips (1960), details of the derivations will not be repeated here. In Pao (1971), the solution to (3) has been given as

$$\eta(\xi) = H(\xi) + \int_0^{\xi} R(\xi, s)\,\{g_n(s)\,H(s) + h_n(s)\}\,ds, \tag{10}$$

where $H(\xi)$ is an arbitrary solution which satisfies the homogeneous wave equation and $R(\xi, s)$ is the resolvent kernel which is conjugate to the kernel $K(\xi, s)$ of the integral equation. As a first approximation, the resolvent kernel

$$R(\xi, s) = K(\xi, s).$$

However, the solution can actually be given in a simpler form:

$$\eta(\xi) = H(\xi) + \int_0^{\xi} R(\xi, s)\,h(s)\,ds. \tag{11}$$

The difference lies in the starting-point of the iteration. In (10), the zeroth-order solution is assumed to be $H(\xi)$, while in (11) the zeroth-order solution is assumed to be zero. In the limit, both iterations will lead to the same analytic solution. For each of the three main solutions, the boundary conditions and the analytical nature of the integrals are different. These solutions will be discussed separately. For clarity of interpretation of results, only the first approximation to the resolvent kernel will be employed in the discussions immediately below. The higher iterations will be discussed later in this paper.

The acoustic mode S0

In the $S0$ solution, no transition point is encountered along the wave propagation path. Hence, the value of M^2q^2 is always positive and bounded away from zero. The homogeneous solutions to (3) are the simple harmonic functions of ξ. The kernel of the integration can be written as

$$K(\xi, s) = (2i)^{-1}\{e^{i(\xi-s)} - e^{-i(\xi-s)}\} = \sin(\xi - s), \tag{12}$$

where s is a dummy variable corresponding to ξ. It should be noted also that the origin of the ξ co-ordinate has been defined to be the same as the origin of the y_3 co-ordinate. Since the first approximation to the resolvent kernel is $K(\xi, s)$, the solution can be given as

$$\Phi_0(y, k_1, k_2, \omega) = \{Mq(y)\}^{-\frac{1}{2}}\left\{a\,e^{i\xi} + b\,e^{-i\xi} + \int_0^{\xi} \sin(\xi - s)h_0(s, k_1, k_2, \omega)\,ds\right\}, \tag{13}$$

where a and b are arbitrary constants to be determined by the boundary conditions.

If the wave is assumed to be propagating away from the shear layer at $y = \pm\infty$ these radiation conditions will serve as the required two boundary conditions. In the present discussion, the shear layer is similar to a jet exhaust flow into a stationary ambient medium. The convection velocity vanishes on the y_3 axis at $y_3 = \pm\infty$. The main shear flow will be confined to the neighbourhood of the y_1, y_2 plane.

For the above-mentioned flow condition, it is easy to verify that the outgoing wave at $+\infty$ is represented by $\exp(i\xi)$ and the outgoing wave at $-\infty$ by $\exp(-i\xi)$ The boundary conditions can be written as

$$\left.\begin{aligned} a + \frac{1}{2i}\int_0^{-\infty} e^{-is}h_0(s, k_1, k_2, \omega)\,ds = 0, \\ b - \frac{1}{2i}\int_0^{\infty} e^{is}h_0(s, k_1, k_2, \omega)\,ds = 0. \end{aligned}\right\} \tag{14}$$

Hence, the solution to the convected wave equation for the $S0$ mode is

$$\Phi_0(y, k_1, k_2, \omega) = (2i)^{-1}\{Mq(y)\}^{-\frac{1}{2}} \times \left\{e^{i\xi}\int_{-\infty}^{\xi} e^{-is}h(s, k_1, k_2, \omega)\,ds + e^{-i\xi}\int_{\xi}^{\infty} e^{is}h(s, k_1, k_2, \omega)\,ds\right\}. \tag{15}$$

From the structure of this solution, some immediate conclusions can be made. First of all, a local frequency can be defined through a Lagrangian transformation of co-ordinates. The local frequency of pressure fluctuations as measured in

a frame of reference which moves with the convection velocity M_c can be written as

$$\omega_0 = \omega + k_1 M_c/M. \tag{16}$$

Once a far-field plane-wave element has been determined, the values of k_1, k_2 and ω will remain constant. The value of Mq, though variable, is directly proportional to the value of ω. In the high frequency limit, there is a straightforward physical interpretation of (15). The value of Mq can be made arbitrarily large as the value of ω increases. Under such conditions, the value of Mq will appear to be constant over many wavelengths in a small interval Δy in the shear layer. If it is further assumed that a correlated turbulence volume lies in Δy, then the integrals in (15) will have the form of a Fourier transformation. These integrals will thus serve to select a harmonic component from the source function and pass it to the far field as a radiated plane-wave element. This source element will have a local frequency ω_0 and a wavenumber vector (k_1, k_2, Mq). However, by definition of Mq (equations (3) and (16)), the following relation holds:

$$\omega_0^2 = (A/M)^2\{k_1^2 + k_2^2 + (Mq)^2\}. \tag{17}$$

Hence the magnitude of the wavenumber vector is related to the local frequency through the local speed of sound. The source element which is responsible for far-field noise radiation is, therefore, an acoustic component of the turbulence structure in the convected frame of reference. Therefore, the $S0$ mode of noise emission can also be called the acoustic mode.

The Doppler effect of frequency shift can be recovered directly from (16). If the angle between the far-field wavenumber vector and the y_1 axis is defined as θ, equation (16) can be written as

$$\omega_0 = \omega(1 - M_c \cos\theta), \quad \text{with} \quad k_1 = k_\infty \cos\theta; \quad \omega = -k_\infty/M, \tag{18}$$

where k_∞ denotes the magnitude of the wavenumber vector in the far field, and the negative sign in the wavenumber–frequency ratio indicates a forward-propagating wave according to the definition of the Fourier transformations. Therefore

$$\omega = \omega_0/(1 - M_c \cos\theta). \tag{19}$$

Since it is known from the above discussion that the local frequency of the source function equals ω_0, the source function and the far-field noise radiation are related by the Doppler shift relation. Equation (19) is derived only from the far-field conditions and the definition of ω_0, its validity does not depend on the details of the shear flow profile. This relation should apply equally well to solutions $S1$ and $S2$.

The S1 solution

In this case one transition point exists between the far field and the source region. The governing differential equation is hyperbolic on the far-field side of the transition point and is elliptic on the other side. In Erdélyi (1956, p. 98) it is shown that the solutions on both sides of the transition point can be made analytically continuous through the use of Airy functions. The matching condition at the transition point has been included in the definition of the Airy

functions. For this reason, it is more convenient to define the transformation in a way which is slightly different from (9):

$$\xi(y) = \left\{\tfrac{3}{2}\int_{y_0}^{y} M|q|\,dy\right\}^{\frac{2}{3}}. \tag{20}$$

According to this definition, ξ is real and positive for points on either side of the transition point. The sign convention for the Airy functions requires, however, that the argument of the functions be negative for the hyperbolic branch of the solution and positive for the elliptic branch. In the present analysis, the ξ co-ordinate is pointing at the opposite direction from the y co-ordinate for wave radiation to plus infinity.

The kernel for the integral equation can be given as

$$K(\xi, s) = \begin{cases} \pi\{\mathrm{Bi}(-\xi)\,\mathrm{Ai}(-s) - \mathrm{Ai}(-\xi)\,\mathrm{Bi}(-s)\} & \text{for} \quad y > y_0, \\ \pi\{\mathrm{Bi}(\xi)\,\mathrm{Ai}(s) - \mathrm{Ai}(\xi)\,\mathrm{Bi}(s)\} & \text{for} \quad y \leqslant y_0. \end{cases} \tag{21}$$

Hence, the first-order approximate solutions to the convected wave equation are

$$\Phi_1(y, k_1, k_2, \omega) = \{Mq(y)\}^{-\frac{1}{4}}\xi^{\frac{1}{4}}\Big\{a\,\mathrm{Ai}(-\xi) + b\,\mathrm{Bi}(-\xi) + \int_0^{\xi}\pi\{\mathrm{Bi}(-\xi)\,\mathrm{Ai}(-s) - \mathrm{Ai}(-\xi)\,\mathrm{Bi}(-s)\}h_1(s, k_1, k_2, \omega)\,ds\Big\} \quad \text{for} \quad y > y_0 \tag{22}$$

and

$$\Phi(y, k_1, k_2, \omega) = \{Mq(y)\}^{-\frac{1}{4}}\xi^{\frac{1}{4}}\Big\{a\,\mathrm{Ai}(\xi) + b\,\mathrm{Bi}(\xi) + \int_0^{\xi}\pi\{\mathrm{Bi}(\xi)\,\mathrm{Ai}(s) - \mathrm{Ai}(\xi)\,\mathrm{Bi}(s)\}h_1(s, k_1, k_2, \omega)\,ds\Big\} \quad \text{for} \quad y \leqslant y_0. \tag{23}$$

Two boundary conditions are required for the $S1$ solution: the pressure wave is outgoing as ξ approaches minus infinity, and the pressure fluctuation vanishes as ξ approaches plus infinity. In order to define the boundary conditions, the asymptotic approximations for the Airy functions with large argument are required:

$$\begin{aligned} \mathrm{Ai}(-\xi) &\sim \pi^{-\frac{1}{2}}\xi^{-\frac{1}{4}}\sin(\zeta + \tfrac{1}{4}\pi), \quad \mathrm{Bi}(-\xi) \sim \pi^{-\frac{1}{2}}\xi^{-\frac{1}{4}}\cos(\zeta + \tfrac{1}{4}\pi), \\ \mathrm{Ai}(\xi) &\sim \tfrac{1}{2}\pi^{-\frac{1}{2}}\xi^{-\frac{1}{4}}e^{-\zeta}, \quad \mathrm{Bi}(\xi) \sim \pi^{-\frac{1}{2}}\xi^{-\frac{1}{4}}e^{\zeta}, \end{aligned} \tag{24}$$

where $\zeta = \frac{2}{3}\xi^{\frac{3}{2}}$. After these values of the Airy functions have been substituted into (22) and (23), it can be seen that the asymptotic value of the solution is a linear combination of the simple harmonic functions $\exp\{\pm i\int M|q|\,dy\}$ in the far field, and the exponential functions $\exp\{\pm i\int M|q|\,dy\}$ in the near field. Hence, the boundary conditions can be written as

$$\begin{aligned} a + \pi\int_0^{\infty}\mathrm{Bi}(-s)\,h_1(s)\,ds - ib - \pi i\int_0^{\infty}\mathrm{Ai}(-s)\,h_1(s)\,ds = 0, \\ b + \int_0^{\infty}\pi\,\mathrm{Ai}(s)\,h_1(s)\,ds = 0, \end{aligned} \tag{25}$$

where $h_1(s)$ is an abbreviation of $h_1(s, k_1, k_2, \omega)$. The solution to the $S1$ case for $y \geqslant y_0$ in the far field can now be written as

$$\Phi_1(y, k_1, k_2, \omega) = \pi\{Mq(y)\}^{-\frac{1}{2}}\xi^{\frac{1}{4}}\Big[\{\mathrm{Bi}(-\xi)+i\,\mathrm{Ai}(-\xi)\} \times\Big\{-\int_0^\infty \mathrm{Ai}(s)\,h_1(s)\,ds+\int_0^\xi \mathrm{Ai}(-s)\,h_1(s)\,ds\Big\} +\mathrm{Ai}(-\xi)\int_\xi^\infty \{\mathrm{Bi}(-s)+i\,\mathrm{Ai}(-s)\}\,h_1(s)\,ds\Big]. \quad (26)$$

Since the present subject is wave radiation into the far field, the solution for the elliptic branch is not shown. However, it can be easily recovered from (23) by substituting into it the values of the constants a and b.

In (26), the last term on the right-hand side vanishes as soon as y is beyond the shear layer. The remainder represents the source contribution of the shear layer along the path of wave propagation. The contributions from the elliptic region and the hyperbolic region are given in separate terms. In the elliptic region, the integral represents an exponentially weighted sum of the source elements located at variable distances from the transition point. The radiation efficiency of a source function decreases rapidly with distance from the transition point. It should be noted that the distance is measured in terms of wavelengths. For the same physical distance along the y axis, the distance would appear to be much greater for high frequency than for low frequency. In this region, the transverse wavenumber of the source element is imaginary, and the ratio of frequency to the real component of the wavenumber is less than the local speed of sound. Hence, the source element can be characterized as hydrodynamic.

In the hyperbolic region, the function $\mathrm{Ai}(-s)$ is oscillatory. When the value of s is large, it can be shown that the noise radiation solution for the hyperbolic region of $S1$ approaches the form of the $S0$ solution asymptotically, if the function $\mathrm{Ai}(-s)$ is replaced by its asymptotic value as given in (24). The interpretation of this part of the solution is, therefore, the same as for the $S0$ mode. From discussions of the contributions of the source function in the elliptic zone and the hyperbolic zone, an interesting conclusion can be made. For low frequencies, source elements in both regions can radiate noise with comparable efficiency. For high frequencies, only sources in the hyperbolic region and those in the neighbourhood of the transition point are responsible for effective emission of noise into the far field.

For shear flows with very large convection Mach numbers, more than one transition point may appear within the half-thickness of the shear layer. The elliptic zone of the differential equation is now bounded. In the presence of a second transition point, the second boundary condition, which states that the pressure fluctuation vanishes at infinity in the elliptic zone, cannot be established. However, the second transition point can be ignored if the frequency of sound under consideration is sufficiently high because the separation between these transition points will appear to be very large, and their influence on each other will be very small. If these transition points are separated by more than two radians of wavelength, the error in the solution due to accepting the second boundary condition in its present form is less than one per cent.

The S2 solution

If the distance between two consecutive transition points is less than two radians, their presence must be considered together. In the limiting case, the transition points are considered to be a single point with a second-order zero for the function M^2q^2. The WKBJ transformation and the resulting differential equation for the present case is given by (7) with $n = 2$. The homogeneous solutions of the wave equation are related to Bessel functions of order one quarter, as given in Phillips (1960). It is more convenient to represent the homogeneous solutions by a pair of functions Pa and Qa:

$$\left.\begin{aligned} \mathrm{Pa}(\xi) &= \tfrac{1}{2}\xi^{\frac{1}{2}}\{J_{-\frac{1}{4}}(\tfrac{1}{2}\xi^2) - \alpha_1 J_{\frac{1}{4}}(\tfrac{1}{2}\xi^2)\}, \\ \mathrm{Qa}(\xi) &= \tfrac{1}{2}\xi^{\frac{1}{2}}\{J_{-\frac{1}{4}}(\tfrac{1}{2}\xi^2) + i\alpha_1 J_{\frac{1}{4}}(\tfrac{1}{2}\xi^2)\}, \\ \alpha_1 &= 2^{-\frac{1}{2}}(1+i). \end{aligned}\right\} \tag{27}$$

The kernel for the integral equation can now be written as

$$K(\xi, s) = \pi\{\mathrm{Qa}(\xi)\,\mathrm{Pa}(s) - \mathrm{Pa}(\xi)\,\mathrm{Qa}(s)\}. \tag{28}$$

It should be noted that the reduced wave equation for $S2$ is hyperbolic on either side of the second-order transition point. In the present study, the origin of the WKBJ transformation is defined along the y axis as follows: it is the upper transition point for the upper branch and the lower transition point for the lower branch. In Phillips (1960), the definition of the origin is somewhat different. Neither definition is exact. In the present case, the derivative of the transformation needs to be defined in the neighbourhood of the transition point such that it remains finite:

$$\lim_{\xi\to 0}\psi'(y) = k_s^{\frac{1}{3}}\left\{\frac{d}{dy}\left(\frac{M_c}{A}\right)\right\}^{\frac{1}{3}} \quad (k_s = (k_1^2 + k_2^2)^{\frac{1}{2}}). \tag{29}$$

On the other hand, the Phillips definition results in an inaccuracy of the transverse wavenumber component in the far field. Since the final solution is given in integral form, an isolated singular point in the definition of ψ' can be removed with affecting the value of the solution. The present definition of the WKBJ variable appears to be acceptable. For both the upper and the lower branches, the solution can be written as

$$\Phi_2(y, k_1, k_2, \omega) = \{Mq(y)\}^{-\frac{1}{2}}\xi^{\frac{1}{2}}\Big\{a\,\mathrm{Pa}(\xi) + b\,\mathrm{Qa}(\xi) + \pi\int_0^{\xi}[\mathrm{Qa}(\xi)\,\mathrm{Pa}(s) - \mathrm{Pa}(\xi)\,\mathrm{Qa}(s)]\,h_2(s, k_1, k_2, \omega)\,ds\Big\}. \tag{30}$$

There is a total of four arbitrary constants: a_1 and b_1 for the upper branch, and a_2 and b_2 for the lower branch. These constants will be determined by four boundary conditions. Two of the boundary conditions require that the pressure wave should be outgoing at $y = \pm\infty$. The other two conditions require that the branch solutions should match at $\xi = 0$. At the second-order transition point the pressure should be in equilibrium, and the wave-induced flow field should be kinematically compatible. For $S2$, the convection velocity has a finite jump across the transition point. Its value is exactly twice the local speed of sound.

The treatment of matching conditions for wave propagation across a shear discontinuity has been discussed in detail by Miles (1957) and Ribner (1957). The same matching conditions are used in the present analysis. The asymptotic values of the functions Pa and Qa for large values of ξ can be written as

$$\left.\begin{aligned} \mathrm{Pa}(\xi) &\cong (2\pi\xi)^{-\frac{1}{2}} \exp\{-i(\tfrac{1}{2}\xi^2+\tfrac{1}{8}\pi)\} \\ \mathrm{Qa}(\xi) &\cong (2\pi\xi)^{-\frac{1}{2}} \exp\{i(\tfrac{1}{2}\xi^2+\tfrac{1}{8}\pi)\} \end{aligned}\right\} \quad \text{as} \quad \xi \to \infty. \tag{31}$$

If these expressions are substituted into (30), the solution will be represented by the harmonic functions $\exp\{\pm i \int M|q|\,dy\}$ in the far field. There are two cases which need to be considered.

First, if the shear flow velocity is extremely large, two transition points may appear simultaneously within the half-thickness of the shear layer. Since the shear gradient is large, these points may be very close together. The shear flow on the two sides of these transition points appears to flow in different directions. Its analysis is quite similar to flows with an antisymmetrical profile. Here, the outgoing wave is represented by the $\mathrm{Qa}(\xi)$ component for both branches. The radiation conditions can now be written as

$$\left.\begin{aligned} a_1 - \pi \int_0^{+\infty} \mathrm{Qa}(s)\, h_2(s, k_1, k_2, \omega)\, ds &= 0, \\ a_2 - \pi \int_0^{-\infty} \mathrm{Qa}(s)\, h_2(s, k_1, k_2, \omega)\, ds &= 0. \end{aligned}\right\} \tag{32}$$

According to Ribner (1957), the matching conditions at the origin of the ξ coordinate can be given as

$$\left.\begin{aligned} a_1 \mathrm{Pa}(0) + b_1 \mathrm{Qa}(0) &= a_2 \mathrm{Pa}(0) + b_2 \mathrm{Qa}(0), \\ a_1 \mathrm{Pa}'(0) + b_1 \mathrm{Qa}'(0) &= -a_2 \mathrm{Pa}'(0) - b_2 \mathrm{Qa}'(0), \\ \mathrm{Qa}(0) = \mathrm{Pa}(0), \quad \mathrm{Qa}'(0) &= -i\,\mathrm{Pa}'(0), \end{aligned}\right\} \tag{33}$$

where Pa′ and Qa′ indicate first derivatives with respect to ξ. It follows that

$$\left.\begin{aligned} b_1 &= \tfrac{1}{2}(1-i)\,a_2 - \tfrac{1}{2}(1+i)\,a_1, \\ b_2 &= \tfrac{1}{2}(1-i)\,a_1 - \tfrac{1}{2}(1+i)\,a_2. \end{aligned}\right\} \tag{34}$$

Hence, the solution to the wave equation can be written as

$$\Phi_2(y, k_1, k_2, \omega) = \pi\{Mq(y)\}^{-\frac{1}{2}} \xi^{\frac{1}{2}} \left[\mathrm{Pa}(\xi) \int_\xi^{+\infty} \mathrm{Qa}(s)\, h_2(s)\, ds + \mathrm{Qa}(\xi) \times \left\{ \int_0^\xi \mathrm{Pa}(s)\, h_2(s)\, ds + \tfrac{1}{2}(1-i) \int_0^{-\infty} \mathrm{Qa}(s)\, h_2(s)\, ds - \tfrac{1}{2}(1+i) \int_0^{+\infty} \mathrm{Qa}(s)\, h_2(s)\, ds \right\}\right] \tag{35}$$

for the upper branch, and

$$\Phi_2(y, k_1, k_2, \omega) = \pi\{Mq(y)\}^{-\frac{1}{2}} \xi^{\frac{1}{2}} \left[\mathrm{Pa}(\xi) \int_\xi^{-\infty} \mathrm{Qa}(s)\, h_2(s)\, ds + \mathrm{Qa}(\xi) \times \left\{ \int_0^\xi \mathrm{Pa}(s)\, h_2(s)\, ds + \tfrac{1}{2}(1-i) \int_0^{+\infty} \mathrm{Qa}(s)\, h_2(s)\, ds - \tfrac{1}{2}(1+i) \int_0^{-\infty} \mathrm{Qa}(s)\, h_2(s)\, ds \right\}\right] \tag{36}$$

for the lower branch. In the above equations, the radiated wave is represented by the $\mathrm{Qa}(\xi)$ term. Its coefficient is composed of three parts: direct outward

radiation from the sources, inward radiation as reflected by the transition zone, and the contribution from sources on the other side of the transition points.

In the second case, the velocity of the shear flow is not necessarily high. Since the velocity profile is symmetric, the transition points come always in pairs. When the frequency of noise radiation is sufficiently low, these transition points have to be considered together. The boundary conditions are different: the solution approaches $\mathrm{Qa}(\xi)$ at $y = +\infty$ and $\mathrm{Pa}(\xi)$ at $y = -\infty$. The WKBJ transformation near the transition point is also different. Since the velocity gradient vanishes at the transition point, the limiting value of ψ' at $\xi = 0$ is given by

$$\psi'(y_0) = k_s^{\frac{1}{3}} \left\{ \frac{1}{2} \frac{d^2}{dy^2} \left(\frac{M_c}{A} \right) \right\}^{\frac{1}{3}}, \tag{37}$$

where the second derivative of M_c/A indicates the mean curvature of the shear flow profile at $\xi = 0$. The matching condition near the origin of the ξ co-ordinate now reads

$$\left.\begin{aligned} a_1 \mathrm{Pa}(0) + b_1 \mathrm{Qa}(0) &= a_2 \mathrm{Pa}(0) + b_2 \mathrm{Qa}(0), \\ a_1 \mathrm{Pa}'(0) + b_1 \mathrm{Qa}'(0) &= a_2 \mathrm{Pa}'(0) + b_2 \mathrm{Qa}'(0), \end{aligned}\right\} \tag{38}$$

which is actually equivalent to stating that both the pressure and the pressure gradient be continuous across the transition point. The solution for the present case can now be written as

$$\Phi_2(y, k_1, k_2, \omega) = \pi \{Mq(y)\}^{-\frac{1}{3}} \xi^{\frac{1}{3}} \left\{ \mathrm{Pa}(\xi) \int_{\xi}^{+\infty} \mathrm{Qa}(s)\, h_2(s)\, ds + \mathrm{Qa}(\xi) \times \int_{-\infty}^{\xi} \mathrm{Pa}(s)\, h_2(s)\, ds \right\}. \tag{39}$$

Equations (35), (36) and (39) are analytically similar. In further discussions in this paper, these cases will not be cited separately.

Since the wavenumber is assumed to be small, the value of ξ will be small throughout the shear layer. The source function is concentrated near the origin as far as the ξ co-ordinate is concerned. Furthermore, the interval between the original transition points along the y axis is reduced to zero in the transformation. Hence, it is more convenient to calculate the integrals in terms of the y co-ordinate. In this case, all the sources are located near the origin of the ξ co-ordinate. The expression for the source integral can be significantly simplified. For example, the coefficient of the $\mathrm{Qa}(\xi)$ term in (36) can be written as

$$\int_0^{\xi} \mathrm{Pa}(s)\, h_2(s)\, ds + \tfrac{1}{2}(1-i) \int_0^{\xi} \mathrm{Qa}(s)\, h_2(s)\, ds - \tfrac{1}{2}(1+i) \int_0^{+\infty} \mathrm{Qa}(s)\, h_2(s)\, ds = \tfrac{1}{2}(1-i) \int_{-1}^{1} \mathrm{Pa}(0) \frac{M^2 \Gamma(y, k_1, k_2, \omega)}{\psi'^{\frac{1}{3}} A^2} dy, \tag{40}$$

where $\mathrm{Pa}(0) = 0{\cdot}5770338$. The coefficients for the $\mathrm{Qa}(\xi)$ term in (37) and (30) can also be reduced to the same form, where the limits of integration in the y co-ordinate are the boundaries of the shear layer. In the interval between the original transition points, the source function can be identified as a hydrodynamic pressure fluctuation. The source in this interval is in fact the most important part for $S2$. In the above equation, the source integral is simply a sum of all

the contributions throughout the shear layer without weighting factors. In common turbulence structures, the hydrodynamic components contain most of the kinetic energy. Hence, the contribution to noise radiation comes mainly from source functions in the elliptical region of the $S2$ wave equation.

Although the $S2$ analysis is based on the assumption of low-frequency noise radiation, the validity of the results here is limited. In the WKBJ transformation, the residue function $g(\xi)$ is proportional to k^{-2} within the shear layer. It becomes very large if k is much smaller than one. Although the iteration of the integral equation will eventually converge, the convergence rate will be very poor. For all practical purposes, the present solution should be applied only to cases where $k \sim 1$.

The inverse Fourier transformation

In most practical studies of noise radiation from turbulence, it is necessary to know the sound intensity and spectrum at given points in space. The solutions obtained so far in the present paper are represented mainly in terms of the wavenumber–frequency co-ordinates. Hence, it is the purpose of the analysis in this section to recover the spatial resolution of the $S0$, $S1$ and $S2$ wave functions. The spatial representation of the solution is advantageous from yet another point of view. It has been noted before in Laufer *et al.* (1964) that the spectral solution diverges at small values of Mq. Evidently, a factor of $(Mq)^{-\frac{1}{2}}$ is contained in all solutions for $S0$, $S1$ and $S2$ as given by (15), (26), (36), (37) and (39). This weak singularity has stirred up serious concern about the validity of the solutions. Such a singularity will not appear in the spatial representation of the solution to the wave equation.

The solutions in all three cases approach asymptotically the harmonic functions $\exp(\pm i\int Mq(y)\,dy)$ in the far field. It is possible to represent $\Phi_n(y, k_1, k_2, \omega)$ entirely in terms of the wavenumber–frequency co-ordinates. In order to keep the mathematical expressions from being too complicated, the shear flow profile and its associated turbulence structure are assumed to be symmetric with respect to the y co-ordinate. As a consequence, the radiated wave field can also be regarded as symmetric with respect to the y co-ordinate. With this assumption, the Fourier transformation of the wave function with respect to y will be the same as a cosine transform, and it can be written as (Erdélyi 1954)

$$\frac{1}{2\pi}\int_{-\infty}^{\infty}\Phi_n(y, k_1, k_2, \omega)\,e^{-ik_3 y}\,dy = \{Mq_\infty\}^{\frac{1}{2}}\frac{1}{k_3^2-(Mq_\infty)^2}\,\Phi_n(k_1, k_2, Mq_\infty, \omega)$$
$$= \{Mq_\infty\}^{\frac{1}{2}}\frac{1}{k_\infty^2-M^2\omega^2}\,\Phi_n(k_1, k_2, Mq_\infty, \omega), \qquad (41)$$

where
$$\Phi_n = \Phi_0(k_1, k_2, Mq_\infty, \omega) = \frac{1}{2\pi}\int_0^\infty e^{-is}h_0(s)\,ds \quad \text{for } S0, \qquad (42)$$

$$\Phi_n = \Phi_1(k_1, k_2, Mq_\infty, \omega) = \frac{i}{\pi^{\frac{1}{2}}}\left\{\int_0^\infty A_i(-s)\,h_1(s)\,ds + \int_{-\infty}^0 A_i(s)\,h_1(s)\,ds\right\} \quad \text{for } S1, \qquad (43)$$

$$\Phi_n = \Phi_2(k_1, k_2, Mq_\infty, \omega) = \frac{1}{2\pi^{\frac{1}{2}}}e^{\frac{1}{4}\pi i}\int_{-1}^{1}\mathrm{Pa}\,(0)\,\frac{M^2\Gamma(y, k_1, k_2, \omega)}{\psi'^{\frac{1}{2}}A^2}\,dy \quad \text{for } S2; \qquad (44)$$

$$k_\infty^2 = k_1^2 + k_2^2 + k_3^2.$$

In (41), the wave function is considered to be harmonic in the far field as well as in the near field. That is, the original wave function has been replaced by one which is harmonic throughout the entire space, while it matches the original solution in the far field.

By using (41), the spatial and temporal resolution of the solutions can be recovered by means of a four-dimensional inverse Fourier transformation:

$$\Phi_n(\mathbf{y},t) = \int\int\int\int \frac{(Mq_\infty)^{\frac{1}{2}}\,\Phi_n(k_1,k_2,Mq_\infty,\omega)}{k_\infty^2 - M^2\omega^2} \exp i(\mathbf{k}.\mathbf{y}+\omega t)\,d\mathbf{k}\,d\omega, \qquad (45)$$

where the limits of integration are $\pm\infty$. This equation has exactly the same form, except for some numerical constants, as the general solution to a simple wave equation in three spatial dimensions (Morse & Feshbach 1953). This equation can then be written alternatively as

$$\begin{aligned} \Phi_n(\mathbf{y},t) &= \frac{1}{4\pi}\int\int\int\int P(\mathbf{y}_0,\omega)\,G(\mathbf{y},\mathbf{y}_0,\omega)\,e^{i\omega t}\,d\mathbf{y}_0\,d\omega, \\ P(\mathbf{y}_0,\omega) &= \int\int\int \{Mq_\infty\}^{\frac{1}{2}}\,\Phi_n(\mathbf{k},\omega)\,e^{+i\mathbf{k}.\mathbf{y}_0}\,d\mathbf{k}, \qquad (46) \\ G(\mathbf{y},\mathbf{y}_0,\omega) &= e^{ik_\infty R}/R, \\ R &= |\mathbf{y}-\mathbf{y}_0| \cong r - \mathbf{y}.\mathbf{y}_0/r \quad (\mathbf{r}=\mathbf{y};\ r=|\mathbf{r}|). \end{aligned}$$

In the above equations, the origin of the y co-ordinates is assumed to be in the source region. The dimension of the entire source region is assumed to be small compared with the distance from a point $\mathbf{y}_0$ in the source region, to a point $\mathbf{y}$ in the far field. Equation (45) can now be written as

$$\Phi(\mathbf{y},t) = \frac{e^{ikr}}{4\pi r}\int_{-\infty}^{\infty}\cdots\int_{-\infty}^{\infty} \{Mq_\infty\}^{\frac{1}{2}}\,\Phi_n(\mathbf{k},\omega)\exp\left[-i\mathbf{y}_0.\left(\mathbf{k}-\frac{k\mathbf{r}}{r}\right)\right]e^{i\omega t}\,d\mathbf{y}_0\,d\mathbf{k}\,d\omega. \quad (47)$$

If this equation is first integrated with respect to $\mathbf{y}_0$, and then integrated with respect to $\mathbf{k}$, the result can be written as

$$\Phi_n(\mathbf{y},t) = \frac{e^{ikr}}{4\pi r}\int_{-\infty}^{\infty}\{Mq_\infty\}^{\frac{1}{2}}\,(2\pi)^3\,\Phi_n\left(\frac{k\mathbf{r}}{r},\omega\right)e^{i\omega t}\,d\omega. \qquad (48)$$

If noise spectrum is preferred, the above equation can be expressed as

$$\Phi_n(\mathbf{y},\omega) = \frac{e^{ikr}}{4\pi r}(2\pi)^3\{Mq_\infty\}^{\frac{1}{2}}\,\Phi_n\left(\frac{k\mathbf{r}}{r},\omega\right). \qquad (49)$$

Hence, the spatial resolution of the solutions to the convected wave equation has been recovered in terms of closed-form expressions.

Throughout the above analysis, it is not necessary to define the equivalent source function $P(\mathbf{y}_0,\omega)$. Therefore, any source function which can produce the correct spectral function in the far field will suffice.

Equation (49) indicates some important properties of the wave emission process. The intensity of the pressure wave depends on the inverse square of the radial distance between the source and the receiving point in the far field. Furthermore, the pressure fluctuation in the neighbourhood of any point in the far field

is dominated by a thin pencil of rays emitted from the source in the direction of the receiving point. Since this solution is extremely similar in form to the solution written in the wavenumber co-ordinates, the inverse transformation has been overlooked in previous studies of the convected wave equation. After the inverse Fourier transformation, (48) and (49) show that the actual noise spectrum at a point differs from the plane wave spectrum, (15), (26) and (30), by a factor of k/r. As a consequence, some previous interpretations by Pao (1972) concerning the parametrical dependences of the solutions in various modes are in error.

Noise emission from random sources

For a random noise source, the source function can only be defined in a statistical sense. The results as obtained above have to be further qualified. It can be assumed that, for any of the above solutions, a complex conjugate problem of the wave propagation process can be posed. After the general solutions for both problems have been obtained, they can be multiplied together, and the ensemble average of the product can then be taken. The result will represent the statistical solution for noise emission from random sources. The $S0$ solution is chosen here to demonstrate the analysis. The general solution of the complex conjugate problem corresponding to the $S0$ case can be written as

$$\Phi_0^*(y, k_1, k_2, \omega) = \{Mq(y)\}^{-\frac{1}{2}} \left\{ e^{-i\xi} \int_{-\infty}^{\xi} e^{+ir} h_0^*(r)\, dr + e^{i\xi} \int_{\xi}^{\infty} e^{-ir} h_0^*(r)\, dr \right\}. \quad (50)$$

Hence, the ensemble average of the product of these solutions can be written as

$$\overline{\Phi_0 \Phi_0^*} = Mq(y)^{-1} \left\{ \iint_{-\infty}^{\xi} e^{-is} e^{ir}\, \overline{h_0(s) h_0^*(r)}\, dr\, ds + \iint_{\xi}^{\infty} e^{is} e^{-ir}\, \overline{h_0(s) h_0^*(r)}\, dr\, ds \right\}, \quad (51)$$

where the ensemble average, denoted by an overbar, of the product of disjoint integrals is assumed to be zero. If the turbulence is assumed to be locally homogeneous in structure, the correlation coefficient of the turbulence at two separate points depends only on the distance of separation, and the intensity of turbulence depends only on the mean value of the co-ordinates of these points. A change of variable can be defined:

$$\lambda_3 = y^* - y, \quad \mu = \tfrac{1}{2}(y + y^*), \quad (52)$$

where y^* and y are points along the y axis which correspond to r and s, respectively, along the ξ co-ordinate.

The correlation function of the turbulence can be written in these co-ordinates as

$$\overline{h(s, k_1, k_2, \omega)\, h^*(r, k_1, k_2, \omega)} = N(\mu)\, \Pi(\lambda_3), \quad (53)$$

where $\Pi(\lambda_3)$ is the correlation function and $N(\mu)$ indicates the source strength distribution. For a small source volume, $N(\mu)$ can be defined as $N(\mu) = 1$ in the source region, and vanishes elsewhere. Unfortunately, (51) cannot be further simplified because the co-ordinate transformation between y and ξ is neither linear nor homogeneous. The origin of the ξ co-ordinate is always fixed at the transition point. A convolution integral for (51) is therefore impossible to derive except for special cases. For practical problems, the integrals will be evaluated by numerical calculations.

The higher iterations of the resolvent kernel

The resolvent kernel of a Volterra integral equation can be obtained from $K(\xi, s)$ by iteration:

$$R(\xi, s) = \sum_{n=1}^{\infty} K^n(\xi, s), \tag{54}$$

where $$K^n(\xi, s) = \int_s^{\xi} K(\xi, r)\, g(r)\, K^{n-1}(r, s)\, dr, \quad K^1(\xi, s) = K(\xi, s),$$

where $g(r)$ is the residue function of the WKBJ transformation as defined in (8). The subscript for this function is omitted here to avoid confusion. For the cases as studied in the present paper, the kernel of the integral equation can be written in general as

$$K(\xi, s) = F_2(\xi)\, F_1(s) - F_1(\xi)\, F_2(s), \tag{55}$$

where $F_1(\xi)$ and $F_2(\xi)$ are the normalized homogeneous solutions for each case. A formalism can now be established for the iterated kernels. If the functions are treated as components of a two-dimensional vector, then

$$K^n(\xi, s) = F_i(\xi)\, G^n_{ij}(\xi, s)\, F_j(s), \tag{56}$$

where $$G^n_{ij}(\xi, s) = \int_s^{\xi} G^1_{ik}(\xi, r)\, F_k(r)\, g(r)\, F_l(r)\, G^{n-1}_{lj}(r, s)\, dr$$

and $$\{G^1_{ij}(\xi, s)\} = \begin{pmatrix} 0 & -1 \\ 1 & 0 \end{pmatrix}.$$

The summation convention is adopted for these equations. Since $g(\xi)$ approaches zero like ξ^{-2} for $\xi \to \infty$, the iteration is expected to converge rapidly.

There are two main reasons for writing the resolvent kernel in the present form. First, this formalism can be adapted directly for numerical computations. Second, an explicit form of the functional dependence of the resolvent kernel is necessary in order to show that the iteration will change only the source integral and not the form of the radiation boundary conditions in the far field.

The radiation boundary condition in the far field requires the knowledge of both $\Phi(\xi)$ and its first derivative. Using the nth approximation of the resolvent kernel, the solution to the wave equation can be written as

$$\Phi(\xi) = aF_1(\xi) + bF_2(\xi) + F_i(\xi) \int_0^{\xi} \sum_1^n G^n_{ij}(\xi, s)\, F_j(s)\, h(s)\, ds. \tag{57}$$

Hence, the derivative of $\Phi(\xi)$ depends on both the derivative of $F_i(\xi)$ and the derivative of the integral. The derivative of the integral contains two terms:

$$\frac{d}{d\xi} \int_0^{\xi} \sum_1^n G^n_{ij}(\xi, s)\, F_j(s)\, h(s)\, ds = \sum_1^n G^n_{ij}(\xi, \xi)\, F_j(\xi)\, h(\xi) + \int_0^{\xi} \sum_1^n \frac{d}{d\xi} G^n_{ij}(\xi, s)\, F_j(s)\, h(s)\, ds. \tag{58}$$

According to the definition of $G^n_{ij}(\xi, s)$, both $G^n_{ij}(\xi, s)$ and its first derivative vanishes at infinity. Hence, the derivative of the integral vanishes at infinity. The boundary conditions are defined by the homogeneous solutions and their derivatives. The analytical form of the radiation boundary conditions are, therefore, not affected by the order of iteration.

4. Discussion

Refraction effects

It has been pointed out earlier that the key wave propagation properties in a shear flow are fixed by the reduced wave equation. Some properties, such as the Doppler shift and the dynamical nature of source elements in a local frame of reference, have been discussed in connexion with $S0$. Closer examination of relations between the source function and far-field plane-wave elements will be given in this section.

In $S0$, the source element for noise radiation in the high frequency limit can be identified as an acoustic component of the local turbulence structure. Hence, such an element has also a local direction of propagation. If the local convection Mach number is M_c, then the local direction of propagation θ_0 will be related to the far-field angle of radiation θ by

$$\cos\theta_0 = A\cos\theta/(1-M_c\cos\theta). \tag{59}$$

This relation is obtained through (19) and the following formulae:

$$k_\infty\cos\theta = k_0\cos\theta_0, \quad k_\infty = M\omega, \quad k_0 = M\omega_0/A, \tag{60}$$

where k_0 is the magnitude of the wavenumber vector of the source element. It should be noted that (59) is identical to the refraction relation for wave propagation in a shear flow. Hence, the refracted path of wave propagation in the shear layer can be traced by means of (59). The above discussion applies also to the noise radiation mechanisms for source functions located in the hyperbolic branch of $S1$.

For sound sources in the elliptic branch of $S1$, the interpretation can be given from a different point of view. Analytically, the wavenumber component in the transverse direction is imaginary. It is well known that in such cases the wave particle velocity is out of phase with the pressure by $\frac{1}{2}\pi$. There is no energy flux in this direction. However, the wavenumber component k_1 in the direction of the flow is real, and the turbulent energy contained within a given source element will be carried forwards through local pressure fluctuations. For a small source volume located beneath the transition point, its pressure fluctuation is felt, with an exponential decay factor, by the fluid layer in the neighbourhood of the transition point. At the transition point, the pressure fluctuations attain the sonic phase velocity. Hence, the pressure fluctuations can now propagate and turn as an acoustic wave, and leave the shear layer as a radiated plane-wave element. For source elements which are located in the elliptic branch of $S1$, equation (59) fails because $|\cos\theta_0| > 1$. Here k_0 is no longer related to ω_0 through the local speed of sound as specified by (60).

For source volumes in $S2$, the transverse wavenumber component cannot be precisely defined. Nevertheless, it can be considered as zero. The turbulence source fluctuation has a real propagation velocity in the direction of the flow. The general solution in $S2$ indicates that the source function in such cases is coupled directly with radiated plane-wave elements in the far field.

The correspondence between the source and the radiated noise as described

here is not the same as that given in the classical analysis of turbulent noise. In both theories, the frequencies are related through the Doppler shift relation. In the classical analysis, the wavenumber vector is the same for a plane-wave element in the far field as for the corresponding turbulent source component. The analysis which leads to this conclusion is similar to the derivation of (48) in connexion with the inverse Fourier transformation. This is perhaps a necessary consequence if the wave propagation process is governed by the simple wave equation throughout the entire space. Owing to such correspondences between wavenumber and frequency, the phase speed for the source component in the convected frame of reference can range from zero to values much greater than the local speed of sound. This phase speed equals the local speed of sound only if $\theta = \frac{1}{2}\pi$, and it is greater than the ambient speed of sound for all $\theta > \frac{1}{2}\pi$. In the present theory, the local phase speed of the source element can only be equal to or smaller than the local speed of sound. In the case of radiation in upstream directions, the transverse wavenumber component changes rapidly in the shear layer such that locally the ratio of frequency to the magnitude of the wavenumber vector is always the speed of sound. The physical interpretation of such requirements appears to be correct. The turbulent source is embedded entirely in the fluid and is not in contact with any solid surface. In addition, only linear wave propagation is considered. Hence, the fluctuations in the turbulence can only have phase speeds which are equal to or less than the local speed of sound.

So far, noise radiation has been considered in one direction at a time. The solutions are given in forms such that all contributions from various source volumes are summed along the path of radiation which leads to a given direction in the far field. On the other hand, it is more familiar to consider a given compact source volume which radiates noise in all directions. It is clear from the above discussions that different spectral components of this volume of turbulence will be responsible for noise radiation in various frequencies. The noise radiation mechanism will also be governed by different modes of solution to the convected wave equation.

For a given convection Mach number for the source volume, the far field can be divided into a maximum of four zones. The governing type of solution which relates the radiated noise to the source function will be different in each zone. The dividing angles θ_1, θ_2 and θ_3 for these zones are given by

$$\left.\begin{aligned} &\cos\theta_1 = 1/(M_c - A), \quad \theta_1 = 0 \quad \text{if} \quad (M_c - A) \leqslant 1, \\ &\cos\theta_2 = 1/(M_c + A), \\ &\cos\theta_3 = 1/(M_c - A), \quad \theta_3 = \pi \quad \text{if} \quad (M_c - A) \geqslant -1. \end{aligned}\right\} \tag{61}$$

For sound radiation between $\theta = 0$ and θ_1 the source element is locally acoustic. However, the pressure wave has to pass through a pair of transition points in order to reach the far field. For high frequency radiation, the pressure wave will be heavily attenuated as it passes through the elliptic segment between the transition points. For low frequency radiation, the radiation mechanism will be governed by $S2$. This zone exists only if the convection Mach number is sufficiently large such that $M_c - A$ is greater than one. In the second zone bounded between θ_1 and θ_2, the source element is hydrodynamic. Here the noise radiation

process is governed by either $S1$ or $S2$, depending on the frequency. It should be noted that θ_2 is always smaller than $\frac{1}{2}\pi$. For noise emission between θ_2 and θ_3, the source element is locally acoustic. Since there is no transition point between the source and the far field, the sound radiation process is governed by $S0$. A fourth zone exists between θ_3 and $\theta = \pi$ in the special case where the flow temperature is high while the convection Mach number is small such that $M_c - A$ is less than -1. The source element for sound emission in this zone is again hydrodynamic, and wave propagation will be governed by $S1$ or $S2$. In most cases, only θ_2 has a non-trivial value. The noise-radiation mechanisms will be only those described above for the second and third zones.

The boundary between zones should not be considered as a sharp line of separation. For example, the source components in the third zone which are responsible for noise radiation near θ_2 and θ_3 are indeed acoustic in nature. However, the source volume is located very close to a transition point. It is more appropriate to describe the radiation process by means of $S1$.

Convection effects

In discussions below, the value of k_2 will be taken as zero. This assumption is made mainly for convenience. With this restriction, the paths of noise radiation will fall on a plane which also contains the normal and the y_1 axis of the shear layer. If the source function is confined to a small volume near the origin, a rotation of co-ordinates in the plane of the shear layer will make any radiation path coincide with such a vertical plane. The value of k_2 in the new co-ordinates will be zero. In this case, the convection Mach number M_c will be replaced by its effective component $M_c \cos\phi$, where ϕ is the angle of rotation.

A simple turbulence structure can now be introduced to serve as the source function:

$$\overline{v_i v_j}(\boldsymbol{\lambda}, \tau) = v_0^2 \left\{ \left(1 - \frac{\lambda^2}{L_1^2}\right) \delta_{ij} + L_1^{-2} \lambda_i \lambda_j \right\} \exp\left[-\left\{ \left(\frac{\lambda}{L_1}\right)^2 + \left(\frac{\tau}{L_t}\right)^2 \right\} \right], \tag{62}$$

or

$$\overline{v_i v_j}(\mathbf{k}, \omega) = \frac{v_0^2 L_1^3 L_t}{32\pi^2} \{(kL_1)^2 \delta_{ij} - L_1^2 k_i k_j\} \exp\left[-\tfrac{1}{4}\{(kL_1)^2 + (\omega L_t)^2\}\right], \tag{63}$$

where $\boldsymbol{\lambda}$ is the spatial separation from the source, τ is the time delay, L_1 is the spatial scale of the turbulence and L_t is the time scale of the turbulence. This turbulence structure satisfies only the equation of continuity of an incompressible fluid. The quadrupole self-noise source can now be written in more precise terms:†

$$\overline{\frac{\partial v_i}{\partial y_j} \frac{\partial v_j}{\partial y_i} \frac{\partial v_k^*}{\partial y_l^*} \frac{\partial v_l^*}{\partial y_k^*}} = \frac{\partial^4}{\partial \lambda_i \partial \lambda_j \partial \lambda_k \partial \lambda_l} \overline{v_i v_j v_k^* v_l^*}(\boldsymbol{\lambda}, \tau), \tag{64}$$

where the turbulence is assumed to be locally incompressible. According to Batchelor (1960, p. 179) the fourth-order correlation can be related to the second-order correlations via

$$\overline{v_i v_j v_k^* v_l^*} = \overline{v_i v_j} \cdot \overline{v_k^* v_l^*} + \overline{v_i v_k^*} \cdot \overline{v_j v_l^*} + \overline{v_i v_l^*} \cdot \overline{v_j v_k^*}. \tag{65}$$

† The shear noise term will not be presented in this paper. Its analytical form is much simpler, while its functional dependence is similar to that of the self-noise term. See Pao & Lowson (1970).

If $k_2 = 0$, then only the derivatives with respect to y_1 and y_3 need to be considered. Equation (64) represents a contraction of the fourth-order correlation function Ψ which contains sixteen terms. These terms can be evaluated through convolution integrals, and their sum turns out to be rather simple:

$$\Psi(\lambda_3, k_1, k_2, \omega) = \frac{v_0^4 L_t}{16\pi(2\pi)^{\frac{1}{2}} L_1^2}\left\{(k_1 L_1)^4 - 2(k_1 L_1)^2 \frac{\partial^2}{\partial\lambda_3^2} + \frac{\partial^4}{\partial\lambda_3^4}\right\} \times \exp\left[-2\left(\frac{\lambda_3}{L_1}\right)^2 - \tfrac{1}{8}\{(k_1 L_1)^2 + (\omega_0 L_t)^2\}\right]. \quad (66)$$

It should be noted that k_2 has been considered as a variable in the convolution integrals. It is given the value of zero only after all the integrations have been completed.

Equation (66) represents the ensemble average of the square of the self-noise term which appears in the convected wave equation. Therefore, it can be used directly in the calculation of the mean-square value of the sound pressure. A formula for the mean-square value of the pressure field has been derived for $S0$ in the previous section. By using the same procedure, it is equally easy to derive formulae for the spectral density function $\overline{\Phi_n \Phi_n^*}(\mathrm{y}, \omega)$ which describes the noise spectrum received at a point in the far field. The general formula for $\Phi_n(\mathrm{y}, \omega)$ is given by (49), and the source integrals for $S0$, $S1$ and $S2$ are given by (42)–(44). A symbolic expression for the mean-square value of the source integral can be written as

$$\overline{\Phi_n \Phi_n^*}(\mathrm{k}, \omega) = \int\int F_1(r) F_1^*(s) \frac{M^4 \Gamma(y^* - y, k_1, k_2, \omega)}{\{\psi'(y)\,\psi'(y^*)\}^{\frac{1}{2}} A^2}\, dy\, dy^*, \quad (67)$$

where $F_1(\xi)$ stands for $\exp\{\pm i\xi\}$, $\mathrm{Ai}(\pm\xi)$, $\mathrm{Pa}(\xi)$ or $\mathrm{Qa}(\xi)$, whichever is appropriate; $F_1^*(\xi)$ is the complex conjugate of $F_1(\xi)$; and the variables r and s are dummies corresponding to the transformed co-ordinate ξ. There are two cases where this integral can be estimated analytically. In the first case, the source function is confined to the neighbourhood of a transition point. In the second the source volume is small and located sufficiently far from a transition point, and it is required also that the function $q(y)$ be approximately constant throughout the source region. The functional dependence of the above integral can reveal important information concerning the convection laws for each of the three solutions. Hence, the estimate of this integral will be examined separately for each case.

If in $S0$ the source volume is sufficiently small, the value of Mq will appear to be constant across the source volume. Consequently, the variables r and s will be related linearly to y and y^*. The function $F_1(r)\,F_1^*(s)$ can be written as a function of λ_3 and μ, which are defined in (52). After a simple analysis, it can be shown that the integral is equivalent to a local Fourier transformation in the variable λ_3. Furthermore, $\psi' = Mq_0$ in the source region. Hence,

$$\begin{aligned}\overline{\Phi_0 \Phi_0^*}(\mathrm{y}, \omega) &= (16\pi^2 r^2)^{-1} (Mq_\infty)\,(2\pi)^6\, \overline{\Phi_0 \Phi_0^*}(\mathrm{k}, \omega) \\ &= \frac{(2\pi)^6}{16\pi^2 r^2}\left\{\frac{Mq_\infty}{Mq_0}\right\} \frac{v_0^4 M^4 L_t}{128\pi^3 L_1 A^2}\{(k_1 L_1)^4 + 2(k_1 L_1)^2 (Mq_0 L_1)^2 + (Mq_0 L_1)^4\} \\ &\qquad \times \exp[-\tfrac{1}{8}\{(k_0 L_1)^2 + (\omega_0 L_t)^2\}] \\ &= \frac{\pi v_0^4 M^4 L_t}{32 r^2 L_1 A^2}\left(\frac{q_\infty}{q_0}\right)(k_0 L_1)^4 [\exp - \tfrac{1}{8}\{(k_0 L_1)^2 + (\omega_0 L_t)^2\}]. \end{aligned} \quad (68)$$

By comparing this equation with the classical results, one finds that the convection law is tremendously different for the present equation. In the classical result, the factor $(k_0 L_1)^4$ will be replaced by $(k_\infty L_1)^4$; the term $(k_\infty L_1)^2$ in the exponential index will be replaced by $(k_\infty L_1)^2$, so that

$$\overline{\Phi_0 \Phi_0^*}(\mathrm{y}, \omega) \sim M^8 (1 - M_c \cos\theta)^{-5} (\omega_0 L_1)^4 \exp\left[-\tfrac{1}{8}\{(k_\infty L_1)^2 + (\omega_0 L_t)^2\}\right], \quad (69)$$

where a bandwidth adjustment of $(1 - M_c \cos\theta)^{-1}$ has been included. If (68) is written in the same form, the convection factor of $(1 - M_c \cos\theta)^{-4}$ will be absent from the expression for sound intensity:

$$\overline{\Phi_0 \Phi_0^*}(\mathrm{y}, \omega) = \frac{\pi v_0^4 M^8 L_t}{32 r^2 A^6 L_1} \left(\frac{q_\infty}{q_0}\right) \frac{(\omega_0 L_1)^4}{(1 - M_c \cos\theta)} \exp\left[-\tfrac{1}{8}\{(k_0 L_1)^2 + (\omega_0 L_t)^2\}\right]. \quad (70)$$

In (68), there is a factor of q_∞/q_0. It is natural to ask what may happen if q_0 vanishes. If this is the case, the source volume will be in the immediate neighbourhood of a transition point, the $S0$ solution will not be valid. Radiation from such source volumes should be calculated by using the $S1$ or $S2$ solution. In the above analysis, the discussion should be valid for all frequencies as long as the source volume remains compact and small. That is, it is not necessary to confine the analysis to the high frequency limit. However, this analysis is not valid for very low frequencies where the WKBJ transformation itself would fail.

In the $S2$ case, the values of r and s are small throughout the shear layer. Hence, the function $F_1(r) F_1^*(s)$ can be replaced by its value at $r = s = 0$. The integral in (67) can be written simply as an integration of the source function over the variables λ_3 and μ. For convenience, the source volume is assumed to be small such that the convection Mach number will be approximately constant for the entire source volume. While this assumption allows a straightforward interpretation of the result, it is not essential to the analysis. The value of ψ' is proportional to $k_1^{\frac{1}{2}}(M\Omega)^{\frac{1}{2}}$ in the present case:†

$$\psi' = \kappa\{M k_1 \Omega\}^{\frac{1}{2}}, \quad \Omega = \frac{1}{M} \frac{d}{dy}\left(\frac{M_c}{A}\right), \quad (71)$$

where κ is a proportionality constant which equals one in the neighbourhood of the transition point. It should be noted that the integral in (67) in its present form can be considered as a Fourier transformation in the λ_3 co-ordinate, while the wavenumber component in this direction vanishes. The result of the integration can now be written as

$$\begin{aligned}\overline{\Phi_2 \Phi_2^*}(\mathrm{y}, \omega) &= \frac{(2\pi)^6 M q_\infty}{16\pi^2 r^2} \overline{\Phi_2 \Phi_2^*}\left(\frac{k\mathbf{r}}{r}, \omega\right) \\ &= \frac{\pi^2 M^4 v_0^4 L_t}{32 r^2 A^2 L_1} \left(\frac{M q_\infty}{\psi'}\right) \mathrm{Pa}^2(0) (k_1 L_1)^4 \exp\left[-\tfrac{1}{8}\{(k_1 L_1)^2 + (\omega_0 L_t)^2\}\right] \\ &= \frac{\pi^2 M^{\frac{7}{2}} v_0^4 L_t}{32 r^2 A^2 L_1} \left\{\frac{\tan\theta}{L_1^{\frac{1}{2}} \Omega^{\frac{1}{2}}}\right\} \mathrm{Pa}^2(0) (k_1 L_1)^{\frac{9}{2}} \exp\left[-\tfrac{1}{8}\{(k_1 L_1)^2 + (\omega_0 L_t)^2\}\right]. \end{aligned} \quad (72)$$

Again, the factor $M q_\infty/\psi'$ deserves some attention. It remains finite for all directions of wave radiation which belong to $S2$. The domain of validity for $S2$ has

† There are two cases of $S2$. In the other one, $\psi' = k^{\frac{1}{2}}\{\frac{1}{2} M \Omega'\}^{\frac{1}{2}}$.

been defined in the last subsection. Here θ will always be smaller than $\frac{1}{2}\pi$, and it can approach $\frac{1}{2}\pi$ only if the value of M_c approaches infinity.

If the wavenumber factor is rewritten in terms of the local frequency ω_0, equation (72) will read

$$\overline{\Phi_2 \Phi_2^*}(\mathbf{y}, \omega) = \frac{\pi^2 M^8 v_0^4 L_t \mathrm{Pa}^2(0)}{32 r^2 A^2 L_1^{\frac{3}{2}} \Omega^{\frac{1}{2}}} \frac{(\omega_0 L_1 \cos\theta)^{\frac{3}{2}}}{\{1 - M_c \cos\theta\}^{\frac{1}{2}}} \exp\left[-\tfrac{1}{8}\{(k_1 L_1)^2 + (\omega_0 L_t)^2\}\right]. \quad (73)$$

The convection law as shown in this equation is different from the classical result in two ways. First, there is an additional factor of $(\cos\theta)^{4.5}$. Second, the convection factor is stronger by a factor of $(1 - M_c \cos\theta)^{-\frac{1}{2}}$. Analytically, the latter effect is a result of the interaction between the noise radiation mechanism and the shear velocity gradient, since an additional factor of $(k_1 L_1)^{\frac{1}{2}}$ comes from the $M q_\infty / \psi'$ factor in (72).

The $S1$ case will be considered in two parts. Again, the source volume is assumed to be small: it is located either in the neighbourhood of the transition point or far away from it. The convection effects associated with the former condition can be analysed in the same way as is the $S2$ case. Here, the value of ψ' in the neighbourhood of the transition point is

$$\psi' = k^{\frac{2}{3}} (2M\Omega)^{\frac{1}{3}} \quad (74)$$

and the function $F_1(r) F_1^*(s)$ will be evaluated at $r = s = 0$. Hence, (67) can be written as

$$\begin{aligned}\overline{\Phi_1 \Phi_1^*}(\mathbf{y}, \omega) &= \frac{\pi^2 v_0^4 M^{\frac{1}{3}} L_t \mathrm{Ai}^2(0) \tan\theta}{8 r^2 A^2 L_1^{\frac{1}{3}} \Omega^{\frac{1}{3}}} (k_1 L_1)^{\frac{1}{3}} \exp\left[-\tfrac{1}{8}\{(k_1 L_1)^2 + (\omega_0 L_t)^2\}\right] \\ &= \frac{\pi^2 v_0^4 M^8 L_t \mathrm{Ai}^2(0) \tan\theta}{8 r^2 A^2 L_1^{\frac{4}{3}} \Omega^{\frac{1}{3}}} \frac{(\omega_0 L_1 \cos\theta)^{\frac{1}{3}}}{(1 - M_c \cos\theta)^{\frac{1}{3}}} \exp\left[-\tfrac{1}{8}\{(k_1 L_1)^2 + (\omega_0 L_t)^2\}\right]. \end{aligned} \quad (75)$$

In (75) the convection factor is different from the classical result by a factor of $(\cos\theta)^{4.33} (1 - M_c \cos\theta)^{-0.33}$. The interaction between the sound emission process and the velocity gradient is slightly weaker than in the $S2$ case.

If the source volume is located in the elliptic branch and far away from the transition point, the Airy functions can be replaced by their asymptotic forms. Consequently,

$$\begin{aligned} F_1(r) F_1^*(s) / \{\psi'(r)\, \psi'(s)\}^{\frac{1}{2}} &= r^{\frac{1}{4}} s^{\frac{1}{4}} F_1(r) F_1^*(s) / \{M^2 q(r)\, q(s)\}^{\frac{1}{4}} \\ &= \frac{1}{4\pi M q_0} \exp\left\{-\int^y M q\, dy\right\} \exp\left\{-\int^{y^*} M q\, dy\right\}. \end{aligned} \quad (76)$$

Since the source volume is small and q remains approximately constant over the source volume, the argument of the exponential function can be written as

$$\begin{aligned} \int^y M q\, dy &= \int^{y_1} M q\, dy + \int_{y_1}^{y} M q\, dy = Q + M q_0 (y - y_1), \\ Q &= \int^{y_1} M q\, dy, \end{aligned} \quad (77)$$

where y_1 is a suitable point in the source volume and q_0 is the value of q at y_1.

It is important to note that the above function depends only on μ and not λ_3.

The integration of (67) over the variables λ_3 and μ has again the meaning of a Fourier transformation of the source function in the λ_3 co-ordinate, while the wavenumber component vanishes. The result of the integration can now be given as

$$\overline{\Phi_1 \Phi_1^*}(\mathrm{y}, \omega) = \frac{\pi v_0^4 M^8 L_t q_\infty}{32 r^2 A^2 L_1 q_0} e^{-2Q} \frac{(\omega_0 L_1 \cos\theta)^4}{(1 - M_c \cos\theta)^5} \exp\left[-\tfrac{1}{8}\{(k_1 L_1)^2 + (\omega_0 L_t)^2\}\right]. \quad (78)$$

The convection factor $(1 - M_c \cos\theta)^{-5}$ is exactly the same as in the classical results. However, the above equation contains also a factor of $(\cos\theta)^4 e^{-2Q}$. From the definition of transition point, one can verify that the transition point is closer to the edge of the shear layer for smaller values of θ. If the source volume is located at a fixed depth in the shear layer, the distance between the source and the transition point will be greater for smaller angles of radiation. For a given frequency, the directivity of noise radiation will be strongly modified by the factor e^{-2Q}. This is perhaps a contributing factor which leads to the observed cardioid pattern of jet noise radiation at high frequencies.

Q is a linear function of ω_0:

$$Q = k_1 W(y_0, \theta) = \frac{M \omega_0 \cos\theta}{(1 - M_c \cos\theta)} W(y_0, \theta), \quad (79)$$

where y_0 is the position of the source function and θ is the angle of noise radiation in the far field. By means of this definition, (78) can be integrated over ω_0 in closed analytical form.

Mach-number and temperature dependence

Equations (70), (73), (75) and (78) can be integrated analytically over ω_0. The result will provide a value for the total amount of noise emission in a given direction for each of these cases. The exponential function in the turbulent source spectrum can be written as a function which depends only on ω_0:

$$\exp\left[-\tfrac{1}{8}\{(k_0 L_1)^2 + (\omega_0 L_t)^2\}\right] = \exp\left[-\frac{1}{8}\left(\frac{M}{M_c}\right)^2 \left(\frac{\omega_0 L_1}{\alpha A}\right)^2 (\alpha^2 M_c^2 + A^2)\right] \quad \text{for } S0, \quad (80)$$

$$\exp\left[-\tfrac{1}{8}\{(k_1 L_1)^2 + (\omega_0 L_t)^2\}\right] = \exp\left[-\frac{1}{8}\left(\frac{M}{M_c}\right)^2 \left(\frac{\omega_0 L_1}{\alpha}\right)^2 \times \frac{(1 - M_c \cos\theta)^2 + \alpha^2 M_c^2 \cos^2\theta}{(1 - M_c \cos\theta)^2}\right] \quad \text{for } S1 \text{ and } S2, \quad (81)$$

$$L_1/L_t = \alpha (M_c/M),$$

where α is a constant which defines the ratio of the integral spatial scale and the integral time scale of the given turbulence structure. The value of α^2 can be taken as 0·1 in jet turbulence. The value of M/M_c is a matter of definition. If a single source volume is under consideration, the reference Mach number M can be defined as the same as the local convection Mach number M_c. Hence, $M/M_c = 1$. Equations (70), (73), (75) and (78) can now be integrated for noise emission in a given direction. The results are, respectively,

$$\overline{\Phi_0 \Phi_0^*}(\mathrm{y}) = \frac{3 \times 2^{\frac{1}{2}} \pi^{\frac{1}{2}} v_0^4 M^8 \alpha^4 q_\infty}{r^2 A^2 L_1 q_0} \left(\frac{M_c}{M}\right)^4 \frac{A}{(1 - M_c \cos\theta)} \{A^2 + \alpha^2 M_c^2\}^{-\frac{5}{2}} \quad \text{for } S0, \quad (82)$$

$$\overline{\Phi_2\Phi_2^*}(y) = \frac{21\times 2^{\frac{1}{2}}\pi^2 v_0^4 M^8 \mathrm{Pa}^2(0)\alpha^{\frac{3}{2}}\tan\theta}{4r^2A^2L_1^{\frac{3}{2}}\Omega^{\frac{1}{2}}}\Gamma(\tfrac{3}{4})\{\cos\theta\}^{\frac{3}{2}}\left(\frac{M_c}{M}\right)^{\frac{2}{3}} \times\{(1-M_c\cos\theta)^2+\alpha^2M_c^2\cos^2\theta\}^{-\frac{11}{6}} \quad \text{for } S2, \tag{83}$$

$$\overline{\Phi_1\Phi_1^*}(y) = \frac{160\times 2^{\frac{1}{2}}\pi^2 v_0^4 M^8 \mathrm{Ai}^2(0)\alpha^{\frac{1}{2}}\tan\theta}{9r^2A^2L_1^{\frac{1}{2}}\Omega^{\frac{1}{2}}}\Gamma(\tfrac{2}{3})\{\cos\theta\}^{\frac{1}{2}}\left(\frac{M_c}{M}\right)^{\frac{1}{3}} \times\{(1-M_c\cos\theta)^2+\alpha^2M_c^2\cos^2\theta\}^{-\frac{5}{6}} \quad \text{for } S1(a), \tag{84}$$

$$\overline{\Phi_1\Phi_1^*}(y) = \frac{3\times 2^{\frac{1}{2}}\pi^2 v_0^4 M^8\alpha^4 q_\infty}{r^2A^2L_1q_0}\left(\frac{M_c}{M}\right)^4 F(b)\cos^4\theta \times\{(1-M_c\cos\theta)^2+\alpha^2M_c^2\cos^2\theta\}^{-\frac{5}{2}} \quad \text{for } S1(b), \tag{85}$$

where $\Gamma(x)$ denotes the gamma function, and the function $F(b)$ and the value of b are defined as

$$F(b) = \int_b^\infty e^{b^2-u^2}(u-b)^4\,du, \tag{86}$$

$$b = \frac{2^{\frac{3}{2}}M|V(y_0,\theta)\cos\theta}{L_t\{(1-M_c\cos\theta)^2+\alpha^2M_c^2\cos^2\theta\}^{\frac{1}{2}}}. \tag{87}$$

It should be noted that the value of b in (87) is defined for self-noise. Its value is smaller for shear noise by a factor of $1/2^{\frac{1}{2}}$. In (82), there is a factor of $(1-M_c\cos\theta)^{-1}$. It is important to note that this term remains finite for all solutions which belong to $S0$. According to (59) and (61), the value of $(1-M_c\cos\theta)^{-1}$ can never be greater than $(M_c+A)/A$. For small values of Mach number, all of the above cases obey an M^8 law. For high Mach numbers, the current results are not the same as the classical results. First of all, the $S0$ case approaches an M^3 law only when M_c^2 becomes significantly greater than A^2. However, this does not mean that $S0$ radiation is necessarily more efficient in the higher Mach number range than $S1$ or $S2$, because this type of noise radiation did not have the advantages of a convection factor to begin with as did the other two cases. It is quite surprising to note that the convection law for the $S2$ and $S1(a)$ case turns out to be less efficient than the M^3 law in the high Mach number range: there is an $M^{2\cdot5}$ law for $S2$ and an $M^{2\cdot67}$ law for $S1(a)$. For the $S1(b)$ case, the Mach-number dependence is identical to the classical results.

It is not clear whether the slight decline of the noise radiation efficiency in the $S1(a)$ and $S2$ cases is experimentally observable, assuming that the above conclusion is correct. The overall noise radiation depends also on the fourth power of the turbulence intensity v_0. If this non-dimensional value depends on even a small positive fractional power of the Mach number, the dependence of v_0^4 on Mach number will largely compensate for small deviations from the M^3 law.

Another unexpected result in this study is the dependence of the radiated sound pressure on c_j/c_0. In (1), both the source function $\gamma(\partial v_i/\partial y_j)\,\partial v_j/\partial y_i$ and the pressure fluctuation $\log(p/p_0)$ are multiplied by a factor A. Since the source function as defined in (8) depends explicitly on A^{-2}, it may appear that the intensity of the radiated noise would depend on A^{-4}. This is not the case if one examines carefully the solutions as given by (15), (26), (36) and (39). While the factor AA^{-2} of the source integrand is evaluated in the shear flow region, the

factor A associated with $\log(p/p_0)$ should be evaluated in the far field, where it has a value of one. Hence, the sound intensity in the far field depends only on A^{-2} instead of A^{-4}. Such a dependence can be written as either T/T_j or ρ_j/ρ_0, and it is much weaker than the corresponding dependence discussed in Ribner (1964).

Limitations to the present theory

In general, the accuracy of the present analysis is limited to the extent where (3) is applicable. Although there may be further improvements of this wave equation under special flow conditions, it appears that the present solution contains a sufficient number of differences from the classical analysis to warrant detailed considerations.

The second limitation of the present analysis is inherent in the WKBJ transformation. The application of the WKBJ method should be restricted to cases where $kL > 1$, where k denotes here a dimensional wavenumber. The value of kL is directly related to the Strouhal number St in aerodynamic noise:

$$St = \omega L/2\pi U = kL/2\pi M \quad (kL = 2\pi StM).$$

For a turbulent round jet, the characteristic dimension is the exit diameter of the jet. For most jets, the peak Strouhal number is between 0·25 and 0·30. If the jet velocity is greater than 0·6 times the ambient speed of sound, all the noise radiation near or above the peak of the spectrum can be studied by the present theory. The same statement can be made also for rocket-noise radiation. The peak Strouhal number for rocket noise ranges from 0·04 down to 0·02. However, the corresponding values of M ranges from a minimum of 6 to well above 10.

In the final discussion, most of the interpretations are made on the assumption that the source volume is small. If the source volume is large, much of the simple interpretation in terms of ray acoustics will no longer apply. Hence, such discussion serves only to indicate the underlying mechanisms of noise emission from a physical point of view of fluid mechanics.

Finally, it should be pointed out that the present formulation is given in terms of Cartesian co-ordinates. It is perhaps more appropriate to study problems such as jet noise radiation in terms of cylindrical co-ordinates. Mechanisms such as low frequency noise radiation and the interaction between jet instability and noise radiation can be described more accurately in cylindrical co-ordinates. Analytical techniques such as Fourier transformations and WKBJ methods remain available for obtaining solutions from the latter case.

This work was supported by the Unsteady Gasdynamics Branch of National Aeronautics and Space Administration – Marshall Space Flight Center, under contract no. NAS 8-28588.

REFERENCES

BATCHELOR, G. K. 1960 *The Theory of Homogeneous Turbulence.* Cambridge University Press.

ERDÉLYI, A. (ed.) 1954 *Tables of Integral Transforms*, vol. 1, chap. 1. McGraw Hill.

ERDÉLYI, A. 1956 *Asymptotic Expansions.* Dover.

FFOWCS WILLIAMS, J. E. 1963 The noise from turbulence convected at high speed. *Phil. Trans. Roy. Soc.* A 255, 469–503.

LAUFER, J., FFOWCS WILLIAMS, J. E. & CHILDRESS, S. 1964 Mechanism of noise generation in the turbulent boundary layer. *AGARDograph*, no. 90.

MILES, J. W. 1957 On the reflection of sound at interface of relative motion. *J. Acoust. Soc. Am.* **29**, 226–228.

MORSE, P. M. & FESHBACH, H. 1953 *Methods of Theoretical Physics*, chaps 9, 10. McGraw Hill.

PAO, S. P. 1971 A generalized theory on the noise generation from supersonic shear layers. *J. Sound Vibr.* **19**, 401–410.

PAO, S. P. 1972 Developments of a generalized theory of jet noise. *A.I.A.A. J.* **10**, 596–602.

PAO, S. P. & LOWSON, M. V. 1970 Some applications of jet noise theory. *A.I.A.A. 8th Aerospace Sci. Paper*, no. 70-233.

PHILLIPS, O. M. 1960 On the generation of sound by supersonic turbulent shear layers. *J. Fluid Mech.* **9**, 1–28.

RIBNER, H. S. 1957 Reflection, transmission, and amplification of sound by a moving medium. *J. Acoust. Soc. Am.* **29**, 435–441.

RIBNER, H. S. 1964 The generation of sound by turbulent jets. *Adv. in Appl. Mech.* **8**, 103–182.